Full-thickness skin-on-a-chip model for *in vitro* drug testing

Combining tissue engineering with organ-on-a-chip technology to produce advanced skin models

Patrícia Alexandra Afonso Zoio

Dissertation presented to obtain the Ph.D degree in Molecular Biosciences

Instituto de Tecnologia Química e Biológica António Xavier | Universidade Nova de Lisboa

Oeiras,
November, 2021

UNIVERSIDADE NOVA DE LISBOA

Full-thickness skin-on-a-chip for *in vitro* drug testing

Combining tissue engineering with organ-on-a-chip technology to produce advanced skin models

Patrícia Alexandra Afonso Zoio

Dissertation presented to obtain the Ph.D degree in Molecular Biosciences

Instituto de Tecnologia Química e Biológica António Xavier | Universidade Nova de Lisboa

Oeiras, November, 2021

Full thickness skin-on-a-chip for *in vitro* drug testing

Supervisor: Doctor Abel González Oliva[1,2]

[1] Instituto de Tecnologia Química e Biológica (ITQB), Universidade Nova de Lisboa, Portugal

[2] Instituto de Biologia Experimental e Tecnológica (IBET), Portugal

Work performed at:

Biomolecular Diagnostic Laboratory
Instituto de Tecnologia Química e Biológica, Universidade Nova de Lisboa (ITQB-NOVA); 2781-901 Oeiras – Portugal

Doctoral programme
Advanced Integrated Microsystems (AIM)

Financial support from Fundação para a Ciência e Tecnologia (FCT) – PhD Grant – PD/BD/128164/2016

Abstract

Human skin represents an important endpoint to access the efficacy and toxicity of cosmetics and pharmaceuticals. In the last few years, there has been an increasing demand for the development and production of *in vitro* skin models for basic and applied research which led to important advancements in the field of skin tissue engineering. However, current *in vitro* skin models still do not recapitulate the complex architecture and physiology of the *in vivo* human skin. The main limitations of the models produced with conventional methods are the use of exogenous animal-derived hydrogels, high contractability, lack of physiologically relevant mechanical forces and perfusion. This results in low mechanical stability and in a significantly weaker skin barrier compared to the native skin. Consequently, there remains a dependence on animal models during preclinical drug trials which results in expensive drug development, high failure rates and ethical issues.

In this work, we combine innovative tissue engineering techniques and rapid prototyping technology to produce advanced biomimetic skin models. First, we developed a protocol for the generation of a pigmented full thickness human skin model (FTSm) compatible with long-term studies. A fibroblast-derived matrix was combined with the use of an inert polystyrene for the development of a tissue with high mechanical stability, avoiding the use of animal-derived materials. A terminally differentiated skin that could maintain its architecture and homeostasis up to 50 days was successfully generated. The model demonstrated structural characteristics and barrier properties parallel to the native human skin. Skin permeation and irritation tests were performed based on OECD guidelines. The results showed the potential of the model to function as an open-source alternative to current commercially available options.

A biomimetic organ-on-a-chip (OoC) system with a dynamic perfusion and a modular architecture was designed and fabricated to increase the physiological relevancy of the FTSm. By imparting a fine control over the microenvironment and by including relevant mechanical cues, we developed a skin-on-a-chip (SoC) model that could circumvent the limitations of conventional cell studies. Finite element analysis (FEA) was performed to characterize the velocity profile and shear stress,

for different flow configurations. The fabricated system included an easy-to-use architecture with a removable culture insert that can be transferred between modules. It was demonstrated that mechanical forces and shear stress impact tissue formation, increasing synthesis and deposition of extracellular-matrix (ECM). The developed SoC resulted in a fully differentiated FTSm with enhanced barrier properties, increased thickness and terminal differentiation. Furthermore, by culturing the FTSm in a scaffold and stimulating the cells to produce their own ECM, a model with superior stability and physiological relevance was produced. Finally, electrodes were integrated in the developed OoC platform for real-time monitoring of the transepithelial electrical resistance (TEER). The TEER was measured during the culture of a FTSm inside the chip and after exposure of a benchmark irritant to evaluate its impact on the skin barrier. The integration of the sensors represents a promising tool to assess the barrier function inside the platform in the context of drug testing and disease modelling.

Overall, in this research work, biomimetic skin models that better recapitulate the complexity of the native human skin were developed. In the future, they could offer a suitable test system for drug testing and for basic investigations on (patho-)physiological aspects of human skin.

Resumo

A pele humana é um órgão importante para o estudo da eficácia e toxicidade de cosméticos e produtos farmacêuticos. Nos últimos anos, tem-se observado um aumento na procura de modelos de pele *in vitro* para investigação fundamental e aplicada, o que levou a avanços importantes na área da engenharia de tecidos cutâneos. No entanto, os modelos de pele *in vitro* existentes atualmente ainda não são capazes de recapitular a arquitetura e fisiologia complexas da pele humana nativa. As principais limitações dos modelos de pele produzidos através de métodos convencionais incluem o uso de materiais exógenos de origem animal, a elevada contratabilidade dos tecidos e ausência de perfusão e de forças mecânicas fisiologicamente relevantes. Estas limitações resultam em modelos com uma baixa estabilidade mecânica e uma barreira de pele significativamente mais fraca em comparação com a pele nativa. Consequentemente, permanece a dependência por modelos animais durante os testes pré-clínicos de fármacos, o que por sua vez resulta em custos elevados, taxas de aceitação baixa e implicações éticas.

Neste trabalho, técnicas inovadoras de engenharia de tecidos foram combinadas com tecnologia de prototipagem rápida para produzir modelos biomiméticos de pele capazes de superar as limitações dos modelos atuais. Primeiro, desenvolvemos um protocolo otimizado para a geração de um modelo de pele humana completa (PHCm) com pigmentação, compatível com estudos de longo prazo. Combinou-se o use de uma matriz extracelular produzida por fibroblastos com um *scaffold* de poliestireno inerte para o desenvolvimento de um tecido com alta estabilidade mecânica, evitando-se o uso de componentes de origem animal. Uma pele terminalmente diferenciada capaz de manter a sua arquitetura e fisiologia até 50 dias foi gerada com sucesso. A PHCm demonstrou características estruturais e propriedades de barreira paralelas à pele humana nativa. Testes de permeação e irritação da pele foram realizados com base nas diretrizes da OCDE. Os resultados mostraram o potencial do modelo para se tornar uma alternativa *open source* aos modelos de pele comercialmente disponíveis .

Um sistema biomimético com base em tecnologia *organ-on-a-chip* (OoC) que inclui uma perfusão dinâmica e uma arquitetura modular foi desenvolvido e

fabricado de forma a aumentar a relevância fisiológica do PHCm. Ao implementar-se um controle do espaço intersticial e ao incluírem-se estímulos mecânicos relevantes, foi possível desenvolver um modelo de pele-em-chip que pode superar as limitações dos modelos convencionais. O sistema incluiu uma arquitetura fácil de usar com cultura celular removível e que pode ser transferida entre módulos diferentes. Foi demonstrado que as forças mecânicas e a tensão de cisalhamento impactam a formação do tecido, aumentando a síntese e deposição de matriz extracelular (MEC). A plataforma de OoC deu origem a um PHCm totalmente diferenciada com propriedades de barreira melhoradas, maior espessura e diferenciação terminal. Além disso, ao cultivar-se o PHCm num *scaffold* e ao estimular-se as células a produzirem sua própria MEC, produziu-se um modelo com estabilidade superior e maior relevância fisiológica. Por fim, elétrodos foram integrados na plataforma OoC de forma a monitorar-se, em tempo real, a resistência elétrica transepitelial (RETE). A RETE foi medida durante a cultura de PHCm dentro do chip e após a exposição de um irritante de referência para avaliar seu impacto na barreira da pele. A integração dos sensores representa uma ferramenta promissora para avaliar a função de barreira dentro da plataforma no contexto de testes de fármacos e simulação de doenças cutâneas.

No geral, neste trabalho, foram desenvolvidos modelos biomiméticos de pele que melhor recapitulam a complexidade da pele humana nativa. No futuro, estes modelos poderão ser usados para testes de toxicidade e para investigações básicas sobre aspetos (patofisiológicos) da pele humana.

Acknowledgments

I want to acknowledge everyone who has contributed directly and indirectly to my PhD research during the past five years. First of all, I would like to express my sincere gratitude to my PhD advisor, Professor Abel Oliva, for giving me the opportunity to join the Biomolecular Diagnostic Laboratory and work on this exciting, interdisciplinary project. Throughout these years, I was able to think and work independently while being guided towards realistic aspirations. The successful completion of this work was only possible due to the support of Dr. Abel.

I want to thank all my colleagues from the Biomolecular Diagnostic Laboratory for all the help and support. A special thanks to Sandro Evaristo for introducing me to the world of cell culture and teaching me the basic techniques during my first year and to Sara Ventura for contributing to this work with her technical knowledge. I also want to express my warm gratitude to Dragana Barros for all the enthusiastic and stimulating conversations not only about work but also life in general.

A sincere thank you to Dr. Joana Marto from University of Lisbon. Joana not only greatly enriched this work with her technical expertise in the area of topical drug delivery but also greatly motivated me with her captivating enthusiasm.

I want to thank my colleagues and professors from the StartUp Research program for expanding my perspective towards scientific research. It provided me with social awareness, innovation mindset and important skills to translate academic research into ideas that create a bigger impact in the world. I believe the skills I gained during this post-graduation positively impacted my PhD thesis.

I would also like to express my gratitude to Dr. Ana Cadete, senior scientist at Moderna, for the guidance and motivation towards the development of a business idea. Although my work did not progress in that direction, I am deeply thankful for her effort. Her enthusiasm, expertise and high productivity were very contagious and inspired me to be a better researcher.

Finally, I want to express my deepest gratitude to my family who have always supported me throughout the highs and lows of this long journey. I want to

specially thank my parents, Vasco Zoio and Ana Afonso, for providing me much needed emotional support. This thesis is dedicated to them.

Table of Contents

List of abbreviations

2D - Two-dimensional

3D - three-dimensional

AC - Alternating current

Ag - Silver

AgCl - Silver chloride

ALI - Air–liquid Interface

AMPs - Antimicrobial peptides

ANOVA - One-way Analysis of Variance

BM - basement membrane

BoC - Barrier-on-chip

CAD - Computer aided design

CC - Current carrying

CGM - Co-culture growth medium

CNC - Computer numerically controlled

DC - Direct current

DEJ - dermo-epidermal junction

e.g. - *Exempli gratia*

ec - electrical current

ECM - Extracellular matrix

ECVAM - European Centre for the Validation of Alternative Methods

EU - European Union

FBS - Fetal Bovine Serum

FDA - Food and Drug Administration

FDM - Fibroblast-derived matrix

FEA - Finite element analysis

FGF - Fibroblast Growth Factor

FITC - Fluorescein isothiocyanate

FTSm - Full thickness skin model

GAGs - Glycosaminoglycans

GelMA - Gelatin-methacryloyl

H&E - Haematoxylin and eosin

HDFns - Human dermal fibroblasts of neonatal origin

HFs - Human fibroblasts

HEKns - Human epidermal keratinocytes of neonatal origin

HKs - Human keratinocytes

HKGS – Human keratinocyte growth supplement

HPAs - Human preadipocytes

HUVECs - Human Umbilical Vein Endothelial Cells

IMDM - Iscove's Modified Dulbecco's Medium

iPSC - induced pluripotent stem cells

IT - Information technology

JAMs - Junctional adhesion molecules

K - Keratin

KGM - Keratinocyte growth medium

LL - Lower limit

LPS - Lipopolysaccharides

LY - Lucifer yellow

MGM - Melanocyte growth medium

MMP - Matrix Metalloproteinase

MTT - 3-[4,5-dimethylthiazole-2-yl]-2,5-diphenyltetrazolium bromide

OD - optical density

OECD - Organization for Economic Co-operation and Development

OoC - Organ-on-a-chip

PAMPA - Parallel artificial membrane permeability assay

PBS - Phosphate buffered saline

PC - Polycarbonate;

PCL - Polycaprolactone;

PCR - Polymerase chain reaction

PDMS - Polydimethylsiloxane

PEEK - Polyether ether ketone

PEG - Polyethylene Glycol

PET - Polyethylene terephthalate

PGs - Proteoglycans

PMMA - Poly(methylmethacrylate)

PS - Polystyrene

PTFE - Polytetrafluoroethylene

PVC - Polyvinyl chloride

PVC - Polyvinyl chloride

R&D - Research and Development

RHEm - Reconstructed human epidermis models

RPM - Rotation per minute

S - sensitivity field

SB - *Stratum basale*

SC - *Stratum corneum*

SD - Standard deviation

SDS - sodium dodecyl sulphate

SG - *Stratum granulosum*

SG - succinimidyl glutarate

SoC - Skin-on-a-chip

SS - *Stratum spinosum*

TEER - Transepithelial/transendothelial electrical resistance

TEWL - Transepidermal water loss

TG - Test guideline

TNF - Tumor necrosis factor

UN GHS - United Nations Globally Harmonized System of Classification

UV - Ultraviolet

VS - Voltage sensing

List of figures

Chapter 2

Chapter 3

Chapter 4

Chapter 5

Chapter 6

Chapter 7

Appendix A

Appendix B

Appendix C

List of tables

Chapter 3

Appendix B

Appendix C

Chapter 1

Aims and thesis outline

1.1 Motivation

1.1.1 The need for advanced organ models

Currently, the biopharmaceutical industry is facing unprecedented challenges, including a significant decline in Research and Development (R&D) productivity. A key aspect of this problem is the decreasing number of new compounds being approved by the regulatory agencies [1]. Every year, pharmaceutical companies are spending more capital in developing drugs that fail at late stages of process, especially the phase II and phase III, the most expensive phases of clinical trials. The success rate of drugs that pass in clinical trials has been reported to be as low as 12% [2]. This reveals a failure in testing methods, particularly those used between the preclinical development and the beginning of clinical trials.

Conventional preclinical testing relies on cell studies and animal models, neither of which recapitulate the complexity of the human body. Recent advances in cell culture, such as three-dimensional (3D) cultures and bioprinted tissues offer better results than traditional two-dimensional (2D) cultures, but are still far from replicating the complex *in-vivo* like interactions between cells and the extracellular matrix [3]. Moreover, they are unable to reproduce the systemic response of the body which is essential for the study of the pharmacokinetics and pharmacodynamics of a drug. On the other hand, animal models can replicate the complex interaction between organs and provide a systemic response but the results cannot be extrapolated to humans. Furthermore, ethical guidelines dictate that animal models should be replaced, reduced and refined, known as the 3R principle. New models capable of improving R&D productivity should include human cells and be capable of replicating human tissue and organ physiology and interactions to replicate the systemic response of the human body.

Recent developments formed at the interface between microscale technology and tissue engineering has led to development of platforms termed organ-on-a-chip (OoC). These platforms aim to reproduce the *in-vivo* tissue composition, function and environment to bridge the gap between human biology

and current *in vitro* models. This new generation of OoC platforms is expected to provide a complex structure and networks for efficiently testing new compounds and for developing specialized in vitro disease models. This was successfully demonstrated by multiple publications which reported, for example, the development lug, heart, liver, kidney, gut on OoC platforms [4]. Furthermore, disease models were generation such as cancer-on-a-chip and inflammation-on-a-chip [5] [6].

1.1.2 Advanced biomimetic skin models

The role of the skin in the human body is indispensable, serving as a barrier against the external environment and representing an important endpoint for both pharmaceuticals and cosmetics. Furthermore, multiple diseases affect this organ, usually due to immune malfunctions, contact with allergens, irritants or pathogen infections. In fact, the global burden of skin diseases is high, affecting approximately one third of global population, ranging from mild disorders to malignant melanoma [7]. The important role of the skin combined with European legislation banning the use of animal testing for cosmetic ingredients and the increasing number of chemicals for which risk assessment must be conducted, pressured the development of new models that could replace animal testing.

The reconstruction of skin models with physiologically relevant cellular and matrix architecture is gaining importance as an *in vitro* tool to study skin diseases and for the pharmaceutical, toxicological and cosmetic industries. Important progress has been achieved in the last years to create 3D models mimicking its complex architecture. However, the existent models using conventional approaches are limited by a weak skin barrier function compared to the native human skin [8]. Probable reasons include the lack of mechanical forces and dynamic flow system that provide necessary mechanistic signals and continuous supply of nutrients and metabolites. Furthermore, major obstacles hampering the quality and reproducibility of the skin models is the contraction of the dermal equivalent. These factors limit the utility of the current *in vitro* skin models in percutaneous penetration and toxicity studies.

At the time of the beginning of this thesis, only a handful of publications reported the use of OoC platforms to culture skin models. Ataç *et al* demonstrated

advantages of a microfluidic culture by prolonging culture and higher cellular viability of a commercial skin model and skin biopsy inserted into a chip [9]. Abaci *et a*l presented a pumpless microfluidic chip, which recirculated the culture medium using a rocking platform, for the purpose of drug testing on a skin model inserted into it [10]. Two studies reported co-cultivation of skin with other organs [11] [12]. The mentioned studies pointed to the potential of the OoC technology in the area of skin tissue engineering. However, in these works, the skin models were not reconstructed directed into the system, limiting the benefits of a dynamic culture.

1.2 Goals of the project

This work aimed at developing a biomimetic skin-on-a-chip device for disease modelling and *in situ* drug testing. It aimed at expanding the potential of current OoC platforms for skin engineering by providing a device for the development of full-thickness skin models that better recapitulate the structure and functionalities of human skin, compared to static culture models.

The first major goal was to develop a full-thickness skin model, including the dermal and epidermal compartments. The Biomolecular Diagnostics Laboratory from ITQB had previous expertise in the development of epidermal models on polycarbonate membranes. However, no protocols were established for the development of the dermal compartment. The first task included the development and optimization of a protocol to produce a mechanically stable dermis, without using animal-derived hydrogels such as collagen from bovine or rat tail origin. The dermis needed to be compatible with the development of a fully differentiated epidermal compartment on top. The final task was to validate the model by performing irritation and permeation testing and comparing the results to conventional approaches.

The second major goal was to design and fabricate an OoC platform in which a mechanically stable full-thickness skin model could be cultivated for multiple weeks. The first task consisted on the design of the device and perform finite element modelling to study the OoC hydrodynamics. The device needed to correctly seal the skin tissue and provide continuous flow and drainage of nutrients at the basal side and air flow at the apical side. The skin developed on chip was

compared with the skin developed off chip using histologic analysis and immunohistochemistry. The final task consisted in performing preliminary drug testing *in situ*.

The final major goal was the integration of sensors in the developed organ-on-a-chip platform for real-time monitoring of skin health. First, the placement and geometry of the electrodes was studied using finite element modelling to access its sensitivity. The sensors were assembled and integrated in the developed SoC. Finally, its performance was experimentally evaluated by following skin formation and by assessing its response to drugs.

1.3 Thesis outline

To provide a background for the development of a biomimetic skin model, in **Chapter 2** an introduction to the skin anatomy and physiology is provided, as well as an overview of the in vitro skin models reported in the literature. Particular attention is given to scaffold-based full-thickness skin models. In **Chapter 3**, an introduction to organ-on-a-chip technology is provided. The most relevant technical and biological factors to the development of a biomimetic skin-on-a-chip are described. A detailed overview of the skin-on-a-chip platforms that have been published up to this date as well as the challenges and future perspectives is presented. **Chapter 4** contains the development of a protocol for the development of pigmented full-thickness human skin model based on a fibroblast-derived matrix for long-term studies. In **Chapter 5**, the protocol described in the previous chapter is used to the development of skin models for preliminary drug permeation and irritation testing, according to OECD guidelines. **Chapter 6** contains the development of a skin-on-a-chip model with a modular architecture and integrated scaffold. **Chapter 7** focuses on the integration of the electrodes on the developed organ-on-a-chip, for measurement of the transepithelial resistance measurement. The applicability of the device is expanded to other organs with barrier function. Lastly, **Chapter 8** concludes this thesis with a summary of the obtained results as well as a list of recommendation for further research.

1.4 Scientific output

The work performed under the scope of this PhD thesis results in the publications, communications and awards listed below:

1.4.1 Original papers in peer-reviewed journals

- **Zoio P,** Lopes-Ventura S, Marto J, Oliva A. Open-source human skin model with an in vivo-like barrier for drug testing. ALTEX - Alternatives to animal experimentation. 2022. https://doi.org/10.14573/altex.2111182.

- **Zoio P,** Oliva A. Skin-on-a-Chip Technology: Microengineering Physiologically Relevant In Vitro Skin Models. Pharmaceutics. 2022; 14(3):682. https://doi.org/10.3390/pharmaceutics14030682.

- **Zoio P**, Lopes-Ventura S, Oliva A. Biomimetic Full-Thickness Skin-on-a-Chip Based on a Fibroblast-Derived Matrix. Micro. 2022; 2(1):191-211. https://doi.org/10.3390/micro2010013

- Hall MJ, Lopes-Ventura S, Neto MV, Charneca J, **Zoio P**, Seabra MC, Oliva A, Barral DC. Reconstructed human pigmented skin/epidermis models achieve epidermal pigmentation through melanocore transfer. Pigment Cell & Melanoma Research. 2022; 00, 1– 11. https://doi.org/10.1111/pcmr.13039

- **Zoio P**, Ventura S, Oliva A. Barrier-on-a-Chip with a Modular Architecture and Integrated Sensors for Real-Time Measurement of Biological Barrier Function. *Micromachines*. 2021; 12(7):816. doi.org/10.3390/mi12070816

- **Zoio P,** Ventura S, Leite M, Oliva A. Pigmented Full-Thickness Human Skin Model Based on a Fibroblast-Derived Matrix for Long-Term Studies. *Tissue Eng Part C Methods*. 2021;27(7):433-443. doi:10.1089/ten.TEC.2021.006

-

1.4.2 Oral Communications

- **Zoio P**, Oliva A. Fully Human Skin-on-a-chip with integrated sensors and a modular architecture for drug screening and disease modelling. Presented at the 11th edition World Conference on Alternatives and Animal Use in the Life Sciences (Maastricht, The Netherlands) (2021).

1.4.3 Poster Communications

- **Zoio P**, Lopes-Ventura S, Oliva A. Fully Human Skin-on-a-chip with integrated sensors and a modular architecture for drug screening and disease modelling. Presented at the 11th WC11 (Maastricht, The Netherlands) (2021).

- Lopes-Ventura S, **Zoio P**, Oliva A. Reconstructed Fully-Humanized Skin model for therapeutic biomedical applications. Presented at the Champalimaud Foundation, Lisbon, Portugal (2020).

- **Zoio P**, Lopes-Ventura S, Oliva A. Fully Humanized Skin-on-a-chip for medical applications: Combining microtechnology with 3D tissue engineering to develop human skin. Presented at the European Commission JRC, Ispra, Italy (2019).

1.4.4 Awards

- Early career Scientist Award attributed by the Physicians Committee for Responsible Medicine (2021)

- Best Poster Award attributed by European Society of Toxicology *in vitro* (ESTIV) at the 11th World Congress on Alternatives to Animal Use in Life Sciences WC11 (2021)

- Early-Career Scientist Award attributed by the People for ethical treatment of animals (PETA) (2019)

- Best Poster award attributed by the European Commission (JRC) at the Conference on "Non-animal approaches in Science" (2019)

1.5 References

[1] I. Khanna, "Drug discovery in pharmaceutical industry: productivity challenges and trends," Drug Discov. Today, vol. 17, no. 19, pp. 1088–1102, 2012.

[2] J. A. DiMasi, H. G. Grabowski, and R. W. Hansen, "Innovation in the pharmaceutical industry: New estimates of R&D costs," J. Health Econ., vol. 47, pp. 20–33, 2016.

[3] K. Duval et al., "Modeling Physiological Events in 2D vs. 3D Cell Culture," Physiology, vol. 32, no. 4, pp. 266–277, Jun. 2017.

[4] J. E. Sosa-Hernández et al., "Organs-on-a-chip module: A review from the development and applications perspective," Micromachines, vol. 9, no. 10, 2018.

[5] R. Portillo-Lara and N. Annabi, "Microengineered cancer-on-a-chip platforms to study the metastatic microenvironment," Lab Chip, vol. 16, no. 21, pp. 4063–4081, 2016.

[6] D. Irimia and X. Wang, "Inflammation-on-a-Chip: Probing the Immune System Ex Vivo," Trends Biotechnol., vol. 36, no. 9, pp. 923–937, 2018.

[7] C. Karimkhani et al., "Global Skin Disease Morbidity and Mortality: An Update From the Global Burden of Disease Study 2013," JAMA dermatology, vol. 153, no. 5, pp. 406–412, May 2017.

[8] G. Sriram et al., "Full-thickness human skin-on-chip with enhanced epidermal morphogenesis and barrier function," Mater. Today, vol. 21, no. 4, pp. 326–340, 2018.

[9] B. Ataç et al., "Skin and hair on-a-chip: In vitro skin models versus ex vivo tissue maintenance with dynamic perfusion," Lab Chip, vol. 13, no. 18, pp. 3555–3561, 2013.

[10] H. E. Abaci, K. Gledhill, Z. Guo, A. M. Christiano, and M. L. Shuler, "Pumpless microfluidic platform for drug testing on human skin equivalents," Lab Chip, vol. 15, no. 3, pp. 882–888, 2015.

[11] I. Wagner et al., "A dynamic multi-organ-chip for long-term cultivation and substance testing proven by 3D human liver and skin tissue co-culture," Lab Chip, vol. 13, no. 18, pp. 3538–3547, 2013.

[12] I. Maschmeyer et al., "A four-organ-chip for interconnected long-term co-culture of human intestine, liver, skin and kidney equivalents," Lab Chip, vol. 15, no. 12, pp. 2688–2699, 2015.

Chapter 2

Advancements in the development of physiologically relevant *in vitro* human skin models

2.1 Introduction

Skin and subcutaneous disorders affect approximately one third of the global population and are associated with a global burden encompassing psychological, social and financial dimensions [1]. In particular, chronic skin diseases, such as psoriasis, eczema and atopic dermatitis result in a significant morbidity and are known to affect patients' quality of life [2]. On the other side, malignant skin diseases, such as malignant melanoma, are frequently fatal [3]. A better understanding of the physiology of healthy and diseased skin would greatly benefit from the existence of a biomimetic skin models that replicate the key components of *in vivo* skin. Moreover, these models could be used to develop and test new substances for pharmaceutical and cosmetic applications.

Drug development is long and costly process, with estimated costs of developing a single new drug reported to be 2.6 billion USD [4]. Furthermore, the success rate of drugs passing preclinical trials and reaching the clinical trial phase is reported to be only 12%. The decline in R&D productivity has been a cause of concern in pharmaceutical industry since the 1950s [5]. In parallel, the emergence of new technologies during the past decades such as combinatorial chemistry and bioinformatic tools resulted in major improvements in the initial stages of drug development. As a consequence of this new technologies, there has been an increase in the volume of drug candidates. Interestingly, these advances combined with an increased investment in R&D did not result in an increased in the number of drugs approved and introduced in the market. The large volume of potential drugs is bottlenecked along different stages of the development pipeline. It has been estimated that for every 5000 to 10000 drug candidates that enter the pipeline, only 1 is approved for clinical use [6].

The lack of correlation between the input and output in the pharmaceutical industry reveals important flaws in the testing methods, specially between preclinical development and the beginning of clinical trials. Conventional preclinical drug testing relies on *in vitro* cell cultures and animal models. Most commonly, *in vitro c*ell culture relies on 2D arrangements of cells (cell monolayers) and, while these models are useful for assessing compound cytotoxicity, they are not good predictors of complex interactions seen *in vivo* [7]. Animal models offer information regarding

systemic effects but cannot replicate the human physiology. Animal models also suffer from low throughput and repeatability and present interspecies variability [8]. Furthermore, they represent significant ethical challenges. In the particular case of the skin, different animal models have been used for research in this area with mouse models being most commonly used because of easily handling and lower cost. The use of mouse models is often mandatory for *in vivo* translational research, to study skin physiology, biochemistry and immunology. However, many comparative studies show significant differences between mouse and human skin. Mouse skin is structurally and functionally different; it is thinner, contains more hair follicles, includes less keratinocyte layers, decreased barrier function and greater absorption [9]. Furthermore, there are multiple differences between mouse and human skin immune systems, including the presence and location of different dominant T cells and differing array of chemokines expressed. All of these differences make mouse models poor predictors of the human skin response to topical drugs. These relevant differences between the animal and human models result in multiple drug candidates failing in clinical trials or in dismissal of drugs that could potentially be effective in humans.

From an ethical perspective, the replacement of animal models satisfies a growing societal concern regarding animal experimentation. Ethical guidelines dictate that, where possible, animal experimentation should be replaced, reduced, or refined (3R principle). The cosmetic industry, another multibillion-dollar field, has been greatly affected by the restrictions imposed on animal testing. Since 2009, the European Commission has been approving regulations on cosmetics establishing a testing and marketing ban: a prohibition to test finished cosmetic product or ingredients on animals and to commercialize any cosmetic product or ingredient that has been tested on animals within the European Union [10]. In 2013 a full marketing ban was put in place for all human health effects including repeated-dose toxicity, reproductive toxicity and toxicokinetic, irrespective of the availability of alternative non-animal tests. The European Centre for the Validation of Alternative Methods (ECVAM) was established in 2010 as a reference laboratory (EURL-ECVAM) for the research and validation of alternative methods, following 3R principles [11].

The combinatory effect of the high prevalence of skin diseases, R&D decline and restrictions on animal testing pressured the development of physiologically relevant skin models that could replace conventional, inefficient models. Recently, 3D culturing techniques have improved relevance of the available models and demonstrated the synergistic effects different cell types have on each other [12]. These models can be assembled into complex structures to simulate more physiologically relevant conditions and cell-matrix interactions. These 3D *in vitro* models could reconstitute human skin and allow the development of new therapeutic agents for treatment of multiple diseases and give insights into skin pathologies. Advances in tissue engineering has resulted in progress towards recapitulating some functions of the native human skin. In the last years, these models have been used in a large array of applications including basic, pharmacological and cosmetic research. However, engineering physiological relevant skin models remains challenging due to skin's structural and functional complexity as it encompasses a variety of specialized cells and physiological subsystems.

2.2 Skin anatomy and physiology

The skin is a complex fibrous multi-layered structure that acts as the first line of defence between the body and the external environment, protecting against pathogens, ultraviolet (UV) radiation, water loss, mechanical trauma and a multitude of toxic chemicals [13]. Furthermore, it provides thermal, tactile and pain sensations, synthesis of vitamin D and participates in thermoregulation by adjusting blood flow to the surface and by liberating sweat. The skin is a functionally heterogeneous and structurally complex organ that can be divided into two main structural layers: the epidermis and dermis (**Figure 2. 1**).

The epidermis is the outermost layer and consists of a stratified epithelium. It is an avascular structure with varying thickness between 60 μm and 100 μm over most areas, and reaching 600 μm in the plantar and palmar regions [14]. This layer predominantly consists of keratinocytes, protein-rich cells composed mostly of keratin and keratohyalin. Keratin provides structure and tensile strength by forming bundles of elastic fibrils that stretch across the cells. Keratohyalin is a histidine-rich

interfilamentous matrix protein now known as filaggrin, filament-aggregating protein. The epidermis is organized into distinct *stratum* (layers) according to the degree of keratinization of the cells: *stratum basale* (basal cell layer), *stratum spinosum* (spinous or prickle-cell layer), *stratum granulosum* (granular cell layer), *stratum lucidum* (clear layer) and *stratum corneum* (horny cell layer) [15].

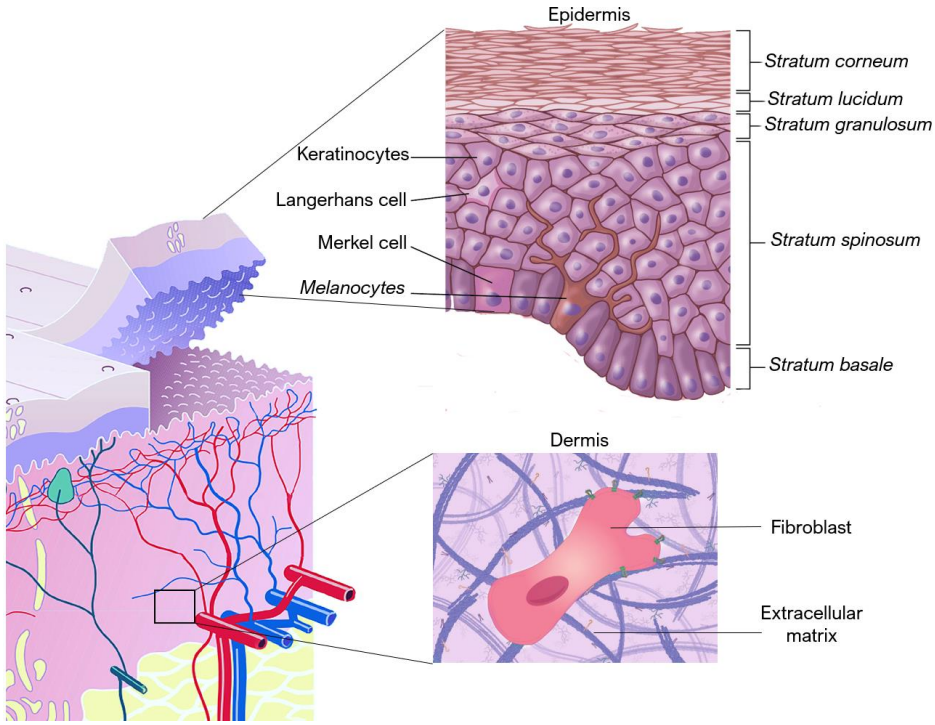

Figure 2. 1. The structure of human skin consisting of two primary layers: the epidermis and the dermis. The two inserts (right site) show their detailed representation of the cellular structure at higher magnification. The epidermis consists mainly of keratinocytes, melanocytes, and Langerhans cells and is organized in the *stratum basale*, *stratum spinosum*, *stratum granulosum*, *stratum lucidum* and *stratum corneum*. The dermis contains fibroblasts and other dermal components embedded within an extracellular matrix rich in collagen and elastin. Adapted from [18].

The *stratum basale* is the innermost layer of the epidermis, separated for the dermis by the basement membrane (basal lamina) and attached to it by hemidesmosomes [16]. This is the only proliferative layer of the skin, containing interfollicular epidermal stem cells and mitotically active cells that are responsible

for tissue renewal. The basal cell layer also contains melanocytes. These cells produce skin pigment or melanin, protecting the deeper skin layers from the harmful effects of the sun [17]. Merkel cells, tactile cells of neuroectodermal origin, are also located in the basal layer of the epidermis. The progeny of the basal keratinocytes migrates to upper layers and undergoes differentiation process. The morphology of the cuboidal cells in the basal layer changes progressively towards squamous in suprabasal layers.

The *stratum spinosum*, also known as the prickle cell layer, contains irregular, polyhedral cells with cytoplasmatic processes, also called "spines" extending outward and connected to those of adjacent cells via desmosomes to generate a network of keratin fibres capable of withstanding high tension. The *stratum spinosum* is the thickest layer of the epidermis and also contains Langerhans cells, residing in this layer as a dense network of immune system sentinels [19]. The *stratum granulosum* (granular layer) contains cells that produce keratohyalin granules and lamellar granules. Keratohyalin granules contain keratin precursors that aggregate, crosslink and form bundles. The lamellar granules contain glycolipids that get secreted to the surface of the cells and function as a glue, keeping the cells stuck together. Cells in the *stratum* degenerate and undergo apoptosis as they migrate towards the upper layers, forming the *stratum corneum* (horny layer). The *stratum lucidum* is only present in thicker skin and consists of eleidin, a transformation product of keratohyalin. The *stratum corneum* is the outermost layer of the skin. It consists of multiple layers of flattened non-nucleated cells devoid of organelles, filled with keratin and surrounded by lipids, forming an impermeable layer that serves as a protection against water loss and foreign substances [20]. The keratinized cells are surrounded by a plasma membrane and a thick submembranous layer that contains involucrin. This protein is synthesized in the *stratum spinosum* and cross-linked in the *stratum granulosum*. It provides structural support to the cells, allowing them to resist invasion by microorganisms. The dead non-nucleated cells in the *stratum corneum* are continuously shed and replaced by cells differentiating from the lower *strata*. Cells in each *strata* are continuously pushed up to the upper *strata*. Throughout the process, cells degenerate and increase their keratin content as they migrate to upper layers, losing their nuclei when they become part of the *stratum corneum*.

The dermis is a thick connective tissue providing the avascular epidermis with nutritional materials and oxygen. This layer contains mesenchymal stem cells that differentiate into fibroblasts and produce connective tissue. It houses blood vessels, sensory nerves and lymphatics and contains inner parts of sweat glands and sebaceous glands [21]. Overall, the dermis is thicker than the epidermis, ranging between 0.5 mm and 5 mm. It is a vascularized fibrous layer supplied with nerves, lymph vessels, hair follicles, sweat glands, sebaceous glands and smooth muscle. The vasculature within the dermis has three main functions, namely nutrition, oxygenation and thermoregulation. The dermis provides tension, strength and elasticity to the skin through extracellular matrix (ECM). It can be divided into two main layers: the papillary layer (*pars papillaris*) and the reticular layer (*pars reticularis*) [22]. **Figure 2. 2** shows histological images of adult human skin containing the epidermis and dermis, the latter subdivided into the papillary and reticular layers. The papillary and reticular layers are separated by a network of vessels called *rete subpapillare*.

2.2.1 Matrix components in the skin

The largest component of normal skin is the ECM, a structural support network that influences a wide number cellular processes including migration, differentiation and wound healing [24]. The ECM can be divided into the cell-adjacent basement membrane (BM) and the interstitial matrix (**Figure 2. 3**). The epidermal BM is a thin layer of ECM containing multiple specialized structures that firmly anchor the epidermis to the interstitial matrix. The interstitial matrix presents the ECM surrounding cells and forms a 3D porous lattice. As mentioned previously, it can be subdivided into the upper papillary matrix with thinner loosely arranged fibrils and into the reticular matrix, which contains thicker, denser and irregular ECM fibril networks. The looser and softer papillary matrix serves as a deformable adhesive joining between the stiffer BM and the deeper reticular ECM [18]. Most of the mechanical toughness of the dermis is provided by the reticular ECM. Dermal fibroblasts are the main synthesizers of the dermal interstitial matrix, and both epidermal keratinocytes and dermal fibroblasts produce the epidermal BM. Some proteins in the BM such as laminin-332 are purely epidermal products, while other

such as nidogen 1 and 2 are solely produced by fibroblasts. A third group of molecules, such as perlecan and collagen VII, are contributed by both cell types [25].

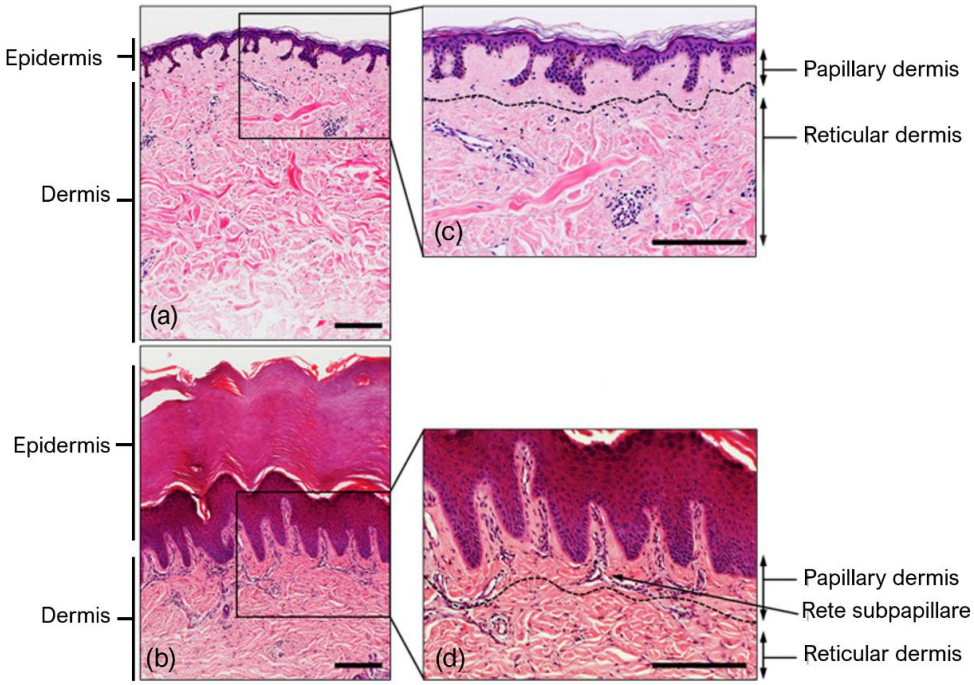

Figure 2. 2. Histological analyses of adult human skin. Human skin consists of two main layers: the epidermis and the dermis**.** The epidermis forms specific folds called rete ridges. Depending on the region of the body, the epidermis and its cornified layer various in thickness. For instance, the skin on the back is thin (a), while the skin on the palms is made of thick epidermis and thick *stratum corneum* (b). The dermis can be divided into papillary and reticular layers (c and d), separates by a vascular network termed the *rete subpapillare* (d). A dashed line in the images represents the interface between the two dermal compartments. The papillary dermis contains higher density of cells and fine collagen bundles compared to reticular dermis that is less cellular and is composed of thick and organized collagen bundles. Scale bar: 200 μm. Adapted from [23].

The ECM is constructed from multiple matrix proteins that form its main components and provide the necessary support to cells and tissues. It is composed of fibre-forming structural molecules, nonfibre-forming structural molecules, and matricellular proteins that do have a structure function but modify cell-matrix interactions [25]. Fibrous-forming molecules such as collagens, fibronectin, laminin and elastin create a 3D framework of rigid proteins, thereby providing structure to

the ECM. The nonfibre-forming molecules such as glycosaminoglycans (GAGS) and proteoglycans (PGs) have important roles in hydration, buffering and force dispersion within tissues. Fibroblasts produce the majority of these ECM components while these same molecules simultaneously act to modify the function of the fibroblasts [26].

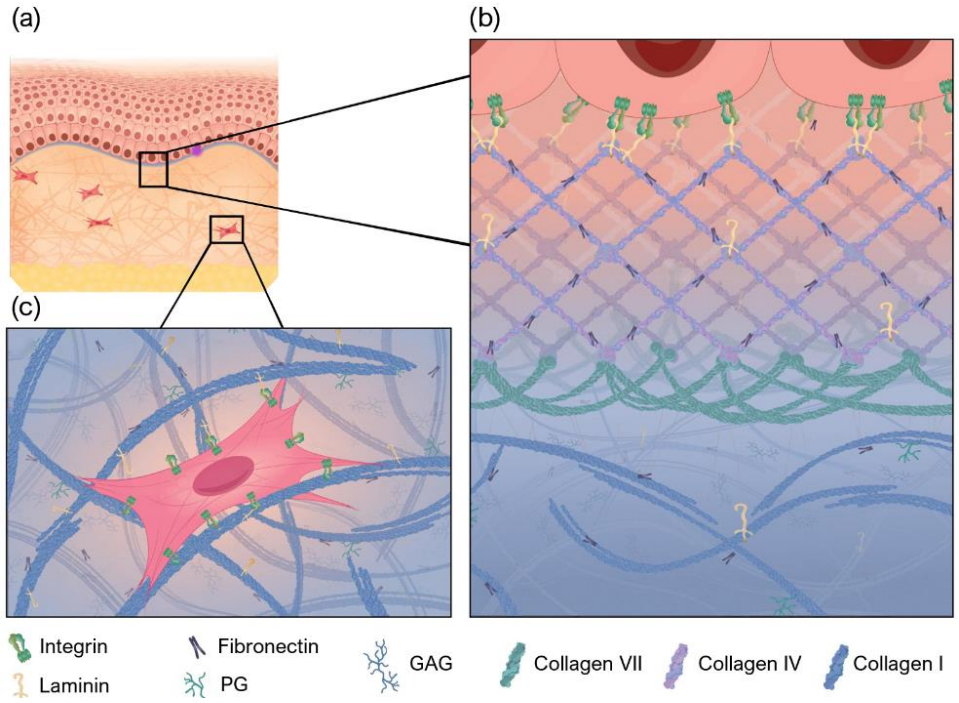

Figure 2. 3. ECM in healthy mammalian skin. (a) Skin is composed of the epidermis and dermis. The BM (purple) connects the epidermis to the dermis, which is comprised of interstitial matrix. (b) The dominant structural component in the BM is collagen type IV, laminin and fibronectin. Together they form a mesh in which the keratinocyte attachment via integrins. Collagen type VII reaches into the papillary dermis and stabilizes the dermal-epidermal junction. (c) In the dermis collagen type I and fibronectin build a fibrillary structure that allows cell adhesion and migration through the matrix. Shown is a fibroblast attaching to collagen and fibronectin via integrins. Adapted from [18]

In the skin, collagens are the largest class of fibre-forming/fibrous ECM molecules, comprising 77% of the fat-free dry weight of human skin, and provide most tensile strength of the skin [27]. The types and molecular organization vary greatly depending on the location within the skin. In the epidermal BM, a network of collagen IV provides strength and stiffness. It associates with other specialized

ECM molecules to form the BM, to which epidermal cells attach. The large collagen VII, assembles into dense anchoring fibrils that laterally span the epidermal BM and anchor it to the papillary matrix. In the dermal interstitial matrix, the major fibrils are heterotypic and contain collagen I, III and V. Collagen I is the most common type (80-85%), collagen III makes 8-11% the fibril content, and collagen V is the minor component. Collagen molecules become cross-linked to adjacent collagen molecule creating additional strength and stability of collagen fibres. Despite being mainly composed of these three collagens, dermal collagen fibrils vary greatly in their diameters depending on the location within the dermis.

Other fibre-forming proteins in the skin include fibronectin, elastin and fibrillin [28]. Fibronectin is a dimeric glycoprotein, abundantly present in the skin, mainly in the dermoepidermal junction area and in the papillary dermis. This glycoprotein is important in cell/cell and cell/fibre interactions and the ability to stimulate fibroblast growth, spreading, migration and contractility [29]. *In vitro* studies revealed that fibronectin is required for deposition of collagen I and other proteins into the ECM [30]. Fibroblasts and fibronectin share a complex dynamic relationship. The intracellular cytoskeleton of fibroblasts can influence the orientation of fibronectin fibrils whereas the fibronectin matrix can influence intracellular events, for example, cell alignment [25]. This glycoprotein plays a role in the phenomenon of fibroblast-mediated collagen gel contraction *in vivo* [31][32]. Furthermore, in wound healing, fibronectin plays a critical role in ECM organization and stability. Rubber-like elastin fibres contribute the resilience and elasticity in the skin. It has a role closely linked with collagen I, providing the dermis of the skin with the ability to recover from continuous stretching alongside with fibrillin [28]. Fibrillin microfibrils are fundamental structural components of the dermis. Together with elastic fibres they provide the skin with elasticity. Furthermore, they assist in anchoring the epidermal BM to the interstitial matrix by directly binding perlecan.

Glycoproteins such as laminins secrete molecules that comprise the BM, integrins that act as membrane-bound receptors and structural proteins that facilitate skin cell adhesion and migration [33]. They are made up of three different chains, α, β and γ which exist in various genetically distinct forms. They are involved on cell adhesion and play important roles in cell differentiation and

migration via their integrins. The major laminins in adult skin are laminin-332, laminin-311 and laminin-511, all contributed by keratinocytes.

The nonfibre-forming molecules, mostly GAGs and PGs are abundant components of the ECM in addition to collagen fibres. They are responsible for the creation of a charged, dynamic and osmotically active space. These nonfibre-forming proteins fill the majority of the tissue's interstitial space [34]. The GAGs include chondroitin sulphate, dermatan sulphate, keratan sulphate, heparan sulphate and hyaluronic acid. Their numerous chains containing negatively charged carboxyl and sulphate groups have important roles in maintaining water in the tissues. Hyaluronic acid is the simplest GAG and it forms PG aggregates. Their crosslinking to other matrix proteins results in the formation of structures that increase tissue stiffness [35]. Other abundant PGs are decorin, versican and dermatopontin, essential for skin architecture and function. They directly interact, either via GAG chains and/or their protein cores with ECM proteins to regulate tissue architecture.

Finally, also present in the ECM are matricellular proteins, a group of structurally unrelated proteins that interact with a wide range of cellular receptors and have the ability to use different domains to interact simultaneously with multiple proteins. Included among the matricellular proteins are osteopontin, secreted protein, acidic and rich in cysteine (SPARC), tenascin-C, fibulins, and the CCN family [36]. Matricellular proteins can be absent in healthy skin and expressed temporarily after skin wounding.

2.2.2 Skin barrier function

The *in vivo* skin barrier function is executed by different components: the microbiome, the *stratum corneum*, tight junctions (TJs), the chemical barrier and the immunological barrier (**Figure 2. 4**) [37]. For drug delivery and skin absorption applications, the mechanical barriers (*stratum corneum* and TJs) play the major role. The other barriers also influence and interact with carriers and ingredients and ideally should be taken into account.

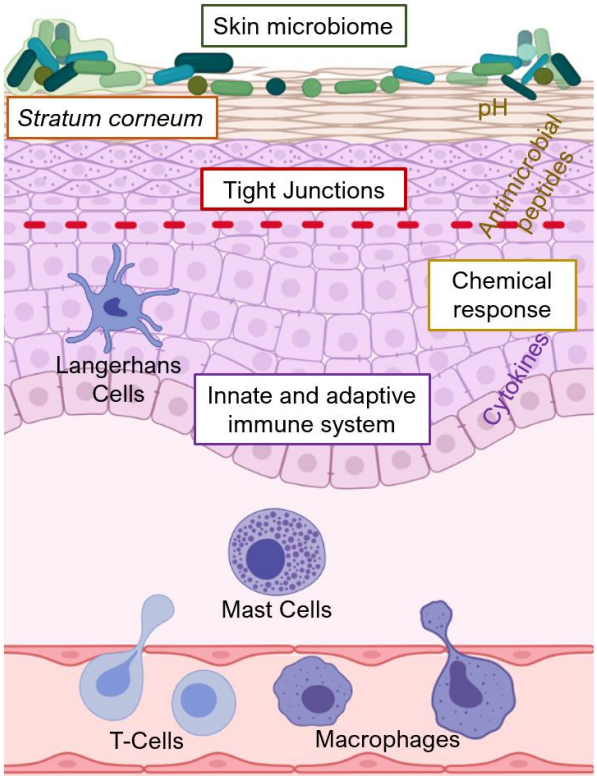

Figure 2. 4. Skin barrier function. Schematic representation denoting the different barriers in the human skin: Skin microbiome, stratum corneum, tight junctions, chemical barrier and immunological barrier, including the innate and adaptative immune system. Image created with software BioRender.

The *stratum corneum* is the foremost front providing a physical barrier of the skin against pathogens, irritants or UV radiation. It can be seen as a heterogenous arrangement analogous to "bricks and mortar" in which corneocytes are considered as hydrophilic "bricks" and the intercellular lipid matrix is considered the hydrophobic "mortar" (**Figure 2. 5**) [38]. Connecting the corneocytes are corneodesmosomes, similar to "iron rods" extending through the "bricks" which provide the *stratum corneum* tensile strength and the ability to resist shearing forces [39]. Corneodesmosomes are composed, among others, by desmoplakin, desmoglein 1, desmocollin 1 and corneodesmosin. In particular, corneodesmosin is delivered to the extracellular space by lamellar bodies at the granular cell layer and is then integrated into desmosomes, which are transformed by corneodesmosomes [40].

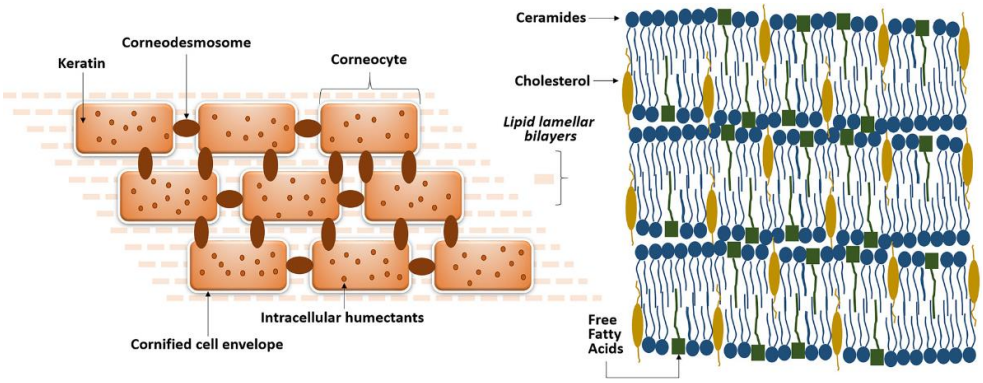

Figure 2. 5. Structure of the stratum corneum, representing the "brick and mortar" model. The image depicts layers of brick-like corneocytes, held together by corneodesmosomes (rivets), embedded in a hydrophobic extracellular lipid matrix (mortar). Corneocytes are composed of keratin and intracellular humectants. The "mortar" lipids are secreted into the intercellular space from the lamellar body secretory system of the granular layer as an intercellular lipid membrane bilayer consisting of three class of lipids: ceramides, cholesterol and free fatty acids. Adapted from [50]

The intercellular space of the *stratum corneum* is filled with densely packed lipid layers, so called lamellae matrix, which aids to prevent access of water-soluble materials and the loss of internal water. The lipid content consists of ceramides, cholesterol, and free fatty acid [41]. The different types of lipids, along their bilayer arrangement and hydrophobicity, all play important roles in the barrier function of the skin. The importance of the *stratum corneum* for the skin barrier function has been shown for decades in many reports [42]. The importance of lipids for skin barrier function can be seen by the impact of its removal using, for example, acetone, which increased trasnepidermal water loss (TEWL) [43]. Furthermore, abnormal lipid organization results in impaired epidermal barrier function. The removal of this layer, e.g., by tape stripping, results in impaired skin barrier function, show by the increased TEWL and enhanced uptake of externally applied substances [46, 47]. Removal of the *stratum corneum* by tape stripping or laser abrasion is also a method to enhance drug delivery [46], [47]. Various distinct components of the *stratum corneum* such as filaggrin, CE-proteins and corneodesmosin have been shown to be involved in skin barrier function. Filaggrin mutations have been related to defective barrier function in patients with ichthyosis vulgaris and atopic eczema [48][49].

The viable epidermis also contributes to the skin physical barrier by adherens junctions, tight junctions (TJs) and desmosomes. Adherens junctions and desmosomes are not directly linked to skin barrier function but are important for keratinocyte adhesion and differentiation that is needed for epidermal integrity. TJs are cell-cell junctions that are present in simple and multi-layered epithelia as well as in endothelia. These proteins seal the paracellular pathway to restrict the movement of molecules within the intercellular space. They consist of transmembrane proteins of the claudin family, TJ-associated marvel proteins (e.g., occluding) and junctional adhesion molecules (JAMS) as well as TJ plaque proteins (e.g., zonula occludens proteins 1-3, MUPP-1 and cingulin). They are connected with the actin filament cytoskeleton. TJs are crucial for skin barrier function as they are directly involved in the inside-out barrier function [51], [52]. TJs are formed in the granular cell layer by several TJ proteins that are all expressed at specific layers of the epidermis, indicating the complexity of the skin barrier function [53]. They are involved in differentiation, proliferation, cell polarity and signal transduction processes of cells [54][55][56].

The chemical barrier is mainly composed of antimicrobial peptides (AMPs). These peptides are mainly produced by keratinocytes and immune cells and are involved in protection, inflammation and wound healing processes in the skin [57]. Different AMPs are permanently present in healthy skin with their expression further induced in case of infection or injury. They are effective against a wide range of microbes including bacteria, fungi and viruses [58], [59].

The immunological barrier in the epidermis consists of components originating from the cellular such as Langerhans and dermal dendritic cells, mast cells, basophils, T cells as well as the humoral immune system such as cytokines. The immunological barrier may also play a relevant role in drug delivery. It has been hypothesized that drug delivery systems may influence the immune cells residing in the skin resulting in an impact on other barrier components [13].

Finally, the native skin is colonized with diverse types of microorganisms, termed microbiome. These microorganisms produce bactericidal compounds and inhibit the growth of pathogenic microorganisms. Furthermore, they prime the adaptive immune system, thereby enhancing the host innate immunity [53].

2.3 Skin mimetic models

The importance of the skin barrier for basic research and to study the effect of drugs and cosmetics pressured the development of models that could mimic the function of human skin. During the years, multiple strategies have been used to produce models with different levels of complexity, using both non-biological and biological components. In general, the different models can be divided in *ex vivo*, artificial and reconstructed skin models. The different approaches result in models with different details of information and resemblance to the *in vivo* human skin. The technical and economic efforts also greatly vary between them

2.3.1 *Ex vivo* skin models

The most commonly used models for preclinical research of new topical drug formulations are *ex vivo* skin models, obtained from humans or animals [60].

Regarding animal *ex vivo* models, various models have been used including pig, primates, mice, rats, guinea pigs, rabbits, bovines (udder), and snakes (shed skin) [9]. The different *ex vivo* animal models differ in the number of epidermal layers, thickness of the *stratum corneum*, lipid profile, and overall morphology. In particular, rat skin is commonly used for permeation studies, due to its high availability, small size and relative low costs. However, studies point to the existence of several limitations in the rat skin model including its higher permeability compared to human skin. Alternatively, pig skin models present more biological similarities with the human skin such as the thickness of the layer, similarity in hair follicle and blood vessel density, content of ceramides, dermal collagen, and elastin.

The use of *in vivo* skin is not always possible due to ethical concerns, regulatory issues and laboratory facilities. Alternatively, *ex vivo* human samples can offer a physiological construct with lesser limitations. Human skin samples used for *ex vivo* permeation assays can be obtained from plastic surgery, amputations or cadavers and are collected from different sites. Full-thickness skin models obtained from excisions containing connective tissue, subcutaneous fat and all skin layers have been reported. *Ex vivo* skins can be prepared in various thicknesses using a dermatome. It is available as epidermis and a portion of dermis or full-thickness skin

samples containing epidermis and dermis (depending on anatomical location up to 1–2 mm). However, *ex vivo* skin models have limited availability and the results obtained with them present significant variability due to donor variation, including age differences, which result in unpredictable features as well as tissues being obtained from different anatomical sites [61]. Furthermore, variations in the sample thickness influence the drug penetration to the receptor compartment.

These observations reinforce the need for reproducible alternative skin models, capable of mimicking healthy and diseased human skin for multiple applications.

2.3.2 Artificial *in vitro* skin models

Currently, the most common methods used to test topical applied drugs rely on animal models. However, as discussed previously, these models suffer from multiple disadvantages including intra- and inter-individual variations. In the last several years attempts have been made to develop reliable high throughput alternatives such as artificial *in vitro* models that could substitute human or animal skin samples [62]. Artificial membranes could offer a simple reproducible alternative to study basic physiochemical mechanisms of drug permeation, ideal as an initial screening approach to narrow the selection of drug formulations. Most artificial models focus on mimicking healthy skin with intact barrier properties. These artificial models have several benefits including low variability, good storage conditions and low costs. In addition, they lack any type of ethical concerns contrary to human or animal tissues. Typically, these artificial membranes are chemically inert, contain pores and have high compatibility with solvents. Different approaches have been applied including, non-lipid-based models such as silicone membranes and lipid models.

Depending of the specific applications, silicon-based membranes, cellulose acetate or cellulose nitrate filters are available for use in the Franz diffusion cell method. The majority of the literature describes the use of silicon-based membrane such as poly(dimethylsiloxane) (PDMS), Silastic and Silatos. Silicone based membranes have been used for decades for evaluating drug transport across human skin. The *in vitro* release pattern from various lipophilic compounds was found to

be in agreement with the *in vivo* data reported in the literature. However, it has been suggested that these membranes are not appropriate for permeation tests using hydrophilic compounds [61]. Taking this int account, an improved model was developed combining PDMS and polyethylene glycol (PEG) 6000 [63]. Although preliminary tests have been performed using this model using aqueous solutions, its potential still has to be elucidated. Alternatively, the traditional cellulose-acetate membranes are also frequently used, mainly in the first phase of the diffusion studies. The first parallel artificial membrane permeability assay (PAMPA) model for assessing skin penetration incorporated silicone oil and isopropyl myristate as membrane components [64]. This model was used to study the permeation of a large variety of molecules [65] [66]. Overall, these simple models are widely applicable and can be used to test basic diffusion mechanisms. However, they have limited quality of prediction, specially to study the permeability of hydrophilic compounds [63].

Lipid-based skin equivalents can improve the complexity of the model and its ability to mimic human skin [9]. The first report describing lipid-based models, used lipids present in the *stratum corneum* (ceramides, cholesterol, FFA and cholesteryl sulphate) in the preparation of the membranes [67]. Sinko et al. designed the skin PAMPA, which consisted of ceramide analogues (certramides) [68]. Several other groups reported the use of PAMPA models to investigate drug permeability of skin [69] [70].

A different type of skin mimetic model, Strat-M® is a recent development in the field of synthetic membranes (**Figure 2. 6**). It mimics the multi-layered architecture of the skin by including multiple layers of different materials, such as porous polyether sulfone and polyolefin, enclosed by a combination of lipids and other components, forming a 3D structure. These multiple layers create a morphology similar to human skin, including a very tight surface layer. Strat-M was used to evaluate the permeation efficiency of hydrophilic molecules [72]. This model lacks the capacity to mimic the complex architecture of the *in vivo* human skin. However, by including a composition that resembles the *stratum corneum* layer it presents a valuable alternative to current methods. The results obtained using Strat-M® are highly reproducible due to the simple nature and standardized construction of this model [73]. However, these artificial models do not fully recreate the

heterogeneous nature of the skin and lack cell metabolism which limits its applicability.

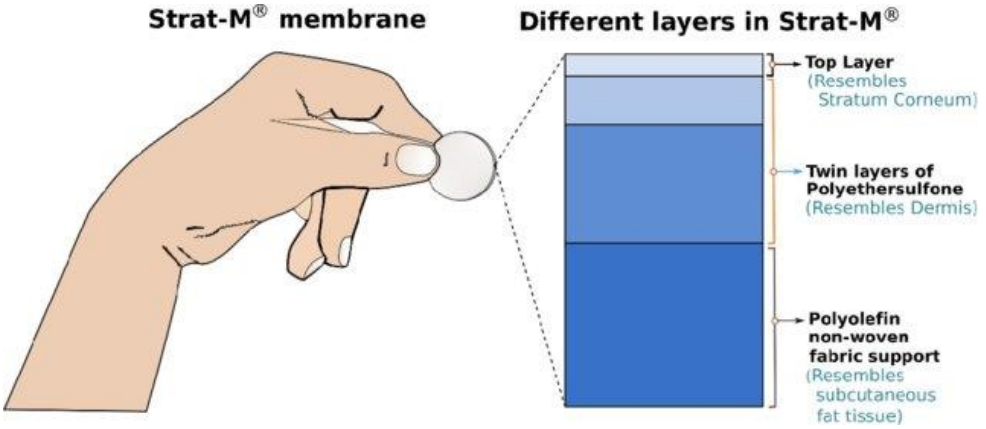

Figure 2. 6. Artificial skin model, Strat-M® and the representation of the different layers resembling the compartments of the native skin. Adapted from [71].

2.3.3 Reconstructed Skin models

2.3.3.1 From 2D to 3D models

Currently, most pathophysiological studies are conducted in two-dimensional (2D) cell culture in which cells are grown as a monolayer on solid flat surfaces such as polycarbonate or glass (**Figure 2. 7.a**). In these cultures, medium containing nutrients and stimulating factors is added to the plates, flasks or Petri dishes to bathe the cells. Cells consume these nutrients and in turn produce metabolic wastes, making it necessary to change the culture medium regularly. Cells proliferate and gradually cover the surface, reaching a stage where they need to be passaged. In this process, cells are harvested and reseeded into multiple cell culture flasks. The simplicity, low cost, high speed of testing and the possibility of high-throughput screening have made 2D cell culture a key component of drug discovery programs. Although these 2D cell culture systems have proven to be a valuable method to quickly identify toxic compounds and further our understanding in molecular signalling and cellular morphology, their limitations have become increasingly recognised [7].

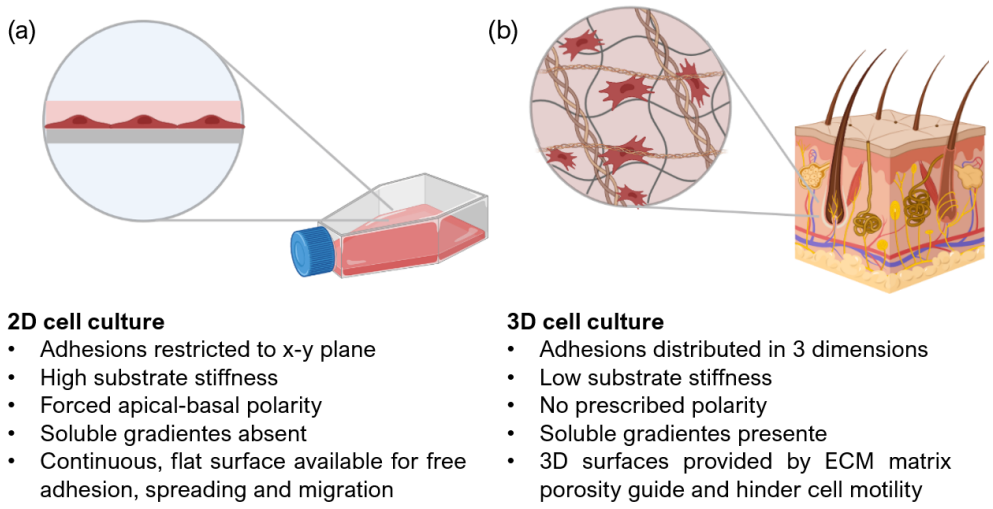

Figure 2. 7. 2D vs. 3D cell culture: (a) Cell behaviour in 2D conventional cell culture. Cells cultured in a 2D manner tend to have a flat shape that does not represent the real physiological cell morphology. (b) Cell behaviour in 3D cell culture. Cells cultured in a 3D system are present in a microenvironment similar to that in vivo, therefore they have a more representative morphology and physiology. Image created with software BioRender.

Currently, it is well known that not all results and conclusions from these 2D cell culture systems are translatable to physiological *in vivo* systems. 2D monolayers lack native tissue complexity, partly due to the altered differentiation status of the cells used in 2D culture as well as due to the culture conditions in which unnatural geometric and mechanical constraints are imposed on cells. Bhadriraju *et al* showed that cells cultured in 2D formats undergo proliferation and de-differentiation and consequently lose their functions [74]. Cells cultured in a three-dimensional (3D) geometry show evident difference in proliferation, differentiation, morphology and functions [75]. Beningo *et al* showed that fibroblasts cultured in 2D have a flat shape, different from the bipolar shape found in tissues [76]. The culture in fibroblasts in a 3D collagen matrix showed a more typical *in vivo* phenotype [77]. Additionally, 2D monolayers lack important factors associated with the 3D *in vivo* environment such as spatial orientation, cell-ECM interactions, physiological oxygen, nutrient and signalling gradients. Consequently, 2D cell culture models are unreliable predictors of *in vivo* drug efficacy and toxicity, giving unsatisfactorily misleading and non-predictive data for *in vivo* responses. The limitations of the 2D

cell cultures contribute to the relative high drug failure rate during preclinical testing.

Multiple studies have shown that the culture of skin cells in 3D results in a more physiologically relevant morphology of both fibroblasts and keratinocytes (including differentiation) compared with cells cultured as monolayers in 2D cultures [78]. *In situ* environment of a cell in a living organism is that almost all the cells are surrounded by other cells and ECM (**Figure 2. 7.b**). It has been shown that 3D ECM containing receptors a matrix stiffness can promote normal epithelial polarity and differentiation. Moreover, 3D culture provide not only the templates for cells to adhere and grow, but also the interconnectivity within 3D constructs to allow nutrients and metabolites to be transported in and out the tissue model. Consequently, 3D cell cultures can support a much larger number of cells than 2D cell cultures. As a result, physiological 3D skin models are required to provide a better platform for predicting clinical outcomes for drug testing.

2.3.3.2 Reconstructed human epidermis

Although 2D cell culture is simple and reproducible, the increased relevance of 3D constructs pressured the development of 3D skin models for a variety of applications. Reconstructed human epidermis models (RHEm) are the simplest form of 3D organotypic skin constructs that include an epidermal barrier. Human keratinocytes can be isolated from skin biopsied and serially propagated *in vitro* [79]. These cells can be used to produce RHEm by seeding them onto a porous membrane, on transwell-like inserts. After a period of submerged culture, the RHEm is exposed to the air from above with the culture medium below. This method of culture stimulates keratinocyte differentiation in which basal keratinocytes migrate upwards to form a stratified epidermal structure ad matured into cornified cells (corneocytes at the *stratum corneum*). For most of these models, stratified epithelium is created in approximately 11 to 14 days at the air-liquid interface.

This method has been used to produce multiple commercial RHEms. In particular, EpiSkin®, EpiDerm®, SkinEthic® and EpiCs® RHEms have already been validated for skin irritation and skin corrosion testing according to OECD test guidelines 439 and 432, respectively [80]. Typically, RHEm are easily and reproducibly implemented, making them compatible with high-throughput

permeability screening of drugs and cosmetics. By including the *stratum corneum*, these models enable hydrophobic components to be tested using relevant vehicles used in in vivo studies. In addition, they release keratinocyte-derived inflammatory cytokines, useful for a more detailed study of skin irritation and sensitization. However, RHEms present multiple limitations due to the presence of keratinocytes alone and the lack of key interactions with dermal cells. This limits their applicability since the cross talk between keratinocytes and fibroblasts drives the inflammatory cytokine response in skin models lacking immune cells. Permeability tests demonstrated that permeability coefficients differ and exceed from the values resulted from tests on human skin. Moreover, the statistical data has shown that the RHEm reproducibility is not convincing compared to the excised skin [81].

2.3.3.3 Full-thickness human skin models (FTSm)

To surpass the limitations of RHEms, more complex FTSm including both the dermal and epidermal components have been developed. Pioneering work in this field involved seeding keratinocytes on decellularized pig skin or human de-epidermised dermis. More recently, the development of multiple technologies expanded the possibility to develop biomimetic FTSm. Currently, two main types of engineered 3D tissue models exist: (1) Scaffold-free and (2) Scaffold-based.

2.3.3.3.1 Scaffold-free FTSm

Scaffold-free FTSm are based on the use of spheroids, non-adherent cell aggregates produced by the self-assembly of cells. These 3D cellular aggregates that can represent the microenvironment of cells more accurately when compared with 2D cell cultures, replicating many organ features including deposition of ECM, cell-cell interactions and formation of nutrient, waste and gas gradients [82]. The most common method of spheroid culture is the hanging drop method, in which droplets having high density of cells are cultured in inverted cell culture plates under physiological conditions until they form 3D spheroids. In this method, cells are in direct contact with each other and the ECM components. This method has some advantages including low costs, increased reproducibility and compatibility with high throughput analysis. Ströbel *et al* described the production of spherical skin microtissues with different keratinocyte layers and a dermal fibroblasts core producing ECM [83]. However, using this technique, the model is fully immersed in

media and does not recapitulate the air-liquid interface of physiological skin. *An in-vivo* like skin should be able to replicate the interface with a gaseous environment, important for the formation of a biomimetic skin barrier. In general, the use of spheroid culture is uncommon in skin research with very few studies reporting culturing keratinocyte and fibroblast cell lines as spheroids. A study showed generation of spheroids by co-culturing three types of cells on a low attachment surface; type IV collagen-rich fibroblast formed the core, surrounded by a ring of keratinocytes with melanoma cells on the outside [84]. However, it was not possible to observe a complete differentiation of keratinocytes for the formation of the stratified epithelium. Spheroids have been used to study skin cancer by the integration of melanoma cancer spheroids placed into skin equivalents [85]. Bioprinting offers the possibility to standardize the deposition of micro-tissues by the exact positioning of spheroids in the raised skin models [86].

2.3.3.3.2 Scaffold-based FTSm

The most conventional approach to generate FTSm is based on the use of scaffolds, structures that support cell growth in a new dimension, escaping the geometrical limitations of 2D cultures. These scaffolds can be comprised of natural and/or synthetic polymers. Unlike scaffold-free approaches, this method allows formation of a FTSm that is structurally, mechanically and functionally similar to the biological tissue [12].

FTSms developed using hydrogels are the most common approach. These are loose scaffolds consisting of natural or synthetic materials, modelling soft tissue due to their tissue-like flexibility and viscoelasticity. The gels can have a porous architecture, allowing mass transfer of drugs, nutrients and oxygen to the cells in a 3D environment. These materials can be derived from multiple sources and tailored for specific application. Natural hydrogels such as collagen, fibronectin, elastin, fibrin, silk, alginate, chitosan, fibrin, or GAGs typically present good differentiation and stratification [87]. These materials are typically non-cytotoxic and provide good support for the epidermal layer. For example, Matrigel® is a popular commercial hydrogel containing collagen IV, laminin, enactin and other undefined constituents that can promote cellular functions by providing the necessary endogenous factors.

Most commonly, collagen (usually type I) is used as a natural polymer to recreate the dermal compartment in bioengineered skin. The collagen hydrogels are typically chosen due to their abundance in the *in vivo* dermal ECM, making it a physiologically relevant matrix component, and presents tissue-like mechanical properties such as viscoelasticity, turgidity and flexibility. However, hydrogels present multiple disadvantages, including their often animal-derived origin such as bovine or rat-tail tendon, weak mechanical stability and batch-to-batch variability [87]. The use of animal-derived materials may introduce interspecies effects, and the presence of only one extracellular matrix component is unable to successfully represent the complex dermal architecture [88]. The weak mechanical stability is due to the very high-water content and the susceptibility of the hydrogels to physical contraction when integrated fibroblasts exert forces on the matrix, a phenomenon known as fibroblast-mediated contraction. The hydrogel contraction during experiment leads to inconsistencies and variability. Furthermore, these hydrogels are prone to enzymatic degradation by action of collagenases (MMP2, MMP9) and gelatinases, limiting their applicability when long-term culture is required [89].

To reduce these limitations, techniques have been developed to improve the mechanical stability of natural scaffolds. For example, cross-linking techniques using multiple components such as glutaraldehyde, GAGs or fibrin to add mechanical strength to the natural hydrogels. Vidal *et al* used a hydrogel produced from cross-linked silk and collagen to recreate the dermal compartment which provided a more resistant structure compared to conventional collagen hydrogels [90]. The use of innovative techniques such as electrospinning and bioprinting can also help solving the problems related to hydrogel contraction. Torres *et al* described electrospinning of elastin-like materials that do not require addition of cytotoxic cross-linkers, while allowing for the incorporation of multiple functionalities to support cell adhesion and proliferation [91]. For bioprinting applications, Shi *et a*l increased the mechanical stability of the used bioink by mixing gelatin-methacryloyl (GelMA) with collagen I and the enzyme tyrosinase [92].

An alternative to hydrogels is the use of solid scaffolds in cell culture. There are multiple potential materials that can be used for the fabrication of solid scaffolds, including naturally derived materials such as collagen, fibrin, silk and gelatine [87]. These materials benefit from being biocompatible and from possessing readily

available adhesion sites, thereby increasing the tissue complexity. Decellularized scaffolds are an example of a natural matrix in which tissues undergo physical, chemical or enzymatic treatment to remove the cellular antigens while preserving the ECM. These scaffolds are typically biodegradable which makes them suitable for transplantation applications. Biodegradable scaffolds enable the creation of 3D cellular structures which can be incorporated into *in vivo* tissues and be replaced by healthy native tissue. However, in the context of *in vitro* cell culture, biodegradable scaffolds present multiple shortcomings including short shelf-life and low reproducibility. Furthermore, scaffold degradation can lead to loss of mechanical properties and the local release of toxic by-products. For the production of reproducible 3D environment, the development of scaffolds should take into account variables such as shelf-life, storage and quality control.

Alternatively, synthetic scaffolds with defined composition have been developed. For this, inert and non-degradable materials such as polymers, titanium and ceramic-based platforms can be used to create scaffold suited for cell culture [93]. Depending on the used methodology, two types of scaffolds can be obtained: fibrous and porous. Fibrous scaffolds are typically developed using electrospinning, a highly flexible technique by which polymer jets are passed through an electric field. The electrospun fibres are used to form complex interlaced structured in which cell positioning can be regulated [94]. Porous scaffolds include a controllable 3D space where cells can enter and grow, forming contacts and interacts with adjacent cells. The dimensions of the voids can be tailored to optimize cell seeding as well as conditioning cell behaviour and growth in the scaffold [95]. Voids are interconnected by small pores, which prevent cells from being isolated within the 3D microenvironment and also contribute to greater cell infiltration.

The pore formation in the scaffold can be achieved using multiple techniques including particulate leaching, emulsion templating and gas foaming. In particulate leaching, a polymer is cast around soluble beads known as porogens such as sugar, salt and paraffin wax. This method results in limited connectivity between pores, which may affect the culture. Gas foaming technology can generate large internal volume and 3D spaces by agitating polymers to create foam. The regulation of agitation and the use of high-pressure gases facilitates control of the porosity of the scaffold. However, this method also results in low pore interconnectivity.

Emulsion templating is an alternative procedure to generate increased interconnectivity, incorporating polymerisation by high internal phase emulsion (HIPE) [96]. Alvetex® scaffold is a synthetic and inert polystyrene scaffold using the technique of emulsion templating to produce a homogeneous network of 30-40 μm pores, linked by interconnects with approximately 13 μm (**Figure 2. 8**) [87]. These commercial scaffolds present a high porosity (90%) which provide a physical space for fibroblasts to infiltrate and retain their 3D geometry and secrete a dynamic network of endogenous ECM. Alvetex® is engineered as a membrane with thickness of 200 μm. This thin scaffold enables mass transfer of gases, nutrients and waste to maintain cellular viability. An increased thickness would result in poor mass transfer since the conventional cell culture are based on static systems. **Figure 2. 9** illustrates the limited mass transfer in a porous scaffold using static cell culture system compared with a dynamic 3D culture.

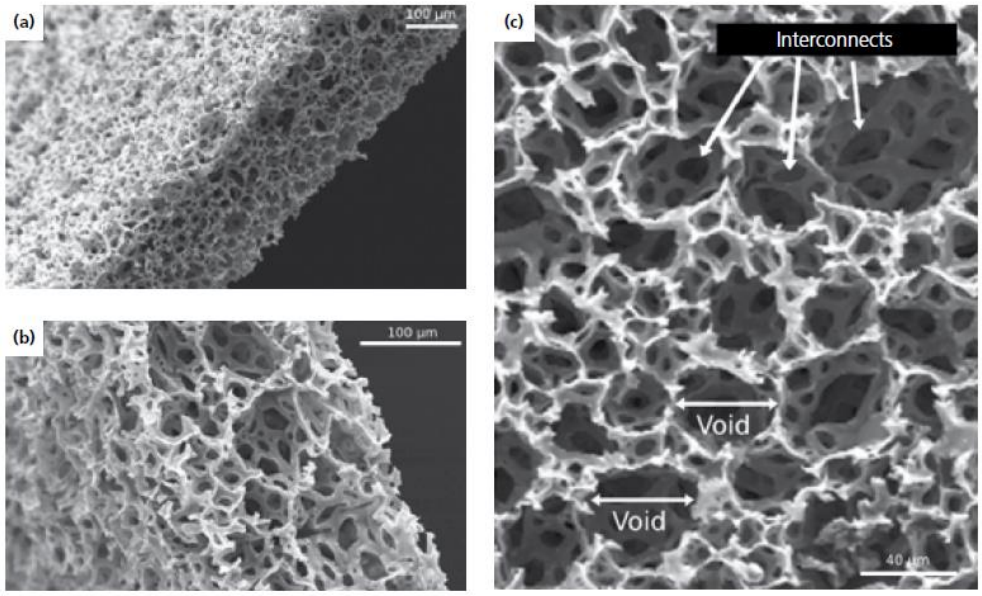

Figure 2. 8. Alvetex viewed by scanning electron microscope, showing its porous structure. (a) A 200 μm thick polystyrene scaffold. (b) Alvetex porosity of > 90% (c) Close-up voids with dimensions of approximately 36 – 40 μm in diameter and interconnects of approximately 12-14 μm in diameter. Adapted from [87].

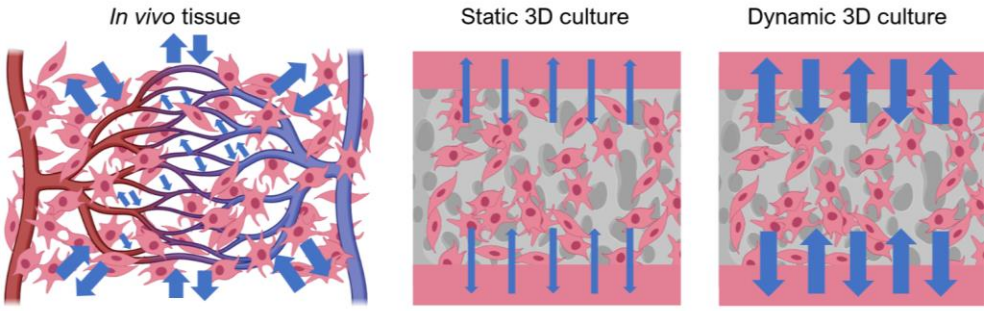

Figure 2. 9. Perfusion model. Unlike real tissue, 3D cell culture models lack a vascular and capillary bed. Exchange of gases, nutrients and waste products occurs by diffusion, most often in a static culture where unstirred layers can build up in stagnant media. Dynamic 3D culture involves perfusion and movement of the media to reduce unstirred layers and increase exchange. Image created with software BioRender.

2.3.4 Skin models with additional cell types

There is a growing interest in building biomimetic skin models integrating not only the dermal and epidermal compartment but also pigmentation, appendages, immunity, innervation, adipose tissue and vascularization [97]. These complex models present multiple challenges including optimization of co-culture conditions and availability of specific cell types.

Melanocytes cells were the first additional cell type to be integrated into the FTSm containing fibroblasts and keratinocytes to reproduce *in vivo* pigmentation [98]. *In vivo*, human skin pigmentation consists of epidermal melanin and relies upon the production of melanin pigment by melanocytes followed by the transfer of melanin from melanocytes to keratinocytes through dendrites. Melanin provides photoprotection against UV radiation and determines the colour of the skin and hair. Various models were able to replicate these mechanisms *in vitro*. A recent developed model generated pigmented skin models using induced pluripotent stem cells (iPSC)-derived melanocytes showed the capability of these cells to transfer their melanin into keratinocytes [99]. This holds potential for high-throughput drug screening studies related to drug-induced skin pigmentation. Pigmented models could also be used to study complex diseases such as vitiligo and some post-inflammatory conditions that result in skin discoloration.

Langerhans cells were further incorporated into the skin models to study the immunological responses [19]. These models have been used to recapitulate responses of these cells to UV radiation and several known allergens [100]. Furthermore, it was shown that Langerhans cells derived from the MUTZ-3 progenitor cell line migrated through the basal membrane to the dermal compartment following exposure to various known irritants [101]. This study demonstrated the immunocompetency of the developed skin models, making it useful for future hazard identification, test allergenics and evaluation of inflammatory responses against therapeutic candidates.

Multiple skin constructs also include the hypodermal laver [102]. In the native skin, the hypodermis is located beneath the dermis and it is attached via collagen and elastin fibres. This layer mainly consists of subcutaneous adipocytes and functions mainly as an energy reserve and heat insulator. However, it also produces many hormones and it has multiple blood and lymphatic vessels traversing in the region. In addition, adipose-derived stem cells have gained attention due to their implication in repair of multiple organs. The inclusion of this layer into the skin models could represent and improved human skin mimetic for cosmetic and pharmaceutical development.

Skin appendages such as hair follicles, sebaceous and sweat glands are essential to maintain a healthy skin barrier [98]. At the moment, many challenges remain before a fully functional human skin model is generated that includes skin appendages. Some models have successfully generated hair follicles *in vivo* or have produced hair-like structures *in vitro*, but none could successfully integrate fully differentiated hair follicle in a skin construct in *vitro* nor to produce sweat glands. The lack of these structures is one of the biggest challenges of current *in vitro* skin models.

Finally, to develop long-lasting biomimetic skin substitute, vascularization has been studied by co-culturing endothelial cells within the dermal compartment and by stimulating capillary formation. Despite the success of these types of studies for promoting viability and functionality of the engineered skin, they do not allow studying systemic delivery of drugs due to lack of perfusion on the formed capillary structures *in vitro*. This capability has been enabled by innovative tissue engineering

strategies. Perfusion culture systems such as microfluidic culture systems and 3D bioreactors can be used to model dynamic biological processes and the in vivo forces. A detailed analysis of perfusion system for skin cultured will be made in Chapter 3.

2.4 Conclusion and Future directions

The human skin is the barrier between the body and the environment, protecting from external assaults. It consists of a wide variety of cell types forming a complex multi-layered and differentiated architecture that it is heterogeneous in nature. Currently, animal models are widely used in the basic research for understanding healthy and diseases state of human skin and in the preclinical phase for identifying the mode of action of drugs and cosmetics. However, animal models often poorly predict the human response due to differences in skin anatomy, physiology and immunity as well as involving ethical concerns. Reconstituting the skin tissue from different cellular building blocks while controlling size, shape, composition and spatial heterogeneity is a real demand in skin engineering and drug discovery.

In recent years, advanced skin tissue models have been developed combining innovative biomaterials and skin cells, offering alternatives to the animal model. From single layer to more complex skin models comprising all the *in vivo* layers, 3D constructs provide a stratified architecture that mimics the native environment. However, most available skin models are limited to specific cell types such as keratinocytes and fibroblasts derived from neonatal and adult skin. Furthermore, conventional skin models typically lack skin appendages and the vascular system. Despite the development of new fabrication techniques, the traditional method based on collagen gel dermal matrix incorporated with fibroblasts and keratinocytes still represents the gold standard in 3D artificial skin engineering.

New protocols will need to be published for incorporating complex co-cultures with additional cells such as melanocytes, Langerhans cells. iPSCs may address some of the current limitations due to their pluripotency and self-renewal

features. Further developments in *in vitro* skin substitutes should include addition of skin appendages. The integration of sweat glands or hair follicles will help to mimic a more realistic *in vivo* situation, offering a more correct experimental setup. The development of biomimetic materials recapitulating the *in vivo*-like ECM enhances the physiologically relevance of the developed tissues. Finally, the creation of vascular networks could be possible with the emergence of new technologies such as organ-on-a-chip technology and bioprinting. Building the next generation of skin constructs by including various skin components and patient-specific cells, while optimizing miniaturization methods, could revolutionize the early stages of drug development and offer advanced tools for modelling skin diseases.

2.5 References

[1] D. Seth, K. Cheldize, D. Brown, and E. F. Freeman, "Global Burden of Skin Disease: Inequities and Innovations," *Curr. Dermatol. Rep.*, vol. 6, no. 3, pp. 204–210, Sep. 2017.

[2] S. Chu, S. Mehrmal, P. Uppal, R. L. Giesey, M. E. Delost, and G. R. Delost, "Burden of skin disease and associated socioeconomic status in Europe: An ecologic study from the Global Burden of Disease Study 2017," *JAAD Int.*, vol. 1, no. 2, pp. 95–103, Jul. 2020.

[3] M. Johansson, J. Brodersen, P. C. Gøtzsche, and K. J. Jørgensen, "Screening for reducing morbidity and mortality in malignant melanoma," *Cochrane database Syst. Rev.*, vol. 6, no. 6, pp. CD012352–CD012352, Jun. 2019.

[4] J. A. DiMasi, H. G. Grabowski, and R. W. Hansen, "Innovation in the pharmaceutical industry: New estimates of R&D costs," *J. Health Econ.*, vol. 47, pp. 20–33, 2016.

[5] J. W. Scannell, A. Blanckley, H. Boldon, and B. Warrington, "Diagnosing the decline in pharmaceutical R&D efficiency," *Nat. Rev. Drug Discov.*, vol. 11, no. 3, pp. 191–200, 2012.

[6] E. Petrova, "Innovation in the Pharmaceutical Industry: The Process of Drug Discovery and Development BT - Innovation and Marketing in the Pharmaceutical Industry: Emerging Practices, Research, and Policies," M. Ding, J. Eliashberg, and S. Stremersch, Eds. New York, NY: Springer New York, pp. 19–81, 2014.

[7] R. Edmondson, J. J. Broglie, A. F. Adcock, and L. Yang, "Three-dimensional cell culture systems and their applications in drug discovery and cell-based biosensors," *Assay Drug Dev. Technol.*, vol. 12, no. 4, pp. 207–218, May 2014.

[8] Y. E. Yun, Y. J. Jung, Y. J. Choi, J. S. Choi, and Y. W. Cho, "Artificial skin models for animal-free testing," *J. Pharm. Investig.*, vol. 48, no. 2, pp. 215–223, 2018.

[9] T. Moniz, S. A. Costa Lima, and S. Reis, "Human skin models: From healthy to disease-mimetic systems; characteristics and applications," *Br. J. Pharmacol.*, vol. 177, no. 19, pp. 4314–4329, Oct. 2020.

[10] I. A. S. Olsson, S. P. da Silva, D. Townend, and P. Sandøe, "Protecting Animals and Enabling Research in the European Union: An Overview of Development and Implementation of Directive 2010/63/EU," *ILAR J.*, vol. 57, no. 3, pp. 347–357, May 2016.

[11] E. Marafante and M. Balls, "The European Centre for the Validation of Alternative Methods (ECVAM)," *Alternatives to Animal Testing*. pp. 21–25, 24-Feb-1994.

[12] M. J. Randall, A. Jüngel, M. Rimann, and K. Wuertz-Kozak, "Advances in the biofabrication of 3D skin in vitro: Healthy and pathological models," *Front. Bioeng. Biotechnol.*, vol. 6, no. OCT, 2018.

[13] A. V Nguyen and A. M. Soulika, "The Dynamics of the Skin's Immune System," *Int. J. Mol. Sci.*, vol. 20, no. 8, p. 1811, Apr. 2019.

[14] Y. I. Wang and J. Sanders, "Skin model studies," *Press. Ulcer Res. Curr. Futur. Perspect.*, pp. 263–285, 2005.

[15] D. W. Scott and W. H. Miller, "CHAPTER 1 - Structure and Function of the Skin," D. W. Scott and W. H. B. T.-E. D. (Second E. Miller, Eds. Saint Louis: W.B. Saunders, pp. 1–34, 2011.

[16] J. A. McGrath and J. Uitto, "Anatomy and Organization of Human Skin," *Rook's Textbook of Dermatology*. pp. 1–53, 22-Mar-2010.

[17] R. L. Maynard and N. Downes, "Chapter 24 - The Skin or the Integument," R. L. Maynard and N. B. T.-A. and H. of the L. R. in T. and B. R. Downes, Eds. Academic Press, pp. 303–315, 2019.

[18] K. Pfisterer, L. E. Shaw, D. Symmank, and W. Weninger, "The Extracellular Matrix in Skin Inflammation and Infection ," *Frontiers in Cell and Developmental Biology* , vol. 9. p. 1578, 2021.

[19] K. Clayton, A. F. Vallejo, J. Davies, S. Sirvent, and M. E. Polak, "Langerhans Cells—Programmed by the Epidermis ," *Frontiers in Immunology* , vol. 8. p. 1676, 2017.

[20] G. K. Menon, G. W. Cleary, and M. E. Lane, "The structure and function of the stratum corneum," *Int. J. Pharm.*, vol. 435, no. 1, pp. 3–9, 2012.

[21] C. A. Brohem, L. B. da Silva Cardeal, M. Tiago, M. S. Soengas, S. B. de Moraes Barros, and S. S. Maria-Engler, "Artificial skin in perspective: concepts and applications," *Pigment Cell Melanoma Res.*, vol. 24, no. 1, pp. 35–50, Feb. 2011.

[22] S. Kusuma, R. K. Vuthoori, M. Piliang, and J. E. Zins, "Skin Anatomy and Physiology BT - Plastic and Reconstructive Surgery," M. Z. Siemionow and M. Eisenmann-Klein, Eds. London: Springer London, pp. 161–171, 2010.

[23] G. Sriram, P. L. Bigliardi, and M. Bigliardi-Qi, "Fibroblast heterogeneity and its implications for engineering organotypic skin models in vitro," *Eur. J. Cell Biol.*, vol. 94, no. 11, pp. 483–512, 2015.

[24] J. K. Kular, S. Basu, and R. I. Sharma, "The extracellular matrix: Structure, composition, age-related differences, tools for analysis and applications for tissue engineering," *J. Tissue Eng.*, vol. 5, pp. 2041731414557112–2041731414557112, Dec. 2014.

[25] L. E. Tracy, R. A. Minasian, and E. J. Caterson, "Extracellular Matrix and Dermal Fibroblast Function in the Healing Wound," *Adv. Wound Care*, vol. 5, no. 3, pp. 119–136, 2016.

[26] B. P., "Wound healing and the role of fibroblasts," *J. Wound Care*, vol. 22, no. 8, pp. 407–412, Aug. 2013.

[27] G. D. Weinstein and R. J. Boucek, "Collagen and Elastin of Human Dermis**From the Divisions of Dermatology and Cardiology of the Department of Medicine, University of Miami School of Medicine and Howard Hughes Medical Institute, Miami, Florida.This investigation was supported in part by Gr," *J. Invest. Dermatol.*, vol. 35, no. 4, pp. 227–229, 1960.

[28] C. Frantz, K. M. Stewart, and V. M. Weaver, "The extracellular matrix at a glance," *J. Cell Sci.*, vol. 123, no. Pt 24, pp. 4195–4200, Dec. 2010.

[29] C. D. Gildner, D. C. Roy, C. S. Farrar, and D. C. Hocking, "Opposing effects of collagen I and vitronectin on fibronectin fibril structure and function," *Matrix Biol.*, vol. 34, pp. 33–45, Feb. 2014.

[30] J. Sottile and D. C. Hocking, "Fibronectin polymerization regulates the composition and stability of extracellular matrix fibrils and cell-matrix adhesions," *Mol. Biol. Cell*, vol. 13, no. 10, pp. 3546–3559, Oct. 2002.

[31] K. K. Sethi, I. V Yannas, V. Mudera, M. Eastwood, C. McFarland, and R. A. Brown, "Evidence for sequential utilization of fibronectin, vitronectin, and collagen during fibroblast-mediated collagen contraction," *Wound Repair Regen.*, vol. 10, no. 6, pp. 397–408, Nov. 2002.

[32] M. Obara and K. Yoshizato, "A novel domain of fibronectin revealed by epitope mapping of a monoclonal antibody which inhibits fibroblasts-mediated collagen gel contraction," *FEBS Lett.*, vol. 412, no. 1, pp. 48–52, Jul. 1997.

[33] J. R. Stanley, D. T. Woodley, S. I. Katz, and G. R. Martin, "Structure and Function of Basement Membrane," *J. Invest. Dermatol.*, vol. 79, no. 1, Supplement, pp. 69–72, 1982.

[34] H. Järveläinen, A. Sainio, M. Koulu, T. N. Wight, and R. Penttinen, "Extracellular matrix molecules: potential targets in pharmacotherapy," *Pharmacol. Rev.*, vol. 61, no. 2, pp. 198–223, Jun. 2009.

[35] D. H. Lee, J.-H. Oh, and J. H. Chung, "Glycosaminoglycan and proteoglycan in skin aging," *J. Dermatol. Sci.*, vol. 83, no. 3, pp. 174–181, Sep. 2016.

[36] P. Bornstein and E. H. Sage, "Matricellular proteins: extracellular modulators of cell function," *Curr. Opin. Cell Biol.*, vol. 14, no. 5, pp. 608–616, 2002.

[37] H. Niehues, J. A. Bouwstra, A. El Ghalbzouri, J. M. Brandner, P. L. J. M. Zeeuwen, and E. H. van den Bogaard, "3D skin models for 3R research: The potential of 3D reconstructed skin models to study skin barrier function," *Exp. Dermatol.*, vol. 27, no. 5, pp. 501–511, 2018.

[38] P. M. Elias, "Skin barrier function," *Curr. Allergy Asthma Rep.*, vol. 8, no. 4, pp. 299–305, 2008.

[39] M. J. Cork *et al.*, "New perspectives on epidermal barrier dysfunction in atopic dermatitis: Gene–environment interactions," *J. Allergy Clin. Immunol.*, vol. 118, no. 1, pp. 3–21, Jul. 2006.

[40] N. JONCA, E. A. LECLERC, C. CAUBET, M. SIMON, M. GUERRIN, and G. SERRE, "Corneodesmosomes and corneodesmosin: from the s *tratum corneum* cohesion to the pathophysiology of genodermatoses," *Eur. J. Dermatology*, vol. 21, no. 2, pp. 35–42, May 2011.

[41] L. Norlén, B. Forslind, I. Nicander, B. L. Rozell, and S. Ollmar, "Inter- and Intra-Individual Differences in Human Stratum Corneum Lipid Content Related to Physical Parameters of Skin Barrier Function In Vivo," *J. Invest. Dermatol.*, vol. 112, no. 1, pp. 72–77, Jan. 1999.

[42] C. Gorzelanny, C. Mess, S. W. Schneider, V. Huck, and J. M. Brandner, "Skin barriers in dermal drug delivery: Which barriers have to be overcome and how can we measure them?," *Pharmaceutics*, vol. 12, no. 7, pp. 1–31, 2020.

[43] G. Grubauer, P. M. Elias, and K. R. Feingold, "Transepidermal water loss: the signal for recovery of barrier structure and function.," *J. Lipid Res.*, vol. 30, no. 3, pp. 323–333, 1989.

[44] S. MONASH and H. BLANK, "Location and Re-Formation of the Epithelial Barrier to Water Vapor," *AMA. Arch. Derm.*, vol. 78, no. 6, pp. 710–714, Dec. 1958.

[45] F. Rancan, M. Giulbudagian, J. Jurisch, U. Blume-Peytavi, M. Calderón, and A. Vogt, "Drug delivery across intact and disrupted skin barrier: Identification of cell populations interacting with penetrated thermoresponsive nanogels," *Eur. J. Pharm. Biopharm.*, vol. 116, pp. 4–11, 2017.

[46] L. R. Sklar, C. T. Burnett, J. S. Waibel, R. L. Moy, and D. M. Ozog, "Laser assisted drug delivery: A review of an evolving technology," *Lasers Surg. Med.*, vol. 46, no. 4, pp. 249–262, Apr. 2014.

[47] M. H. Asfour, "Advanced trends in protein and peptide drug delivery: a special

emphasis on aquasomes and microneedles techniques," *Drug Deliv. Transl. Res.*, vol. 11, no. 1, pp. 1–23, 2021.

[48] S. Kezic and I. Jakasa, "Filaggrin and Skin Barrier Function," in *Current Problems in Dermatology*, vol. 49, pp. 1–7, 2016.

[49] W. H. I. McLean, "Filaggrin failure – from ichthyosis vulgaris to atopic eczema and beyond," *Br. J. Dermatol.*, vol. 175, no. S2, pp. 4–7, Oct. 2016.

[50] J. M. Abdo, N. A. Sopko, and S. M. Milner, "The applied anatomy of human skin: A model for regeneration," *Wound Med.*, vol. 28, no. September 2019, p. 100179, 2020.

[51] N. Kirschner, P. Houdek, M. Fromm, I. Moll, and J. M. Brandner, "Tight junctions form a barrier in human epidermis," *Eur. J. Cell Biol.*, vol. 89, no. 11, pp. 839–842, 2010.

[52] T. Sugawara *et al.*, "Tight junction dysfunction in the stratum granulosum leads to aberrant stratum corneum barrier function in claudin-1-deficient mice," *J. Dermatol. Sci.*, vol. 70, no. 1, pp. 12–18, Apr. 2013.

[53] K. Bäsler, S. Bergmann, M. Heisig, A. Naegel, M. Zorn-Kruppa, and J. M. Brandner, "The role of tight junctions in skin barrier function and dermal absorption," *J. Control. Release*, vol. 242, pp. 105–118, 2016.

[54] M. S. Balda and K. Matter, "Tight junctions and the regulation of gene expression," *Biochim. Biophys. Acta - Biomembr.*, vol. 1788, no. 4, pp. 761–767, 2009.

[55] N. Kirschner, R. Rosenthal, D. Günzel, I. Moll, and J. M. Brandner, "Tight junctions and differentiation – a chicken or the egg question?," *Exp. Dermatol.*, vol. 21, no. 3, pp. 171–175, Mar. 2012.

[56] K. Matter, S. Aijaz, A. Tsapara, and M. S. Balda, "Mammalian tight junctions in the regulation of epithelial differentiation and proliferation," *Curr. Opin. Cell Biol.*, vol. 17, no. 5, pp. 453–458, 2005.

[57] A. L. Hilchie, K. Wuerth, and R. E. W. Hancock, "Immune modulation by multifaceted cationic host defense (antimicrobial) peptides," *Nat. Chem. Biol.*, vol. 9, no. 12, pp. 761–768, 2013.

[58] M. H. Braff, A. Bardan, V. Nizet, and R. L. Gallo, "Cutaneous Defense Mechanisms by Antimicrobial Peptides," *J. Invest. Dermatol.*, vol. 125, no. 1, pp. 9–13, 2005.

[59] R. Gläser *et al.*, "The Antimicrobial Protein Psoriasin (S100A7) Is Upregulated in Atopic Dermatitis and after Experimental Skin Barrier Disruption," *J. Invest. Dermatol.*, vol. 129, no. 3, pp. 641–649, 2009.

[60] E. Abd *et al.*, "Skin models for the testing of transdermal drugs," *Clin. Pharmacol. Adv. Appl.*, vol. 8, pp. 163–176, 2016.

[61] G. E. Flaten, Z. Palac, A. Engesland, J. Filipović-Grčić, Ž. Vanić, and N. Škalko-Basnet, "In vitro skin models as a tool in optimization of drug formulation," *Eur. J. Pharm.*

Sci., vol. 75, pp. 10–24, 2015.

[62] R. Neupane, S. H. S. Boddu, J. Renukuntla, R. J. Babu, and A. K. Tiwari, "Alternatives to biological skin in permeation studies: Current trends and possibilities," *Pharmaceutics*, vol. 12, no. 2, 2020.

[63] R. Miki *et al.*, "Development of a membrane impregnated with a poly(dimethylsiloxane)/poly(ethylene glycol) copolymer for a high-throughput screening of the permeability of drugs, cosmetics, and other chemicals across the human skin," *Eur. J. Pharm. Sci.*, vol. 66, pp. 41–49, 2015.

[64] G. Ottaviani, S. Martel, and P.-A. Carrupt, "Parallel Artificial Membrane Permeability Assay: A New Membrane for the Fast Prediction of Passive Human Skin Permeability," *J. Med. Chem.*, vol. 49, no. 13, pp. 3948–3954, Jun. 2006.

[65] V. Dobričić, B. Marković, K. Nikolic, V. Savić, S. Vladimirov, and O. Čudina, "17β-carboxamide steroids – in vitro prediction of human skin permeability and retention using PAMPA technique," *Eur. J. Pharm. Sci.*, vol. 52, pp. 95–108, 2014.

[66] D. Karadzovska and J. E. Riviere, "Assessing vehicle effects on skin absorption using artificial membrane assays," *Eur. J. Pharm. Sci.*, vol. 50, no. 5, pp. 569–576, 2013.

[67] W. Abraham and D. T. Downing, "Preparation of model membranes for skin permeability studies using stratum corneum lipids," *J. Invest. Dermatol.*, vol. 93, no. 6, pp. 809–813, 1989.

[68] B. Sinkó *et al.*, "Skin–PAMPA: A new method for fast prediction of skin penetration," *Eur. J. Pharm. Sci.*, vol. 45, no. 5, pp. 698–707, 2012.

[69] M. Köllmer *et al.*, "Investigation of the Compatibility of the Skin PAMPA Model with Topical Formulation and Acceptor Media Additives Using Different Assay Setups," *AAPS PharmSciTech*, vol. 20, no. 2, p. 89, 2019.

[70] H. Wu, Z. Deng, B. Zhou, M. Qi, M. Hong, and G. Ren, "Improved transdermal permeability of ibuprofen by ionic liquid technology: Correlation between counterion structure and the physicochemical and biological properties," *J. Mol. Liq.*, vol. 283, pp. 399–409, 2019.

[71] J. Ponmozhi *et al.*, "Development of skin-on-a-chip platforms for different utilizations: Factors to be considered," *Micromachines*, vol. 12, no. 3, pp. 1–25, 2021.

[72] A. Haq, B. Goodyear, D. Ameen, V. Joshi, and B. Michniak-Kohn, "Strat-M® synthetic membrane: Permeability comparison to human cadaver skin," *Int. J. Pharm.*, vol. 547, no. 1, pp. 432–437, 2018.

[73] L. Yue *et al.*, "Targeting ALDH1 to decrease tumorigenicity, growth and metastasis of human melanoma," *Melanoma Res.*, vol. 25, no. 2, 2015.

[74] K. Bhadriraju and C. S. Chen, "Engineering cellular microenvironments to improve cell-based drug testing," *Drug Discov. Today*, vol. 7, no. 11, pp. 612–620, 2002.

[75] S. Mitragotri and J. Lahann, "Physical approaches to biomaterial design," *Nat. Mater.*, vol. 8, no. 1, pp. 15–23, 2009.

[76] K. A. Beningo, M. Dembo, and Y. Wang, "Responses of fibroblasts to anchorage of dorsal extracellular matrix receptors," *Proc. Natl. Acad. Sci.*, vol. 101, no. 52, pp. 18024 LP – 18029, Dec. 2004.

[77] E. Cukierman, R. Pankov, and K. M. Yamada, "Cell interactions with three-dimensional matrices," *Curr. Opin. Cell Biol.*, vol. 14, no. 5, pp. 633–640, 2002.

[78] Y. Fang and R. M. Eglen, "Three-Dimensional Cell Cultures in Drug Discovery and Development," *SLAS Discov. Adv. life Sci. R D*, vol. 22, no. 5, pp. 456–472, Jun. 2017.

[79] N. Ali, M. Hosseini, S. Vainio, A. Taïeb, M. Cario-André, and H. R. Rezvani, "Skin equivalents: Skin from reconstructions as models to study skin development and diseases," *Br. J. Dermatol.*, vol. 173, no. 2, pp. 391–403, 2015.

[80] A. Almeida, B. Sarmento, and F. Rodrigues, "Insights on in vitro models for safety and toxicity assessment of cosmetic ingredients," *Int. J. Pharm.*, vol. 519, no. 1, pp. 178–185, 2017.

[81] M. H. Mohammadi *et al.*, "Skin Diseases Modeling using Combined Tissue Engineering and Microfluidic Technologies," *Adv. Healthc. Mater.*, vol. 5, no. 19, pp. 2459–2480, 2016.

[82] F. Hirschhaeuser, H. Menne, C. Dittfeld, J. West, W. Mueller-Klieser, and L. A. Kunz-Schughart, "Multicellular tumor spheroids: An underestimated tool is catching up again," *J. Biotechnol.*, vol. 148, no. 1, pp. 3–15, 2010.

[83] S. Ströbel, N. Buschmann, A. Neeladkandhan, S. Messner, and J. M. Kelm, "Characterization of a novel in vitro 3D skin microtissue model for efficacy and toxicity testing," *Toxicol. Lett.*, vol. 258, pp. S156–S157, 2016.

[84] J. Klicks, C. Maßlo, A. Kluth, R. Rudolf, and M. Hafner, "A novel spheroid-based co-culture model mimics loss of keratinocyte differentiation, melanoma cell invasion, and drug-induced selection of ABCB5-expressing cells," *BMC Cancer*, vol. 19, no. 1, p. 402, 2019.

[85] H. Vörsmann *et al.*, "Development of a human three-dimensional organotypic skin-melanoma spheroid model for in vitro drug testing," *Cell Death Dis.*, vol. 4, no. 7, pp. e719–e719, 2013.

[86] N. I. Moldovan, N. Hibino, and K. Nakayama, "Principles of the Kenzan Method for Robotic Cell Spheroid-Based Three-Dimensional Bioprinting," *Tissue Eng. Part B Rev.*, vol. 23, no. 3, pp. 237–244, Dec. 2016.

[87] S. Sanyal, M. Kosovsky, "Materials and assay systems used for three-dimensional cell culture," *Technology Platforms for 3D Cell Culture*, 2017

[88] A. El Ghalbzouri, S. Commandeur, M. H. Rietveld, A. A. Mulder, and R. Willemze,

"Replacement of animal-derived collagen matrix by human fibroblast-derived dermal matrix for human skin equivalent products," *Biomaterials*, vol. 30, no. 1, pp. 71–78, 2009.

[89] M. A. Karsdal *et al.*, "The good and the bad collagens of fibrosis – Their role in signaling and organ function," *Adv. Drug Deliv. Rev.*, vol. 121, pp. 43–56, 2017.

[90] S. E. L. Vidal, K. A. Tamamoto, H. Nguyen, R. D. Abbott, D. M. Cairns, and D. L. Kaplan, "3D biomaterial matrix to support long term, full thickness, immuno-competent human skin equivalents with nervous system components," *Biomaterials*, vol. 198, pp. 194–203, 2019.

[91] I. González de Torre, A. Ibáñez-Fonseca, L. Quintanilla, M. Alonso, and J.-C. Rodríguez-Cabello, "Random and oriented electrospun fibers based on a multicomponent, in situ clickable elastin-like recombinamer system for dermal tissue engineering," *Acta Biomater.*, vol. 72, pp. 137–149, 2018.

[92] Y. Shi *et al.*, "Tyrosinase-doped bioink for 3D bioprinting of living skin constructs," *Biomed. Mater.*, vol. 13, no. 3, p. 35008, 2018.

[93] A. R. Boccaccini and J. J. Blaker, "Bioactive composite materials for tissue engineering scaffolds," *Expert Rev. Med. Devices*, vol. 2, no. 3, pp. 303–317, May 2005.

[94] D. H. Reneker and I. Chun, "Nanometre diameter fibres of polymer, produced by electrospinning," *Nanotechnology*, vol. 7, no. 3, pp. 216–223, 1996.

[95] E. Knight and S. Przyborski, "Advances in 3D cell culture technologies enabling tissue-like structures to be created in vitro," *J. Anat.*, vol. 227, no. 6, pp. 746–756, Dec. 2015.

[96] A. Barbetta, N. R. Cameron, and S. J. Cooper, "High internal phase emulsions (HIPEs) containing divinylbenzene and 4-vinylbenzyl chloride and the morphology of the resulting PolyHIPE materials," *Chem. Commun.*, no. 3, pp. 221–222, 2000.

[97] C. Rodrigues Neves and S. Gibbs, "Progress on Reconstructed Human Skin Models for Allergy Research and Identifying Contact Sensitizers BT - Three Dimensional Human Organotypic Models for Biomedical Research," F. Bagnoli and R. Rappuoli, Eds. Cham: Springer International Publishing, 2021, pp. 103–129.

[98] H. E. Abaci, Z. Guo, Y. Doucet, J. Jacków, and A. Christiano, "Next generation human skin constructs as advanced tools for drug development," *Exp. Biol. Med.*, vol. 242, no. 17, pp. 1657–1668, 2017.

[99] K. Gledhill, Z. Guo, N. Umegaki-Arao, C. A. Higgins, M. Itoh, and A. M. Christiano, "Melanin transfer in human 3D skin equivalents generated exclusively from induced pluripotent stem cells," *PLoS One*, vol. 10, no. 8, pp. 1–16, 2015.

[100] N. Bechetoille, C. Dezutter-Dambuyant, O. Damour, V. André, I. Orly, and E. Perrier, "Effects of Solar Ultraviolet Radiation on Engineered Human Skin Equivalent

Containing Both Langerhans Cells and Dermal Dendritic Cells," *Tissue Eng.*, vol. 13, no. 11, pp. 2667–2679, Sep. 2007.

[101] I. J. Kosten, S. W. Spiekstra, T. D. de Gruijl, and S. Gibbs, "MUTZ-3 derived Langerhans cells in human skin equivalents show differential migration and phenotypic plasticity after allergen or irritant exposure," *Toxicol. Appl. Pharmacol.*, vol. 287, no. 1, pp. 35–42, 2015.

[102] B. Huber, A. Link, K. Linke, S. A. Gehrke, M. Winnefeld, and P. J. Kluger, "Integration of Mature Adipocytes to Build-Up a Functional Three-Layered Full-Skin Equivalent," *Tissue Eng. - Part C Methods*, vol. 22, no. 8, pp. 756–764, 2016.

Chapter 3

Skin-on-a-chip technology: the future of skin disease models and pharmacological studies

3.1 Introduction

Modern cell culture techniques aim to surpass the limitations of the conventional cell-based cell culture platforms and increase the predictive power of *in vitro* models. The need for physiologically relevant and functional tissue models led to the emergence a new technology for cell culture known as organ-on-a-chip (OoC) or microphysiological systems. OoCs combine the advances in tissue engineering and the field of microfluidics to reproduce key functional aspects of organs and tissues [1]. These systems have the potential to achieve experimental controllability and reproducibility similar to two-dimensional (2D) cell culture while allowing for an increased physiological relevance and complexity (**Figure 3. 1**). The possibility of connecting OoC systems that mimic different organs will allow the study of systemic effects which, until now, were only possible using animal models.

The key features of OoC platforms include the presence of biomechanical forces typically to model fluid flow and the integration of multiple cell types to model the complex interaction between them [2]. To model fluid flow across the tissues, perfusion channels are included on the OoCs. These channels act as engineered vasculature, delivering cell culture media to the cells within the culture chamber and removing associated cell metabolites and detritus. By growing tissues inside a controlled environment while mimicking *in vivo*-like forces and medium perfusion, it has been possible to create more advanced models better suited for pharmaceutical applications and disease modelling. This technology has the potential to substantially reduce the total costs of drug screening due to the decrease of reagent volumes and the possibility of testing various drug candidates in parallel [3]. Also, the close-loop environment in OoC makes it possible the integration of various biosensors for real-time monitoring of tissue function [4]. The sensors can be useful not only for monitoring the formation of healthy tissues but also for monitoring disease conditions in response to drug candidates.

The potential of these platforms has been extensively demonstrated in the last decade. It was shown that the stimuli applied on chip leads to alterations in cell behaviour, including improved cell morphology and differentiation and more *in vivo*-like interactions between cells and the extracellular matrix (ECM) [5]. Some important examples include the reconstruction of a lung-on-a-chip capable of

recreating relevant *in vivo* mechanical forces (stretching) [6], a liver-on-a-chip mimicking parenchymal hepatocytes and the sinusoidal space [7] and a cardiac muscle grown on chip mimicking topographical and electrical cues, important to achieve the alignment and maturation in cardiac tissue [8]. Other relevant models produced on the chip include bone, blood-brain barrier, skeletal muscle, eye, gut and spleen [9].

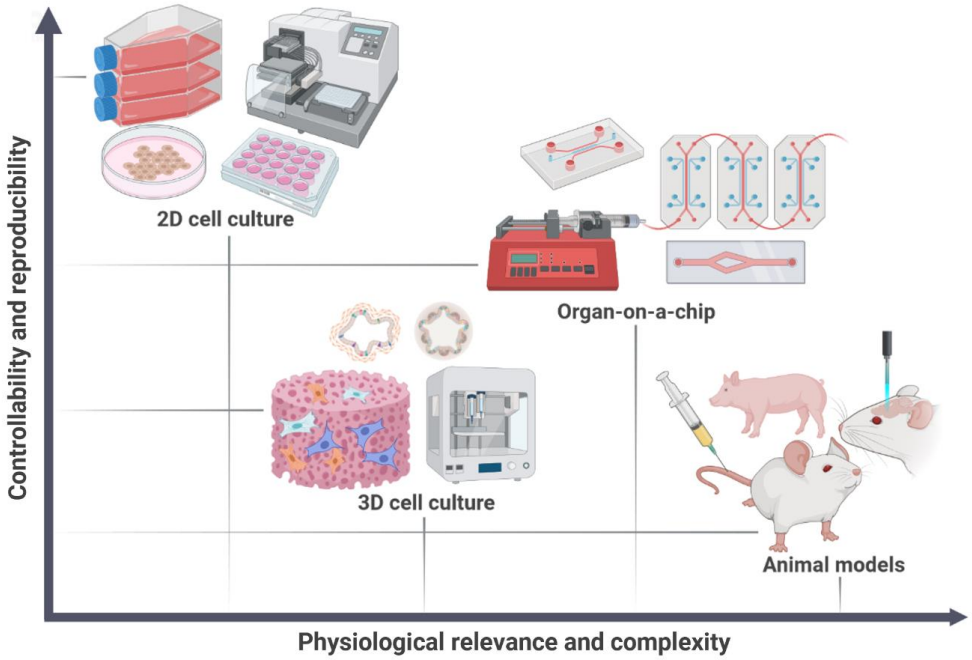

Figure 3. 1. Organ-on-a-Chip platforms. Methods used for preclinical studies of topical, dermal and transdermal drugs. Comparison between the different methodologies regarding controllability and reproducibility as well as physiological relevance and complexity. The figure highlights the potential significance of organ-on-a-chip technology to provide a simple yet more physiologically relevant platform to systematically evaluate skin responses. Figure generated in BioRender.

Additionally, these platforms have been used to recreate multiple pathological conditions, important for future evaluation of drug candidates and therapies [10]. One important example has been the field of cancer research. Despite its complexity, various groups are successfully using OoC technology to study the

basic cellular and molecular biology of cancer. Since the failure in drug development for cancer treatment is in part a result of conventional cancer models failing to recapitulate the *in vivo* tumour microenvironment, OoC can be an important tool for future drug development in this field. Currently, important models have been developed to model tumour microenvironment, cancer cells trans-endothelial migration and cancer-related angiogenesis [11].

One of the most exciting applications of OoC is the development of multi-organ-on-a-chip (multi-OoC) platforms to mimic the interplay between different organs. This could further advance the development of biomimetic *in vitro* models for drug testing and discovery [12,13]. Some examples of multi-OoC include the coculture of a liver and kidney model to study changes in metabolism for repeated dose multi-drug toxicity screening [14] and the coculture of an intestine model with liver cells to study intestinal absorption and liver metabolism of drugs [15]. Other groups focused on the goal of creating a body-on-a-chip and are studying the connection for up to four organs [16, 17]. For examples, Oleaga *et al.* reported the development of a multi-OoC to study the interactions between cardiac, muscle, neuronal and liver tissues [18].

To date, multiple approaches have been employed for the design and fabrications of OoC devices, depending of the final objectives of the research, available equipment and know-how. However, most of them include porous substrate dividing the microchannels to create different compartments [19]. This common practice makes it possible to study barrier function and simulate various interfaces (tissue-liquid, tissue-tissue, air-tissue).

3.2 Skin-on-a-chip technology

Tissue engineered skin models are still deficient in several essential key components to be able to reproduce the full architecture and physiology of *in vivo* skin in healthy and diseased state. One of the main limitations is the lack of vascularization, resulting in restricted nutrition supply, cell-cell interactions and cell-ECM interactions. This justifies the need for modern cell cultures techniques capable of reproducing key features such as vascularization and the mechanical

forces acting on the skin [20]. The limitations of current *in vitro* skin models and the advantages offered by OoC technologies motivated the development of skin-on-a-chip (SoC) models [21]. SoCs are promising tools to increase the predictive ability of skin models, thereby reducing the failures during the preclinical testing. In this chapter, key aspects of the anatomy and physiology of the human skin will be discussed in the context of developing a physiologically relevant skin model using OoC technology. Both technical and biological aspects will be discussed in the section. In the following section, the current state-of-the-art SoC devices will be discussed in detail and the key achievements will be compared.

3.2.1 Main factors in the development of skin-on-a-chip devices

An ideal SoC is expected to include the main layers of skin, presented in **Chapter 2**, as well as the vasculature layer. The integration of mechanical forces such as cyclic stretching and shear stress should also be considered to reproduce the *in vivo* like microenvironment. Other factors such as cell source and type of scaffold are crucial to obtain a final model with the desired architecture and physiology. Finally, the integration of sensors in the SoC should be considered for real-time monitoring of skin function. **Figure 3. 2** gives an overview of the main considerations when developing a SoC model.

3.2.1.1 Perfusion and vascularization

The native human skin includes a complex blood vascular architecture that serves multiple functions. The vasculature of the skin is located within the dermis and serves important nutritional functions, delivering nutrients to the cells and removing unwanted metabolic waste [22]. Furthermore, it serves as a conduit for elements of the immune system and plays a role in thermoregulation, being able to dissipate heat by dilation of superficial vessels

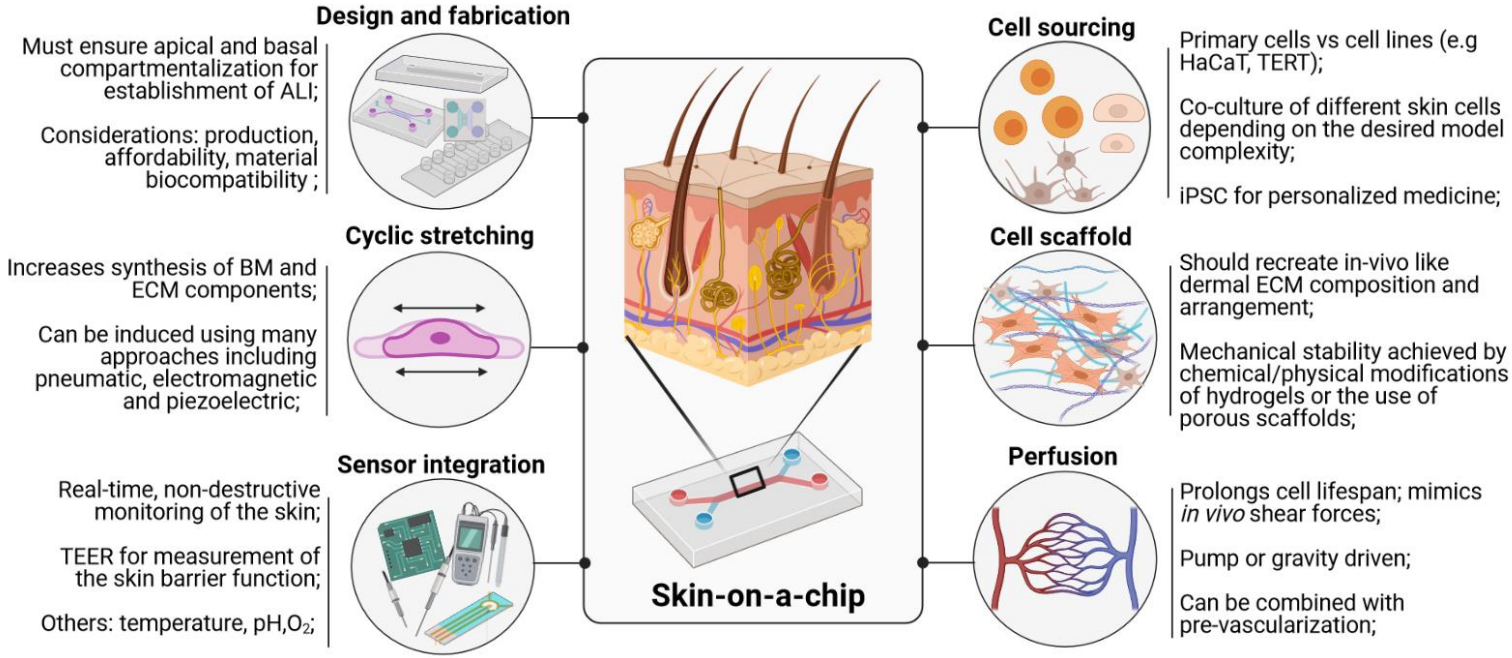

Figure 3. 2. Development of biomimetic Skin-on-a-chip platforms. Schematic drawing representing the main factors to be considered when developing a physiologically relevant skin-on-a-chip model, including technical and biological factors (cell sourcing, cell scaffold, perfusion, cyclic stretching, design and fabrication and sensor integration). The different factors should be evaluated taking into account the specific application as well as available equipment and know-how. ALI: Air-liquid interface; BM: Basement membrane; ECM: Extracellular matrix; TEER: Transepithelial electrical resistance; iPSC: induced pluripotent stem cells. Figure generated in BioRender.

The cutaneous vasculature is also involved in various pathological conditions including acute and chronic inflammatory conditions, tumour growth, metastasis of malignant melanoma and wound healing [23-25]. It is also important when studying the transdermal penetration of substances and the response to irritants [26]. Thus, the cutaneous vasculature is important not only to model physiological *in vitro* skin but also to model pathophysiological conditions.

Conventional reconstructed skin models do not include vascularization which limits their value in regards to their ability to reflect the function of *in vivo* human skin. To overcome these limitations, endothelial cells can be seeded into the dermal part of full-thickness skin model (FTSm), which results in the alignment of endothelial cells to vessel-like structures [27]. More complex methods can induce vascularization in the models and used in studies of angiogenesis, skin grafting and drug testing. Recently, the importance of vascularization for implanted skin, pressured the development of innovative approaches to recreate *in vivo* like vasculature [28]. These are usually classified as prevascularization-based or angiogenic/cell-based [29]. In the prevascularization approach, microvessel channels are fabricated prior to endothelial cell inoculation. Using this method, Groeber *et al* generated a skin model with a perfusable network [30]. The group combined a biological vascular scaffold based on a decellularized segment of porcine jejunum and a tailored bioreactor system. Alternatively, in the angiogenic/cell-based approach endothelial cells are stimulated by growth factors to vascularize the tissue [31]. However, this is a complex and slow process, not suited for high-throughput applications. Furthermore, the vascular channels formed in these studies have a random formation and are inaccessible to external pumps. Consequently, these models do not have functional perfusable vascular channels which limits their applicability.

An advanced skin model should include perfusion of culture media to prolong cell lifespan *in vitro* and recreate the relevant *in vivo*-like biomechanical forces, for example, shear stress. Shear stress refers to the force acting parallel to an object caused by particles flowing or slipping past the object. It can be imparted by fluid flowing over an object and its prevalent throughout the human body [32]. This effect is more pronounced on the endothelial cells lining our blood vessels which are sensitive to changes in fluid flow, with well-established links between disturbed

fluid flow on arterial walls and atherosclerotic build-up. OoC technology can be used for the introduction of biochemical forces similar to what organs and tissues experience *in vivo* and, simultaneously, to allow continuous deliver of cell culture media and removal of cell metabolites and detritus.

Various approaches have been explored for perfusing culture media that can be categorized into pump- or gravity driven solutions [33]. The most common methods for generating fluid flow are the use of an external pump, including a syringe pump or peristaltic pump. These systems deliver accurate, fine-tuned fluid flow but are usually time consuming. Furthermore, the use of tubing can increase the risk of contamination. To overcome some of the limitations of external pumping, pumps have been integrated within microfluidic chips to miniaturize the systems. While internal on-chip pumping makes it possible to reduce the setup footprint, the integration of such an internal pump is typically complicated for both fabrication and operation. Alternatively, passive flow, typically gravity driven, has recently emerged as an alternative [34]. For this, rocking platforms are custom-built to recirculate culture media through the microfluidic channels. These approaches exclude the use of tubing and the use of complex setups with a big footprint. However, these methods typically lack fine control on flow rate, are prone to changes in hydrostatic pressure over time and diminish the advantage of fresh media perfusion and waste removal.

A combination of 3D printing with perfusion could enable the generation of complex structures mimicking the native skin, such as blood vasculature [35], [36]. 3D printing facilitates the precise extrusion and localization of multiple cell types and biomaterials [37]. The fabrication of a vascularized skin equivalent has the potential to enhance the understanding of paracrine signalling within the skin and improve the relevance of current skin models [38]. Blood vessels modelled in microfluidic skin equivalents are not yet at the dimensions relevant to model capillaries as seen in skin models fabricated angiogenically. Despite this, vascularized microfluidic skin equivalents present the opportunity to connect multiple OoCs to create a human on a chip. In conjunction with 3D bioprinting, microfluidics may also address the limitation of low throughput in vascularized skin models [39].

3.2.1.2 Integration of cyclic stretch

In addition to the shear stress induced by perfusion, tissues in the body are continuously subjected to other forces, including tensile and compressive forces (**Figure 3. 3**). Cellular mechanotrasduction is a well-known phenomenon, with various studies describing the cellular mechanisms where mechanical forces are transduced into biochemical signals [40]. These responses are integral parts of the cellular microenvironment that modulate various processes in tissue and organ level in health and disease.

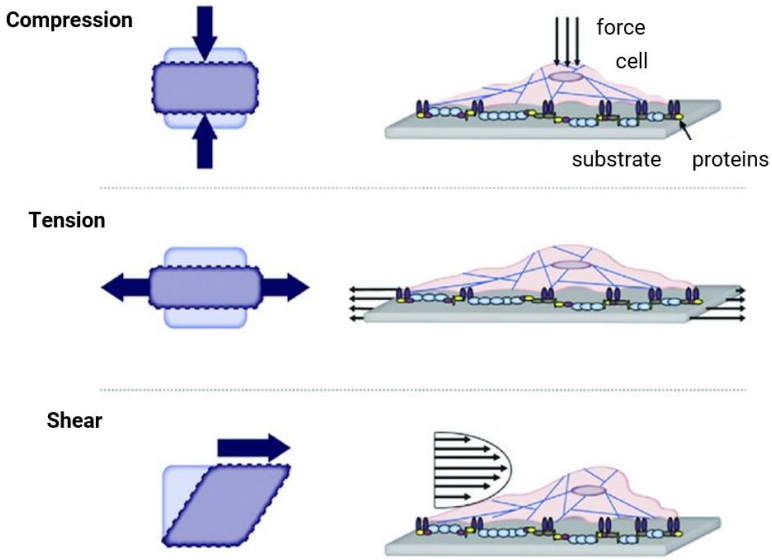

Figure 3. 3. Different mechanical stress types acting on cells. Externally applied forces result in compressive, stretch (tension) and shear stresses on cells. Simplified illustrations of the effect of each force in planar culture have been shown for an idealized square (left) and a cell (right). Compression and stretch (tension) act normal to the cell membrane, while shear stress induces an angle change between opposing sides of the cell. Adapted from [41].

The tensile forces applied to the cellular microenvironment result in stretching of the tissue. The human skin is exposed to various types of mechanical stimuli including cyclic stretch. This is a result of environmental effects, growth and various internal processes. Various experiments investigated the effects of stretch stimuli on 2D skin cells including epidermal keratinocytes and dermal fibroblasts.

According to the reports, application of tensile forces to dermal fibroblasts triggers signal transduction from ECM into cells, resulting in increased synthesis of collagen I, collagen III and elastin [42]. Furthermore, an increased production of protease inhibitors such as tissue inhibitor of metalloproteinase was reported [43]. In epidermal keratinocytes, stretch stimulation promoted cellular adhesiveness, proliferation and protein synthesis [44].

Given the complex interactions between keratinocytes and fibroblasts, other groups studied the importance of these forces and the effect on skin models containing both cells. Lü *et al* developed an *in vitro* tensile device to study the mechanisms regulating keratinocyte migration under application of mechanical stretch [45]. Their results showed that, when exposed to these forces, dermal fibroblasts increase secretion of epidermal growth factor, promoting an asymmetric keratinocyte migration. This phenomenon results in accelerated wound repair. Tokuyama *et al* designed an experimental system wherein stretch was applied during the formation of an FTSm [44]. The group analysed the effects of these stimuli on the keratinization of epidermal keratinocytes and the formation of a basement membrane. Cyclic stretch resulted in an increased in the synthesis of basement membrane proteins and the formation of a thicker epidermal layer.

Various actuation approaches have been developed to induce cyclic stretch on cells [46]. Researchers either use their own stretching platforms typically employing pneumatic approaches or use commercially available systems (Bioequip, Flexcell, STRETX Inc). Although multiple solution exists to apply cyclic stretch, OoC technology presents a unique opportunity to create customizable solutions and to combine it with other relevant forces such as shear stress. Various OoC platforms have reproduced the use of different types of mechanical strains including cyclic stretch. Huh *et al* reported a lung-on-a-chip made of a central chamber divided by an elastic porous membrane that could be stretched unidirectionally by providing vacuum in two adjacent chambers [47-48]. This platform was used to study inflammatory responses and to recreate drug toxicity induced pulmonary edema. The same approach was used simulate the peristaltic movements of the gastro-intestinal barrier [49]. Others groups improved on this model by generating a 3D mechanical strain, better simulating the *in vivo* forces [50].

3.2.1.3 Design and fabrication

Conventional methods for the development of biological barriers typically involve the use of permeable supports (e.g transwell), establishing two chambers that separate the apical and basal surfaces of the tissue. For the formation of 3D skin models with an *in-vivo* like barrier, this correct compartmentalization is crucial. It allows a leakage-free separation between the apical and basal surfaces of the skin, allowing correct establishment of the air-liquid interface.

Advances in biomaterials and microfabrication have allowed researchers to integrate compartmentalization inside OoC platforms for the development of innovative barrier models. The most common approach to create separated domains inside an OoC is by integration of a semipermeable membrane between the elastomeric microfluidic channels. This approach has been successfully used to create biological barrier models of the lung, blood-brain barrier, gut and liver [51]. However, it also presents important limitations specially for the development of a complex 3D tissues such as the FTSm. For its development, the dermal compartment needs to be generated, a process usually involving polymerization of a hydrogel and cell mixture on top of a membrane [39]. For the formation of the epidermis on top of the dermis, the apical chamber must ensure correct formation of a stratified epithelium and the circulation of air (or drugs at a later stage) and the lower chamber must ensure correct medium perfusion. At the end, the tissue should be retrieved to perform well established analysis of its architecture and physiology. Most approaches for integrating cell culture membranes rely on their irreversible bonding between the apical and basolateral culture environments, using adhesive glues or oxygen plasma treatment [52]. For FTSm generation, this presents several limitations including difficulties related to cell seeding, introduction of dermal matrix on top of the membrane, culture maintenance as well as challenges accessing the tissue for end-point analysis.

Furthermore, the use of PDMS for fabrication of SoC platforms should be reconsidered. A fully realized SoC model with the potential to replace animal experiments needs to be able to replicate the structure and function of *in vivo* skin on a relatively low-cost and to be compatible with high-throughput studies. Traditional lithography technology used for the fabrication of PDMS devices present

a limited scalability and inherent high costs [53]. This can hinder large-scale production and commercialization of the developed SoC device. Furthermore, PDMS has other limitations, including the tendency to absorb small hydrophobic molecules and shrinkage during the curing process [19]. Thermoplastics are gaining more attention since they offer several advantages compared to PDMS: thermoplastics are cheaper, present less tendency to absorption and evaporation and provide higher chemical resistivity. Furthermore, these materials feature comparable transparency to PDMS. The use of thermoplastics can lead to an easier transition from academia to industry since they can be fabricated both by rapid prototyping and industrial scale fabrication techniques.

Integration of membranes on thermoplastics can be performed using various techniques such as thermal bonding, ultrasonic welding, laser welding, solvent boding and surface functionalization [19]. Alternatively, these materials can be reversible sealed using clamps or magnets, providing minimal requirements with respect to membrane materials. This technique is compatible with the development of modular microfluidic circuits, a concept that has been explored by several groups. Abhyankar *et al* developed a module-based approach in which magnetic latching allows culture membranes to be sandwiched between fluidic channels and sealed in place to support compartmentalized cultures [54]. The flexibility of this design could be interesting for a future SoC, allowing easy removal of the skin tissue for histological and immunohistochemistry analysis and allowing direct cell seeding and introduction of the hydrogel mixture for dermis formation onto the membrane. Furthermore, different modules could be developed, e.g a drug testing module, enabling the user to select the modules that meet their requirements. Additionally, a user-friendly interface is an important consideration when designing a SoC device. This could streamline experimental procedures and encourage adoption in laboratories not familiarized with OoC technology. For development of useful platform for drug testing, attention should also be given to the importance of performing experiments on a large number of specimens in a highly automatized manner.

If commerciality and large-scale production is not required, other alternative approaches can be considered for the development of SoC devices. One alternative is the establishment of gel-liquid interfaces that can physically support

cells while enabling a direct contact interaction between them. This interface is typically microfabricated using phaseguides acting as capillary pressure barriers or by using equally spaced post structures. This technique was used to construct a neurovascular unit including human endothelial cells simulating the cerebral blood vessels as well as primary rat neurons and astrocytes [55]. It is also possible to engineer embedded tubules in an ECM for SoC development. Homan *et al* used bioprinting to generate convoluted tubule by printing a sacrificial ink embedded within the ECM [56]. The printed ink was then removed and the channel was filled with cells and perfused with cell culture medium. This structure modelled 3D renal tubules and recreated cyclosporine-dependent nephrotoxicity. Although these approaches have several limitations, including high production costs, the need for specialized personnel and reproducibility problems, they can be useful for studying specific aspects of skin diseases.

3.2.1.4 Sensor integration

Conventional analyses of tissue function mainly depend on endpoint assessment techniques. In particular, for 3D cell culture using scaffolds or membranes, this monitoring cannot be done using conventional microscopy techniques due to difficulties with light penetration and scattering effects [57]. The conventional process usually includes the removal of the tissue from the wells, chemically fixing, and labelling. Alternatively, assays based on the transport of tracer compounds (e.g., fluorescein isothiocyanate-labelled dextran) are performed. However, these compounds can affect the tissue's integrity and lack the sensitivity to detect subtle changes in their function [58]. With OoC system it is possible to surpass this limitation by integrating microsensors for measuring relevant physical/chemical parameters *in situ*.

To maintain a suitable environment for tissue growth inside OoC systems it is necessary to monitor physiological parameters in real-time [4]. Integrated sensors can characterize the engineered tissue and tissue interactions with different stimulants, giving prompt insight. First attempts to integrate sensors inside the OoC systems have shown the relevance of monitoring in real-time to capture changes in the properties of living cells to obtain a complete information about what is happening inside the OoC A recent automated multi-tissue organ system integrated

an impressive array of on- chip sensors, including electrochemically activated immune biosensors attached to physical microelectrodes, mini microscopes and optical pH, oxygen and temperature monitors [59]. This technical feat highlights the ongoing engineering advances that are enabling real- time non- invasive monitoring of OoC microenvironments.

In the context of SoC platforms, the integration of sensors would be extremely relevant. Growing a FTSm inside a platform is a very long process ranging from 2 weeks to 1.5 months. Using conventional endpoint assays, no information is acquired during the period necessary for skin formation, resulting in low experiment reproducibility. An ideal future platform should integrate physical sensors for monitoring extracellular microenvironment parameters (e.g., pH, O_2, temperature), electrochemical sensors for measuring soluble protein biomarkers as well as transepithelial/transendothelial electrical resistance (TEER) sensors to measure skin barrier.

TEER has become a widely accepted method to evaluate the tissue barrier function in *in vitro* systems. This method is a label-free alternative to the widely used conventional assays based on the transport of tracer compounds. TEER enables non-destructive, real-time quantification of the barrier function. Conventional TEER measurements are performed by introducing commercially available chopstick type electrodes at both sides of a cellular barrier (**Figure 3. 4.a**). However, TEER readings using handheld chopstick electrodes have low reproducibility due to variations in depth and/or the angle of immersion [60]. Also, chopstick type electrodes cannot deliver a uniform current density when large tissue culture inserts are used (> 12 mm in diameter). As an alternative, EndOhm chambers contain a pair of concentric electrodes, generating a more uniform current density across the tissue when compared to the chopstick electrodes (**Figure 3. 4.b**). Also, Endohm's fixed geometry increases reproducibility.

Just as in conventional systems, the TEER of a cellular barrier inside an OoC device can be measured by introducing electrodes on both sides of the cellular barrier [61]. This has been achieved by inserting electrodes on the chip inlets/outlets, in a process similar to the introduction of the chopstick electrodes. Alternatively, the OoC with integrated TEER electrodes has been fabricated for development and

monitoring of the blood–brain barrier, gastrointestinal tract and airway epithelium [62]. TEER can be used to evaluate the stage of skin differentiation and the impact of a topical irritant.

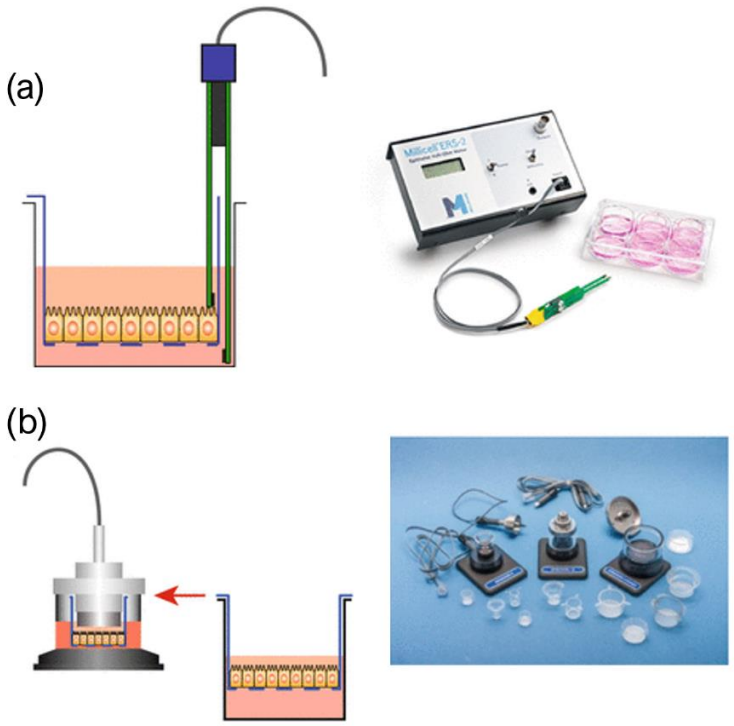

Figure 3. 4.Transepithelial/transendothelial electrical resistance (TEER) measurements. (a) Using chopstick/STX2 electrode pairs connected to voltohmeter and (b) using an EndOhm chamber. The uniformity of the current density generated by the electrodes across the cell layer has significant effect on the TEER measurement. The chopstick electrodes cannot deliver uniform current density. As an alternative, the EndOhm chamber generates a more uniform current density. Adapted from [63].

3.2.1.5 Cell sourcing

Multiple *in-house* culture protocols have been developed and optimized over the last decades to allow incorporation of different cell types with different origins and disease-specific phenotypes. Conventional FTSm are generally constructed using primary human skin cells (epidermal keratinocytes and dermal fibroblasts). These cells originate from freshly isolated healthy human skin obtained from standard surgical procedures. The clear advantage of using primary cells from

human donors is that they capture the *in vivo* phenotype [64]. These cells can also be successfully used to model pathologies when sourced from donors with that particular disease, reflecting clinical population variance in their phenotypes. However, primary cells also present important disadvantages including limited availability of donor skin, donor variation that may hamper experimental readout parameters and restricted proliferation and amplification capacity.

As an alternative, cell lines with validation of purity and viability can be used. The advantage of cell lines is the availability of reliable protocols, responding in a stable and predictable and contributing to a higher reproducibility. However, cells lines are only approximations for the primary cell types found *in vivo* and can deviate from the original phenotype. This is the case of the self-renewable keratinocyte cell line, HaCaT which has been extensively investigated for its ability to undergo differentiation. Although epidermal tissue formation is possible using HaCaT cells, owing to their low differentiation potential compared to primary keratinocytes, HaCaT cannot be easily used to generate the *stratum corneum* [65]. Specifically, it was difficult to observe whether it had reproduced the full layers of skin relative to those observed *in vivo* [66]. The widely used HaCaT keratinocyte cell line is unsuitable for organotypic cultures as it fails to develop a fully stratified epidermis and lacks a functional *stratum corneum*.

Alternatively, hTERT-immortalized keratinocyte cell lines have been proved to develop high quality epidermal and skin equivalents and faithfully mimic primary keratinocyte gene and protein expression with regard to epidermal proliferation, differentiation, skin barrier function and inflammatory responses. Reijnders *et al* were able to develop a fully differentiated FTSm generated from human TERT-immortalized keratinocytes and fibroblasts [67]. The group reported the successful production of a FTSm with a fully differentiated epidermis and a fibroblast-populated dermis comparable to a model originated from primary cells. Models including TERT-immortalized cells have the potential of providing higher throughput screening of new products and drugs and should be considered for incorporating into reproducible SoC platforms. However, donor variation can be an important feature to accurately resemble the population and should not be forgotten when using cell lines. Depending on the context of use, primary cells can be the better choice for development of a physiologically relevant epidermis. In general,

when choosing the ideal cell types for integration in the SoC platform, the context of use needs to be considered and the key aspects and components needed for function needs to be identified.

Induced pluripotent stem cells (iPSC) are a promising alternative source of cells for tissue engineering. These cells are derived from adult somatic cells via reprogramming with ectopic expression factors (Oct3/4, Sox2, c-Myc and Klf4) [68]. The expression of this factors results in the suppression of genes responsible for differentiation, reverting the cells to a pluripotent state. IPSC offer an approach to circumvent the limitations associated with current FTSm due to their unlimited growth and ability to differentiate into multiple cell types. Furthermore, cells differentiated from iPSC retain characteristics of the original donor, such as disease phenotype, offering an alternative source for modelling skin diseases. Various groups developed FTSm containing iPSC-derived fibroblasts and/or keratinocytes. Gledhill *et al* generated a functional FTSm from iPSC-derived keratinocytes, melanocytes and fibroblasts containing a function epidermal-melanin unit [69]. This model showed similar morphology and functionality to primary healthy skin model. This approach has the potential to create relevant SoC platforms. To obtain a more functional and physiological complete model it would be useful the introduction of iPSC-derived immune cells and appendages in these models. However, many hurdles still exist before iPSC-derived FTSm can reach a level of complexity nearing that of human skin. Additionally, cost, retention of epigenetic memory, genomic instability and lack of complex structures like appendages are other factors which remain to be fully addressed.

3.2.1.6 Cell Scaffolds

One of the major challenges for the production of a biomimetic skin model is the development of a dermal matrix with *in vivo*-like composition and mechanical environment while assuring its stability and reproducibility. The dermis is an integrated system of fibrous, filamentous and amorphous connective tissue, responsible for the elasticity and tensile strength of the skin. The fibroblasts are surrounded by this system, composed of a variety of proteins, including collagens, glycosaminoglycans, proteoglycans and adhesive proteins such as fibronectin and laminin [70]. All of these components are secreted and remodelled by the fibroblasts,

resulting in an organized meshwork which provides a soft and elastic environment for cellular growth and interactions. Dermal fibroblasts communicate extensively with the keratinocytes within the epidermis, located on top of this elastic dermal layer. The top of the dermal layer acts as a soft substrate for keratinocyte adherence and formation of an extracellular basement membrane. Type IV collagen is found in the basement membrane zone, and the major structural component of anchoring fibrils is collagen type VII, mainly produced by keratinocytes [71]. A detailed description of the ECM in the skin can be found in **Chapter 2.2.1**.

The correct development of a SoC device requires an understanding of the interplay of the different cell types and the effect of the ECM on cellular function and architecture. The ECM composition and 3D arrangement affect cell morphology, polarity and survival and must be carefully engineered to promote the formation of appropriate tissue architecture and physiology.

Conventional methods to develop the dermal compartment involve the use of natural hydrogels, typically animal-derived collagen, to create an environment conductive to cell adhesion and growth [72]. However, as fibroblasts proliferate, the ECM tends to contract and degrade, limiting their lifespan and application due to the lack of reproducibility. This also frequently results in detachment of the compartment from the membrane leading to leakage problems. The use of conventional hydrogel materials constitutes a relevant limitation for the standardization of FTSm and their reliable application, making them unsuitable for integration on SoC device. To overcome these problems, various groups proposed chemical and physical modifications of the matrix. Lotz *et al* were able to generate cross-linked collagen hydrogels that were more mechanically stable and less prone to enzymatic degradation when compared with non-cross-linked collagen hydrogels [73]. The produced dermal compartments could support a fully differentiated epidermis on top. Overall, these stable structures are more suitable for integration on a SoC device. However, they typically comprise exclusively of one ECM component (e.g., collagen type I) which does not represent the *in vivo* dermal composition. Alternate polymers or hydrogels should be developed specifically to mimic the biophysical properties of the skin. One interesting possibility could be to generate of a fibroblast-derived matrix in which fibroblasts are stimulated to synthetize the different components of the in vivo ECM [74]. This strategy can be

combined with the use of a scaffold of high porosity to achieve good mechanical stability.

When combining an *in-vivo* like ECM with a perfusion system it is possible to recreate physiological interstitial flow. This flow refers to the movement of fluid through the ECM or *interstitium* of a tissue and constitutes and important component of microcirculation (**Figure 3. 5**). These forces provide the convection necessary for transport of molecules and provide a specific mechanical environment to cells. A biomimetic skin model should recreate interstitial flow. This is possible by generating a pressure gradient across the SoC through fluidic flow in the basal chamber, especially during culture at ALI which increases interstitial flow in the FTSm. This not only enhances transport of nutrients but also induces morphogenic effects in both fibroblasts and keratinocytes. In particular, *in vitro* studies showed that interstitial flow affects both alignment and differentiation human fibroblasts [75]. A comprehensive consideration of the interstitial flow and how it is sensed by cells to drive morphogenic responses and other biological responses is relevant for development of a SoC platform, with important implications on the delivery of drugs and therapeutics.

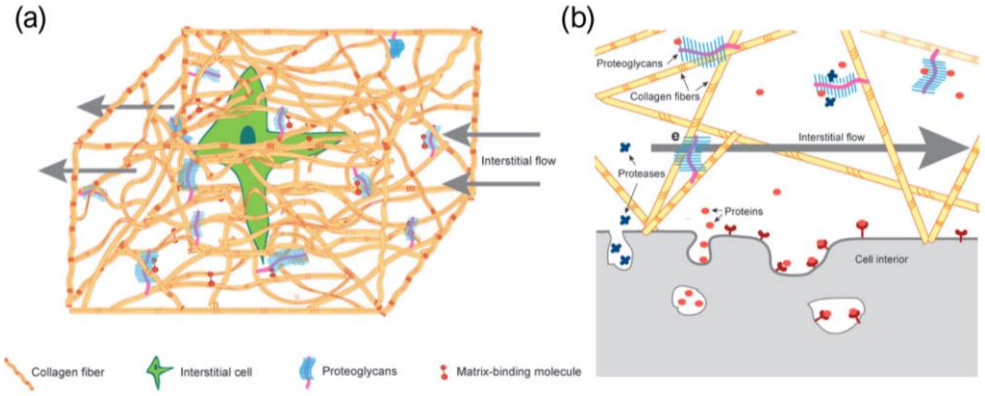

Figure 3. 5. Interstitial flow. a) Schematic of the interstitium showing major features and components of typical ECM. Here collagen fibbers are intertwined along with proteoglycans and interstitial cells. b) A microscopic view of the ECM-cell interface reveals the many events that play a role in interstitial transport. The ECM components provide resistance to convection and diffusion as well as serving as a storage site for ECM-binding proteins. Adapted from [76].

3.2.2 The evolution of skin-on-a-chip platforms

Here, the evolution of SoC platforms in the last years is presented. The platforms are divided into transferred SoC, SoC using 2D cell cultures, SoC using 3D cell cultures and SoC platforms for permeation assays. All the available SoC with key achievements made to date are summarized in **Table 3. 1**.

3.2.2.1 Transferred skin-on-a-chip

The most common application of SoC devices has been the maintenance of skin tissues under dynamic perfusion to increase its longevity and/or to establish a co-culture of tissues modelling different organs [39]. The published work using this approach typically includes in the developed SoC a commercially available FTSm or a skin biopsy from a donor.

The use of OoC platforms for skin cultivation is still in its infancy with the first paper showing the potential of this field being published by Ataç *et al* in 2013 [77]. In this work, a PDMS-based microfluidic platform was used to apply dynamic perfusion and mechanical shear stress to an *in vitro* skin model and single hair follicular units **(Figure 3. 6.a**). In these experiments, two types of tissues were used, namely, a commercial FTSm (EpiDermFT®, Mattek, Ashland, MA, USA) and an *ex vivo* skin model. The group was able to extend the suggested culture period for the *in vitro* commercial model using the chip-based platform. Furthermore, the architecture of the *ex vivo* skin was better preserved by integration in the platform. The group hypothesized that these positive effects could be explained by the inclusion of dynamic perfusion and the shear stress influencing, for example, the relative distances between cells and the ECM components. The successful long-term maintenance of the *in vitro* skin models in the developed platform showed the potential of SoC devices and inspired many publications in this field in the last five years.

Model type	Tissue (Cell types)	Dermal matrix	Duration on-chip	Fabrication method; materials	Flow type; velocity	Main features	Ref.
Transferred skin and hair follicle-on-chip	Commercial FTSm (EpiDermFT®) + *ex vivo* subcutaneous tissue	Collagen	7-14 days	Lithography; PDMS + glass + PC (TissUse' HUMMIMIC)	Integrated micropump; 30 µL/min	Ex vivo skin and hair follicle on chip; prolonged lifespan	Ataç *et al* (2013) [77]
Transferred skin-on-chip	FTSm (Primary Hks + primary HFns)	Collagen	28 days	Lithography; PDMS + PC membrane	Gravity driven flow; 3.28 µL/min	Drug toxicity studies (doxorubicin)	Abaci *et al* (2015) [78]
Transferred skin-on-chip	Human skin biopsy	Human skin biopsy	4 h	Lithography; PDMS	Static	Neutrophil responses to *Staphylococcus aureus* skin infection studies	Kim *et al* (2019) [79]
Transferred skin-on-chip	Commercial RHEm (EpiDerm®)	None	50 h	Commercial platform (IMOLA-IVD)	Peristaltic pump; 60 µL/min (ON/OFF pump cycles)	Automated perfusion; TEER monitored after SDS stimuli	Alexander *et al* (2018) [80]
Multi organ-on-a-chip	Human skin biopsy	Human skin biopsy	14 days	Commercial platform (TissUse' HUMMIMIC)	Integrated micropump; 30 µL/min	Co-culture of 2 organs (skin and liver); Exposure to toglitazone	Wagner *et al* (2013) [81]
Multi organ-on-a-chip	Human Skin biopsy	Human skin biopsy	28 days	Commercial platform (TissUse' HUMMIMIC)	Integrated micropump; 2.58 µL/min	Co-culture of 4 organ models (skin, liver, intestine and kidney);	Maschmeyer *et al* (2015) [82]
Multi organ-on-a-chip	Commercial RHEm (EpiDerm®)	None	5 days	Commercial platform (TissUse' HUMMIMIC)	Integrated micropump; 2.7 µL/min	Co-culture of 2 organ models (skin and liver); Pharmacokinetics (hyperforin and permethrin)	Kühnl *et al* (2020) [83]

Table 3. 1. Summary of the SoC devices reported in the literature. Data shown for multi-organ-on-a-chip corresponds to the skin section of the platform. Abbreviations: dECM, decellularized extracellular matrix; FTSm, full thickness skin model; HKs, Human keratinocytes; HFs, Human fibroblasts; HPAs; Human preadipocytes subcutaneous; HUVECs, human umbilical vein endothelial cells; iPSCs, induced pluripotent stem cells; PC, polycarbonate; PCL, polycaprolactone; PDMS, polydimethylsiloxane; PEG, polyethylene glycol; PET, polyethylene terephthalate; PMMA, poly(methylmethacrylate); PS, polystyrene; PTFE, polytetrafluoroethylene; PVC, polyvinyl chloride; RHEm, Reconstructed epidermis model; TEER, Transepithelial electrical resistance

Model type	Tissue (Cell types)	Dermal matrix	Duration on-chip	Fabrication method; materials	Flow type; velocity	Main features	Ref.
Multi organ-on-a-chip	FTSm (Primary HKns + primary HFns)	Collagen	3 days	Commercial platform (TissUse' HUMMIMIC)	Integrated micropump; $3x10^4$ µL/min	Co-culture of 2 organ models (skin and liver); Topical and systemic toxicity testing (terbinafine)	Tavares et al (2020) [84]
2D skin-on-a-chip	Cell monolayers (Immortalized HaCaT HKs + Immortalized HS27 HFns + HUVECs)	Fibronectin coating	3 days	Lithography; PDMS + PET membrane	Gravity driven flow; Not stated	TNF-α induced skin inflammation; Simulation of skin edema	Wufuer *et al* (2016) [85]
2D skin-on-a-chip	Cell monolayers (Immortalized HaCaT HKs + U937 dendritic cells)	None	20 days	Rapid prototyping; PMMA, PDMS and PET membrane	Syringe pumping; 0.6 – 1.2 µL/min	Immune competent model; TEER measurements	Ramadan *et al* (2015) [86]
2D skin-on-a-chip	Cell monolayer (Immortalized HaCaT HKs)	None	15 days	Laser cutter; PMMA + PDMS + PET membrane	Syringe pumping; 10 µL/min	Photolithography-free; Irritation testing (potassium dichromate)	Sasaki *et al* (2019) [87]
3D vascularized skin-on-a-chip	FTSm (Primary HKns + primary HFns) + iPSC-derived endothelial cells	Collagen	1 h 22d w/o perfusion	3D printing; Transwell inserts+ PET membranes	Syringe pump; Not stated	Integration of iPSC; Promotion of neovascularization during wound healing in rat model	Abaci *et al* (2016) [88]
3D vascularized skin-on-a-chip	FTSm (Primary HKns + primary HFns + HUVECs)	Collagen	10 days	3D printing; Not stated	Peristaltic pumping; 33 – 50 µL/min	Vascular channels coated with endothelial cells; Permeation testing (caffeine and ISDN)	Mori *et al* (2016) [89]
3D vascularized skin-on-a-chip	FTSm (Primary HKns + primary HFns) + HUVECs + Hypodermis model (Primary HPAs)	Fibrinogen + dECM porcine skin	7 days	3D printing; PCL	Peristaltic pumping; 50 –100 µL/min	3D cell printing; Integration of hypodermis	Kim et al (2019) [90]

Table 3.1. (Continued)

Model type	Tissue (Cell types)	Dermal matrix	Duration on-chip	Fabrication method; materials	Flow type; velocity	Main features	Ref.
3D skin-on-a-chip	FTSm (HaCaT + primary HFs + HUVECs)	Collagen	12 -14 days (5 – 7 for dermis)	Lithography; PDMS + PC membrane	Gravity driven; 5 - 10 µL/min	Studies of mass transport with Fluorescein isothiocyanate-dextran	Lee *et al* (2017) [91]
3D skin-on-a-chip	FTSm (Primary HKs + Primary HFs)	Collagen	7 days	Lithography; PDMS + PC membrane	Gravity driven; Not stated	Study of collagen contraction;	Song *et al* (2017) [92]
3D skin-on-a-chip	FTSm (Primary HKs + Primary HFs	Collagen	11 days	Lithography; PDMS + PC membrane	Gravity driven; Not stated	Uniaxial stretch applied for modelling wrinkled skin	Lim *et al* (2018) [93]
3D skin-on-a-chip	FTSm (Primary HKs + Primary HFs	Collagen	7 days	Not stated; PTFE; PET membrane	Peristaltic pumping; 20 - 167 µL/min	Formation of a thicker stratum corneum with perfusion	Strüver *et al* (2017) [94]
3D skin-on-a-chip	FTSm (Primary HKs + primary HFs)	Commercial Matriderm®	7 days	Commercial platform (TissUse' HUMMIMIC)	Integrated micropump; Not stated	Permeation of fluorescein sodium salt; TEER measurements	Schimek *et al* (2018) [95]
3D skin-on-a-chip	FTSm (Immortalized N/TERT-1 HKs + primary HFs)	Fibrin + PEG	21 days	Micromiling; PMMA + PC membrane	Peristaltic pumping; 1 µL/min	Improved differentiation and barrier function; Stable dermis;	Sriram *et al* (2018) [96]
3D skin-on-a-chip	FTSm (Immortalized HaCaT HKs + Primary HFs)	Fibrin	Not stated	Edge plotter; PMMA + PDMS + Vinyl + PC membranes	Syringe pumping; 0.67 µL/min	Parallel flow method for bilayer tissue formation	Valencia et *al* (2021) [97]

Table 3.1. (Continued)

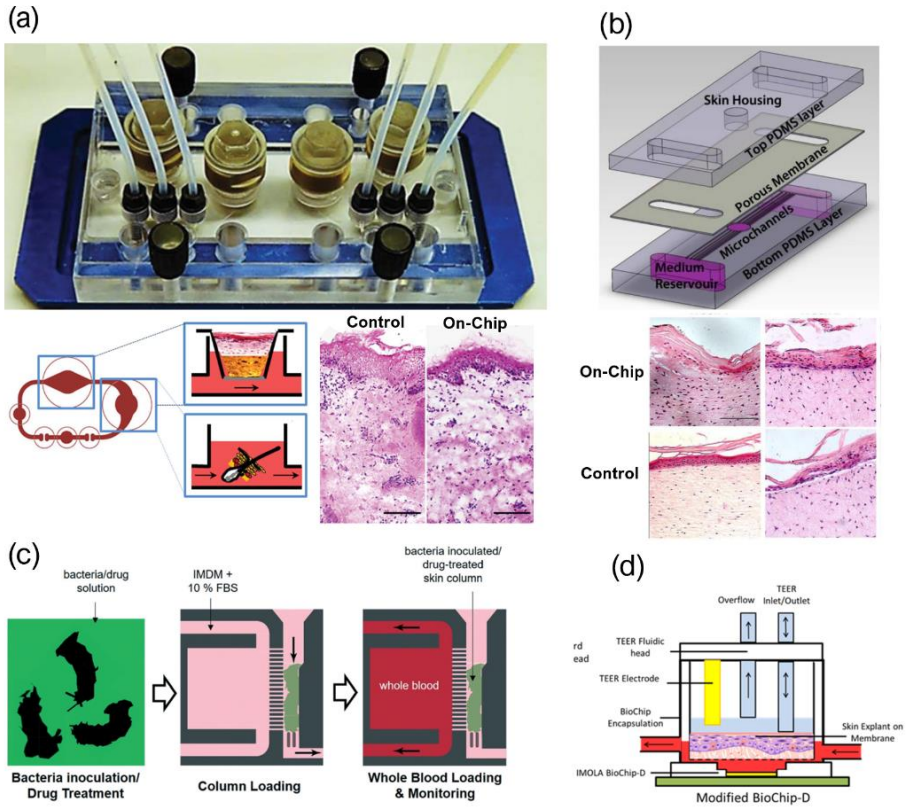

Figure 3. 6. Transferred SoC devices. (a) Multi-organ-chip for culturing a commercially available skin equivalent or ex vivo skin and a single hair follicular unit extract, developed by Ataç *et al*. Histological analysis showing maintenance of ex vivo skin for 14 days in culture [77]. (b) Pumpless SoC for the maintenance of a FTSm generated off chip, developed by Abaci *et al*. Histological analysis for skin maintained on chip for 1 week (left) and two weeks (right) [78]. (c) SoC device for simulating neutrophil responses to skin infection and antibiotic treatments, developed by Kim et al. Schematics of the ex vivo human skin and blood samples loading [79]. (d) Schematic diagram of a SoC with TEER fluidic head, developed by Alexander et al. The fluidic system with medium is highlighted in red [80]. Figure adapted from a) [77]; b) [78]; c) [79]; d) [80].

In 2015, similarly to the work by Ataç *et al*, Abaci *et al* designed and fabricated a platform for long-term maintenance of an *in vitro* FTSm (**Figure 3. 6.b**) [78]. However, instead of establishing media perfusion with the use of an integrated micropump, the group established recirculating gravity-driven flow by placing the SoC on a rocking platform. This design excluded the necessity of an external pump and tube connections resulting in easier operation. In this work, it was possible to maintain the skin barrier

function for 3 weeks. To validate the use of the developed SoC for drug toxicity studies, the group added an anticancer drug (doxorubicin) in the culture medium and compared these results with untreated SoC models. They performed H&E and immunostaining, showing the toxic effects of the drugs which affected the proliferative activity and spatial detachment of the basal layer.

More recently, Kim *et al* developed a SoC device to study neutrophil response to the presence of a bacterial infection (**Figure 3. 6.c**) [98]. The skin tissues included in the device were fragments of a human skin biopsy which was previously cultured with the bacteria. The device was fabricated using standard photolithography procedures and was composed of a blood loading channel, a channel for inserting the skin tissues. The two channels are separated by a red blood cell filter that selectively allows neutrophils to pass. As a proof of concept, the model was used to distinguish between cellulitis and pseudo-cellulitis patient samples, showing its potential for diagnosis and treatment optimization.

Alexander Jr. *et al* used an intelligent mobile lab for in vitro diagnostics (IMOLA-IVD) to monitor the TEER of a commercially available RHEm (MatTek EpiDerm®) during a period of 48h (**Figure 3. 6.c**) [80]. The group demonstrated that the system with integrated sensors could maintain a stable RHEm inside the chip while monitoring various metabolic parameters.

Recent studies focused on the development of multi-organ-chips capable of maintaining a co-culture of 3D tissues representing different organs. Until now, all the published work combining skin tissues with other organ models used the device first described by Ataç *et al* [77]. The device is commercially available by TissUse (HUMIMIC®) which enables the integration of up to four different organ models (HUMIMIC® Chip 2- Chip 4). Using TissUse' HUMIMIC® Chip2, Wagner *et al* established a co-culture of a human artificial liver model and skin biopsies [99]. The crosstalk between the tissues was observed during 2 weeks through the consumption of albumin produced in the liver by the skin tissue. Furthermore, the multi-tissue sensitivity to troglitazone, a liver toxic substance, was evaluated. The experiments revealed a sensitivity of the multi-OoC co-cultures of liver and skin equivalents to a liver toxic substance at different levels of analyses.

Maschmeyer *et al* used TissUse' HUMIMIC® Chip 4 to maintain the function of four organs (intestine, liver, skin and kidney) over 28 days in co-culture [82]. The group performed in depth metabolic and gene analysis which revealed the establishment of reproducible homeostasis among the co-cultures. This study showed the potential of the platform for repeated dose systemic toxicity of drug candidates over multiple days.

Kuhnl *et al* used the same platform for incorporation of a RHEm (EpiDerm®) and liver (HepaRG-stellate) spheroids [83]. The model was used to analyse the pharmacokinetics and pharmacodynamics of two topical substances (hyperforin and permethrin). The device made it possible to preserve the skin barrier of the model during the necessary days for drug testing. Furthermore, the group was able to use the system to provide relevant information regarding how different routes of application impact the systemic concentrations of the substances (parent and metabolites) over the course of the experiments.

Tavares *et al* also used TissUse' HUMIMIC (Chip 2) to co-culture a RHEm developed in-house and a liver model (HepaRG spheroids) [84]. The group used the device to study the topical and systemic administration of terbinafine, an antifungal medication. They assessed the substance irritancy/toxicity with 3-[4,5-dimethylthiazole-2-yl]-2,5-diphenyltetrazolium bromide (MTT) cell viability test, lactate dehydrogenase, lactate and glucose levels and gene expression The group concluded that the combination of the two tissues in the device allowed a more sensitivity assessment of the toxic effects resultant from topical application of 5% terbinafine and SDS and system application of 0.1% terbinafine.

While these studies provide valuable information regarding the use of SoC devices and their clinical and testing purposes including the multi-organ crosstalk and drug sensitivity and toxicity, the fact that the skin models are generated outside the chip limits the benefits of the dynamic culture.

3.2.2.2 Skin-on-a-chip models based on 2D cell cultures

Several research groups have been developing SoC platforms to simulate diseases and the complex interactions with the immune system. One popular approach to mimic the structure and functional responses of the human skin consists on the use of layers of 2D cells cultured on chip, mimicking different skin compartments. Using

this approach, Wufuer *et al* proposed a model consisting of 3 layers (epidermal, dermal and vascular) co-cultured inside a SoC device (**Figure 3. 7.a**) [85]. Each layer was separated by a porous membrane to allow interlayer communication. A model of skin inflammation was generated by perfusion of the model with tumour necrosis factor (TNF-α), followed by measurement of proinflammatory cytokines levels and tight junction analysis. Furthermore, the efficacy of the drug dexamethasone was evaluated using the developed inflammation model. The study demonstrated that this drug could attenuate the effects of TNF-α including endothelial barrier dysfunction.

In the same year, Ramadan *et al* described a SoC for the development of an immune competent *in vitro* skin model (**Figure 3. 7.b**) [101]. The model included a confluent layer of a human skin keratinocyte cell line (HaCaT), cultured on top of a porous membrane acting as a model of the epidermis and immune cells (leukemic monocyte lymphoma cell) positioned beneath the membrane. Silver/Silver chloride (Ag/AgCl) wires were inserted into the platform to measure the TEER, thereby monitoring the cell layer integrity through the course of cell culture and in response to chemical/physical stimuli. The group found that the perfusion-based culture promoted the barrier function and the lifespan of the cellular system. Furthermore, they investigated the effects of lipopolysaccharides (LPS) and the effects of UV radiation stimulus on the developed model. These experiments allowed the understanding of the role of the human keratinocyte (HK) layer as a protection barrier.

Sasaki *et al* developed a photolithography-free device to culture an HaCaT monolayer and perform permeation assays (**Figure 3. 7.c**) [87]. In this work, the group developed a simple platform without the use of complex microfabrication techniques which could be a barrier to some researchers. A porous membrane was sandwiched between branched microchannels and bonded using a PDMS mortar. The group tested the effect of potassium dichromate on the permeability of the cell monolayer by introducing fluorescein isothiocyanate-dextran (FITC-Dextran) solution on the top channel.

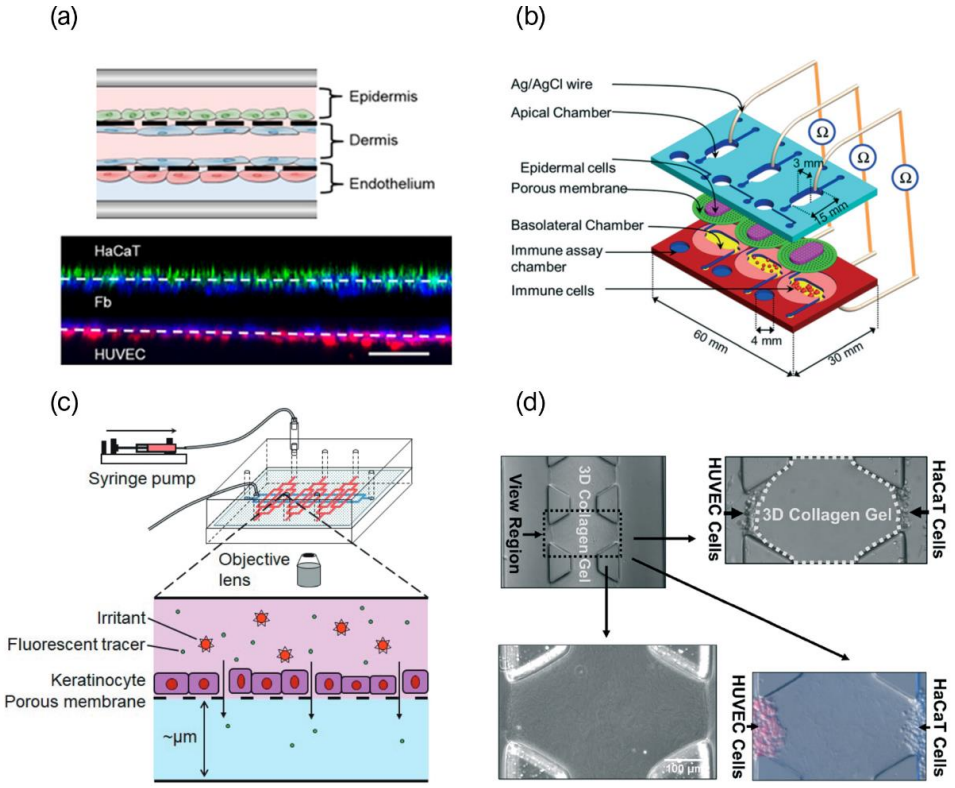

Figure 3. 7. SoC devices based on 2D cell cultures. (a) Schematic representation of SoC device, including three separate channels with four vertically stacked cell layers, developed by Wufuer et al. Z-stacked fluorescence image showing the cells adhered to the membranes [85]. (b) Schematic 3D view of the SoC device and TEER electrodes, developed by Ramadan et al. Device includes HaCat and human leukemic monocyte lymphoma cell line [86]. (c) Schematic representation of SoC for HaCat culture and parallel permeation assays, developed by Sasaki et al [87]. (d) Image showing a collagen gel in the middle gel channel of the SoC device, developed by Ren et al. HUVEC and HaCaT cells are introduced in the device, to study cell transmigration [100]. Figures adapted from a) [85]; b) [86]; c) [87]; d) [100].

More recently, Ren *et al* developed a microfluidics-based SoC model to study the effect of transendothelial and transepithelial migration of human T lymphocytes, mimicking skin inflammatory microenvironments (**Figure 3. 7.d**) [100]. The group included collagen from rat tail to mimic the *in vivo* ECM with a porous fibre structure. The gel was injected into an inlet to fully fill the channel. HaCaT and human umbilical vein endothelial cells (HUVEC) solutions were loaded into the chip and attached to both sides of the collagen gel. The device allowed the quantitative analyses of human T cell

migration under controlled chemical gradient conditions. Furthermore, the potential of the SoC for drug screening, studying the involvement of T cell trafficking during cytokine-stimulated skin inflammation.

Although several of the described studies using cell monolayers mention the creation of 3D environments, no differentiated skin structure is developed. In these studies, the skin cells are cultured directly in the microfluidic chip. However, they do not represent the 3D complexity of human skin.

3.2.2.3 Skin-on-a-chip models based on 3D cell cultures

In the last 5 years, various groups developed OoC devices for 3D skin tissue formation inside the platform. For this, two different approaches have been used, one based on the construction of dermal compartments with integrated hollow channels, mimicking the vascular networks, for medium perfusion and the other based on the use of channels, usually designed on a PDMS layer, below the skin tissue.

3.2.2.3.1 3D SoC models with vascular networks

Using the first approach, Abaci *et al* developed FTSm with micropatterned vascular networks inside the dermal compartment (**Figure 3. 8.a**)[88]. The group used 3D printing to build the moulds used to make sacrificial channels of cross-linked alginate. These microchannels were embedded in the dermal compartment composed of collagen type I and were subsequently removed using sodium citrate after epidermal cornification. The group introduced either endothelial cells derived from iPSCs or HUVECs to cover the inner surface of these channels. These cells made it possible to recapitulate the endothelial barrier function, decreasing the permeability and diffusivity of the channels when compared to the control. Furthermore, the group grafted the vascularized human skin models to immunodeficient mice. It was possible to obtain neovascularization during wound healing, showing its potential for treatment of cutaneous wounds.

Mori *et al* fabricated a culture device composed of anchoring structures and nylon wires strung across the connectors of the device (**Figure 3. 8.b**) [89]. A collagen structure was fixed into the device and perfusable vascular channels were created by removing the nylon wires. The group could recreate some features of the dermal/epidermal morphology and *in vivo* tight junctions on the vascular channel.

Furthermore, they observed an increased cell density of the perfused skin model when compared to a non-perfused skin model. However, the contraction of the collagen used for the dermal compartment impacted the permeation testing which had to be restricted to the central portion of the model.

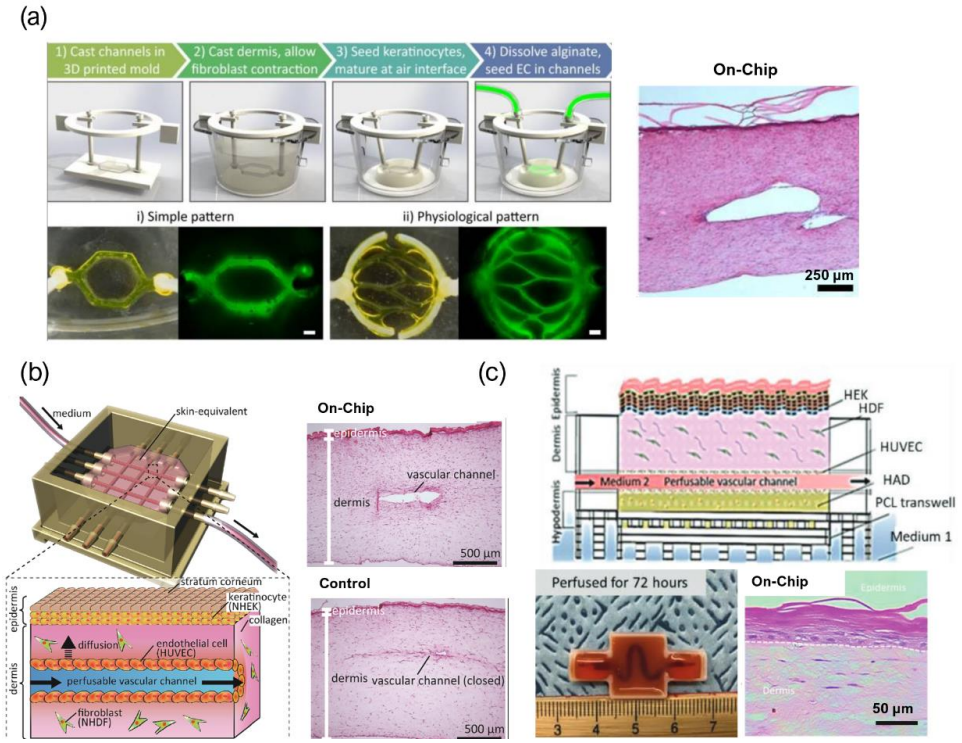

Figure 3. 8. 3D Skin-on-a-chip models with vascular networks. (a) Schematic description of the protocol to develop a vascularized skin, developed by Abaci et al. In this method, a sacrificial layer of alginate microchannels is created using 3D-printed moulds. Histological analysis of the generated SoC [88]. (b) Schematic of the SoC with integrated perfusable vascular channels, developed by Mori et al. Histological analysis of perfused and non-perfused skin [89]. (c) Schematic representation of the SoC model with vascularization developed by Kim et al, including epidermis, dermis and hypodermis. Perfusion test after 72 hours and histological analysis of the skin grown on chip [90]. Figures adapted from a) [88]; b) [89]; c) [90];

Recently, Salameh *et al* used the same device and technique as described by Mori *et al* to developed a vascularized FTSm which includes a more complex vasculature system than the models previously described [102]. The model was created with a combination of moulding, auto-assembly techniques and microfluidics and

included HFs, HKs and HUVECs. The technique used to produce hollow channels inside the collagen matrix was similar to the work by Mori et al, using nylon wires. However, to induce vasculogenesis, an additional step was included by seeding HUVECS transduced with Turbo-RFP lentiviruses (RFP-HUVECS) after pouring a first layer of collagens and HFs. After removing the nylon wires, the hollow channels were seeded with HUVECS and perfusion was initiated using a peristaltic pump. It was possible to generate a differentiated epidermis, perfusable vascular channels with angiogenic sprouts and an adjacent microvascular network. Furthermore, the potential of the model for topical and systemic applications were validated. Two compounds (caffeine and minoxidil) were topically applied to measure skin permeability and a pollutant (benzo[a]pyrene) was systemically applied.

An alternative approach for generating perfusable vascularized human skin models consists on the use of 3D cell printing. Kim *et al* used this technique for engineering a complex vascularized 3D human skin composed of epidermis, dermis and hypodermis (**Figure 3. 8.c**) [90]. Decellularized hypodermal and dermal extracellular matrices were used for casting the corresponding compartments. For vasculature generation, a bioink composed of gelatine, glycerol, and thrombin with endothelial cells embedded was printed with a cylindrical shape; once finished, the construct was incubated at 37 ºC, eliminating the gelatine and leaving hollow tubes inside the tissue. Proper tissue formation and maturation are shown in this work, along with good vascular permeability properties that could lead to a promising platform for drug and cosmetic testing and skin diseases modelling.

3.2.2.3.2 3D SoC models with basal channels

Using the most conventional approach for OoC fabrication, Lee *et al* created an device with a simple structure and gravity-induced flow system to generate 3D tissues (**Figure 3. 9.a**) [91]. The chip consisted of two layers of PDMS assembled on top of a glass base. The bottom PDMS layer consisted of the fluidic chamber and the top PDMS layer had a central chamber for the skin model formation. A polycarbonate membrane was bonded between the bottom and top layers. The skin model was composed of collagen and primary human dermal fibroblasts of neonatal origin (HDFns) mimicking the dermal compartment and primary human epidermal keratinocytes of neonatal

origin (HEKns) representing the epidermal layer. Also, to represent the vascular structure, HEKns were cultured on the bottom-side surface of the membrane. The group observed comparable expression of keratin-14, keratin-10 and loricrin when comparing with conventional, transwell-based skin models. However, the *stratum corneum* of the perfused skin was less homogeneous that the one from the conventional model. The authors hypothesized that this could be caused by and inhomogeneous distribution of nutrients or due to a "leaky" barrier function. The SoC developed by this group was used in various subsequent studies.

In the same year, Song *et al* used the described platform to compare the shrinkage of collagen between static and dynamic systems [92]. The group also studied the expression of key marker proteins (fibronectin, collagen IV and keratin 10). They observed that the contraction of the hydrogel was lowest in the dynamic system. However, the markers were less expressed in the SoC model. Furthermore, the platform was also used for studying skin aging and the effect of different drugs and formulations. By inserting permanent magnets into a dedicated cavity on the PDMS layer, Lim *et al* could stretch the membrane and develop wrinkle skin. Jeon *et al* were able to use the platform to replicate the side effects of the drug sorafenib on the skin [92]. Kim *et al* tested *Curcuma longa* leaf extract using the SoC device [103]. The group found that the skin barrier function of the epidermis was enhanced by the extract.

Strüver *et al* developed a perfusion platform to apply mechanical forces and shear stress to *in vitro* skin models (**Figure 3. 9.b**) [104]. They used bovine collagen and HDFns to develop the dermal compartment and, after solidification added primary HEKns on top of the matrix. After 1 day under submerged conditions, the skin models were transferred to the developed platform and grown for 6 days at the air-liquid interface. The device was constructed to be compatible with 6-well cell culture inserts. To assess the barrier function of the skin models, skin permeability studies were performed using reference substances (testosterone and caffeine). The perfusion resulted in the thickening of the stratum corneum and a higher compaction of the dermis equivalent. Furthermore, the group observed increased expression of filaggrin and involucrin following dynamic perfusion. However, it was not possible to obtain an improved barrier function on the dynamically cultivated skin. The group concluded that the simple perfusion of skin models might not be sufficient to produce and enhanced barrier function similar to in vivo skin.

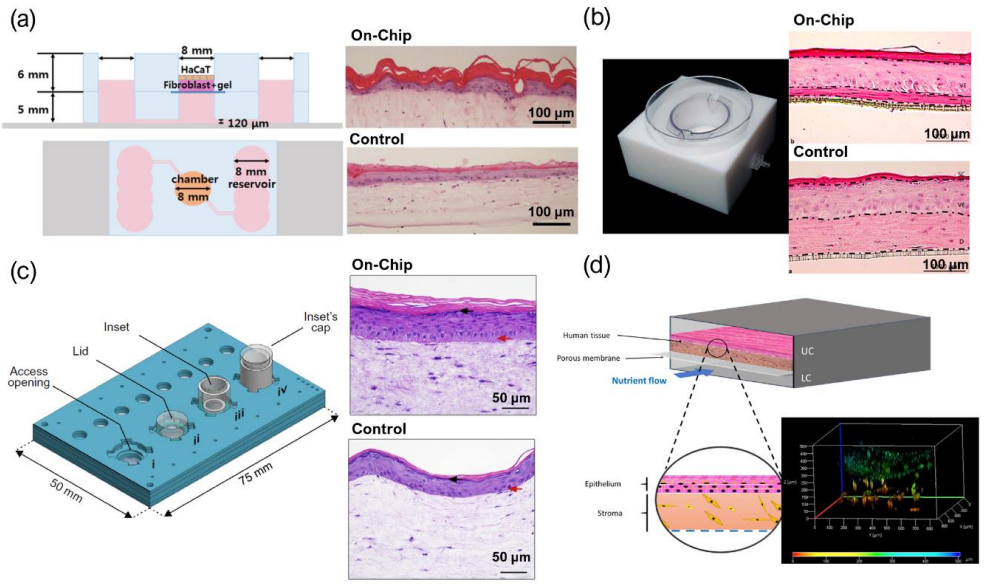

Figure 3. 9. 3D Skin-on-a-chip models with basal channels. (a) Cross section and top schematic of the SoC device developed by Lee et al. Histological evaluation of the skin tissue grown on chip and control [91]. (b) Image of the SoC platform equipped with cell culture insert, lid, and tub connectors, developed by Strüver *et al.* Histological evaluation of the skin cultured on chip and control after 7 days of cultivation [94]. (c) Schematic representation of the 4-chamber SoC device showing each unit in a different operation configuration, developed by Sriram et al. Histological evaluation of skin grown on chip for 2 weeks [96]. (d) Representative cross section of the bilayer SoC chambers, developed by Valencia et al. Confocal image of a bilayer dermo-epidermal equivalent generated on chip using parallel flow [97]. Figures adapted from a) [91]; b) [94]; c) [96]; d) [97].

Schimek *et al* used the platform provided by the company TissUse to grow a FTSm [95]. For the dermal compartment, the group used Matriderm®, a porous structure composed of bovine collagen and elastin, seeded with dermal HFns. These skin equivalents developed *in vivo*-like histological architecture, with normal differentiation marker expressions and proliferation rates.

Most of the mentioned studies included the use of animal-derived collagens to produce the dermal compartment. Consequently, they reported the poor mechanical properties resultant from the fibroblast-mediated matrix contraction and matrix degradation. These phenomena decreased reproducibility, limited the SoC lifespan as well its applicability. Moreover, the groups also reported lack of attachment of the

culture to the membrane and chip walls due to acute shrinkage. Recently, to overcome these problems, groups proposed chemical and physical modification of the matrix adding synthetic or natural polymers.

Sriram *et al* developed a model based on the use of fibrin that could overcome the typical limitations of current SoC devices which use animal-derived hydrogel for the dermal compartment (**Figure 3. 9.c**) [96]. As both pure collagen and fibrin present poor mechanical stability, the group developed a modified biomaterial by combining fibrinogen with PEG. This mixture was combined with fibroblasts and the gelation was initiated by adding human thrombin. The volume of the final mixture to be pipetted into the SoC device was optimized to produce a flat surface on the day of keratinocytes seeding pipetted. The device was composed of a multi-chamber microfluidic chip consisting of two fluidic compartments separated by a permeable microporous membrane. The device also included interchangeable lids and insets to switch from bioreactor to an in vitro analysis system. Using the developed device, the group generated a stratified epidermis with enhanced basement membrane. In particular, the deposition of collagen IV, VII and XVII were enhanced when comparing with the control. The TEER values were also higher than the controls, pointing to an enhanced barrier function.

Valencia *et al* developed a 3D skin model including a dermal and epidermal compartment using a different approach (**Figure 3. 9.d**) [97]. The group developed a controlled parallel flow method to generate a bilayer tissue by using syringe pumps. The HaCaT cell line and HFs were used to generate the model. In a similar approach to Sriram *et al*, the group used human fibrinogen to form a fibrin hydrogel for the dermal compartment. Thrombin and tranexamic acid were added to the fibrinogen to prepare a pregel (no gelled fibrinogen solution). The device was fabricated using and edge plotter and included two PMMA layers, one PDMS layer, vinyl upper and lower chambers and an integrated polycarbonate membrane. Contrary to conventional systems where cells are manually pipetted into the culture channels, the group was able to inject all components (cells and ECM) directly into the channels using syringe pumps. With the developed approach, it was possible to obtain a 3D dermal compartment with HFs and HKs on top to simulate the epithelial compartment. Although this is a promising approach that could increase automatization and standardization, no differentiated epidermis was produced and no air-liquid interface was established.

3.2.2.4 Skin-on-a-chip models for permeation

Traditional permeation methods, typically using Franz diffusion cells, present multiple limitations including low precision, low throughput and relatively high costs. Microfluidic platforms can offer an alternative to the traditional permeation methods. Multiple SoC platforms have been proposed that focus exclusively on skin permeation tests, typically using synthetic skin substitutes or *ex vivo* animal skin.

Mah *et al* developed a miniaturized flow-through diffusion cell to study the permeation of endoxifen, an anti-estrogenic agent with limited availability (**Figure 3. 10.a**) [105]. The device was fabricated using PDMS and utilized minimal amounts of drug for the permeation studies. Rat abdominal skin was mounted between the donor and receptor compartments with the stratum corneum facing the donor compartment. The permeation studies of endoxifen attained the targeted flux and demonstrated the potential of the platform to investigate expensive and/or limited drugs during the pre-formulation studies.

Provin *et al* fabricated a device for percutaneous absorption assays of molecules for pharmaceutical and cosmetology purposes (**Figure 3. 10.b**) [109]. The device consisted of a donor and a receptor compartment made of PDMS and a middle membrane coated with lipids to act as an artificial stratum corneum. The different compartments and the membrane were bonded together using oxygen plasma. The measurement of the diffusion profile followed by the calculation of the permeability coefficients and time lag were performed on seven different molecules and obtained data positively fit with those available from literature on human skin penetration.

Both of the described permeability devices were made of PDMS, a material unsuitable for industrial mass production, incompatible with organic solvents and known to exhibit significant adsorption of small hydrophobic compounds. Recently, Alberti *et al* and Lukács *et al* developed SoC for permeation assays using materials alternative to PDMS [107, 108].

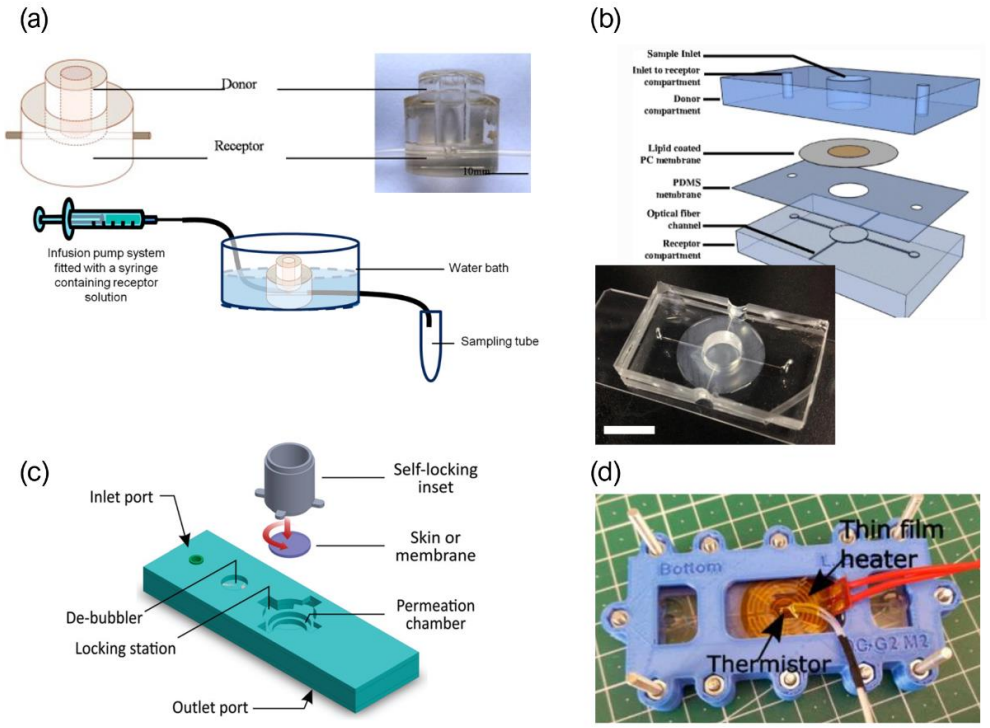

Figure 3. 10. Skin-on-a-chip platforms for permeation assays. (a) Schematic diagram of the donor and receptor compartments and fully assembly of miniaturized flow-through cell, developed by Mah *et al* [105]. (b) Exploded schematic view of the device developed by Provin *et al*. Photograph of the final microdevice bonded on a glass slide. Scale bar is 1 cm [106]. (c) Illustration of a single permeation unit including a self-locking inset mechanism that enables sealing of the skin tissue or membrane, developed by Alberti *et al* [107]. (d) Bottom side of the developed SoC including a circular film heater and thermistor, developed by Lukács *et al* [108]. Figures adapted from a) [105]; b) [106]; c) [107]; d) [108].

Alberti *et al* presented a novel microfluidic platform enabling high throughput skin permeation testing in a flow-through design at a fraction of the material cost of Franz diffusion cells (**Figure 3. 10.c**) [107]. The SoC were made of polycarbonate and included PTFE filter membranes and silicone rubber connectors. The group validated the platform against the Franz cells by comparing the transport of 3 chemicals of varying lipophilicity (caffeine, salicylic acid and testosterone). The group used a reconstructed FTSm and showed that the platform minimizes the effect of unstirred water layers that occur in conventional Franz diffusion cells.

More recently, Lukács *et al* developed a microfluidic diffusion chamber for *in vitro*/*ex vivo* monitoring of transdermal delivery of topical drugs (**Figure 3. 10.d**) [108]. The device is made of three functional elements: on top is a donor compartment where the examined compound (in this case cream) is poured; in the middle is an integrated skin sample (or alternatively a membrane), and in the bottom is the receptor compartment. The device was fabricated using polymer-based techniques, surrounded by PMMA and polylactic acid (PLA) and it included a temperature-controlled module The group used caffeine as a hydrophilic model drug and an *ex vivo* animal model (rat origin). The group concluded that the SoC device provided similar information to the Frans cells regarding the characteristics, degree, and speed of absorption of the test drug through the dermal barrier.

3.3 Challenges and future perspectives

Taken together, these studies demonstrate the potential of SoC platforms for a multitude of applications ranging from disease modelling to drug testing. However, by comparing the observations from the different groups it is possible to observe inconsistencies regarding the effects of the OoC technology on the skin architecture and physiology. Some groups even report negative effects from the development of skin models inside the chip, with dynamic perfusion. This is the case of the work from Lee *et al* in which dynamic perfusion resulted in a negative effect on the *stratum corneum* homogeneity, resulting in a "leakier" barrier [91]. Moreover, Song *et al* observed that key differentiation markers were less expressed in the SoC model when comparing to the control. Other groups reported a comparable architecture between SoC and conventional skin models [92]. Strüver *et al* reported that the dynamically cultivated skin did not present an improved barrier function and hypothesized that simple perfusion of skin models might not be sufficient to produce and enhanced barrier function similar to *in vivo* skin [104]. Schimek *et al* also reported the development of SoC with architecture and differentiation markers comparable to the conventional skin models generated without perfusion [95]. One of the most promising results comes from the works of Sriram *et al* [96]. This group demonstrated that the dynamic perfusion and control of the microenvironment can improve the epidermal differentiation and consequently the skin barrier function. They hypothesised that the dynamic perfusion

can enhance the transport of nutrients inside the SoC and induce *in vivo*-like shear stress and mechanotransduction mechanisms. Furthermore, the peristaltic flow could induce mechanical stretching, which was previously shown to yield higher expression of basement membrane components and a thicker epidermis.

The different results obtained by the groups working with SoC devices can be explained by their widely different approaches regarding the materials used and the cell types, chip design and type of flow. In particular, the nature of cells used in the FTSm can compromise the ability to generated fully-differentiated SoC models and their overall reproducibility. Many researchers use primary cells to generate the SoC models, which is considered a key point for the development of physiological relevant *in vitro* skin. However, these cells present limited population doublings and limited reproducibility. Other groups report the use of cell lines, such as HaCaT cells without successful reproduction of 3D structure. At present, Sriram *et al* are the only group that developed a SoC using TERT-immortalized keratinocytes [96]. It would be important to understand, for example, if the effects of perfusion and mechanical forces on the generated SoC depend on the types of cells used.

An important parameter that also extensively varies in the reported studies and that can affect the final structure and applicability of the SoC model is the material used for generating the dermal compartment. The *in-vivo* ECM comprises multiple types of collagens, various fibrous proteins and proteoglycans. It is common for SoC models to comprise exclusively type 1 collagen. Not only this is not representative of the *in-vivo* like microenvironment but also results in fibroblast-mediated matrix contraction and matrix degradation. This phenomenon limits their lifespan and reproducibility. Furthermore, collagen detachment inside the SoC platform can lead to a multitude of problems including the maintenance of a leak-free fluid-tissue-air barrier. The use of collagen to generate several SoC models can explain some of the inconsistencies specially regarding the results from permeation testing which require leak-free barriers. The polymers or hydrogels should not only mimic the biophysical properties of the skin but also remain stable during cell culture. To achieve this, some groups proposed chemical or physical modifications of the matrix adding synthetic or natural polymers. In particular the combination of fibrinogen and PEG proposed by Sriram *et al* can be a promising approach to generate stable and physiological relevant dermis structures towards a successfully model.

Other relevant parameters should be further investigated and fine-tuned towards the development of reproducible and standardized SoC models. This is the case of the perfusion rates which, at the moment, range from 1 μL/min to 125 μL/min depending on the publication. Air flow and gas composition of the skin compartment exposed to the air can also be relevant parameters to produce models with improved stratification and homeostasis. This also differs between the different studies with some groups employing active ventilation using peristaltic pumping and other groups employing passive ventilation.

Although the use of SoC devices for production of biomimetic skin is still in its infancy, much progress has been made in this field. These devices have been used to simulate diseases, bacterial infection and test drugs and compounds regarding toxicity, efficacy and permeation. Furthermore, the first steps have been done to establish a co-culture of different tissues to study the systemic effect of topically applied drugs. However, to achieve an advanced platform capable of replacing animal testing for topically applied drugs, further improvement is needed.

First, for these SoC devices to become mainstream tools in biology laboratories it is important to solve current challenges related to design, manufacturability and usability. Most of the mentioned works used traditional lithography technology for the fabrication of PDMS devices, limiting its potential to be mass produced. Alternative techniques using different micropatterning technologies and materials such as PMMA, PVC or polycarbonate should be used. Importantly, these platforms should be self-sufficient, robust, simple to operate and allow multiple specimens to be cultured in parallel, reducing the production costs.

Furthermore, an advanced SoC device should include integrated sensors, chosen depending on the particular context and goal. Conventional OoC are irreversibly sealed, usually through plasma bonding, making it difficult the complete removal of the tissue at the end of an experiment. Most of the studies use fluorescent-labelled cells for visual inspection under the microscope. However, this becomes increasingly more difficult when producing physiologically relevant 3D models. Other groups complement their analysis with TEER measurements. This is a promising parameter for quantitative analysis of the skin barrier. Integrated biosensors will be crucial to monitor the skin in real time for quality control and also to study the effect of

test drugs. Furthermore, since the standard characterization of the skin model requires histological analysis and immunohistochemistry it should be possible to easily open the device for tissue retrieval. Ideally, the SoC device should have a modular microfluidic circuit with interchangeable modules and sensors to suit the specific requirements of an experiment.

Regarding the biological components, the dermal compartment should not include animal derived materials. In the advanced SoC model, the ECM should reflect the *in vivo* human microenvironment. This could be achieved, for example, using a fibroblast-derived-matrix in which the dermal cells are stimulated to produce their own components. This could be combined with a scaffold structure to give the necessary mechanical stability during tissue culture inside the chip. Alternatively, a stable human-derived hydrogel should be used. Furthermore, current biomimicry is limited by the cells and appendages incorporated in the SoC. Additional cell types such as melanocytes, Merkel cells and immune cells as well as appendages such as sweat glands could also be integrated to expand the applicability of future models. However, the trade-off between complexity and reproducibility needs to be considered. The need for additional cells and appendages will be dependent on the application and, in a first instance, the main focus should be to optimize and standardize a SoC with co-culture of a differentiated epidermis and 3D dermis. Additionally, the use of iPSCs derived from specific patients could become an important tool for personalized medicine, to model healthy and disease characteristics tailored to the patient. Taking into account the high costs and low yield and reproducibility when using iPSC, it is crucial for lab-automation to be implemented in parallel.

The development of physiological relevant SoC models is crucial to obtain a useful tool to study the efficacy and toxicity of transdermally delivered drugs and to evaluate the systemic effects of compounds if connected with other OoCs (multi-OoC). It could also be important to model both physiological and pathological skin conditions including skin cancer, expanding our comprehension of skin biology and making it possible to develop better drugs.

3.4 References

[1] Q. Wu *et al.*, "Organ-on-a-chip: recent breakthroughs and future prospects," *Biomed. Eng.*

Online, vol. 19, no. 1, p. 9, 2020.

[2] C. L. Thompson, S. Fu, M. M. Knight, and S. D. Thorpe, "Mechanical Stimulation: A Crucial Element of Organ-on-Chip Models," *Front. Bioeng. Biotechnol.*, vol. 8, p. 602646, Dec. 2020.

[3] N. Franzen, W. H. van Harten, V. P. Retèl, P. Loskill, J. van den Eijnden-van Raaij, and M. IJzerman, "Impact of organ-on-a-chip technology on pharmaceutical R&D costs," *Drug Discov. Today*, vol. 24, no. 9, pp. 1720–1724, 2019.

[4] T. Kilic, F. Navaee, F. Stradolini, P. Renaud, and S. Carrara, "Organs-on-chip monitoring: sensors and other strategies," *Microphysiological Syst. Vol 2 (September 2018) Microphysiological Syst.*, 2018.

[5] K. Ronaldson-Bouchard and G. Vunjak-Novakovic, "Organs-on-a-Chip: A Fast Track for Engineered Human Tissues in Drug Development," *Cell Stem Cell*, vol. 22, no. 3, pp. 310–324, 2018.

[6] A. O. Stucki *et al.*, "A lung-on-a-chip array with an integrated bio-inspired respiration mechanism," *Lab Chip*, vol. 15, no. 5, pp. 1302–1310, 2015.

[7] J. Deng *et al.*, "Engineered Liver-On-A-Chip Platform to Mimic Liver Functions and Its Biomedical Applications: A Review," *Micromachines* , vol. 10, no. 10. 2019.

[8] A. Agarwal, J. A. Goss, A. Cho, M. L. McCain, and K. K. Parker, "Microfluidic heart on a chip for higher throughput pharmacological studies," *Lab Chip*, vol. 13, no. 18, pp. 3599–3608, 2013.

[9] R. Mittal *et al.*, "Organ-on-chip models: Implications in drug discovery and clinical applications," *J. Cell. Physiol.*, vol. 234, no. 6, pp. 8352–8380, Jun. 2019.

[10] O. Yesil-Celiktas *et al.*, "Mimicking Human Pathophysiology in Organ-on-Chip Devices," *Adv. Biosyst.*, vol. 2, no. 10, p. 1800109, Oct. 2018.

[11] A. Sontheimer-Phelps, B. A. Hassell, and D. E. Ingber, "Modelling cancer in microfluidic human organs-on-chips," *Nat. Rev. Cancer*, vol. 19, no. 2, pp. 65–81, 2019.

[12] V. Palaninathan *et al.*, "Multi-organ on a chip for personalized precision medicine," *MRS Commun.*, vol. 8, no. 3, pp. 652–667, 2018.

[13] S. Basak, "Unlocking the future: converging multi-organ-on-a-chip on the current biomedical sciences," *Emergent Mater.*, vol. 3, no. 5, pp. 693–709, 2020.

[14] N. Lin *et al.*, "Repeated dose multi-drug testing using a microfluidic chip-based coculture of human liver and kidney proximal tubules equivalents," *Sci. Rep.*, vol. 10, no. 1, p. 8879, 2020.

[15] V. De Gregorio *et al.*, "Intestine-Liver Axis On-Chip Reveals the Intestinal Protective Role on Hepatic Damage by Emulating Ethanol First-Pass Metabolism ," *Frontiers in Bioengineering and Biotechnology* , vol. 8. p. 163, 2020.

[16] J. H. Sung *et al.*, "Recent Advances in Body-on-a-Chip Systems," *Anal. Chem.*, vol. 91, no. 1, pp. 330–351, 2019.

[17] N. Picollet-D'hahan, A. Zuchowska, I. Lemeunier, and S. Le Gac, "Multiorgan-on-a-Chip: A Systemic Approach To Model and Decipher Inter-Organ Communication," *Trends Biotechnol.*, vol. 39, no. 8, pp. 788–810, 2021.

[18] C. Oleaga *et al.*, "Multi-Organ toxicity demonstration in a functional human in vitro system composed of four organs," *Sci. Rep.*, vol. 6, no. August 2015, pp. 1–17, 2016.

[19] S. Schneider, D. Gruner, A. Richter, and P. Loskill, "Membrane integration into PDMS-free microfluidic platforms for organ-on-chip and analytical chemistry applications," *Lab Chip*, vol. 21, no. 10, pp. 1866–1885, 2021.

[20] M. H. Mohammadi *et al.*, "Skin Diseases Modeling using Combined Tissue Engineering and Microfluidic Technologies," *Adv. Healthc. Mater.*, vol. 5, no. 19, pp. 2459–2480, 2016.

[21] E. Sutterby, P. Thurgood, S. Baratchi, K. Khoshmanesh, and E. Pirogova, "Microfluidic Skin-on-a-Chip Models: Toward Biomimetic Artificial Skin," *Small*, vol. 16, no. 39, pp. 1–17, 2020.

[22] L. Celleno and F. Tamburi, "Chapter 1 - Structure and Function of the Skin," in *Personal Care & Cosmetic Technology*, A. Tabor and R. M. B. T.-N. C. Blair, Eds. Boston: William Andrew Publishing, pp. 3–45, 2009.

[23] R. Huggenberger and M. Detmar, "The Cutaneous Vascular System in Chronic Skin Inflammation," *J. Investig. Dermatology Symp. Proc.*, vol. 15, no. 1, pp. 24–32, Dec. 2011.

[24] D. S. Foster, R. E. Jones, R. C. Ransom, M. T. Longaker, and J. A. Norton, "The evolving relationship of wound healing and tumor stroma," *JCI insight*, vol. 3, no. 18, p. e99911, Sep. 2018.

[25] M. Kashani-Sabet, R. W. Sagebiel, C. M. M. Ferreira, M. Nosrati, and J. R. Miller III, "Vascular Involvement in the Prognosis of Primary Cutaneous Melanoma," *Arch. Dermatol.*, vol. 137, no. 9, pp. 1169–1173, Sep. 2001.

[26] G. Cevc and U. Vierl, "Spatial distribution of cutaneous microvasculature and local drug clearance after drug application on the skin," *J. Control. Release*, vol. 118, no. 1, pp. 18–26, 2007.

[27] M. Lovett, K. Lee, A. Edwards, and D. L. Kaplan, "Vascularization strategies for tissue engineering," *Tissue Eng. Part B. Rev.*, vol. 15, no. 3, pp. 353–370, Sep. 2009.

[28] H. Shahin, M. Elmasry, I. Steinvall, F. Söberg, and A. El-Serafi, "Vascularization is the next challenge for skin tissue engineering as a solution for burn management," *Burn. trauma*, vol. 8, pp. tkaa022–tkaa022, Aug. 2020.

[29] L. Chen *et al.*, "Pre-vascularization Enhances Therapeutic Effects of Human Mesenchymal Stem Cell Sheets in Full Thickness Skin Wound Repair," *Theranostics*, vol. 7, no. 1, pp. 117–131, Jan. 2017.

[30] F. Groeber *et al.*, "A first vascularized skin equivalent as an alternative to animal experimentation," *ALTEX*, vol. 33, no. 4, pp. 415–422, 2016.

[31] M. W. Laschke and M. D. Menger, "Vascularization in Tissue Engineering: Angiogenesis versus Inosculation," *Eur. Surg. Res.*, vol. 48, no. 2, pp. 85–92, 2012.

[32] L. C. Delon *et al.*, "A systematic investigation of the effect of the fluid shear stress on Caco-2 cells towards the optimization of epithelial organ-on-chip models," *Biomaterials*, vol. 225, p. 119521, 2019.

[33] K. Kaarj and J. Y. Yoon, "Methods of delivering mechanical stimuli to Organ-on-a-Chip," *Micromachines*, vol. 10, no. 10, 2019.

[34] Y. I. Wang and M. L. Shuler, "UniChip enables long-term recirculating unidirectional perfusion with gravity-driven flow for microphysiological systems," *Lab Chip*, vol. 18, no. 17, pp. 2563–2574, 2018.

[35] Y. Zhang *et al.*, "Recent advances in 3D bioprinting of vascularized tissues," *Mater. Des.*, vol. 199, p. 109398, 2021.

[36] D. G. B.-B. V. T. M. M. T.-S. A. and P. for in vitro S. Hwang, Y.-M. Choi, and J. Jang, "3D Bioprinting-Based Vascularized Tissue Models Mimicking Tissue-Specific Architecture and Pathophysiology for in vitro Studies," *Front. Bioeng. Biotechnol.*, vol. 9, p. 685507, May 2021.

[37] J. Vanderburgh, J. A. Sterling, and S. A. Guelcher, "3D Printing of Tissue Engineered Constructs for In Vitro Modeling of Disease Progression and Drug Screening," *Ann. Biomed. Eng.*, vol. 45, no. 1, pp. 164–179, Jan. 2017.

[38] R. Augustine, "Skin bioprinting: a novel approach for creating artificial skin from synthetic and natural building blocks," *Prog. Biomater.*, vol. 7, no. 2, pp. 77–92, Jun. 2018.

[39] L. Valencia and J. L. Jorcano, "Skin-on-a-chip models : General overview and future perspectives Skin-on-a-chip models : General overview and future perspectives," vol. 030901, no. May, 2021.

[40] F. Martino, A. R. Perestrelo, V. Vinarský, S. Pagliari, and G. Forte, "Cellular Mechanotransduction: From Tension to Function," *Front. Physiol.*, vol. 9, p. 824, Jul. 2018.

[41] M. M. Janaszak, R. P. Wolfe, and T. Ahsan, "Chapter 2 - Biomechanics in Stem Cell Manufacturing," J. M. S. Cabral, C. Lobato de Silva, L. G. Chase, and M. B. T.-S. C. M. Margarida Diogo, Eds. Boston: Elsevier, pp. 27–42, 2016.

[42] J. H.-C. Wang, B. P. Thampatty, J.-S. Lin, and H.-J. Im, "Mechanoregulation of gene expression in fibroblasts," *Gene*, vol. 391, no. 1–2, pp. 1–15, Apr. 2007.

[43] L. Shelton and J. S. Rada, "Effects of cyclic mechanical stretch on extracellular matrix synthesis by human scleral fibroblasts," *Exp. Eye Res.*, vol. 84, no. 2, pp. 314–322, Feb. 2007.

[44] E. Tokuyama, Y. Nagai, K. Takahashi, Y. Kimata, and K. Naruse, "Mechanical stretch on human skin equivalents increases the epidermal thickness and develops the basement membrane," *PLoS One*, vol. 10, no. 11, pp. 1–12, 2015.

[45] D. Lü *et al.*, "Asymmetric migration of human keratinocytes under mechanical stretch and cocultured fibroblasts in a wound repair model," *PLoS One*, vol. 8, no. 9, pp. e74563–e74563, Sep. 2013.

[46] W. Zhang, G. Huang, and F. Xu, "Engineering Biomaterials and Approaches for Mechanical Stretching of Cells in Three Dimensions ," *Frontiers in Bioengineering and Biotechnology* , vol. 8. p. 1151, 2020.

[47] D. D. Huh, "A human breathing lung-on-a-chip," *Ann. Am. Thorac. Soc.*, vol. 12 Suppl 1, no. Suppl 1, pp. S42–S44, Mar. 2015.

[48] D. Huh *et al.*, "A human disease model of drug toxicity-induced pulmonary edema in a lung-on-a-chip microdevice," *Sci. Transl. Med.*, vol. 4, no. 159, 2012.

[49] C. P. Gayer and M. D. Basson, "The effects of mechanical forces on intestinal physiology and pathology," *Cell. Signal.*, vol. 21, no. 8, pp. 1237–1244, Aug. 2009.

[50] Q. Zhao, T. Cole, Y. Zhang, and S.-Y. Tang, "Mechanical Strain-Enabled Reconstitution of Dynamic Environment in Organ-on-a-Chip Platforms: A Review," *Micromachines*, vol. 12, no. 7, p. 765, Jun. 2021.

[51] C. M. Sakolish, M. B. Esch, J. J. Hickman, M. L. Shuler, and G. J. Mahler, "Modeling Barrier Tissues In Vitro: Methods, Achievements, and Challenges," *EBioMedicine*, vol. 5, pp. 30–39, 2016.

[52] T. Pasman, D. Grijpma, D. Stamatialis, and A. Poot, "Flat and microstructured polymeric membranes in organs-on-chips," *J. R. Soc. Interface*, vol. 15, no. 144, 2018.

[53] D. I. Walsh, D. S. Kong, S. K. Murthy, and P. A. Carr, "Enabling Microfluidics: from Clean Rooms to Makerspaces," *Trends Biotechnol.*, vol. 35, no. 5, pp. 383–392, 2017.

[54] V. V. Abhyankar, M. Wu, C. Y. Koh, and A. V. Hatch, "A reversibly sealed, easy access, modular (SEAM) microfluidic architecture to establish in vitro tissue interfaces," *PLoS One*, vol. 11, no. 5, pp. 1–20, 2016.

[55] Q. Xue *et al.*, "A novel brain neurovascular unit model with neurons, astrocytes and microvascular endothelial cells of rat," *Int. J. Biol. Sci.*, vol. 9, no. 2, pp. 174–189, 2013.

[56] K. A. Homan *et al.*, "Bioprinting of 3D Convoluted Renal Proximal Tubules on Perfusable Chips," *Sci. Rep.*, vol. 6, no. 1, p. 34845, 2016.

[57] B. W. Graf and S. A. Boppart, "Imaging and Analysis of Three-Dimensional Cell Culture Models BT - Live Cell Imaging: Methods and Protocols," D. B. Papkovsky, Ed. Totowa, NJ: Humana Press, pp. 211–227, 2010.

[58] Y. B. Arlk *et al.*, "Barriers-on-chips: Measurement of barrier function of tissues in organs-

on-chips," *Biomicrofluidics*, vol. 12, no. 4, pp. 1–13, 2018.

[59] Y. S. Zhang *et al.*, "Multisensor-integrated organs-on-chips platform for automated and continual in situ monitoring of organoid behaviors," *Proc. Natl. Acad. Sci. U. S. A.*, vol. 114, no. 12, pp. E2293–E2302, 2017.

[60] J. Yeste, X. Illa, C. Gutiérrez, M. Solé, A. Guimerà, and R. Villa, "Geometric correction factor for transepithelial electrical resistance measurements in transwell and microfluidic cell cultures," *J. Phys. D. Appl. Phys.*, vol. 49, no. 37, 2016.

[61] O. Y. F. Henry, R. Villenave, M. J. Cronce, W. D. Leineweber, M. A. Benz, and D. E. Ingber, "Organs-on-chips with integrated electrodes for trans-epithelial electrical resistance (TEER) measurements of human epithelial barrier function," *Lab Chip*, vol. 17, no. 13, pp. 2264–2271, 2017.

[62] B. Srinivasan, A. R. Kolli, M. B. Esch, H. E. Abaci, M. L. Shuler, and J. J. Hickman, "TEER Measurement Techniques for In Vitro Barrier Model Systems," *J. Lab. Autom.*, vol. 20, no. 2, pp. 107–126, 2015.

[63] Ebrary, "Measurement of Transepithelial Electrical Resistance (TEER)." [Online]. Available: https://ebrary.net/24380/health/measurement_transepithelial_electrical_resistance_teer.

[64] L. J. van den Broek, L. I. J. C. Bergers, C. M. A. Reijnders, and S. Gibbs, "Progress and Future Prospectives in Skin-on-Chip Development with Emphasis on the use of Different Cell Types and Technical Challenges," *Stem Cell Rev. Reports*, vol. 13, no. 3, pp. 418–429, 2017.

[65] C. A. Brohem, L. B. da Silva Cardeal, M. Tiago, M. S. Soengas, S. B. de Moraes Barros, and S. S. Maria-Engler, "Artificial skin in perspective: concepts and applications," *Pigment Cell Melanoma Res.*, vol. 24, no. 1, pp. 35–50, Feb. 2011.

[66] M. H. Jung, S. M. Jung, and H. S. Shin, "Co-stimulation of HaCaT keratinization with mechanical stress and air-exposure using a novel 3D culture device," *Sci. Rep.*, vol. 6, no. May, pp. 1–7, 2016.

[67] C. M. A. Reijnders, A. Van Lier, S. Roffel, D. Kramer, R. J. Scheper, and S. Gibbs, "Development of a Full-Thickness Human Skin Equivalent in Vitro Model Derived from TERT-Immortalized Keratinocytes and Fibroblasts," *Tissue Eng. - Part A*, vol. 21, no. 17–18, pp. 2448–2459, 2015.

[68] K. Takahashi and S. Yamanaka, "Induction of Pluripotent Stem Cells from Mouse Embryonic and Adult Fibroblast Cultures by Defined Factors," *Cell*, vol. 126, no. 4, pp. 663–676, Aug. 2006.

[69] K. Gledhill, Z. Guo, N. Umegaki-Arao, C. A. Higgins, M. Itoh, and A. M. Christiano, "Melanin transfer in human 3D skin equivalents generated exclusively from induced pluripotent stem cells," *PLoS One*, vol. 10, no. 8, pp. 1–16, 2015.

[70] C. Frantz, K. M. Stewart, and V. M. Weaver, "The extracellular matrix at a glance," *J. Cell Sci.*, vol. 123, no. Pt 24, pp. 4195–4200, Dec. 2010.

[71] E. Roig-Rosello and P. Rousselle, "The Human Epidermal Basement Membrane: A Shaped and Cell Instructive Platform That Aging Slowly Alters," *Biomolecules* , vol. 10, no. 12. 2020.

[72] S. Sanyal, M. Kosovsky, "Materials and assay systems used for three-dimensional cell culture," *Technology Platforms for 3D Cell Culture*, 2017

[73] C. Lotz, F. F. Schmid, E. Oechsle, M. G. Monaghan, H. Walles, and F. Groeber-Becker, "Cross-linked Collagen Hydrogel Matrix Resisting Contraction to Facilitate Full-Thickness Skin Equivalents," *ACS Appl. Mater. Interfaces*, vol. 9, no. 24, pp. 20417–20425, 2017.

[74] A. El Ghalbzouri, S. Commandeur, M. H. Rietveld, A. A. Mulder, and R. Willemze, "Replacement of animal-derived collagen matrix by human fibroblast-derived dermal matrix for human skin equivalent products," *Biomaterials*, vol. 30, no. 1, pp. 71–78, 2009.

[75] C. P. Ng and M. A. Swartz, "Fibroblast alignment under interstitial fluid flow using a novel 3-D tissue culture model," *Am. J. Physiol. Circ. Physiol.*, vol. 284, no. 5, pp. H1771–H1777, May 2003.

[76] M. A. Swartz and M. E. Fleury, "Interstitial Flow and Its Effects in Soft Tissues," *Annu. Rev. Biomed. Eng.*, vol. 9, no. 1, pp. 229–256, Jul. 2007.

[77] B. Ataç *et al.*, "Skin and hair on-a-chip: In vitro skin models versus ex vivo tissue maintenance with dynamic perfusion," *Lab Chip*, vol. 13, no. 18, pp. 3555–3561, 2013.

[78] H. E. Abaci, K. Gledhill, Z. Guo, A. M. Christiano, and M. L. Shuler, "Pumpless microfluidic platform for drug testing on human skin equivalents," *Lab Chip*, vol. 15, no. 3, pp. 882–888, 2015.

[79] J. J. Kim *et al.*, "A microscale, full-thickness, human skin on a chip assay simulating neutrophil responses to skin infection and antibiotic treatments," *Lab Chip*, vol. 19, no. 18, pp. 3094–3103, 2019.

[80] F. A. Alexander, S. Eggert, and J. Wiest, "Skin-on-a-chip: Transepithelial electrical resistance and extracellular acidification measurements through an automated air-liquid interface," *Genes (Basel).*, vol. 9, no. 2, 2018.

[81] I. Wagner *et al.*, "A dynamic multi-organ-chip for long-term cultivation and substance testing proven by 3D human liver and skin tissue co-culture," *Lab Chip*, vol. 13, no. 18, pp. 3538–3547, 2013.

[82] I. Maschmeyer *et al.*, "A four-organ-chip for interconnected long-term co-culture of human intestine, liver, skin and kidney equivalents," *Lab Chip*, vol. 15, no. 12, pp. 2688–2699, 2015.

[83] J. Kühnl *et al.*, "Characterization of application scenario-dependent pharmacokinetics

and pharmacodynamic properties of permethrin and hyperforin in a dynamic skin and liver multi-organ-chip model," *Toxicology*, vol. 448, no. November 2020, 2021.

[84] R. S. N. Tavares *et al.*, "Toxicity of topically applied drugs beyond skin irritation: Static skin model vs. Two organs-on-a-chip," *Int. J. Pharm.*, vol. 589, no. April, p. 119788, 2020.

[85] M. Wufuer *et al.*, "Skin-on-a-chip model simulating inflammation, edema and drug-based treatment," *Sci. Rep.*, vol. 6, no. October, pp. 1–12, 2016.

[86] Q. Ramadan and F. C. W. Ting, "In vitro micro-physiological immune-competent model of the human skin," *Lab Chip*, vol. 16, no. 10, pp. 1899–1908, 2016.

[87] N. Sasaki, K. Tsuchiya, and H. Kobayashi, "Photolithography-free skin-on-a-chip for parallel permeation assays," *Sensors Mater.*, vol. 31, no. 1, pp. 107–115, 2019.

[88] H. E. Abaci *et al.*, "Human Skin Constructs with Spatially Controlled Vasculature Using Primary and iPSC-Derived Endothelial Cells," *Adv. Healthc. Mater.*, vol. 5, no. 14, pp. 1800–1807, 2016.

[89] N. Mori, Y. Morimoto, and S. Takeuchi, "Skin integrated with perfusable vascular channels on a chip," *Biomaterials*, vol. 116, pp. 48–56, 2017.

[90] B. S. Kim, G. Gao, J. Y. Kim, and D. W. Cho, "3D Cell Printing of Perfusable Vascularized Human Skin Equivalent Composed of Epidermis, Dermis, and Hypodermis for Better Structural Recapitulation of Native Skin," *Adv. Healthc. Mater.*, vol. 8, no. 7, pp. 1–11, 2019.

[91] S. Lee, S. P. Jin, Y. K. Kim, G. Y. Sung, J. H. Chung, and J. H. Sung, "Construction of 3D multicellular microfluidic chip for an in vitro skin model," *Biomed. Microdevices*, vol. 19, no. 2, 2017.

[92] H. J. Song *et al.*, "Development of 3D skin-equivalent in a pump-less microfluidic chip," *J. Ind. Eng. Chem.*, vol. 60, pp. 355–359, 2018.

[93] H. Y. Lim *et al.*, "Development of wrinkled skin-on-a-chip (WSOC) by cyclic uniaxial stretching," *J. Ind. Eng. Chem.*, vol. 68, pp. 238–245, 2018.

[94] K. Strüver, W. Friess, and S. Hedtrich, "Development of a Perfusion Platform for Dynamic Cultivation of in vitro Skin Models," *Skin Pharmacol. Physiol.*, vol. 30, no. 4, pp. 180–189, 2017.

[95] K. Schimek *et al.*, "Bioengineering of a full-thickness skin equivalent in a 96-well insert format for substance permeation studies and organ-on-a-chip applications," *Bioengineering*, vol. 5, no. 2, pp. 1–19, 2018.

[96] G. Sriram *et al.*, "Full-thickness human skin-on-chip with enhanced epidermal morphogenesis and barrier function," *Mater. Today*, vol. 21, no. 4, pp. 326–340, 2018.

[97] L. Valencia, V. C. Tejero, M. Clemente, I. Fernaud, and M. Holgado, "OPEN A new microfluidic method enabling the generation of multi - layered tissues - on - chips using skin cells as a proof of concept," pp. 1–14, 2021.

[98] J. J. Kim *et al.*, "A microscale, full-thickness, human skin on a chip assay simulating neutrophil responses to skin infection and antibiotic treatments," *Lab Chip*, vol. 19, no. 18, pp. 3094–3103, 2019.

[99] I. Wagner *et al.*, "Skin and hair-on-a-chip: Hair and skin assembly versus native skin maintenance in a chip-based perfusion system," *BMC Proc.*, vol. 7, no. S6, p. 13355, 2013.

[100] X. Ren *et al.*, "Investigations on T cell transmigration in a human skin-on-chip (SoC) model," *Lab Chip*, vol. 21, no. 8, pp. 1527–1539, 2021.

[101] Q. Ramadan and F. C. W. Ting, "In vitro micro-physiological immune-competent model of the human skin," *Lab Chip*, vol. 16, no. 10, pp. 1899–1908, 2016.

[102] S. Salameh *et al.*, "A perfusable vascularized full-thickness skin model for potential topical and systemic applications," *Biofabrication*, vol. 13, no. 3, p. 35042, 2021.

[103] K. Kim, H. M. Jeon, K. C. Choi, and G. Y. Sung, "Testing the effectiveness of curcuma longa leaf extract on a skin equivalent using a pumpless skin-on-a-chip model," *Int. J. Mol. Sci.*, vol. 21, no. 11, pp. 1–15, 2020.

[104] K. Strüver, W. Friess, and S. Hedtrich, "Development of a Perfusion Platform for Dynamic Cultivation of in vitro Skin Models," *Skin Pharmacol. Physiol.*, vol. 30, no. 4, pp. 180–189, 2017.

[105] C. S. Mah, S. J. Kochhar, P. S. Ong, and L. Kang, "A miniaturized flow-through cell to evaluate skin permeation of endoxifen," *Int. J. Pharm.*, vol. 441, no. 1–2, pp. 433–440, 2013.

[106] C. Provin, A. Nicolas, S. Grégoire, and T. Fujii, "A microfluidic diffusion cell for fast and easy percutaneous absorption assays," *Pharm. Res.*, vol. 32, no. 8, pp. 2704–2712, 2015.

[107] M. Alberti *et al.*, "Multi-chamber microfluidic platform for high-precision skin permeation testing," *Lab Chip*, vol. 17, no. 9, pp. 1625–1634, 2017.

[108] B. Lukács *et al.*, "Skin-on-a-chip device for ex vivo monitoring of transdermal delivery of drugs—design, fabrication, and testing," *Pharmaceutics*, vol. 11, no. 9, 2019.

[109] C. Provin, A. Nicolas, S. Grégoire, and T. Fujii, "A microfluidic diffusion cell for fast and easy percutaneous absorption assays," *Pharm. Res.*, vol. 32, no. 8, pp. 2704–2712, 2015.

Chapter 4

Pigmented full-thickness human skin model based on a fibroblast-derived matrix for long-term studies

The contents of this chapter have been published in:

Zoio P, Ventura S, Leite M, Oliva A. Pigmented Full-Thickness Human Skin Model Based on a Fibroblast-Derived Matrix for Long-Term Studies. *Tissue Eng Part C Methods*. 2021;27(7):433-443. doi:10.1089/ten.TEC.2021.006

Author contributions:

Zoio P. developed the protocol for production of full-thickness skin, generated both skin models, performed part of the characterization and the data analysis. **Zoio P**. wrote the manuscript. Ventura S. developed the protocol to produce pigmentation and performed the immunofluorescence analysis. Leite M contributed to the immunofluorescence analysis. Oliva A. supervised the project and revised the manuscript.

4.1 Abstract

Reconstructed human skin models are a valuable tool for drug discovery, disease modelling and basic research. In the last decades, major progress has been made in this field leading to the development of full-thickness skin models (FTSms) better representative of the native human skin by including the cellular crosstalk between the dermal and epidermal layers. However, current available FTSms still present important limitations since they are only suitable for short-term studies, include non-human extracellular matrix components and have a weak skin barrier function compared to *in vivo* human skin. In this work, a fibroblast-derived matrix was combined with the use of an inert polystyrene scaffold for the development of a fully human dermis capable of supporting a differentiated epidermis. To produce a pigmented FTSm, a co-culture with keratinocytes, melanocytes and fibroblasts was established. The structure and functionality of the developed FTSms were studied for short and long-term cultivation using histological and immunofluorescence staining. The integrity of the skin barrier was evaluated using transepithelial electrical resistance (TEER) measurements. It was possible to obtain a mature dermis capable of supporting an epidermis without keratinocyte infiltration in only 6 days. Extracellular matrix components (collagen, fibrin) were secreted by the fibroblasts and accumulated in the scaffold structure, recreating the microenvironment of the native human dermis. Moreover, the use of a scaffold resulted in a structure with mechanical stability due to its non-contracting nature. The co-culture of primary human keratinocytes resulted in a terminally differentiated skin equivalent that could maintain its architecture and homeostasis up to 50 days. Melanocytes were correctly integrated within the epidermal basal layer and made it possible to reproduce constitutive pigmentation. TEER levels increased during culture time, reaching values of 1.1 ± 0.2 $k\Omega.cm^2$ for the FTSm, indicative of a functional skin barrier.

4.2 Introduction

In recent years, there has been an increase in the demand for physiologically relevant *in vitro* human skin models for evaluating the safety and efficacy of new drug formulations or cosmetic ingredients and for studying skin biology and skin-related diseases. This need has been further amplified by EU regulations that encourage the 3Rs concept, calling for Replacement, Reduction and Refinement of animal experimentation and bans the use of animals for testing active compounds for cosmetics (Cosmetics regulation EC No 1223/2009) [1].

The majority of the available skin models are reconstructed human epidermis models (RHEms) generated by seeding keratinocytes on a porous membrane. Although these models provide highly standardized conditions for drug testing, they do not include the cellular epidermal-dermal crosstalk, which limits its applicability [2]. More recently, full-thickness skin models (FTSms) have been developed by seeding keratinocytes onto a dermal compartment composed of fibroblasts embedded in a matrix. Most FTSms are generated using collagen-based hydrogels, usually of bovine or rat-tail origin [3, 4]. Although these hydrogels offer a good support for epidermis formation, they are susceptible to fibroblast-mediated contraction during culture, resulting in excessive deformation [5, 6]. The high contractibility of the dermal matrix renders the models unsuitable for long-term studies.

To overcome this, solutions based on chemically crosslinking the dermal layer or creating more stable composites have been proposed. In particular, Vidal S. *et al* presented a new matrix consisting of a silk-collagen composite system which reduced contraction and degradation over time [7]. Lotz C. *et al* prolonged the skin longevity by using succinimidyl glutarate polyethylene glycol (PEG-SG) to crosslink cell seeded collagen [8]. However, most of these systems include animal-derived components and are not able to completely inhibit contraction. Matrices including non-human extracellular matrix components (ECM) components introduce batch-to-batch variability and are not representative of the healthy *in-vivo* human skin microenvironment, which contains lipids, fibrin, glycosaminoglycans and proteoglycans [9].

An alternative approach for the generation of FTSm is based on the use of human fibroblast-derived matrices (FDMs) as dermal equivalents. For this, multi-layered human fibroblasts are stimulated to generate ECM by modulation of various culture conditions. This approach results in a stratified FTSm with higher concentration of natural moisturizing factors and longer-lifespan compared to animal collagen-based skin equivalents [10]. However, a major disadvantage of using FDMs is the requirement for extended culture periods to produce sufficient quantities of ECM ranging from weeks to months due to the lack of a scaffold [11, 12]. Also, some features such as thickness and mechanical stability of the FDMs introduce high variability [13].

Hill *et al* generated a mechanically stable 3D microenvironment mimicking the native skin by seeding fibroblasts on an inert porous scaffold, enabling the formation of a FDM with defined thickness [14]. This model was successfully used to investigate early melanoma invasion within a fully human microenvironment. However, one of the main limitations of using scaffolds for generating FDMs is the potential for keratinocyte infiltration into the dermis resulting in the absence of a continuous epidermal layer and epidermis disorganization. Considering this, Roger *et al* studied the optimized timeframe for dermis formation [15]. Although the group could generate a skin model that recapitulates various features of *in vivo* skin, their protocol still required more than 40 days to produce the FTSms.

We report the development of a robust and stratified FTSm in a total of 21 days. By seeding a high density of human dermal fibroblasts on a porous scaffold and stimulating the cells to produce FDM, a dermal equivalent capable of supporting an epidermis, is produced in only 6 days. The resultant FTSm is highly differentiated and closely mimic aspects of the architecture of the *in vivo* skin tissue. Moreover, a pigmented version of the FTSm is produced by introducing melanocytes. A complex structure with co-culture with 3 different skin cell types is obtained, ideal to study pathologies that require advanced.

4.3 Methods

4.3.1 Primary cells and cell maintenance

Primary human dermal fibroblasts isolated from neonatal foreskin (HDFn, CellnTec) were maintained in Fibroblast Growth medium (FGM) composed of Iscove's Modified Dulbecco's Medium (IMDM, Gibco®, Waltham, MA USA) supplemented with 10% fetal bovine serum (FBS, Gibco®, Waltham, MA USA). Primary human epidermal keratinocytes isolated from neonatal foreskin (HEKn, Gibco®, Waltham, MA USA) were maintained in keratinocyte growth medium (KGM) composed of EpiLife medium (Gibco®, Waltham, MA USA), supplemented with 0.06 mM calcium and keratinocyte growth factor (HKGS, Gibco®, Waltham, MA USA). Primary human melanocytes (HEM, Gibco®, Waltham, MA USA) were maintained in Melanocyte growth medium (MGM) composed of M254 medium (Gibco®, Waltham, MA USA) supplemented with melanocyte growth factor (HMGS, Gibco®, Waltham, MA USA). All cells were maintained at 37ºC and 5% CO_2 in a humidified incubator.

4.3.2 Generation of the FTSm

The process of developing full-thickness and fully human skin can be divided in the main steps depicted in **Figure 4. 1**: the generation of a mature dermis, the expansion of keratinocytes on top of the dermis under submerged conditions and the development of the epidermis at the air-liquid interface (ALI). Fully-human dermal equivalents were generated by seeding HDFns within inert porous polystyrene scaffolds (Alvetex®, REPROCELL Europe Ltd., UK) with void sizes of 33-55 μm and 90% porosity. This makes them the ideal structure for the HDFns to penetrate and lay down FDM. Briefly, scaffolds were pre-treated with 70% ethanol to render them hydrophilic followed by two washes with PBS. 1.0×10^6 HDFs were seeded onto the scaffolds in 100 μL FGM and incubated at 37ºC, in a humified atmosphere of 5% CO_2 for 1.5 hours. After the cell adhesion period, FGM supplemented with 100 $\mu g/mL$ L-Ascorbic acid 2-phosphate (Sigma-Aldrich) was applied to the bottom of each well to flood the insert prior to incubation and maintained up to a further 18 days at 37ºC in a

5% CO_2 humidified incubator, changing the media every 3 days, to study the formation of the dermal equivalent.

FTSms were generated by seeding 5.0 x 10^5 HEKn cells onto the dermal equivalents. HEKns were incubated under submerged conditions in KGM containing high calcium concentration (1.5 mM) and maintained at 37ºC, in a humified atmosphere of 5% CO_2. After 3 days, the models were raised to ALI by removal of the medium in the upper compartment and cultured in KGM containing 1.5 mM calcium, supplemented with 10 ng/mL KGF and 50 μg/mL of L-Ascorbic acid 2-phosphate. The FTSms were maintained up to a further 50 days.

4.3.3 Generation of the pigmented FTSm

Pigmented FTSms were developed by seeding 5.0 x 10^4 HEMs on top of the dermis compartment. The tissues were incubated in MGM under submerged conditions at 37ºC and 5% CO_2 for cell adhesion. After 24h, 5.0 x 10^5 HEKns were seeded on top of the dermis and HEM layer. The cells were maintained in co-culture growth medium (CGM) composed of 80% KGM containing high calcium (1.5 mM) and 20% MGM under submerged conditions. After 3 days, ALI was established and the models were maintained in CGM supplemented with 10 ng/mL KGF and 50 μg/mL of L-Ascorbic acid 2-phosphate for 12 days.

4.3.4 Generation of a RHEm on a polycarbonate membrane

Cell culture inserts with polycarbonate membranes (Merck Millipore) were used for RHEm generation. The polycarbonate membranes were selected for HEKn attachment without matrix. Briefly, the inserts were placed in 6-well plates containing 2.5 ml KGM with high calcium concentration (1.5 mM) and seeded with 1.5 x 10^5 HEKns in 500 μL FGM medium. After 24h, the models were raised to ALI. The medium was replaced by 1.5 ml KGM supplemented with 1.5 mM calcium, 50 μg/mL L-Ascorbic acid 2-phosphate and 10 ng/ml KGF and renewed every other day.

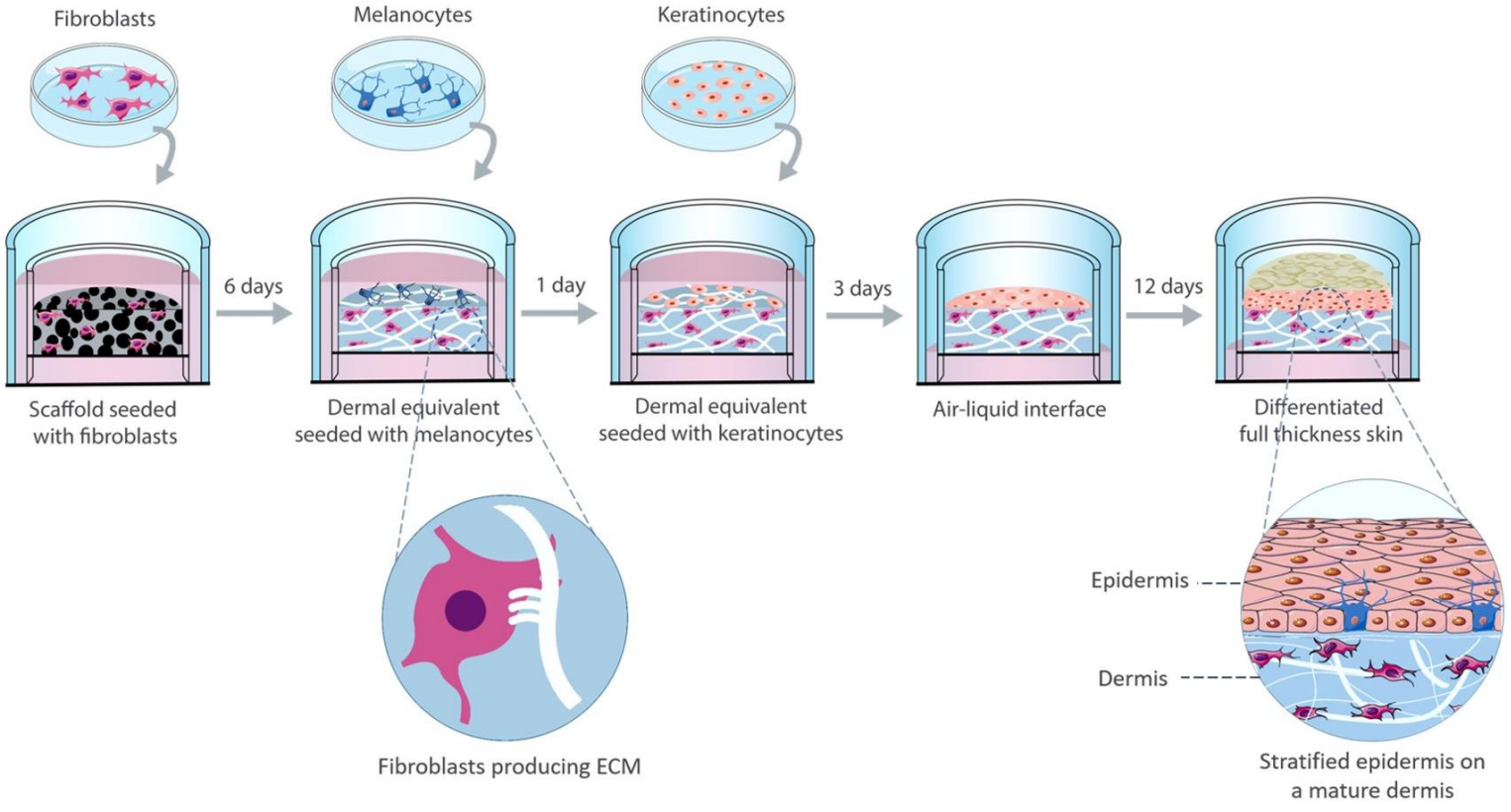

Figure 4. 1. Schematic representation of the developed methodology for pigmented FTSm generation using co-culture with 3 cell types (HDFns, HEKns and HEMs). The process can be divided in four main steps: the development of a mature dermis, the culture of HEMs on top of the dermis, the culture of epidermal cells under submerged conditions, and the culture of the epidermis at the ALI until a fully differentiated skin is generated. After 12 days, a stratified epidermis on top of a mature dermis is obtained.

4.3.5 Experimental Design

4.3.5.1 Strategy

The presented method was used to produce fully human dermal equivalents with different maturation times. FTSm were generated using the developed dermal equivalents and maintained for up to 50 days. The morphology and functionality of the produced FTSm was evaluated and compared to an *in house* RHEm. This was performed through histological and immunofluorescence analysis and through transepithelial electrical resistance (TEER) measurements. For each experiment, an N=3 and n=3 were used.

4.3.5.2 Histological analysis and immunohistochemistry

The reconstructed tissues were fixed immediately after being taken out of culture in 10% neutral buffered formalin (Sigma-Aldrich). The samples were embedded in paraffin to allow for transverse sectioning. Paraffin-embedded sections were de-paraffined and re-hydrated for morphological evaluation by staining with haematoxylin and eosin (H&E) through standard methods.

Skin sections (5-µm-thick) were mounted on slides and incubated during 30 minutes in a dry chamber. Sections were stained with anti-ki67 (Roche), anti S-100 (Roche) and anti-tyrosinase (Roche) primary antibodies diluted in a solution of PBS containing 1% bovine serum albumin (PBS-BSA 1%; BSA, Sigma-Aldrich).

4.3.5.3 Immunofluorescence analysis

Skin sections were deparaffinized using HistoChoice® (Sigma-Aldrich) and incubated in a dry chamber at 65ºC during 30 minutes. Then, skin sections were hydrated during 5 minutes in a gradient of ethanol solutions (100%, 96% and 70%). The antigen retrieval was performed by heating in citrate buffer (pH=6). For anti-collagen IV antibody, the antigen retrieval was followed by proteinase K (20µg/mL in TE Buffer) incubation for 30 seconds at 37ºC with 10 minutes of cooling at room temperature. Immunofluorescence staining of sections was performed using the following primary antibodies: 1:500 anti-collagen IV (Abcam), 1:10 anti-cytokeratin

10 (Progen), 1:1000 anti-cytokeratin 14 (Abcam), 1:100 anti-cytokeratine 15 (Sigma-Aldrich), 1:250 anti-fibronectin (Abcam), 1:50 anti-filaggrin (Invitogen) and 1:100 anti-collagen I (Abcam) diluted in a solution with PBS-BSA 1% with overnight incubation in humidified chamber at 4°C. Secondary antibodies, 1:1000 Alexa Fluor® 488 Goat Anti-Rabbit IgG (Invitrogen) or 1:1000 FITC Goat Anti-Mouse IgG (Sigma-Aldrich), diluted in a solution with PBS-BSA 1%, were then added with an incubation of 2 hours. Nuclei were stained with 1 µg/mL of 4,6-diamidino-2-Phenylindole (DAPI, Invitrogen) and slides were mounted with Vectashield (Vector Laboratories). Images were obtained using the Nikon Eclipse TE2000-S fluorescence microscope (Nikon instruments, USA) and analysed with the ImageJ software.

4.3.5.4 **Transepithelial electrical resistance evaluation**

The barrier integrity of developed models was evaluated by TEER. Measurements were taken using an EVOM Epithelial Volt/Ohm Meter and a pair of Ag/AgCl probes (WPI Europe, UK). Measurements were performed during 14 days of cell culture for FTSm and RHEm. TEER values were calculated according to the following equation:

$$TEER = \left(R_{sample} - R_{blank}\right) \times A \quad [4.1]$$

Where R_{sample} is the resistance value for the skin model, R_{blank} is the resistance value of an insert without cultured cells and A the effective culture area (1.12 cm² for FTSm and 0.63 cm² for RHEm). For the RHEms, the KGM was replaced with 300 µl PBS in the apical region and 2 ml PBS in the basal region. For FTSm, for the time required to measure electrical resistance, the tissues were placed in an adapted 6-well plate containing 2 ml PBS. The KGM was aspirated and replaced with 250 µl of PBS in the apical region. For both models, the probe was placed such that one electrode was submerged in the upper compartment and the other was submerged in the lower compartment. TEER values were recorded during culture time from the last day under submerged conditions (day 0) until day 14 at ALI. These measurements were performed for 3 batches of 3 skins at each time point for FTSm and RHEm.

4.4 Results

4.4.1 Generation of a mature dermis capable of supporting a differentiated epidermis

The first step to obtain an organized FTSm was the optimization of the culture times to produce a mature dermal equivalent capable of supporting the epidermis and minimize keratinocyte infiltration. As can be seen in **Figure 4. 2.a**, dermal HDFns cultured for 3 to 12 days in the porous scaffold show a homogeneous distribution within the scaffolds. HDFns are stimulated to produce FDM which build up and accumulate inside the scaffold. This can be seen in **Figure 4. 2.b** which shows ECM markers expressed in the dermal construct from 3 to 12 days of HDFn culture. Collagen I, collagen IV and fibronectin were detected within the dermal equivalents since day 3 of culture. An increase in the color intensity could be observed over time, which shows an increase in quantities of FDM being produced by the HDFns and being deposited within the scaffold structure.

The influence of the dermis maturation on the epidermis formation was evaluated by seeding HEKns on top of dermal equivalents cultured for different times. **Figure 4. 3** shows cross sections of FTSm generated using dermal constructs matured from 3 to 18 days. Epidermis grown on a 3-day dermal construct shows keratinocyte infiltration, resulting in areas of epidermal disorganization. From 6 to 18 days of dermis formation, a differentiated and organized epidermis is achieved. No signs of keratinocyte infiltration can be seen in these constructs. During culture time, a layer of fibroblasts and ECM starts to deposit at the basal and apical sides of the scaffold, reaching 50±15 μm thickness at day 33 of culture (data not shown).

4.4.2 FTSm resembling in vivo human skin morphology and homeostasis

The morphology of the FTSm was evaluated and compared to the RHEm. After 12 days at ALI, both FTSm and RHEm displayed native human skin-like morphology, including a well-organized and stratified epidermis (**Figure 4. 4**). H&E

staining reveals all layers of the epidermis: *stratum basale* (SB), *stratum spinosum* (SS), *stratum granulosum* (SG) and *stratum corneum* (SC).

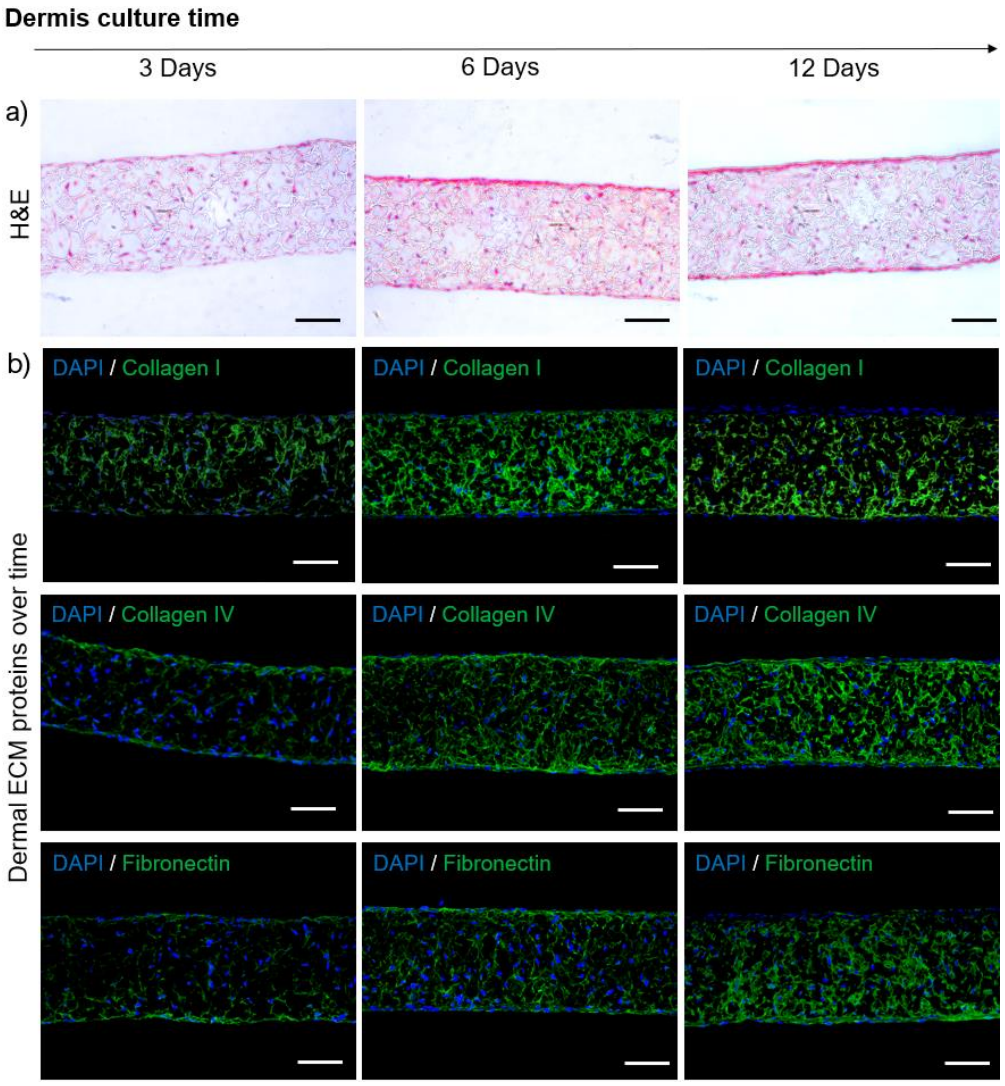

Figure 4. 2. HDFns seeded on inert porous scaffolds and stimulated to produce ECM for 3, 6 and 12 days a) Representative H&E images of dermal models cultured over time. b) Representative immunofluorescence images showing ECM proteins (collagen I, collagen IV and fibronectin) deposited on the dermal models cultured over time. Scale bars: 100 μm.

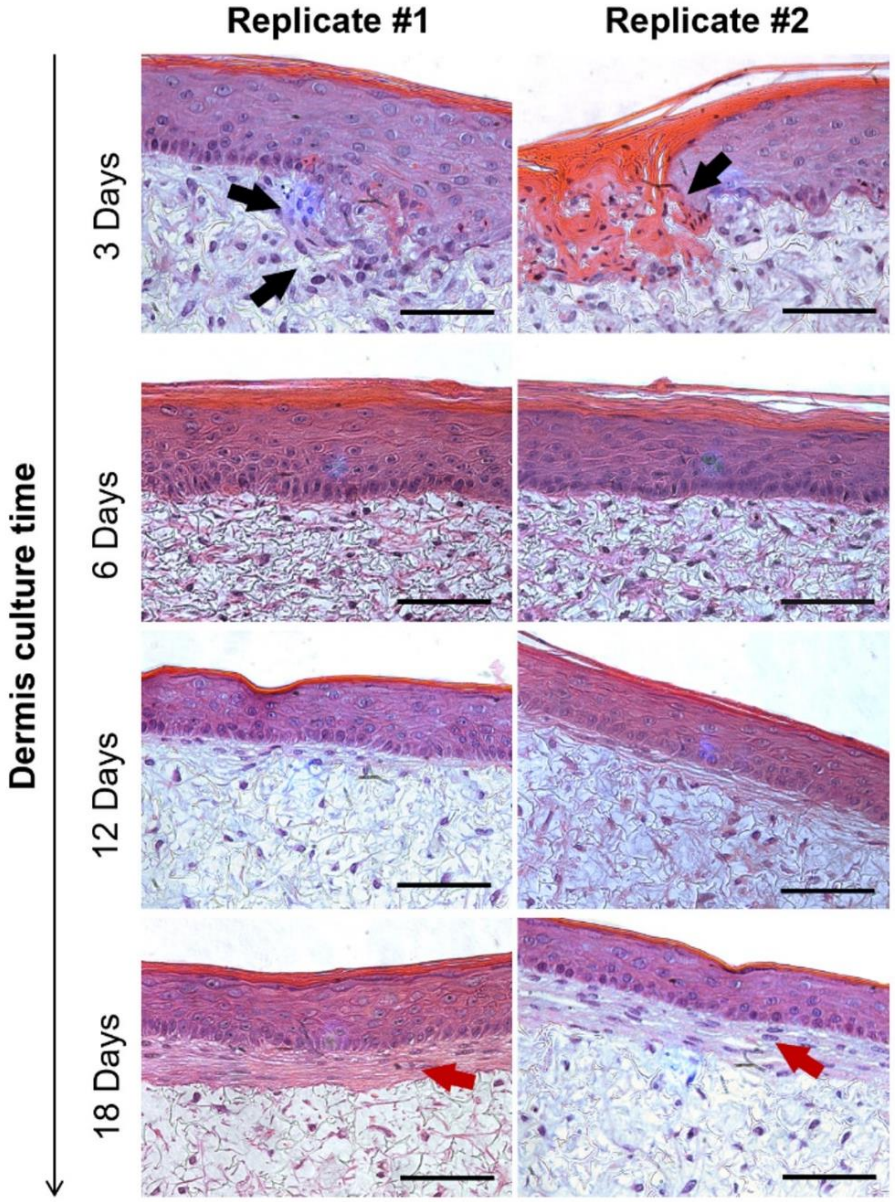

Figure 4. 3. Representative H&E images of two independent replicates of FTSm (HDFns+HEKns) developed using dermis with different maturation times (from 3 to 18 culture days) and maintained at ALI for 12 days to promote epidermal differentiation. Black arrows point to keratinocyte infiltration on a dermis cultured for 3 days. Red arrows point to ECM deposition on top of the scaffold on a dermis cultured for 18 days. Scale bars: 100 μm.

FTSm and RHEm were kept at ALI for up to 50 days and its structure was monitored over time, confirming the suitability of the developed model for long-term studies. Histological sections after a cultivation time of 30 days show a differentiated epidermis, including the presence of all layers characteristic of the *in vivo* human epidermis. Although there is a reduction in epidermal thickness when compared to the models cultured for 12 days at ALI, the pattern of uniform cuboid basal keratinocytes and preserved architecture indicates the model maintains their functionality.

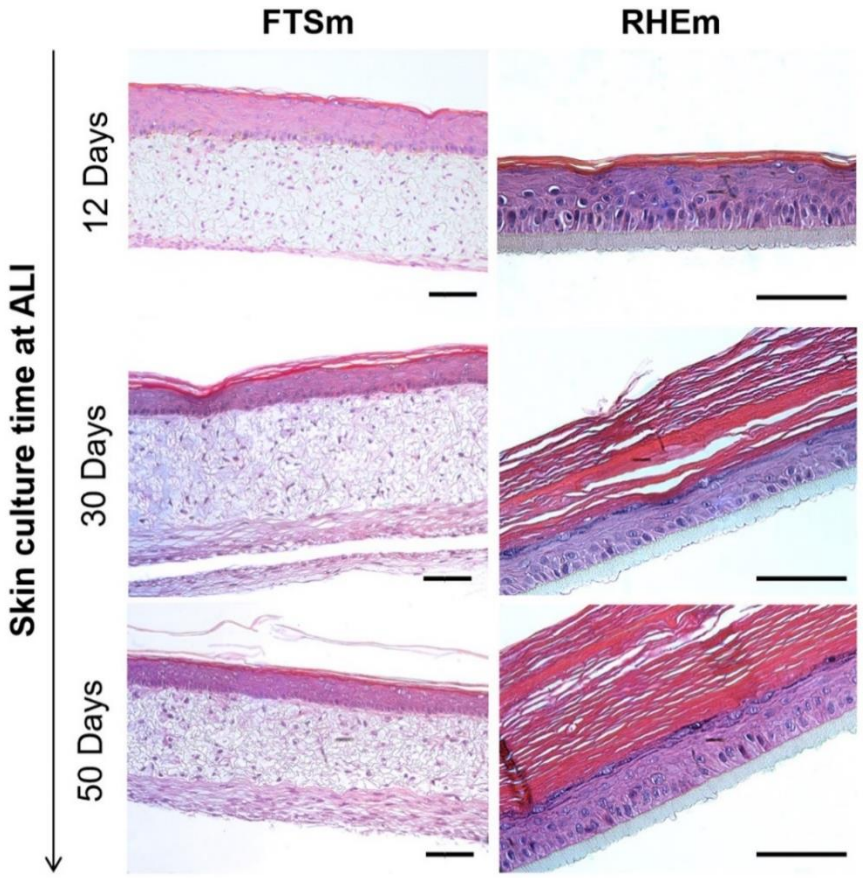

Figure 4. 4. Representative H&E images of skin models (FTSm and HEKns) maintained over time at ALI (up to 50 days). For the FTSm (HDFns+HEKns) a 6-day dermis was used. Scale bars: 100 μm.

From day 30 to 50 of culture at ALI, both RHEm and FTSm remained stable, maintaining the same thickness and identifiable epidermal layers. For RHEm, the reduction in thickness of the lower cellular layers was accompanied by an increase in cornified acellular upper layers, with the SC reaching a thickness of approximately 200 ± 25 μm at day 50 of culture. FTSm cultured long-term did not show an increase in the SC thickness.

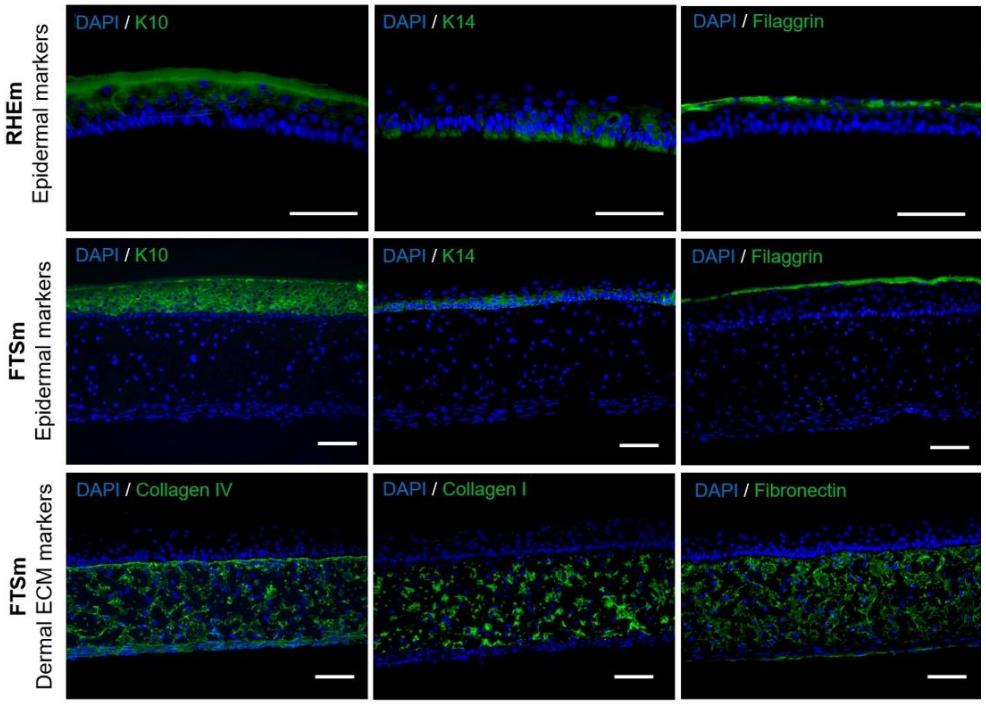

Figure 4. 5. Immunofluorescence analysis of FTSm (HDFns+HEKns) and RHEm. The FTSm was generated by culturing the dermal compartment for 6 days, then allowing epidermal differentiation for 12 days ALI. The RHEm was generated by allowing epidermal differentiation at ALI for 12 days. Data show protein expression patterns for key biomarkers typically associated with epidermal differentiation (K10, K14 and filaggrin) and with ECM compounds found in the dermis (collagen I, collagen IV and fibronectin). Scale bars: 100 μm.

The presence and distribution of protein biomarkers representing various stages of epidermal differentiation was assessed by immunofluorescence staining in FTSm and RHEm (**Figure 4. 5**). Keratin (K) 14, an intermediate filament in the SB of the epidermis, was expressed in the SB and immediate suprabasal layer. K10 was expressed and distributed in the SS layers and extended to all suprabasal layers.

These two markers were similarly expressed in FTSm and RHEm. Filaggrin, a terminal differentiation marker, was correctly deposited at the SG and SC layers for the FTSm and RHEm. This demonstrates the differentiated nature of the models. Collagen IV, a major component of the *lamina densa*, was present within the dermis and showed an increase staining intensity along the dermo-epidermal junction of the FTSm. Collagen I and fibronectin, major components of the dermis, presented a homogenous distribution within this compartment. Proliferative activity of HEKns was identified by immunohistological staining with Ki67, a protein accumulated within the nucleus during mitosis. The results show that the FTSm was actively proliferating via mitosis with Ki67-positive cells restricted to the SB (**Figure 4. 6**). This is expected since, on *in vivo* skin, the stem and progenitor cells reside on the SB, undergoing self-renewing or differentiative cell divisions.

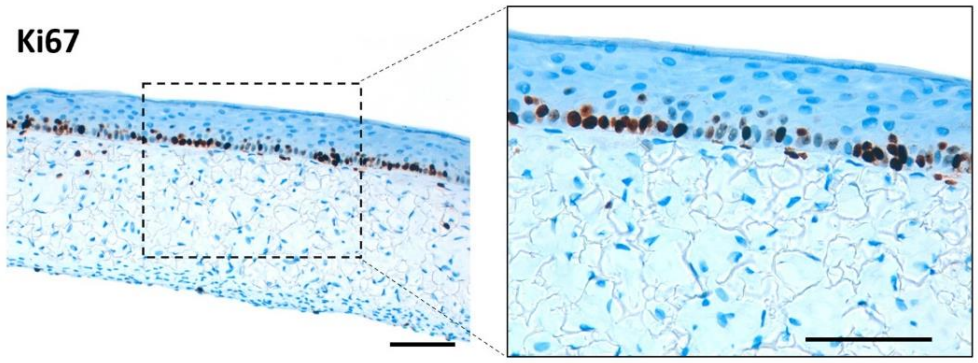

Figure 4. 6. Analysis of HEKn proliferation during FTSm formation. immunohistological staining performed with Ki67, showing proliferative activity in the basal layer. Scale bars: 100 μm.

4.4.3 FTSm with active melanocytes resembling in vivo pigmentation

After 12 days at ALI, a stratified epidermal structure with HEMs correctly integrated was achieved. Macroscopically, the presence of pigmentation on the FTSm can be clearly seen when compared to a FTSm without added HEMs (**Figure 4. 7.a**). The macroscopic pictures show pigmentation across the culture area with decreased intensity at the centre. The presence of melanocytes in the epidermis was evaluated by S-100 protein staining (**Figure 4. 7**.**b**) on FTSm cross sections, revealing their localization in the basal cell layer interspersed with basal cell HEKns. In

addition, tyrosinase, a key enzyme for controlling the production of melanin, was identified through immunohistochemistry. Tyrosinase was highly expressed in the basal layer of the epidermis.

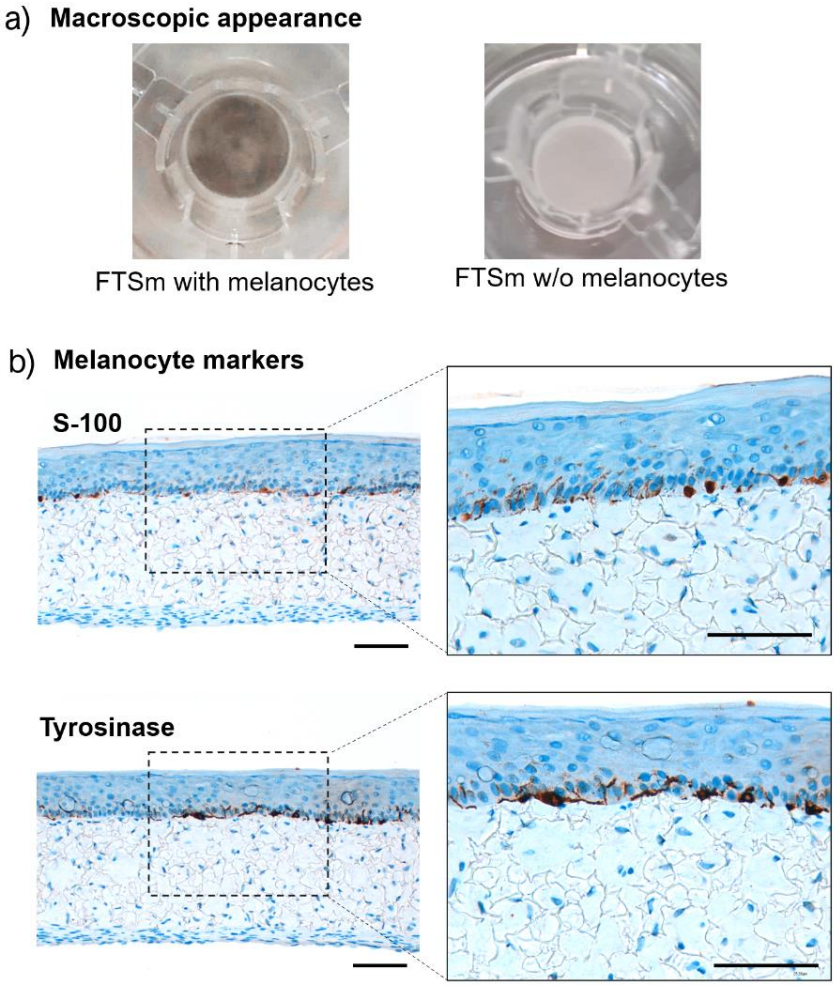

Figure 4. 7. Examination and measurement of pigmentation in the developed FTSm after 6 days of dermis formation and 12 days at ALI for epidermis differentiation. a) Macroscopic appearance of the FTSm with melanocytes (left) in comparison with FTSm without melanocytes (right). Left picture shows the pigmentation caused by the presence of melanocytes. b) Representative immunohistochemistry sections evaluating S-100 protein (top) and tyrosinase (bottom) to detect the presence of melanocytes in the epidermal compartment. Scale bars: 100 μm

4.4.4 TEER as an indicator of the skin barrier formation

The barrier integrity of the stratifying cultures was evaluated by TEER, measured during skin culture from day 0 (submerged conditions) until day 14 at ALI for RHEm and FTSm (**Figure 4. 8**). For both models, TEER values under submerged conditions started bellow 0.2 kΩ.cm² and, as the epidermis gradually developed, increased significantly reaching values of 1.1±0.2 kΩ.cm² for FTSm (**Figure 4. 8.a**) and 9.3 ±1.1 kΩ.cm² for RHEm (**Figure 4. 8**.**b**).

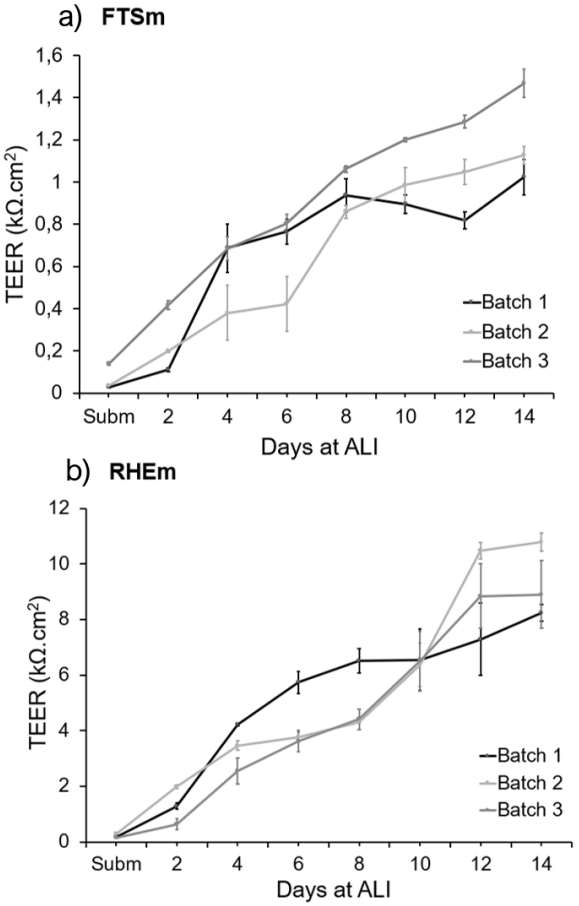

Figure 4. 8. TEER measurements performed with an EVOM system and chopstick electrodes obtained from day 0 to day 12 at ALI for FTSm (HDFns+HEKns) and RHEm. For the FTSm, a 6-day dermis was used. Data represents the average TEER of 3 biological replicates and for 3 technical replicates at each time point. Reported TEER as kΩ.cm² tissue surface area. Error bars represent mean ± standard deviation.

4.5 Discussion

4.5.1 Overview of the FTSm

We present a fully human FTSm based on a FDM with an *in-vivo* like architecture and optimized co-culture with three different skin cell types (fibroblasts, melanocytes and keratinocytes), compatible with long-term cultivation. The developed FTSm includes a mechanically stable dermal compartment with a physiological 3D microenvironment, a fully differentiated epidermis resembling the structure and function of the native counterpart as well as pigmentation by including active melanocytes at the basal layer. Moreover, we evaluate the suitability of using TEER measurements as a non-destructive technique to quantify in real-time the barrier integrity of FTSm during the various stages of skin differentiation.

4.5.2 Dermal compartment based on an FDM

The first goal was the development of a robust dermis that could reproduce the physiological matrix and microenvironment of the native human dermis and that could support a stratified epidermis. Adding a dermis to the skin model fits the need to better mimic the physiological architecture of human native skin since dermal fibroblasts interact with keratinocytes, playing a role in skin tissue morphogenesis, homeostasis and histopathological conditions [16]. FTSms using animal-derived hydrogels present several limitations including batch variability, species-specific effects and lack of mechanical stability due to fibroblast-mediated contraction during cell culture. These characteristics greatly diminish their applicability and negatively impact studies requiring topically application of substances [5] and integration in various platforms such as organ-on-a-chip devices [6,17].

We present an alternative approach where human fibroblasts are seeded in a porous inert scaffold and stimulated to produce a FDM resulting in a fully human dermal component that maintains their mechanical structure long-term. In the developed dermis we could observe expression of collagen I, collagen IV and

fibronectin with accumulation of ECM with time. Previous works using a similar technique needed around 4 weeks to produce a mature dermis capable of supporting the epidermis, followed by an epidermal differentiation of at least 14 days [15]. This long process greatly minimizes their applicability in industry and clinical contexts. Here, we were able to reduce the necessary time for dermal formation to less than 1 week by optimizing the cell seeding density and medium composition. Contrary to conventional FTSms, the developed model shows no reduction of the epidermal surface area due to shrinkage, resulting in a more accurate model of the skin barrier. The 6-day dermis was able to support an epidermis without signs of keratinocyte infiltration and, at the same time, minimized the accumulation of a thick layer of fibroblasts and ECM on the apical and basal sides of the scaffold which leads to a faster nutrient depletion from the cell culture medium. The developed fully human dermal model can be useful to study the effect of drugs on ECM deposition and remodelling.

4.5.3 Fully differentiated pigmented FTSm for long-term studies

It was possible to reproduce the complex multi-layered structure present in healthy *in vivo* skin, with an observable stratified squamous epithelium structured in a basal, spinous, granular and corneal layers. This stratification is a critical feature of a relevant skin models and correlates with its barrier function. The developed FTSm reflected the expected expression pattern of keratins, with expression of K14 in the basal layer and K10 in the suprabasal layers. Filaggrin, a component of the cornified cell envelope, important for the structural ad integrity of the SC, was correctly expressed in the FTSm.

We show that the developed FTSm can maintain its viability and function for at least 50 days at ALI. Conventional FTSm not only contract over time but are also prone to degradation by matrix metalloproteases after two weeks [18]. This extended life-span compared to standard models makes it more suitable to study physiological and biochemical processes over a long period of time. Interestingly, the developed in-house RHEm also demonstrated the same longevity, maintaining *in vivo* architecture for 50 days at ALI. Contrary to other long-term FTSm, the presented model does not include animal-derived hydrogels and does not require

complex methods to generate a stable dermis which could hamper its reproducibility. Recently, given the increased interest in prolonging the experimental testing phase, a long-term skin model became commercially available (Phenion® Full-thickness LONG-LIFE skin model). This model can be kept in culture for up to 50 days. However, these commercial systems lack flexibility since they arrive pre-made and the methods used to generate them are not transparent. With our developed open-source FTSm, it will be possible to study skin reactions taking multiple days to manifest or requiring repeated dose administration as well as recovery or regeneration after tissue treatment.

Thickening of the SC during a prolonged culture period is a common phenomenon for *in vitro* skin models, indicating the accumulation of the corneocytes layer without proper desquamation [19]. The gradual thickening of the SC indicates a lack of epidermal homeostasis. This phenomenon was observed in the developed RHEm, with the SC reaching a thickness of 200 ± 25 μm at day 50 of culture at ALI. Histological analysis of the FTSm showed an absence of SC accumulation with extended culture time. This observation can indicate an optimized epidermal homeostasis with a desquamation process mimicking the native skin [20]. These results point to the potential of the FTSm to study mechanisms in epidermal regeneration and tissue homeostasis. Further studies should be performed to clarify this observation by analysis of the enzymatic activity in SC.

We also developed a pigmented version of the FTSm with active melanocytes at the dermo-epidermal junction. The pigmentation could be clearly seen macroscopically. This model could be of great interest for drug screening studies and disease modelling. Since drug-induced pigmentation accounts for approximately 20% of all cases of hyperpigmentation, this model could be useful to study this side effect of new developed drugs [20]. Skin hyperpigmentation has been shown to be potentially induced by antibiotics, pain relievers, diuretics and anti-inflammatory drugs [21].

4.5.4 Real-time TEER measurement

TEER analysis was used to evaluate the stage of skin differentiation and as a method of quality control. TEER reflects skin barrier functionality by measuring

overall barrier to ions. It takes into account the contributions from the SC barrier and cell-to-cell tight junctions (TJ) which regulate the movement of ions across the paracellular pathway [22]. During RHEm and FTSm culture for two weeks at ALI there is an increase in TEER values, reflecting progressive SC accumulation and TJ formation. RHEm reached values of 9.3 ±1.1 kΩ.cm^2 and FTSm reached values of 1.1 ±2.3 kΩ.cm^2. Although the FTSm does not experience contraction during cell culture, an increased collagen accumulation at the insert wall interface results in an area where keratinocyte adhesion is reduced. This explains why the TEER values are lower when compared with RHEm. In fact, it is documented that a tissue surface coverage of less than 99.6% causes an 80% drop in barrier function [23], resulting in dramatic decrease in TEER values. Still, TEER values for both FTSm and RHEm fall within the range of some validated *in vitro* skin models including Epiderm™ (0.5 ± 0.1 kΩcm^2) [24] and other models without formal regulatory acceptance including Keraskin™-VM (> 0.5 kΩcm^2) [25] and dermo–epidermal skin equivalents (> 1 kΩcm^2) [26].

4.6 Conclusion

We have developed an advanced FTSm which does not include animal-derived components. In this model, human fibroblasts are stimulated to produce FDM resulting in a fully human structure that resembles the *in vivo* microenvironment. The use of an inert scaffold results in a non-contracting and stable structure, increasing reproducibility and applicability. The model exhibits *in vivo-like* characteristics, including a well-differentiated and organized epidermis. We showed the FTSm can be maintained for at least 50 days, making it ideal for long-term studies, for example, modelling melanoma and aging. Moreover, the potential of this model for achieving higher complexity is demonstrated by successfully reproducing skin pigmentation. In the future, other cell types could be introduced in the FTSm such as immune and endothelial cells to recreate a more advanced platform for disease modelling.

4.7 References

[1] Vinken, M. 3Rs toxicity testing and disease modeling projects in the European Horizon 2020 research and innovation program. EXCLI J 19, 775, 2020.El

[2] Ghalbzouri A, Jonkman MF, Dijkman R, Ponec M. Basement membrane reconstruction in human skin equivalents is regulated by fibroblasts and/or exogenously activated keratinocytes. J Invest Dermatol. 2005;124(1):79-86..

[3] Rossi A, Appelt-Menzel A, Kurdyn S, Walles H, Groeber F. Generation of a three-dimensional full thickness skin equivalent and automated wounding. J Vis Exp. 2015;(96):52576

[4] El Ghalbzouri A, Siamari R, Willemze R, Ponec M. Leiden reconstructed human epidermal model as a tool for the evaluation of the skin corrosion and irritation potential according to the ECVAM guidelines. Toxicol In Vitro. 2008;22(5):1311-1320.

[5] Ackermann K, Borgia SL, Korting HC, Mewes KR, Schäfer-Korting M. The Phenion full-thickness skin model for percutaneous absorption testing. Skin Pharmacol Physiol. 2010;23(2):105-112.

[6] Mori N, Morimoto Y, Takeuchi S. Skin integrated with perfusable vascular channels on a chip. Biomaterials. 2017;116:48-56.

[7] Vidal, S.E.L., Tamamoto, K.A., Nguyen, H., Abbott, R.D., Cairns, D.M., and Kaplan, D.L. 3D biomaterial matrix to support long term, full thickness, immuno-competent human skin equivalents with nervous system components. Biomaterials 198, 194, 2019

[8] Lotz, C., Schmid, F.F., Oechsle, E., Monaghan, M.G., Walles, H., and Groeber-Becker, F. Cross-linked collagen hydrogel matrix resisting contraction to facilitate fullthickness skin equivalents. ACS Appl Mater Interfaces 9, 20417, 2017.

[9] Sorrell, J.M., and Caplan, A.I. Fibroblast heterogeneity: more than skin deep. J Cell Sci 117(Pt 5), 667, 2004.

[10] El Ghalbzouri, A., Commandeur, S., Rietveld, M.H., Mulder, A.A., and Willemze, R. Replacement of animalderived collagen matrix by human fibroblast-derived dermal matrix for human skin equivalent products. Biomaterials 30, 71, 2009.

[11] Auger, F.A., Pouliot, R., Tremblay, N., et al. Multistep production of bioengineered skin substitutes: sequential modulation of culture conditions. In Vitro Cell Dev Biol Anim 36, 96, 2000.

[12] Hata, R., Sunada, H., Arai, K., et al. Regulation of collagen metabolism and cell growth by epidermal growth factor and ascorbate in cultured human skin fibroblasts. Eur J Biochem 173, 261, 1988.

[13] Throm, A.M., Liu, W.C., Lock, C.H., and Billiar, K.L. Development of a cell-derived matrix: effects of epidermal growth factor in chemically defined culture. J Biomed Mater Res A 92, 533, 2010.

[14] Hill, D.S., Robinson, N.D., Caley, M.P., et al. A novel fully humanized 3D skin equivalent to model early Melanoma invasion. Mol Cancer Ther 14, 2665, 2015.

[15] Roger, M., Fullard, N., Costello, L., et al. Bioengineering the microanatomy of human skin. J Anat 234, 438, 2019.

[16] Niehues, H., Bouwstra, J.A., El Ghalbzouri, A., et al. 3D skin models for 3R research: the potential of 3D reconstructed skin models to study skin barrier function. Exp Dermatol 27, 501, 2018.

[17] Schimek, K., Hsu, H.H., Boehme, M., et al. Bioengineering of a full-thickness skin equivalent in a 96-well insert format for substance permeation studies and organ-on-a-chip applications. Bioengineering (Basel) 5, 43, 2018.

[18] Karsdal, M.A., Nielsen, S.H., Leeming, D.J., et al. The good and the bad collagens of fibrosis - Their role in signaling and organ function. Adv Drug Deliv Rev 121, 4356, 2017.

[19] Vicanova´, J., Mommaas, A.M., Mulder, A.A., Koerten, H.K., and Ponec, M. Impaired desquamation in the in vitro reconstructed human epidermis. Cell Tissue Res 286, 115, 1996.

[20] Pierard, G.E., Goffin, V., Hermanns-Le, T., and PierardFranchimont, C. Corneocyte desquamation. Int J Mol Med 6, 217, 2000.

[21] Dereure, O. Drug-induced skin pigmentation. Epidemiology, diagnosis and treatment. Am J Clin Dermatol 2, 253, 2001.

[22] Benson, K., Cramer, S., and Galla, H.J. Impedance-based cell monitoring: barrier properties and beyond. Fluids Barriers CNS 10, 5, 2013.

[23] Florin, L., Maas-Szabowski, N., Werner S, Szabowski, A., and Angel, P. Increased keratinocyte proliferation by JUNdependent expression of PTN and SDF-1 in fibroblasts. J Cell Sci 118(Pt 9), 1981, 2005.

[24] Kanda´rova´, H., Liebsch, M., Schmidt, E., et al. Assessment of the skin irritation potential of chemicals by using the SkinEthic reconstructed human epidermal model and the common skin irritation protocol evaluated in the ECVAM skin irritation validation study. Altern Lab Anim 34, 393, 2006.

[25] Jung, K.M., Lee, S.H., Jang, W.H., et al. KeraSkin-VM: a novel reconstructed human epidermis model for skin irritation tests. Toxicol In Vitro 28, 742, 2014.

[26] Akagi, T., Nagura, M., Hiura, A., Kojima, H., and Akashi, M. Construction of three-dimensional dermoepidermal skin equivalents using cell coating technology and their utilization as alternative skin for permeation studies and skin irritation tests.

Tissue Eng Part A 23, 481, 2017.

Chapter 5

Open-source human sin model with an *in vivo*-like barrier for drug irritation and permeation testing

The contents of this chapter are an extended version of the accepted paper: Zoio P, Ventura S, Marto J, Oliva A. Open-source human skin model with an in vivo-like barrier for drug testing. ALTEX - Alternatives to animal experimentation. 2022. https://doi.org/10.14573/altex.2111182.

Author contributions:

Zoio P. developed the skin models, performed the irritation tests, characterization and the data analysis. Zoio P. wrote the article. Ventura S. contributed to the skin characterization. Marto J. performed the permeation tests and the related data analysis. Oliva A. supervised the project and revised the article/chapter.

5.1 Abstract

There is a global trend towards the development of physiologically relevant *in vitro* skin models to reduce and/or replace animal testing in the evaluation of therapeutic drug candidates. However, until now, only commercial reconstructed human epidermis models (RHEms) have undergone formal validation. Although these commercial models are suitable for a wide range of applications, they are costly, lack flexibility and the protocols used to generate them are not transparent. Furthermore, due to the presence of keratinocytes alone, the RHEms lack key interactions with the dermal cells. In this study, we developed a RHEm and a full thickness skin model (FTSm) based on open-source protocols. In particular, an innovative approach was used to generate the FTSm using endogenous extracellular matrix to recreate the dermal compartment, thereby avoiding animal-derived hydrogels. The integrity of the skin barrier was analysed in depth by challenging the surface with detergents and measuring cell viability as well as through transepithelial electrical resistance (TEER) measurements. Skin irritation studies were performed based on OECD guidelines and complemented with evaluation of the impact on the cell barrier using TEER. The comparative permeation study of the developed models and a commercial membrane (Strat-M®) was performed using Franz diffusion cells and an infinite dose approach. Both models demonstrated structural characteristics and barrier properties parallel to the native human skin. Histochemical staining of the models showed an organized, multi-layered epidermal structure. Although the RHEm presented an overall better performance for irritation and permeations assays, both models showed the potential to become open-source alternatives to the existent solutions. These skin model platforms will be a valuable contribution to accelerate the development and dissemination of innovative alternatives to animal testing, circumventing the limitations of commercial models.

5.2 Introduction

Skin diseases are ranked as the fourth leading cause of non-fatal morbidity worldwide, affecting approximately one third of the global population [1]. This is fuelling the growth of the topical drug delivery market and leading to the development of new and better technologies [2–4]. To investigate their mode of action and evaluate potential toxicity, animal models are extensively used in the preclinical phase of topical drug development [5]. However, they frequently lack predictive value for human skin conditions, resulting in high drug attrition rates at later stages of drug development [6]. All of these factors combined with the global legislation commitment to the development of test methods in accordance to the 3Rs (reduction, refinement and replacement of animal experimentation) and the European Union directives prohibiting the use of animal models for cosmetics increased the demand for non-animal alternatives for testing topical formulations [7, 8].

In the last decade, major progress in the development of physiologically relevant *in vitro* human skin models has been made [9]. These models have been extensively used for evaluating the safety and efficacy of new drug formulations or cosmetic ingredients and for studying skin biology and skin-related diseases. However, the complex multi-layered structure and physiology of the native human skin makes it challenging to develop reproducible models that accurately mimic its behaviour [10].

From a histological point of view, the skin is composed of two main layers: the epidermis and the dermis, tightly connected by the dermo-epidermal junction (DEJ) [11]. The epidermal layer is a stratified squamous epithelium containing mainly keratinocytes in close association with melanocytes. Keratinocytes form a proliferative basal layer and differentiate as they move towards the surface of the skin [12]. This process gives rise to the different layers of the epidermis including the *stratum basale* (SB), *stratum spinosum* (SS), *stratum granulosum* (SG) and the most superficial portion, the *stratum corneum* (SC). This outer layer is formed by dead and denucleated keratinocytes (corneocytes), filled with keratin and surrounded by lipids, forming a water-resistant and protective barrier [13]. Melanocytes proliferate

less frequently and remain at the epidermal-dermal junction where they interact with basal layer, playing a crucial role in UV protection [14].

The dermis lies between the epidermis and subcutis and it is mainly composed of human dermal fibroblasts embedded in a collagen matrix. Fibroblasts secrete and remodel extracellular matrix (ECM) components, such as collagen and fibronectin, forming most of this connective tissue and providing the framework and mechanical support to the skin cells [15]. *In vivo*, the epidermis is bound tightly to the dermal component via the basement membrane, which is composed of ECM proteins secreted as a result of interactions between keratinocytes and fibroblasts. The DEJ facilitates the exchange of substances and the polarity of the basal keratinocytes [16].

Engineered skin models are incrementally advancing in emulating the anatomy of the skin. For reconstructed human epidermal models (RHEm), many researchers rely on commercially available *in vitro* skin models such as EpiSkin®, SkinEthic® and EpiDerm® [17]. Most frequently, these models are generated by seeding keratinocytes on a polycarbonate membrane followed by establishment of an air-liquid interface to achieve epidermal differentiation. However, due to the presence of keratinocytes alone, they lack the crosstalk with the dermis which limits their application [18]. Alternatively, more complex full-thickness skin models (FTSm) are commercially available, namely, Phenion®, Epiderm-FT®, Stratatest® and T-Skin® [19 – 21]. These models are created using hydrogel-based technologies, usually animal-derived collagen, into which fibroblasts are integrated. Although these structures mimicking the dermis provide good support to the epidermis and allow communication between keratinocytes and fibroblasts, they present several disadvantages. These include the use of exogenous animal-derived hydrogels, the fibroblast-mediated collagen contraction that result in detachment from the insert, low mechanical stability and batch-to-batch variability [22, 23].

All commercially available skin models have in common the fact that the methods used to generate them are not fully transparent since they are partly based on confidential and legally protected protocols [24]. Moreover, these models are costly and arrive pre-made, lacking the flexibility to be tailored for specific applications. The use of commercial models can also be affected by quality loss after

shipment over long periods of times and distances. To surpass these restrictions, it is crucial to develop open-source protocols to generate reconstructed skin models. The open-source concept was first described in information technology (IT) with LINUX being the most popular example of a free and open software [25]. Reconstructed skin models based on this open concept could lead to independence from commercial suppliers and cost reduction for users. Recently, attempts have been made to develop *in vitro* skin irritation tests based on open-source RHEm with openly accessibly protocols [26]. However, the same validation for open-source FTSm is still lacking.

In the present study, we test the feasibility of using a previously developed open-source FTSm based on a fibroblast-derived matrix (FDM) and scaffold technology for drug testing applications [27]. The developed model avoids the use of animal-derived hydrogels and the consequent problems arising from the use of collagen-based techniques, making it ideal for applications where reproducibility is needed. The integrity of the epidermal barrier was assessed by challenging the surface of the epithelium and by performing transepithelial electrical resistance (TEER) measurements. Irritation tests were performed according to the OECD test guidelines (TG) and complemented with TEER measurements [28]. Finally, permeation studies using Franz diffusion cells were performed on the open source FTSm and compared with an open-source RHEm and the commercial membrane Strat-M®.

5.3 Materials and Methods

5.3.1 Primary cells and cell maintenance

Primary human foreskin-derived dermal fibroblasts (HDFn; CellnTec, Bern, Switzerland) were maintained in Fibroblast Growth medium (FGM) composed of Iscove's Modified Dulbecco's Medium (IMDM, ThermoFisher, Loughborough, UK) supplemented with 10% fetal bovine serum, at 37°C in a 5% $C0_2$ humidifier, following supplier's instructions. HDFs were used for up to 8 passages and subcultured at confluency between 80 and 90%.

Primary human epidermal keratinocytes isolated from neonatal foreskin (HEKn, ThermoFisher, Loughborough, UK) were maintained in keratinocyte growth medium (KGM) composed of EpiLife medium (ThermoFisher Scientific), supplemented with 0.06 mM calcium and keratinocyte growth factor (HKGS, ThermoFisher), at 37°C and 5% CO_2 in a humidified incubator. The KGM medium was changed every other day until the cells reached 50% confluency. At this point the medium was changed every day until reaching 70-80% confluency. A low passage (3-4) and actively proliferating keratinocytes were used for successful 3D culture.

5.3.2 Generation of the open-source FTSm

The development of a FTSm based on a FDM comprises the development of a mature dermis composed of fibroblasts and ECM and the formation of a differentiated epidermis on top of the dermis. The in-depth protocol can be seen in Chapter 4 [27]. **Figure 5. 1.a** shows a schematic representation of the FTSm with a scaffold structure and HDFns to generate the dermal compartment and the HEKns generating a stratified epidermal compartment.

Briefly, for the formation of the fully-human dermal equivalent, HDFns ($1.0x10^6$ cells) were seeded within inert porous polystyrene scaffolds (REPROCELL Europe Ltd, Glasgow, UK) in 100 µL FGM medium and incubated at 37°C, in a humified atmosphere of 5% CO_2 for 1.5 hours. After the cell adhesion period, FGM supplemented with 100 µg/mL ascorbic acid 2-phosphate (Sigma-Aldrich) was applied to the bottom of each well to flood the insert prior to incubation and maintained for 9 days at 37°C in a 5% CO_2 humidified incubator, changing the media every 3 days. During this period, HDFns were stimulated to proliferate and secrete endogenous dermal ECM.

The FTSms were generated by seeding HEKn onto the dermal equivalents. As a first step, HEKns ($5.0x10^5$ cells) were incubated under submerged conditions in KGM containing high calcium concentration (1.5 mM) and maintained at 37°C, in a humified atmosphere of 5% CO_2. After 3 days, the models were raised to the air-liquid interface (ALI) by removal of the medium in the upper compartment and cultured in KGM containing 1.5 mM calcium, supplemented with 10 ng/mL KGF and 100 µg/mL L-ascorbic acid 2-phosphate. The medium was changed every other

day and the FTSms were maintained for 12 days. at 37°C in a 5% CO_2 humidified incubator.

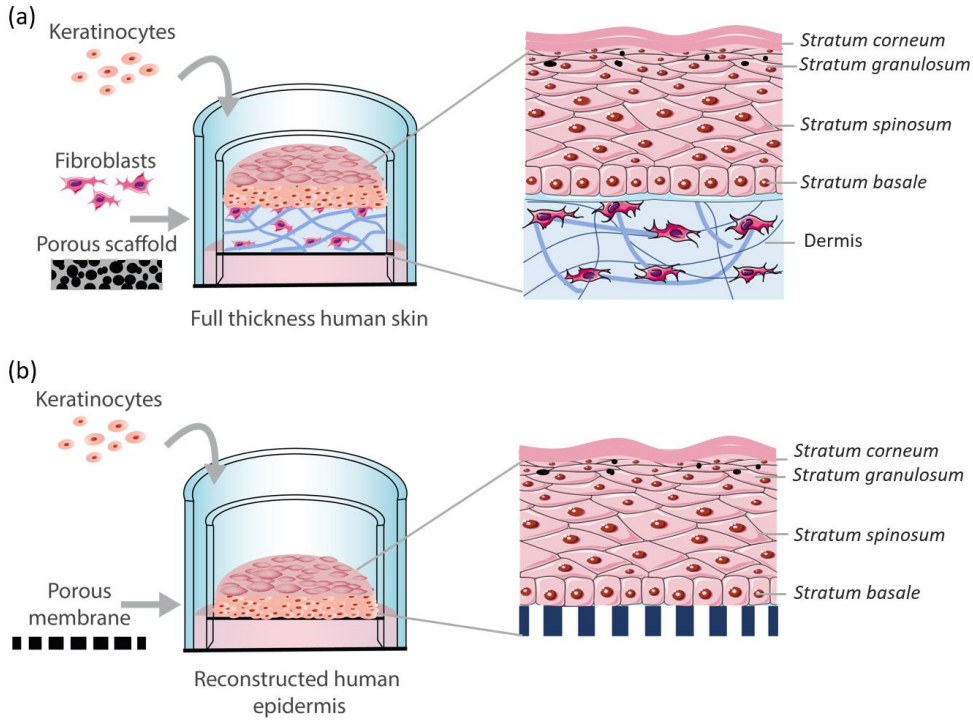

Figure 5. 1. Schematic depiction of an open-source (a) full-thickness model (FTSm) and (b) reconstructed human epidermis model (RHEm). FTSm are generated using a porous polystyrene scaffold seeded with fibroblasts to recreate the dermal compartment and keratinocytes are seeded on top of the dermal compartment. RHEm are generated by seeding keratinocytes on top of a porous membrane. An air-liquid interface is established to generate a fully-differentiated epidermis with the layers present in the *in vivo* skin.

5.3.3 Generation of an open-source RHEm

Epidermal models were generated by seeding HEKns in porous polycarbonate cell culture inserts with a 0.4 μm pore size (Merck Millipore, Beeston, UK). **Figure 5. 1.b** shows a schematic representation of an RHEm generated on top of a porous membrane. Briefly, HEKns were harvested by trypsinization, centrifuged, and $3.0x10^5$ cells/mL were re-suspended in KGM containing high (1.5 mM) calcium concentration. The polycarbonate culture inserts were placed in 6-well plates containing 2.5 mL medium and seeded with 500 μL keratinocyte suspension.

HEKns were incubated at 37 °C in a humidified 5% CO_2 incubator. After 24h, the models were raised to ALI. The medium was replaced by 1.5 mL of modified EpiLife culture medium, supplemented with 1.5 mM Calcium, 100 µg/mL ascorbic acid 2-phosphate and 10 ng/mL KGF and renewed every other day. The epidermal models were maintained for 12 days.

5.3.4 Histological analysis

The reconstructed tissues were fixed immediately after being taken out of culture in 10% neutral buffered formalin (Sigma). The samples were embedded in paraffin to allow for transverse sectioning. Paraffin-embedded sections (5-µm-thick) were de-paraffined and re-hydrated for morphological evaluation by staining with haematoxylin and eosin (H&E) through standard methods.

5.3.5 Barrier function

5.3.5.1 Effective concentration at 50% viability

The barrier function was studied by determination of the concentration at which a benchmark chemical reduces the viability of the tissues by 50% (IC_{50}) after a fixed exposure time. For this, a range of concentrations of sodium dodecyl sulphate (SDS) from 0 to 5 mg/mL were topically applied (70 µL for the RHEm and 150 µL for FTSm) for 18 h. After exposure, samples were washed in PBS to remove medium containing phenol red.

For the FTSm, scaffold discs were removed from the support by unclipping the plastic base and placed in 12-well plates. 1 mL MTT [3-(4,5-dimethylthiazol-2-yl)-2,5-diphenyltetrazolium bromide, 1 mg/mL in phosphate buffered saline (PBS), Sigma-Aldrich] was added to each well and incubated at 37°C in a 5% CO_2 incubator for 1.5 h. The MTT solution was replaced by 1 ml acidified isopropanol. The plates were covered with parafilm, protected from light and left at room temperature on a rotating platform for 30 min at 100 rpm to ensure blue formazan product was fully solubilized.

For the RHEm, inserts were removed from the 6-well plates, washed with PBS and transferred into the 24-well plates prefilled 300 µL of MTT solution (1

mg/mL). RHEs were incubated at 37 °C in a 5% CO_2 incubator for 3 h. After MTT incubation was completed, the culture inserts were then immersed in 2 mL/well of acidified. The plates were left for 2 hours temperature on a rotating platform (100 rpm).

After the extraction period was completed for RHEm and FTSm, samples of the formazan solution of each well were mixed and transferred in two aliquots of 200 µL each into 96-well plates. Absorbance was read at 570 nm using a plate reader. Relative MTT values were calculated with control cultures being set at 100%. Values were normalized to nontreated skin models.

5.3.5.2 Barrier integrity evaluation by passive dye diffusion

The barrier function of the skin models was further assessed by the penetration of the passive dye lucifer yellow (Sigma) in combination with a detergent treatment. Solutions of various SDS concentrations (0-0.5% w/v in PBS) were applied topically (70 µL epidermal models and 150 µL full thickness model). After 2 h incubation at 37°C, the models were washed three times with PBS and 1 mg/mL Lucifer yellow was topically applied to the models for 30 minutes, followed by three washes with PBS. The tissues were fixed with a neutral buffered 10% formalin solution (Sigma) and embedded in paraffin. Tissue sections were rehydrated and nuclei were stained with 1 µg/mL of 4,6-diamidino-2-phenylindole (DAPI, Invitrogen, Waltham, MA, USA) and slides were mounted with VECTASHIELD (Vector Laboratories, Burlingame, CA, USA). Images were obtained using the Nikon Eclipse TE2000-S fluorescence microscope (Nikon instruments, Melville, NY, USA) and analysed with the ImageJ software.

5.3.5.3 Transepithelial electrical resistance

The barrier integrity of RHE and FTSm models were also evaluated by monitoring the TEER. Measurements were taken using an EVOM Epithelial Volt/Ohm Meter and pair of Ag/AgCl probes (WPI Europe, Friedberg, Germany). For both FTSm and RHEm, measurements were performed on the last day of culture, after 12 days of cell culture at the ALI, before their fixation in formalin. TEER values were calculated according to the equation 4.1. For RHEm, the KGM was replaced

with 300 µL PBS in the apical region and 2 mL PBS in the basal region. For FTSm, for the time required to measure electrical resistance, the tissues were placed in adapted 6-well plates containing 2 mL PBS. The KGM was aspirated and replaced with 250 µL of PBS in the apical region. For both models, the probe was placed such that one electrode was submerged in the upper compartment and the other was submerged in the lower compartment. These measurements were performed for four different skin batches for FTSm and RHEm. TEER values measured for skin batches used in previous studies (historical TEER values) were also considered. These values were used to determine a lower threshold by correlating the measurements with skin defects detected macroscopically and through histological analysis. FTSm and RHEm with TEER values lower than the threshold were not used.

5.3.6 Skin Irritation test

5.3.6.1 Study design and Test protocol

The irritation tests were performed according to the OECD TG 439 [28]. The reference substances were 5% aqueous potassium hydroxide (Sigma) and 1-bromohexane (Sigma) both classified as irritants (category 2 substance) according to the United Nations Globally Harmonized System of Classification and Labelling of Chemicals (UN GHS), and isopropanol (Sigma) and diethylene glycol monoethyl (Transcutol®, Sigma) either classified as non-irritant (no category substance). Two controls were included in each test run. PBS was applied to the top of the models as a negative control (non-irritant) and 5% aqueous SDS served as positive control (irritating). Three tissue replicates were used for each chemical substance and duplicates for the controls. All test compounds were pre-checked prior to its use for direct MTT reduction and colour interference as described in the OECD TG 439.

Figure 5. 2 shows the steps performed for skin irritation testing. Briefly, RHEms and FTSms were topically treated with the test substances for 20 minutes. Following exposure, tissues were washed with PBS and incubated for 42 h at 37°C in a CO_2 incubator. At the end of chemical treatment, tissue viability was evaluated by the MTT assay using the protocol described in section 5.3.5.1. The optical density

(OD) of the samples was read in a 96-well plate spectrophotometer at 570 nm and corrected against blanks. The reduction of cell viability in tissues treated with test substances was compared to treated tissues with negative control (100% viability) and expressed a %, according to equation 5.1.

$$\%Viability = \frac{OD_{sample}}{OD_{negative\ control}} \times 100 \quad [5.1]$$

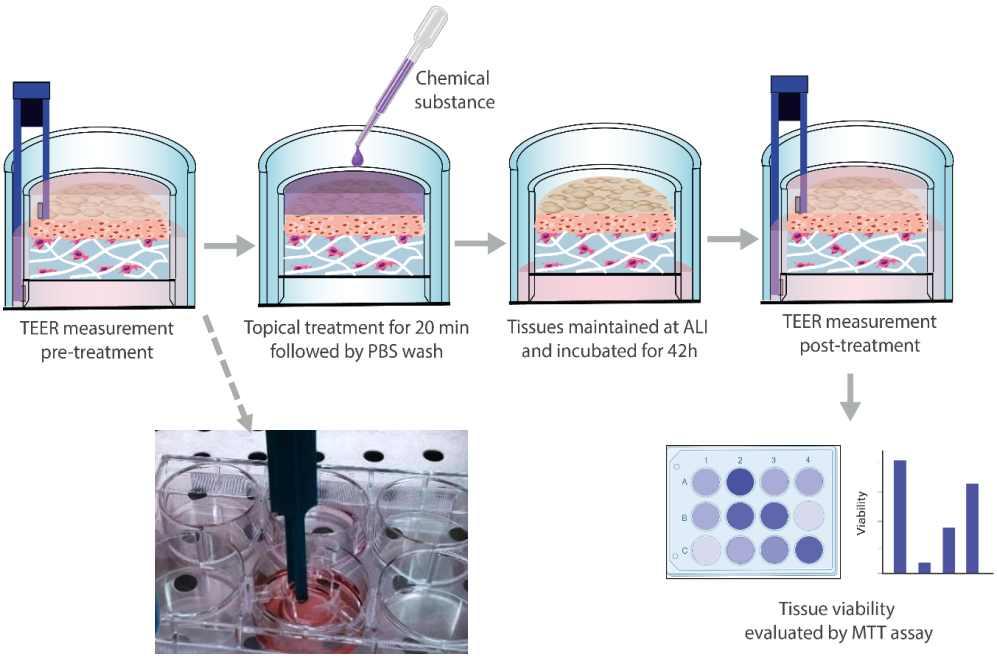

Figure 5. 2. Schematic of the protocol for skin irritation testing. TEER measurements were performed before application of the test substances using chopstick electrodes. Models were topically treated for 20 minutes followed by washes with PBS. The skin tissues were then incubated for 42 h at 37 °C in a CO_2 incubator. After this incubation period, TEER measurements were performed and the tissue viability was evaluated by an MTT assay.

5.3.6.2 Prediction/Evaluation model

The prediction/evaluation model to assess chemical hazard based on OECD TG 439 uses a viability threshold to classify a substance [28]. A substance was classified as "irritating" or "category 2" when the average viability after skin irritation test obtained using the MTT assay was below 50%. A substance was

classified “non-irritating” or “no-category” when the mean viability was above 50%. Also, a tissue was considered as conforming if the mean OD values of the negative control were between 0.6 and 2.8 for every exposure time, as it is the range that includes all OECD validated models, the mean viability of the tissue replicates exposed for 1 h with the positive control were <15% and the standard deviation (SD) was ≤18.

5.3.6.3 TEER for skin irritation test

TEER measurements were also performed as a complement of the skin irritation test. To evaluate the effects of chemical substances on the TEER values of fully matured RHEs and FTSm (day 12 of ALI), measurements were taken before and 42h hours after exposing the tissue to the test substances. TEER measurements were performed as described in section 2.5.3. Raw reads of the TEER value for tissue were reported for the test substances in 3 replicates. The means and SDs of TEER values of selected compounds were normalized to untreated skins and reported as fold of change over control.

5.3.7 Permeation assays using Franz diffusion cells

In vitro permeation tests were performed for different formulations in Franz cells of static flow (volume 4 mL, diffusion area of 1 cm^2), using the RHEms, FTSms and Strat-M® (Merck Millipore, Tullagreen, Carrigtwohill, Ireland). Three test compounds with varying polarity were used for the permeation testing: clotrimazole (FIS – Fabbrica Italina Sintetici S.p.A., Montecchio Maggiore, Italy) and hydrocortisone (Tianjin Jinjin Pharmaceutical Co.,LTD., Tianjin, China), both applied as a 1% (w/v) solution in propylene and salicylic acid (Quimidroga, Barcelona, Spain), applied as a 1% (w/v) solution in propylene glycol/water 9:1. The experiments were performed in triplicate (n=3) for both FTSms, RHEms and Strat-M® membranes. The RHEms and FTSms were visually inspected for any defects. Since both FTSms and RHEms were too small to be directly mounted into the Franz diffusion cells, dedicated adaptor modules were designed in AutoCad (Autodesk, Inc.) and fabricated using 3D-printing (**Figure A. 1** and **Figure A. 2**). The adaptors

allowed correct placement of the skin models in the centre of the Franz cells (**Figure A. 3**).

The receptor medium, a mixture of PBS: ethanol 3:1, was appropriately screened based on solubility studies to ensure the sink conditions during the experiment. The release media was continuously stirred with a magnetic bar and maintained at (32 ± 2)°C by a thermostatic water pump, assuring a temperature of 32°C at the membrane surface (to mimic skin conditions). Aliquots of the receptor phase (200 μL) were withdrawn after 1, 2, 4, 5, 6, 8 and 24 h, and analysed via UV at 298 nm for salicylic acid, 263 nm for clotrimazole and 254 nm for hydrocortisone.

The cumulative amount of permeated drug (*Qt*) through the different models was plotted as function of time and determined based on the following equation 5.2:

$$Qt = \frac{Vr \times Ct + \sum_{t=0}^{t-1} Vs \times Ci}{S} \quad [5.2]$$

where, *Ct* is the drug concentration of the receiver solution at each sampling time, *Ci* is the drug concentration of the sample applied on the donor compartment, and *Vr* and *Vs* are the volumes of the receiver solution and the sample, respectively. S represents the skin surface area.

According to Fick's first law of diffusion, the steady-state flux (J_{ss}, μg/cm²/h) was calculated:

$$J_{ss} = DC_0P/h = C_0K_p \quad [5.3]$$

where *D* is the diffusion coefficient of the drug, C_0 represents the drug concentration in the donor compartment, *P* is the partition coefficient between the vehicle and the skin, *h* is the diffusional path length, and K_p stands for the permeability coefficient.

The flux and K_p of the formulations were measured and compared accordingly. The J_{ss} and K_p of the yielded solutions were calculated and compared.

The permeation lag time, a parameter related to the required time to achieve the steady-state flux of a drug through the skin, was also considered for analysis.

5.3.8 Statistical analysis

Data are presented as mean ± SD. Quantitative differences between samples was assessed by the one-way ANOVA and a p value <0.05 was considered statistically significant (*), p<0.01 very significant (**) and p<0.001 highly significant (***).

5.4 Results

5.4.1 Open-source skin models recapitulate the morphology of human skin

The FTSm and RHEm were developed based on the open-source methodology first presented by Zoio *et al* [27]. The basic morphology of the generated models was analysed by conducting H&E staining on transverse sections. **Figure 5. 3** shows that both skin models formed a complex architecture with a multi-layered epidermis after 12 days of culture at ALI. The models replicated the normal process of epidermal stratification, presenting the four main layers: SB, SS, SG and SC. As expected, in the lower part of the epidermis (SB), HEKns show a cuboid morphology, followed by the cells of the SS and SG with a flatter architecture and anucleated cells closer to the surface. At the apical surface, a cornified layer can be clearly seen in both models.

The FTSm includes a fully human dermis capable of supporting the multi-layered epidermis without HEKn infiltration. **Figure 5. 3** (top) shows the dermis compartment with HDFns distributed along the scaffold and FDM which built up and accumulated in the pores mimicking the composition of the native human dermis.

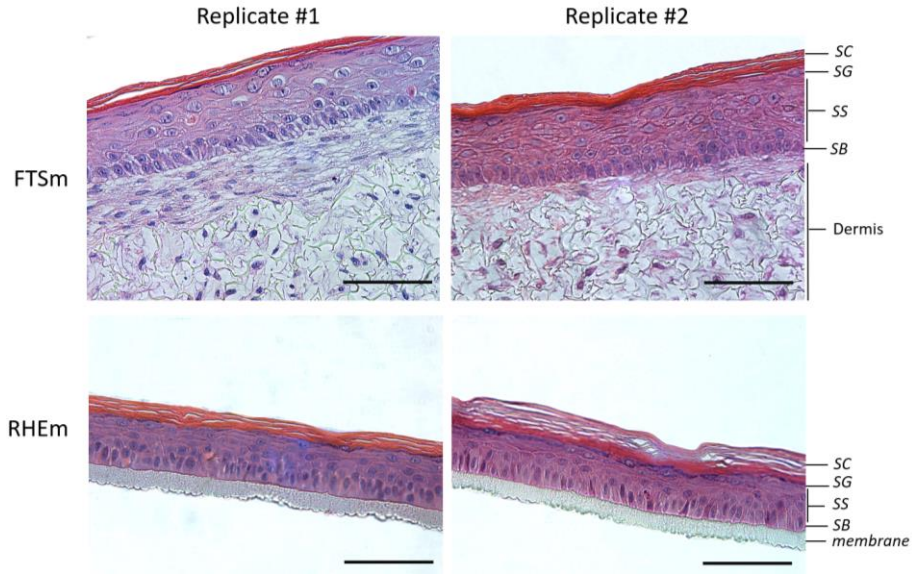

Figure 5. 3. Representative H&E images of two independent replicates of a full thickness skin model (FTSm) composed of dermal and epidermal compartment and a reconstructed human epidermal model (RHEm). Both models were maintained at the air-liquid interface for 12 days to promote epidermal differentiation. Stratum corneum (SC), Stratum granulosum (SG), stratum spinosum (SS) and Stratum basale (SB). Scale bars: 100 μm

5.4.2 Reconstructed full-thickness skin models show improved barrier function

The barrier function of the RHEm and FTSm was assessed by testing the capability of the SC and its lipid composition to resist the rapid penetration of a cytotoxic benchmark (SDS) as estimated by IC_{50}. The viability of the models cultured at ALI for 12 days were assessed by MTT colorimetric assay. Upon application of various SDS concentrations, IC_{50} values of 1.5 mg/mL and 1.8 mg/mL were determined for RHEm and FTSm, respectively (**Figure 5. 4.a**). The calculated values for the effective concentrations that reduce tissue viability by 50% were within OECD acceptance limits. Moreover, the tissue damage induced by a cytotoxic benchmark and the resultant disruption of the skin barrier was visualized by topical application of increasing concentrations of SDS (0.15 to 0.5%) for 2h followed by the observation of the passive diffusion of the hydrophilic fluorescent dye, lucifer yellow, for FTSm (**Figure 5. 4.b**) and RHEm (**Figure 5. 4.c**).

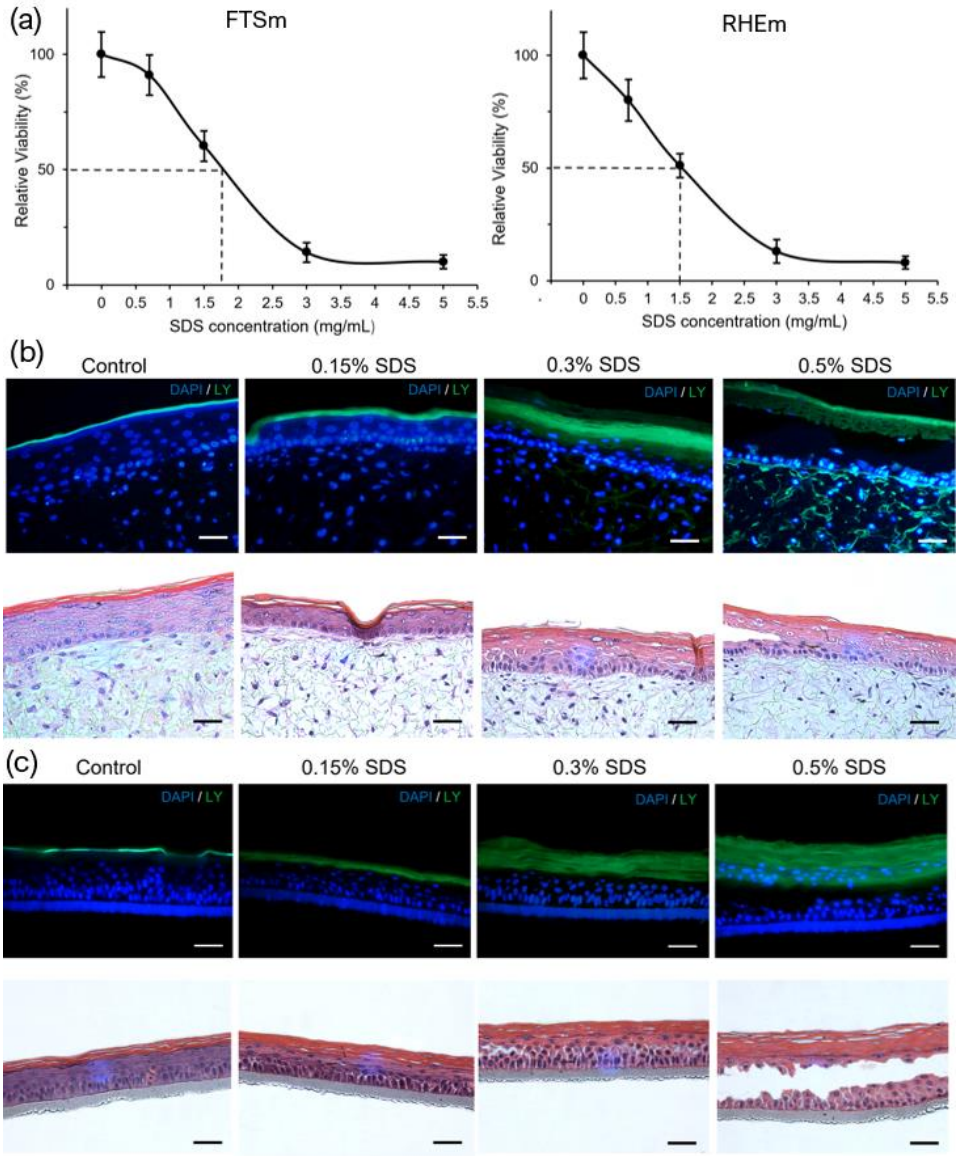

Figure 5. 4. Assessment of barrier properties in epidermal and full thickness models. (a) Analysis of metabolic activity (MTT conversion) in the epidermal model cultured for 10 days at the air–liquid interface before being exposed for 18 h to a concentration range of SDS to determine an IC50 value. Assessment of barrier resistance in (b) Full thickness models and (c) reconstructed skin models. Representative fluorescence (top) and H&E images (bottom) of full thickness skin models and epidermal models cultured for 12 days at ALI. Samples were exposed to a concentration range of SDS for 2 h, followed by the application of the dye lucifer yellow (LY) for 30 min to assess the penetration of dye diffusion and barrier integrity. Nuclei are stained with DAPI (blue colour). Scale bar = 50 μm

When the dye was applied to an untreated skin model it was retained in the SC and no diffusion was observed in the epidermis or into the dermal layer, showing the integrity of the skin barrier for this molecule. For skin models treated with SDS, the diffusion of the dye was dose-dependent, with the dye being mostly retained in the stratum corneum at lower SDS concentrations and with higher penetration for higher SDS concentrations (> 3 mg/mL). A complete lack of epidermal integrity was observed for skin models treated with 0.5% SDS and it was possible to observe tissue damage.

To further assess the integrity of the stratifying cultures, TEER measurements were performed. This technique is useful to study the integrity of tight junctions (TJ) and the presence of barrier dysfunction. TEER was measured after cell culture for 12 days at ALI, for both models. Considering both 4 batches/biological replicates (N=4) with different technical replicates each (n=8,4,4,9) as well as the historical TEER values, FTSm presented mean TEER values of 953±398 $\Omega.cm^2$ (**Figure 5. 5.a**) and the RHEm presented mean TEER values of 11424±6033 $\Omega.cm^2$ (**Figure 5. 5.b**).

For FTSm, evaluation of the skin models macroscopically and through histological analysis led to the establishment of a lower limit for TEER values. Models with TEER values lower than 500 $\Omega.cm^2$ presented macroscopic defects. An extreme macroscopic defect can be seen in **Figure A. 4**. The most common observation was the presence of small holes on the surface of the model. Histologic analysis showed that, on these regions, the epidermal compartment was not present. However, no signs of keratinocyte infiltration were present. This problem possibly occurs due to irregularities in the scaffold structure and affected 15% of the produced FTSm, showing a need for protocol optimization. Only 3% of the produced FTSm presented lower TEER values caused by an undifferentiated epidermis. Taking the overall observations into account, FTSm with TEER < 500 $\Omega.cm^2$ were not used in other experiments.

For RHEm, a lower limit of 1500 $\Omega.cm^2$ for TEER values was established. In models with these lower values, it was not possible to establish an ALI and the inserts remained submerged. As expected, histological evaluation of these

submerged models showed an undifferentiated structure. Taking this into account, RHEm with TEER < 1500 Ω.cm² were not used in other experiments.

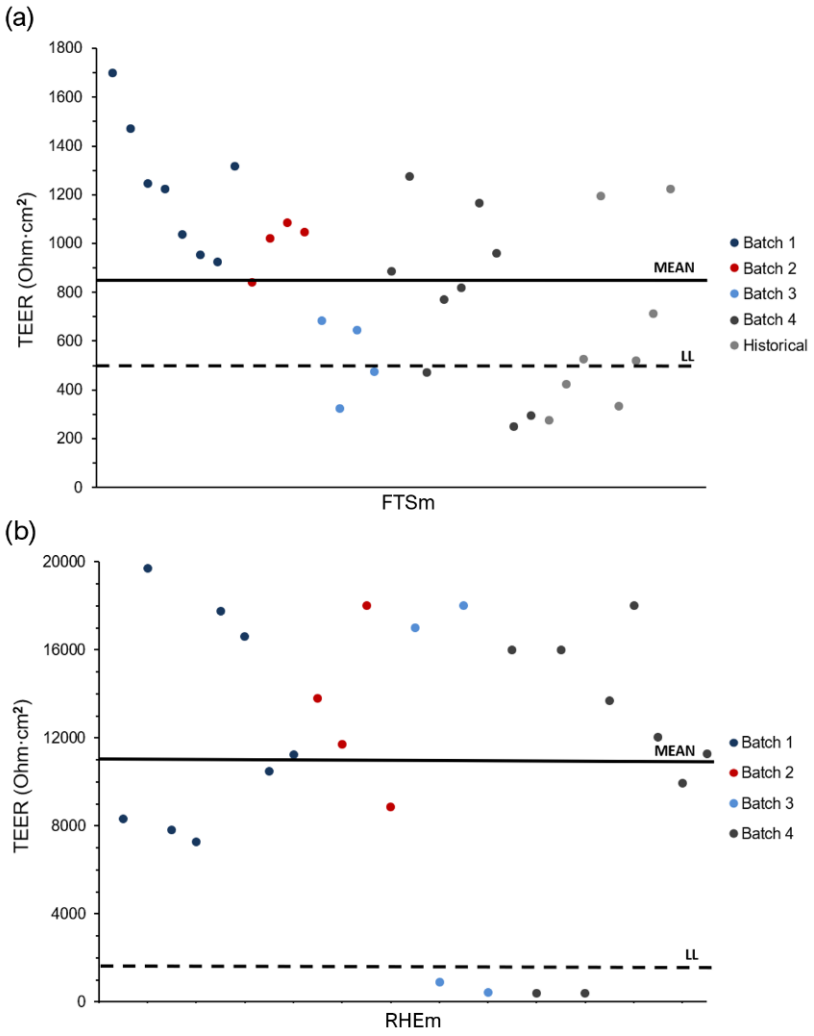

Figure 5. 5. Transepithelial electrical resistance (TEER) measurements performed with an EVOM system and chopstick electrodes obtained after 12 days of culture at the ALI, before fixing tissues in formalin, for (a) Full thickness model (FTSm) and (b) Reconstructed skin model (RHEm). Data represent the different technical replicates, for each batch and historical values. Reported TEER as Ω·cm² tissue surface area. The solid line represents the mean value and the dashed line represents the defined lower limit (LL). EVOM, Epithelial Volt/Ohm Meter; TEER, transepithelial electrical resistance.

5.4.3 Open-source skin models are suitable to test irritation potential of substances

To evaluate the performance of the developed FTSm and RHEm for skin irritation tests, the effect of different chemical substances on the cell viability and impedance was evaluated (**Figure 5. 6**). A negative (PBS) and positive control (5% SDS solution) were included in every test run. Three substances suggested by OECD TG 439 were included (5% potassium hydroxide, isopropanol and 1-Bromohexane), as well as one substance commonly used as a skin penetration enhancer in pharmaceuticals and cosmetic products (diethylene glycol monoethyl ether, Transcutol®).

After topical application of the chemical substances and a subsequent post-incubation time, cell viability was assessed using MTT assay. The relative cell viability was normalized to the PBS-only treated tissues and the relative values of FTSm were compared with values of RHEm (**Figure 5. 6.a**). The OD values of the negative controls were 1.73±0.27 for FTSm and 0.89±0.03 for RHEm, meeting the acceptance criteria of $0.6 \leq OD \leq 2.8$. The positive control demonstrates the sensitivity of the tissue model to a known irritant. The mean viability of the positive control (relative to negative control) varied between 0.5% and 3%, meeting the acceptance criteria of <15%. The SD for both models was always ≤18%. To identify the predictive capacity of the models, the *in vitro* classification obtained was compared to the reference *in vivo* classifications using animal testing [28]. MTT staining confirmed the irritative characteristics of 5% potassium hydroxide for both RHEm and FTSm. However, 1-bromohexane was only correctly identified on the RHE model (48% relative viability). On the FTSm, treatment with this substance resulted in a relative viability of 63.7% which would lead to a classification of non-irritant (or category 2). Isopropanol and diethylene glycol monoethyl ether were correctly identified as non-irritants (no category) in both models.

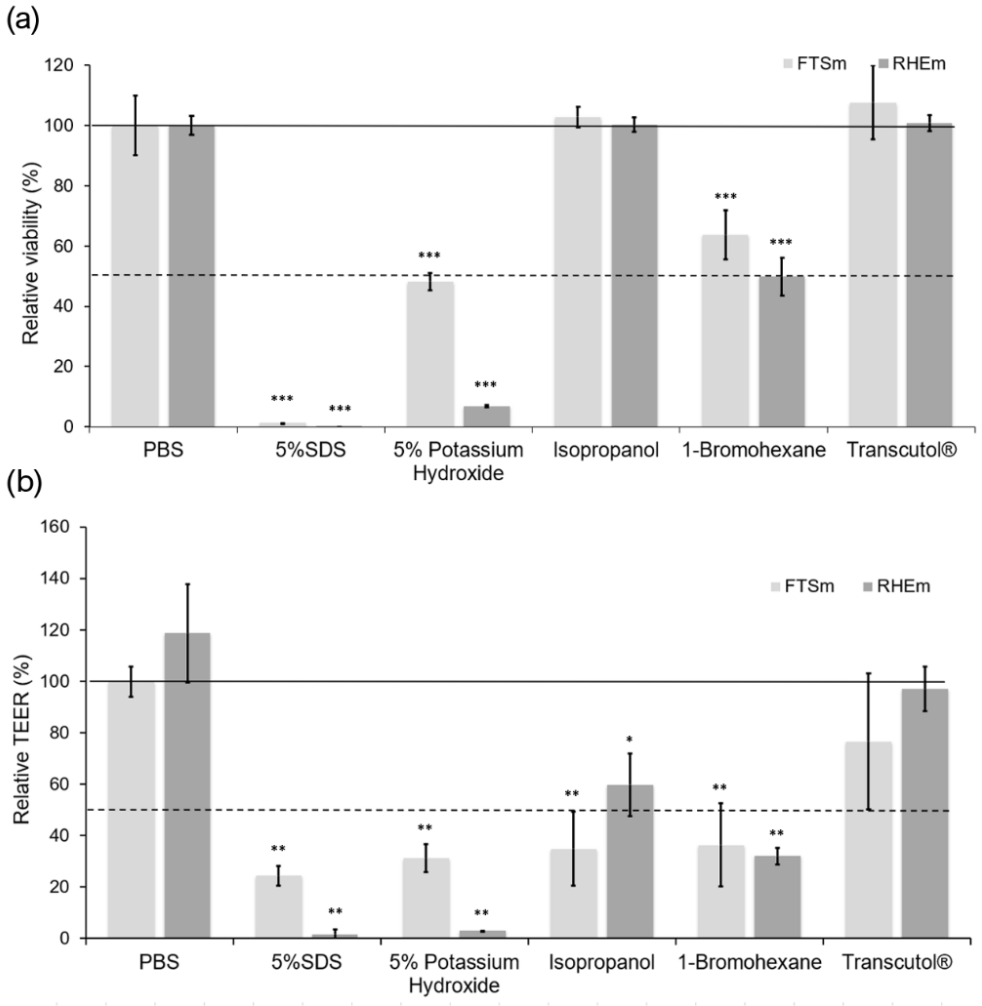

Figure 5. 6. Effect of the test substances on the skin models (FTSm and RHEm). a) Irritation tests evaluated by MTT analysis. Treatment with PBS was set as negative control and treatment with 5% SDS was set as a positive control. The relative increase/decrease in viability was normalized to the change (in %) over the negative control (set to 100%, black solid line). The black dashed line highlights the threshold of 50% viability compared to the negative control. b) Irritation tests evaluated by TEER measurements. The relative increase/decrease in TEER values after treatment with test substance were normalized to the change (in %) over the TEER values before treatment (set to 100%, black dashed line). Black dashed highlights the threshold of 50% compared to the TEER values before treatment with test substance. Data is expressed as mean ± SD from triplicate experiments.

In addition to viability, TEER was measured for RHEm and FTSm before the application of the test formulations and before the MTT assay (**Figure 5. 6.b**). For both models, the application of the irritants 5% SDS, 5% potassium hydroxide and 1-Bromohexane resulted in a marked decrease in TEER values. This effect was more pronounced in the case of RHEm. However, in both models, treatment with the irritants resulted in a reduction of at least 50% comparative to TEER values before their application. Although the viability measurements correctly identified isopropanol as non-irritant, for FTSm, treatment with this substance reduced TEER values in a range that was comparable to the SDS group (70 % reduction). For RHEm, the reduction in TEER values after treatment with isopropanol was less pronounced but showed a significant decrease of approximately 40% the TEER values. For RHEm, when testing diethylene glycol monoethyl ether, no significant changes were detected in TEER which correlates with the data from cell viability. For FTSm, the substance resulted in a 25±25% decrease in TEER values.

5.4.4 Comparative permeation between the reconstructed skin models and artificial membranes

In the permeation assays, FTSms, RHEms and Strat-M® membranes were mounted in Franz diffusion cells. Three test substances (Salicylic acid, hydrocortisone and clotrimazole) were applied to the models. The cumulative amounts of permeated drugs in the models and the steady-state flux were obtained. The steady-state fluxes calculated for salicylic acid using both RHEm and FTSm were not significantly different from the Strat-M® (**Figure 5. 7.a**). The cumulative amount of permeated salicylic acid at 24 h was significantly lower using the FTSm. For hydrocortisone, high permeation fluxes through the FTSms were observed, compared to Strat-M® and RHEm (**Figure 5. 7.b**). RHEm shows a 15% lower permeation rate that the Strat-M membranes. The amount of permeated hydrocortisone after 24 h was not significantly different between the skin models and Strat-M. For the experiment with hydrocortisone, FTSms show high standard deviations. The permeation flux of clotrimazole using both FTSm and RHEm were approximately double the flux compared to using Strat-M® membranes (**Figure 5. 7.c**). The cumulative amount of clotrimazole at the 24 h was not significantly different between the models.

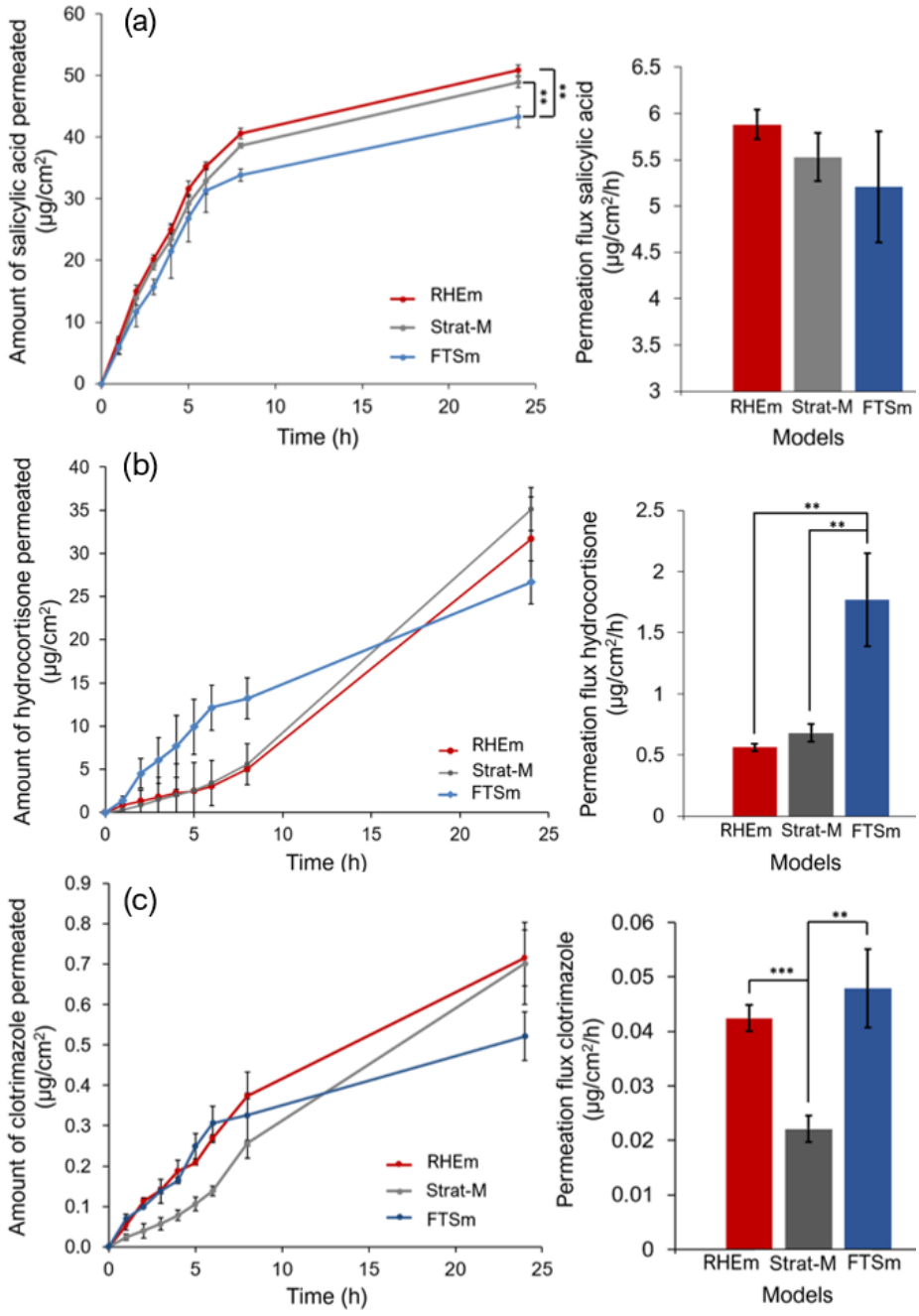

Figure 5. 7. *In vitro* permeation tests performed for a) Salicylic acid, b) Hydrocortisone and c) Clotrimazole. Experiments performed in Franz cell of static flow, using the RHEms, FTSms and Strat-M®. Cumulative amount of permeated (mean values ± SD) (left) and the steady-state flux (mean values ± SD) (right).

5.5 Discussion

5.5.1 Open-source skin models with *in vivo*-like morphology and barrier function

In this work, we studied the potential applications of an open-source FTSm with an *in-vivo* like architecture and optimized co-culture of fibroblasts and keratinocytes. The in-depth protocol to produce the FTSm was previously published by our group [27]. In this protocol, an inert porous scaffold is used as a support for the dermal compartment. Fibroblasts are seeded onto the scaffold and stimulated to secrete endogenous extracellular matrix, thereby avoiding the use of animal-derived collagen matrices. In the previous publication, we showed that this model, contrary to conventional commercial models, presents good mechanical stability and is compatible with long-term cultivation. Furthermore, melanocytes can be added to recreate *in vivo*-like pigmentation.

Here, multiple batches of FTSm with a fully differentiated epidermis were generated. The produced skin models mimicked the structure and function of the native counterpart and recreated the layers characteristic of the native epidermis (SC, SG, SS, SP) on top of the mature dermis. Furthermore, an open source RHEm was also developed and evaluated in parallel. The feasibility of using the developed skin models for skin irritation testing was assessed by applying multiple chemical substances, following OCDE guidelines and skin permeation tests. Furthermore, suitability of using TEER measurements as a non-destructive technique to quantify the barrier integrity of FTSm and RHEm was evaluated. This technique was also implemented for quality control and as a complement of irritation tests.

The development of a relevant FTSm for drug permeation and irritation depends on the recreation of the skin barrier function, similar to *in vivo* healthy human skin. The characterization of the barrier function was performed using a cytotoxic benchmark known to erode the barrier structure (SDS) and by comparing its permeation profile with accepted models. The open-source FTSm and RHEm present IC_{50} values within the OECD acceptance limits. Moreover, the tissue damage induced by a cytotoxic benchmark and the resultant disruption of the skin barrier

was visualized by passive diffusion of the aqueous-soluble lucifer yellow. The ability of the produced models to retain the dye in the SC with absence of passive diffusion showed the integrity of the skin barrier. These findings attest the presence of an intact barrier function on these models, demonstrating their potential as future *in-vitro* test systems.

5.5.2 TEER as a tool for skin quality control

The feasibility of using TEER analysis as a multi-purpose tool to evaluate the stages of skin differentiation was assessed by evaluating the impact of topically applied substances on the skin barrier. TEER reflects skin barrier functionality by measuring overall barrier to ions [29]. It takes into account the contributions from the SC barrier as well as the viable epidermis by including cell-to-cell TJs which regulate the movement of ions across the paracellular pathway [30], [31]. In a previous publication, we showed that, during RHEm and FTSm culture for two weeks at ALI, there is an increase in TEER values reflecting progressive SC accumulation and TJ formation [27].

Here, the TEER was measured at the final day of culture, for multiple tissue batches. A mean TEER value of 953±398 $\Omega \cdot cm^2$ was obtained for the FTSm and a 11424±6033 $\Omega \cdot cm^2$ for the RHEm. This high TEER values are consistent with the presence of barrier function integrity. The high variability of these measurements is not only of biological origin but it is also a result from the use of chopstick-type electrodes. An in-depth discussion related to the limitations of the tetrapolar electrode system for TEER measurements can be seen here [32]. In this is paper, it is hypothesized that the lower TEER values measured in the FTSms compared to the RHEms is a result of lower keratinocyte adhesion at the interface between the scaffold and the insert wall. In general, it is possible to conclude that a meaningful comparison between TEER values can only be performed between inserts/setups with comparable characteristics/geometry. Other factors can affect the accuracy of the measurements including the selection and usage of electrodes, the temperature during measurement and medium formulation [29]. This explains why, for the same cell type, a wide range of TEER values have been reported in the literature [33]. Still, TEER values for the developed skin models are within the range of validated commercial models (Epiderm™: 510 ± 120 Ωcm^2) and models that still misses formal

regulatory acceptance (Keraskin™-VM [34]: > 500 Ωcm²; FTSm using cell coating technology [35]: >1000 Ωcm²).

TEER was also used to evaluate the integrity of the barrier function of each FTSm prior their use in the subsequent assays. By detecting various skin defects using histology analysis and macroscopic evaluation and by correlating these observations with the measured TEER values, a lower threshold was established for both models. For the FTSm, the established lower limit was TEER ≤ 500 Ωcm² and for RHEm the lower limit was TEER ≤ 1500 Ωcm². Wei *et al* also reported the use of tissues with TEER values above 500 Ωcm² in compound screening. Although the group measured different mean TEER values between their FTSm and RHEm, they established the same lower limit for both models. Interestingly, their RHEms also presented values considerable higher than their FTSms.

5.5.3 Skin irritation assays

After studying the developed FTSm and RHEm regarding morphology, viability and barrier function, preliminary skin irritation tests were performed. Since the ban of animal testing for cosmetic research, the need for reconstructed human skin models have increased significantly [5]. OECD published specific guidelines which models must meet to be used in a standardized manner for the evaluation of skin irritation. In this study, we used the OECD TG 439 as a basis to study the performance of the open-source RHEm and FTSm in its capability of correctly classifying a test substance as irritating (category 2) or non-irritating (no category). When skin models are used in the assessment of skin irritants, substances are classified as irritants or non-irritants by their effect on the viability of RHEs and/or the levels of interleukins [36]. Using the MTT assay, RHEm correctly identified 4/4 substances and the FTSm correctly identified 3/4 substances.

Interestingly, the FTSm determined that 1-bromohexane was a non-irritant and RHEm showed viability of 48%, which could be considered as a "borderline" substance. Similar results were also obtained in [26] and [34]. In a human patch test, 1-bromohexane was identified as an irritant but a large variation was observed [37]. Mewes *et al* hypothesized that the variability seen in the patch tests could be

mirrored in the irritation tests using tissue models [26]. The genetic backgrounds of the keratinocyte donor, including the ethnic background, could be responsible for the observed differences in the sensitivity to 1-bromohexane. However, additional studies are needed to confirm this hypothesis. In general, the FTSm shows and increased viability when exposed to irritants comparing to RHEm, which is evident when looking at the case of 5% potassium hydroxide. This can be explained by the added contribution of the dermal layer. It can be hypothesized that less of the test substance is able to penetrate in the dermal compartment and cause fibroblast death.

TEER measurements were performed as a complement of viability measurements for skin irritation tests. If we consider a threshold of 50% TEER value when compared to skin without treatment (normalized to 100%), all the substances are correctly identified except for the case of treatment with isopropanol on FTSm (and with TEER being reduced in 40 +-10% for RHEm). The significant reduction of the measured TEER values is contradictory to the results of the viability test. This phenomenon was also observed in other studies [30]**.** One relevant consideration is that, although the outer epidermal layers are responsible for the major part of the skin barrier function, MTT based assays assess the viability of only the basal cell layer in RHEs [38]. This means that no direct information can be gathered of the effect of a test substance on the outer epidermal layers, such as the SC. The extracellular space of SC layer is filled with lipids such as free fatty acids which contribute to the skin barrier [39]. One hypothesis for the TEER reduction with isopropanol is the capability of this substance to dissolve these lipids in the SC, impairing barrier function. In an *in vitro* model, Cartner *et al* showed that isopropanol causes significant SC perturbation whereas ethanol does not [40]. The group concluded that ethanol should be the ingredient of choice for sanitizers and not isopropanol. Taking into account that a defective barrier can, for example, cause an inflammatory reaction [41] as well as sub-irritative effects (stinging, burning, itching), it could be useful to complement the viability assays with TEER measurements. Ideally, an integrated assessment of tissue damage (MTT assay), barrier function (TEER measurement) and inflammatory response (IL-1α secretion) should be performed to provide a comprehensive evaluation of irritation potential.

5.5.4 Skin permeation assays

Finally, the feasibility of using the developed open-source models for permeation assays was evaluated by comparing with a commercial product that has been tested for a wide range of compounds (Strat-M® membrane) [42]. This multi-layered artificial membrane was engineered to mimic key features of human skin [43]. It possesses a top layer coated with a lipid blend to mimic the *in vivo* SC and porous layers mimicking the dermal and epidermal compartment. By comparing the performance of the models with a highly tested commercial product, it was possible to avoid the use of skin tissues from animal or human origin. It is a well-known problem that permeation of reconstructed skin models (both FTSm and RHEm) exceeds that of human and pig skin [20], [44], [45]. Schmook *et al* showed that both a FTSm (Graftskin LSE®) and a RHEm (Skinethic HRE®) were very permeable for hydrophobic compounds presenting 900 and 800-fold higher flux of clotrimazole as compared to human skin, respectively. The group concluded that the available models could not be regarded as useful for *in vitro* penetration studies [44]. Other works testing commercial RHEms showed that the permeation values for EpiDerm® ranged from two-fold to seven-fold higher than the values obtained with human skin, while EpiSkin® and SkinEthic® overestimated permeation even to a greater extent [45]. Finally, studies focused on the evaluation of the FTSm Phenion FT® found that the barrier of the model was weaker that the barrier of pig skin while showing similarities to the commercially available RHEm [20].

It is well known that the permeability coefficient of topically applied substances (both drugs and vehicle components) is highly dependent on their physicochemical characteristics such as lipophilicity [46]. In this work, permeation studies were performed for three standard compounds (salicylic acid, hydrocortisone and clotrimazole) with different polarities [*n*-octanol-water partition coefficient (log P) of 1.98, 1.61 and 5.84, respectively]. Comparing to Strat-M®, both FTSm and RHEm provided an adequate barrier to salicylic acid, with FTSm presenting the lowest cumulative amounts at 24 hours. However, for a more hydrophobic compound (clotrimazole), the use of reconstructed skin models resulted in approximately double the flux rate compared to Strat-M®. One possible explanation for the different permeation fluxes is the different effect of the propylene

glycol on the artificial membrane compared to the cell-based reconstructed models. Propylene glycol was used as a solvent for the topical drugs and as a skin enhancer, by acting on the intercellular lipid matrix. Carrer *et al* showed that propylene glycol modifies both the epidermis and the dermis by altering the lipidic order of the bilayer structure to a more disordered lipid structure [47]. It has been hypothesized that this effect on the lipid structure could be one of the reasons for the poor correlation between permeation methodologies when the compounds are formulated with propylene glycol. In this study, the different compositions of the Strat-M® and reconstructed skin models could have resulted in a different action of propylene glycol in regards to its skin enhancing capabilities.

The differences between the RHEm and FTSm for hydrocortisone were not expected and probably reflect the different cell batches used for both models. Furthermore, incorrect tissue manipulation when removing the scaffold from the insert and when placing the tissues in the fabricated supports could also explain some incoherencies in the results as well as the increased variability. Overall, the permeation was close between the developed models and commercial Strat-M®, especially regarding the quantities of permeated substances at 24h. However, the results point to the need to further optimize the model, especially to reduce variability. Studies should also be performed to understand the different impact of propylene glycol on Strat-M®, compared to the reconstructed skin models.

Overall, preliminary studies were performed to access the potential of the open-source models for skin irritation and skin permeation testing. Contrary to conventional models, the proposed approach excludes the use of animal components to generate the dermal compartment. However, in the present study, for each experiment, only one batch of cells was used (N=1, n=3). Especially since primary cells were used, the specific batch and passage number could have highly affected the outcome and conclusions. This was possible the case of the permeation tests for the FTSm using hydrocortisone and for the false negative during irritation tests for 1-bromohexane. Future experiments should expand the present analysis, by using more cell batches and by testing a larger array of chemical substances. In particular, for irritation tests, the next step should be to test the 20 reference chemicals defined in the OECD performance standards for *in vitro* skin irritation

testing. Moreover, the potential of this open-source model should also be directly compared to available commercial models, for example the EpiSkin® (RHEm) and Phenion® (FTSm).

5.6 Conclusion

These preliminary studies show the potential of the developed open-source skin models to be used for skin irritation and permeation studies, according to OECD Performance Standards. This work shows that the innovative approach based on the use of an inert scaffold and a fibroblast-derived matrix results in a well differentiated epidermis with *in-vivo* like barrier function. The preliminary irritation tests performed using MTT lead to a correct classification of all the test substances, except for 1-bromohexane. However, this result can reflect the varying responses to 1-bromohexane seen in *in vivo* models. The complement of the tissue viability assays with TEER measurements, resulted in a more comprehensive analysis of skin irritation and opened the possibility of identifying sub-irritative effects. During permeation assays, both skin models showed similar barrier to salicylic acid comparing to the commercial produce Strat-M®. For more hydrophobic compounds, the FTSm presented at least two-fold permeation flux compared to the Strat-M®. Further studies including more skin batches and a larger array of test substances should be performed. Considering the overall results, the proposed open-source skin models show potential to be used for safety profiling of topically applied drugs, as well as in the early stages of drug discovery. In the future, the proposed open-source models could help speed up the translation of a new candidate therapeutics to the clinic and/or the market and circumvent the current limitations of the available commercial models.

5.7 References

[1] D. Seth, K. Cheldize, D. Brown, and E. F. Freeman, "Global Burden of Skin Disease: Inequities and Innovations," *Curr. Dermatol. Rep.*, vol. 6, no. 3, pp. 204–210, Sep. 2017.

[2] M. Cui, C. Wiraja, S. W. T. Chew, and C. Xu, "Nanodelivery Systems for Topical Management of Skin Disorders," *Mol. Pharm.*, vol. 18, no. 2, pp. 491–505, Feb. 2021.

[3] A. R. Tadros *et al.*, "STAR particles for enhanced topical drug and vaccine delivery," *Nat. Med.*, vol. 26, no. 3, pp. 341–347, 2020.

[4] M. Yamada and T. W. Prow, "Physical drug delivery enhancement for aged skin, UV damaged skin and skin cancer: Translation and commercialization," *Adv. Drug Deliv. Rev.*, vol. 153, pp. 2–17, 2020.

[5] A. Almeida, B. Sarmento, and F. Rodrigues, "Insights on in vitro models for safety and toxicity assessment of cosmetic ingredients," *Int. J. Pharm.*, vol. 519, no. 1, pp. 178–185, 2017.

[6] G. A. Van Norman, "Limitations of Animal Studies for Predicting Toxicity in Clinical Trials: Is it Time to Rethink Our Current Approach?," *JACC Basic to Transl. Sci.*, vol. 4, no. 7, pp. 845–854, 2019.

[7] V. Zuang et al., EURL ECVAM Status Report on the Development, Validation and Regulatory Acceptance of Alternative Methods and Approaches (2015) EURL ECVAM Status Report 2015, no. September. 2015.

[8] A. C. Gray, S. S. Sidhu, P. C. Chandrasekera, C. F. M. Hendriksen, and C. A. K. Borrebaeck, "Animal-Friendly Affinity Reagents: Replacing the Needless in the Haystack," *Trends Biotechnol.*, vol. 34, no. 12, pp. 960–969, 2016.

[9] H. Niehues, J. A. Bouwstra, A. El Ghalbzouri, J. M. Brandner, P. L. J. M. Zeeuwen, and E. H. van den Bogaard, "3D skin models for 3R research: The potential of 3D reconstructed skin models to study skin barrier function," *Exp. Dermatol.*, vol. 27, no. 5, pp. 501–511, 2018.

[10] L. J. van den Broek, L. I. J. C. Bergers, C. M. A. Reijnders, and S. Gibbs, "Progress and Future Prospectives in Skin-on-Chip Development with Emphasis on the use of Different Cell Types and Technical Challenges," *Stem Cell Rev. Reports*, vol. 13, no. 3, pp. 418–429, 2017.

[11] R. Joffe, J. A. Plaza, and A. Kajoian, "Tip Chapter: Histology," *Minim. Invasive Aesthetic Proced. A Guid. Dermatologists Plast. Surg.*, p. 179, 2020.

[12] G. Rice and P. Rompolas, "Advances in resolving the heterogeneity and dynamics of keratinocyte differentiation," *Curr. Opin. Cell Biol.*, vol. 67, pp. 92–98, 2020.

[13] S. Perticaroli *et al.*, "Translating chemometric analysis into physiological insights from

in vivo confocal Raman spectroscopy of the human stratum corneum," *Biochim. Biophys. Acta - Biomembr.*, vol. 1861, no. 2, pp. 403–409, 2019.

[14] S. Del Bino, C. Duval, and F. Bernerd, "Clinical and Biological Characterization of Skin Pigmentation Diversity and Its Consequences on UV Impact," *International Journal of Molecular Sciences* , vol. 19, no. 9. 2018.

[15] F. Urciuolo, C. Casale, G. Imparato, and P. A. Netti, "Bioengineered Skin Substitutes: The Role of Extracellular Matrix and Vascularization in the Healing of Deep Wounds," *Journal of Clinical Medicine* , vol. 8, no. 12. 2019.

[16] K. Natsuga, M. Watanabe, W. Nishie, and H. Shimizu, "Life before and beyond blistering: The role of collagen XVII in epidermal physiology," *Exp. Dermatol.*, vol. 28, no. 10, pp. 1135–1141, Oct. 2019.

[17] F. Netzlaff, C. M. Lehr, P. W. Wertz, and U. F. Schaefer, "The human epidermis models EpiSkin®, SkinEthic® and EpiDerm®: An evaluation of morphology and their suitability for testing phototoxicity, irritancy, corrosivity, and substance transport," *Eur. J. Pharm. Biopharm.*, vol. 60, no. 2, pp. 167–178, 2005.

[18] J. X. Wang, M. Fukunaga-Kalabis, and M. Herlyn, "Crosstalk in skin: melanocytes, keratinocytes, stem cells, and melanoma," *J. Cell Commun. Signal.*, vol. 10, no. 3, pp. 191–196, 2016.

[19] B. De Wever, S. Kurdykowski, and P. Descargues, " Human Skin Models for Research Applications in Pharmacology and Toxicology: Introducing NativeSkin ® , the 'Missing Link' Bridging Cell Culture and/or Reconstructed Skin Models and Human Clinical Testing ," *Appl. Vitr. Toxicol.*, vol. 1, no. 1, pp. 26–32, 2015.

[20] K. Ackermann, S. Lombardi Borgia, H. C. Korting, K. R. Mewes, and M. Schäfer-Korting, "The phenion® full-thickness skin model for percutaneous absorption testing," *Skin Pharmacol. Physiol.*, vol. 23, no. 2, pp. 105–112, 2010.

[21] C. Rasmussen *et al.*, "The StrataTest® human skin model, a consistent in vitro alternative for toxicological testing," *Toxicol. Vitr.*, vol. 24, no. 7, pp. 2021–2029, 2010.

[22] R. A. Redden and E. J. Doolin, "Collagen crosslinking and cell density have distinct effects on fibroblast-mediated contraction of collagen gels," *Ski. Res. Technol.*, vol. 9, no. 3, pp. 290–293, Aug. 2003.

[23] S. Radhakrishnan, S. Nagarajan, M. Bechelany, and S. N. Kalkura, "Collagen Based Biomaterials for Tissue Engineering Applications: A Review BT - Processes and Phenomena on the Boundary Between Biogenic and Abiogenic Nature," pp. 3–22, 2020.

[24] B. De Wever *et al.*, "'Open Source'–Based Engineered Human Tissue Models: A New Gold Standard for Nonanimal Testing Through Openness, Transparency, and Collaboration, Promoted by the ALEXANDRA Association," *Appl. Vitr. Toxicol.*, vol. 1, no. 1, pp. 5–9, Jan. 2015.

[25] A. Fuggetta, "Open source software—an evaluation," *J. Syst. Softw.*, vol. 66, no. 1, pp. 77–90, 2003.

[26] K. R. Mewes *et al.*, "Catch-up validation study of an in vitro skin irritation test method based on an open source reconstructed epidermis (phase I)," *Toxicol. Vitr.*, vol. 36, pp. 238–253, 2016.

[27] P. Zoio, S. Ventura, M. Leite, and A. Oliva, "Pigmented full-thickness human skin model based on a fibroblast-derived matrix for long-term studies," *Tissue Eng. Part C Methods*, pp. 1–12, 2021.

[28] OECD, "Test No. 439: In Vitro Skin Irritation - Reconstructed Human Epidermis Test Method," *OECD Publ.*, no. 439, 2013.

[29] B. Srinivasan, A. R. Kolli, M. B. Esch, H. E. Abaci, M. L. Shuler, and J. J. Hickman, "TEER Measurement Techniques for In Vitro Barrier Model Systems," *J. Lab. Autom.*, vol. 20, no. 2, pp. 107–126, 2015.

[30] F. Groeber *et al.*, "Impedance Spectroscopy for the Non-Destructive Evaluation of in Vitro Epidermal Models," *Pharm. Res.*, vol. 32, no. 5, pp. 1845–1854, 2015.

[31] C. Gorzelanny, C. Mess, S. W. Schneider, V. Huck, and J. M. Brandner, "Skin barriers in dermal drug delivery: Which barriers have to be overcome and how can we measure them?," *Pharmaceutics*, vol. 12, no. 7, pp. 1–31, 2020.

[32] P. Zoio, S. Lopes-ventura, and A. Oliva, "Barrier-on-a-chip with a modular architecture and integrated sensors for real-time measurement of biological barrier func- tion," pp. 1–20, 2021.

[33] M. Odijk *et al.*, "Measuring direct current trans-epithelial electrical resistance in organ-on-a-chip microsystems," *Lab Chip*, vol. 15, no. 3, pp. 745–752, 2015.

[34] K.-M. Jung *et al.*, "KeraSkin™-VM: A novel reconstructed human epidermis model for skin irritation tests," *Toxicol. Vitr.*, vol. 28, no. 5, pp. 742–750, 2014.

[35] T. Akagi, M. Nagura, A. Hiura, H. Kojima, and M. Akashi, "Construction of Three-Dimensional Dermo–Epidermal Skin Equivalents Using Cell Coating Technology and Their Utilization as Alternative Skin for Permeation Studies and Skin Irritation Tests," *Tissue Eng. Part A*, vol. 23, no. 11–12, pp. 481–490, Mar. 2017.

[36] A. El Ghalbzouri, R. Siamari, R. Willemze, and M. Ponec, "Leiden reconstructed human epidermal model as a tool for the evaluation of the skin corrosion and irritation potential according to the ECVAM guidelines," *Toxicol. Vitr.*, vol. 22, no. 5, pp. 1311–1320, 2008.

[37] D. Jírová *et al.*, "Comparison of human skin irritation patch test data with in vitro skin irritation assays and animal data," *Contact Dermatitis*, vol. 62, no. 2, pp. 109–116, Feb. 2010.

[38] J. Cotovio, M.-H. Grandidier, P. Portes, R. Roguet, and G. Rubinstenn, "The In Vitro

Acute Skin Irritation of Chemicals: Optimisation of the EPISKIN Prediction Model within the Framework of the ECVAM Validation Process," *Altern. to Lab. Anim.*, vol. 33, no. 4, pp. 329–349, Aug. 2005.

[39] V. S. Thakoersing, J. van Smeden, A. A. Mulder, R. J. Vreeken, A. El Ghalbzouri, and J. A. Bouwstra, "Increased Presence of Monounsaturated Fatty Acids in the Stratum Corneum of Human Skin Equivalents," *J. Invest. Dermatol.*, vol. 133, no. 1, pp. 59–67, 2013.

[40] T. Cartner *et al.*, "Effect of different alcohols on stratum corneum kallikrein 5 and phospholipase A2 together with epidermal keratinocytes and skin irritation," *Int. J. Cosmet. Sci.*, vol. 39, no. 2, pp. 188–196, Apr. 2017.

[41] S. R. Seo, S. G. Lee, H. J. Lee, M. S. Yoon, and D. H. Kim, "Disrupted skin barrier is associated with burning sensation after topical tacrolimus application in atopic dermatitis," *Acta Derm. Venereol.*, vol. 97, no. 8, pp. 957–958, 2017.

[42] T. Uchida, W. R. Kadhum, S. Kanai, H. Todo, T. Oshizaka, and K. Sugibayashi, "Prediction of skin permeation by chemical compounds using the artificial membrane, Strat-M™," *Eur. J. Pharm. Sci.*, vol. 67, pp. 113–118, 2015.

[43] F. J. Arce, N. Asano, G. L. See, S. Itakura, H. Todo, and K. Sugibayashi, "Usefulness of artificial membrane, strat-M®, in the assessment of drug permeation from complex vehicles in finite dose conditions," *Pharmaceutics*, vol. 12, no. 2, 2020.

[44] F. P. Schmook, J. G. Meingassner, and A. Billich, "Comparison of human skin or epidermis models with human and animal skin in in-vitro percutaneous absorption," *Int. J. Pharm.*, vol. 215, no. 1–2, pp. 51–56, 2001.

[45] M. Schäfer-Korting *et al.*, "The use of reconstructed human epidermis for skin absorption testing: Results of the validation study," *ATLA Altern. to Lab. Anim.*, vol. 36, no. 2, pp. 161–187, 2008.

[46] S. E. Cross, B. M. Magnusson, G. Winckle, Y. Anissimov, and M. S. Roberts, "Determination of the Effect of Lipophilicity on the in vitro Permeability and Tissue Reservoir Characteristics of Topically Applied Solutes in Human Skin Layers," *J. Invest. Dermatol.*, vol. 120, no. 5, pp. 759–764, 2003.

[47] V. Carrer *et al.*, "Effect of propylene glycol on the skin penetration of drugs," *Arch. Dermatol. Res.*, vol. 312, no. 5, pp. 337–352, 2020.

Chapter 6

Full-thickness skin-on-a-chip with an *in vivo*-like microenvironment and a modular architecture

The contents of this chapter are an extended version of the published paper: Zoio P, Lopes-Ventura S, Oliva A. Biomimetic Full-Thickness Skin-on-a-Chip Based on a Fibroblast-Derived Matrix. Micro. 2022; 2(1):191-211. https://doi.org/10.3390/micro2010013

Author contributions:

Zoio P. performed the simulations (finite element analysis), designed and fabricated the platform, generated the skin models and performed permeation experiments and TEER measurements on-chip. **Zoio P**. wrote the manuscript. Ventura S. performed the immunofluorescence analysis. Oliva A. supervised the project and contributed to the integration of the electrodes inside the chip..

6.1 Abstract

In vitro human skin models have been widely used as alternatives to animal testing for basic research and clinical applications. However, current commercially available models do not fully reproduce the structure and function of human skin, mainly due to their use of animal-derived collagen and their lack of a dynamic flow system to mimic vascularization. In this study, we present an innovative, full thickness skin-on-a-chip (SoC) system that reproduces key aspects of the *in vivo* cellular microenvironment. Our approach combines the production of a fibroblast derived matrix with the use of an inert porous scaffold for long-term, stable cultivation of a human skin model, without the use of animal components. This advanced skin model is developed inside a biomimetic organ-on-a-chip system with a dynamic perfusion arrangement for continuous supply of nutrients and metabolites. The system is reversibly sealed and has a modular architecture providing an easy-to-use workflow, efficient and precise cell seeding and a removable culture insert that can be transferred between modules. We demonstrate that culture of the dermal compartment under fluid flow results in an increased synthesis and deposition of extracellular-matrix (ECM). The developed SoC includes a fully differentiated epidermal compartment with increased thickness and barrier function and a dermal compartment with an *in vivo*-like ECM. Contrary to other SoC platforms that include a collagen-based matrix, our platform presents superior stability and physiological relevance. We also show that skin integrity can be evaluated directly on-chip via transepithelial electrical resistance (TEER) measurements and *in situ* permeation tests. In the future, this innovative low-cost platform could reduce the dependence on animal models and provide a new *in vitro* tissue system compatible with long-term studies to study skin diseases and evaluate the safety and efficacy of novel drugs and delivery technologies.

6.2 Introduction

The global topical drug delivery market is growing at a fast rate due to the increasing ageing population and the high prevalence of chronic skin diseases [1]. New and better technologies for topical drug delivery are also expected to boost the growth of this market [2]. To test the efficacy and toxicity of topical drugs, animal models have been widely used all over the world; however, animal experimentation raises important ethical and regulatory concerns [3, 4]. In addition, there is a lack of accuracy of the animal to human extrapolation with approximately 90% of the drug candidates that appear safe and effective in animal studies failing to win approval when tested in humans [5–7]. These factors resulted in an increasing need of replacing and/or complement animal testing with physiologically relevant reconstructed human skin models, suitable for topical drug delivery and disease modelling [8, 9].

Over the last few decades, techniques for culturing three-dimensional (3D) skin cells have been developed resulting in significant advancements in the field of skin tissue engineering [9, 10]. However, current commercially available human skin models still lack complexity, present weaker barrier properties compared to *in vivo* human skin and lack vascularization which results in restricted nutrient supply and cell-cell interactions [11]. Organ-on-a-chip (OoC) technology aims to surpass the limitations of conventional cell-based culture platforms and increase the predictive power of *in vitro* models by creating customized cellular microenvironments with precise fluidic, mechanical and structural control [12]. Furthermore, the possibility of integrating sensors in OoC allows real-time monitoring of tissue viability and function [13].

In the last few years, several skin-on-a-chip (SoC) platforms have been reported and their physiological relevance have been shown. However, most of these platforms have been limited to the maintenance of transferred skin tissues, usually skin biopsies to increase it longevity and/or establish a co-culture with other organ models [14–20]. While these studies provide valuable information regarding the potential of SoC devices for clinical and testing purposes, the integration of

models previously developed off-chip limits the potential benefits of the dynamic culture.

Alternatively, groups have generated skin models directly on the chip. Wufuer *et al* developed a simplistic model consisting of 3 cell layers (keratinocytes, fibroblasts and endothelial cells) separated by two porous membranes to simulate inflammation and edema [21]. Ramadan *et al* further explored the potential of the SoC devices by including an immune component, describing the interaction between the HaCaT cell line and a monocytic cell line in a bi-channel microfluidic device [22]. Although these studies replicated some important features of healthy and diseased skin, they included monolayer systems which do not replicate the 3D environment of *in vivo* human skin.

Only a handful of publications have reported OoC devices for 3D skin tissue formation inside the platform. Mori *et al* fabricated a culture device composed of anchoring structures and nylon wires across the connectors of the device to produce full thickness human skin (FTSm) including the dermis and the epidermis [23]. Although this study was an important first step in development of 3D skin inside the platform and to mimic *in vivo* vascularization, the limitations of using collagen were apparent. Collagen contraction made it necessary to develop a complex system based on anchoring structures treated with oxygen plasma and also compromised the reproducibility the model, frequently resulting in clogged channels. Lee *et al* also developed 3D FTSm inside a SoC device composed two polydimethylsiloxane (PDMS) fluidic chambers. However, the *stratum corneum* of the SoC was less homogeneous that the controls [24]. The group also reported contraction of the skin during the differentiation process, resulting in detachment of the scaffold.

Both of the mentioned studies showed the limitations of using natural hydrogels to generate the dermal compartment. These systems reported fibroblast-mediated contraction and matrix degradation leading to distortion and disruption of the skin model. Moreover, by including dermal compartments comprising exclusively of animal-derived collagen type I, they are fully not representative of the *in-vivo* extracellular matrix (ECM) which includes multiple types of collagens, proteins and proteoglycans. Recently, Sriram *et al* used a combination of fibrin and PEG to produce a stable dermal component capable of sustaining the epidermis,

without signs of contraction [25]. The group was able to produce a SoC with improved epidermal differentiation and barrier function.

Here, we present an alternative approach to the production a 3D full-thickness SoC with a dermal compartment better representative of the *in-vivo* microenvironment. A porous scaffold is integrated in the device and dermal cells are seeded and stimulated to produce their own endogenous extracellular matrix (fibroblast-derived matrix, FDM) onto it. This results in a mechanically stable structure and excludes the use of animal-derived components. Furthermore, the device presented here has various advantages over the previously described SoCs, such as reversible sealing, reusability and modular architecture. The SoC platforms described in the literature systems are irreversible sealed, usually through plasma bonding, making it difficult the complete tissue retrieval for endpoint assays (e.g. histological analysis and immunohistochemistry) [26]. We propose a SoC with a removable culture insert and interchangeable modules and integrated sensors, including transepithelial electrical resistance (TEER) measurement electrodes for real-time quantitative analysis of the skin barrier.

To our knowledge, this work is the first to demonstrate the use of an inert porous scaffold integrated on a resealable OoC device for the production of a 3D fully human skin with *in-vivo* like ECM composition and a stable, leak-free, fluid-tissue-air barrier.

6.3 Materials and Methods

6.3.1 Fabrication and assembly of the organ-on-chip device

A SoC device with a modular architecture and a "user friendly" approach was designed and fabricated for the production of a FTSm and for drug testing directly on-chip. The device is composed of 3 main layers: two fluidic compartments (apical and basal) and a central insert layer for cell culture. The design of the SoC was optimized to ensure stability during long-term skin culture while providing a flexible and modular geometry compatible with different types of studies. The lower fluidic compartment comprises of a basal

chamber bellow the scaffold, the inlet and outlet channels. It is intended for perfusion of tissue with culture media during the culture process or for flow-through of a receiver solution during *in vitro* drug tests. The upper compartment comprises an apical chamber connected to inlet and outlet channels. During the culture process, it is used for perfusion of culture media or ventilation on the apical side of the tissue culture. The addition of magnetic latching allows membranes and scaffolds to be sandwiched between the apical and basal fluidic channels and sealed in place to support a compartmentalized skin culture. A closed schematic and exploded view of the SoC device is shown in **Figure 6. 1.**

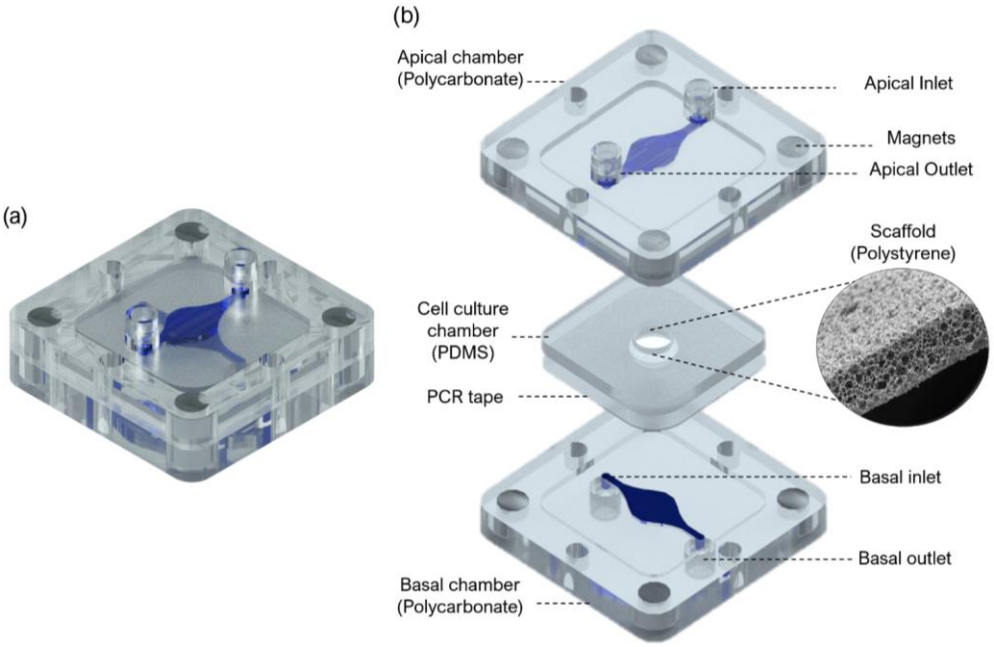

Figure 6. 1. Design of the skin-on-a-chip (SoC) device with modular and a reversible sealing approach (a) Closed device with blue dye showing the apical and basal chamber (b) Schematic exploded view of the SoC platform. The device consists of central insert for cell culture and two external compartments (apical and basal) for top and bottom perfusion with air and/or medium and integrated electrodes. The central insert layer is composed of polydimethylsiloxane (PDMS) and a thin layer of polymerase chain reaction (PCR) tape sealing a membrane/scaffold. The top and bottom compartments are made of polystyrene and include magnets at the corners to correctly seal the insert layer and establish interfaces (air–liquid and liquid–liquid).

First, the fluid compartments and the mould used for the central cell culture layer were designed through computer-aided design (CAD) using AutoCAD 2017 (Waltham, MA, USA). The parts were fabricated though a combination of computer numerically controlled (CNC) micromachining and laser cutting. The apical and basal layers were constructed in polycarbonate (31.5 x 31.5 x 4 mm, length x width x heigh) and included a central cavity designed to accept the cell culture layer (21 x 21 x 1 mm, length x width x heigh). Polycarbonate was chosen due to its low-cost, transparency, mechanical resistance and biocompatibility. The fluidic features oriented to the interior of the device were generated by micromilling (Xometry Europe GmbH, Ottobrunn, DE, Germany). For the access ports, mini female luer interfaces (microfluidic ChipShop, Jena, DE, Germany) were glued to the inlets and outlets in both the upper and lower polycarbonate housings. This provided an easy and leakage-free chip-to-world interface. Each of the fabricated layers contained 4 neodymium magnets with 4 mm diameter and 3 mm height with a force of 3N each (Supermagnete©, Webcraft GmbH, Gottmadingen, DE, Germany). The magnets were placed with polar opposites facing each other on the basal and apical layer. Holes were drilled through both layers along the outer edge to allow screws to pass through both sheets and tighten the compression frame.

Dedicated moulds were fabricated using laser cutting (Epilog Mini 24, EpilogLaser©, Golden, CO, USA) and CNC machining (Carvey, Inventables©, Chicago, IL, USA) to generate a central layer for cell culture that could fit in the polycarbonate cavities. The base of the mould was fabricated in PMMA and had 21 mm in length and 21 mm in width and included a central cylinder with 5 mm diameter and 2 mm height. The lateral and top pieces of the mould were fabricated with laser cutting using PMMA with 2 mm in thickness. To obtain the PDMS layers for cell culture that could fit in the polycarbonate cavities, moulds were fabricated using CNC machining and laser cutting. The base of the mould with a central cylinder of 5 mm diameter and 2 mm height has 21x21 mm and a 2 mm thickness and the lateral and top of the mild were fabricated using laser machining. The middle cavity was filled with degassed PDMS prepolymer mixed with curing agent (Sylgard 184, Dow Corning, Midland, MI, USA) at a 10:1 (*w*/*w*) base to catalyst ratio.

The assembled molds were clamped and placed in an oven for 12 hours at 65°C. The resulting PDMS layer was removed from the mould with the help of a razor blade.

The generation of 3D FTSm inside the platform was achieved by integrating polystyrene scaffolds (Alvetex®, REPROCELL Europe Ltd., Glasgow, UK) onto the SoC device. The scaffolds were cut in a circular shape of 6 mm diameter with a puncher and carefully sandwiched between the PDMS insert layer and a PCR adhesive tape (ThermalSeal RTS®, Sigma) with 21 x 21 mm and an open central region of 5 mm for cell culture. The PCR adhesive tape was chosen due to its biocompatibility for cell culture, transparency and good sealing properties [27]. To better seal the PDMS insert against the polycarbonate housing and avoid leakage, the PCR tape was covered with a thin PDMS layer.

A SoC device with integrated electrodes for TEER measurement and a module compatible with drug testing and direct cell seeding were also designed and fabricated (**Figure 6. 2**). The fabrication of device with integrated electrodes was described by Zoio et al [28]. It includes Ag/AgCl-sintered pellet electrodes concentric placed in both apical and basal perfusion layers. A module for *in situ* drug testing and/or cell seeding consisted of a top polycarbonate housing with embedded magnets and a central reservoir, fabricated using CNC machining (Xometry Europe GmbH, Ottobrunn, DE, Germany). A 6 mm diameter O-ring was added to ensure a leakage free seal around the culture insert. With this module an experimental compound can be easily introduced to test permeation or toxicity effects. Furthermore, this module can be used for direct cell seeding at the basal side of the scaffold and/or for pipetting a cell suspension with a volume ≥ 35 µL at the apical side (smaller volumes can be directly seeded at the PDMS layer). After the period of cell adhesion, the module for cell seeding is exchanged for the apical perfusion module. The detailed dimensions and designs of the SoC and the dedicated modules can be seen in the **Figure B. 1 – Figure B. 6**. The detailed protocols used to fabricate the preliminary SoC devices using precision milling and its assembly are described in **Appendix B.2** and **Appendix B.3**.

The chips were sterilized using UV radiation. The lids, insets, tubing and fittings were sterilized in autoclave before assembling them onto the chip on the setup days.

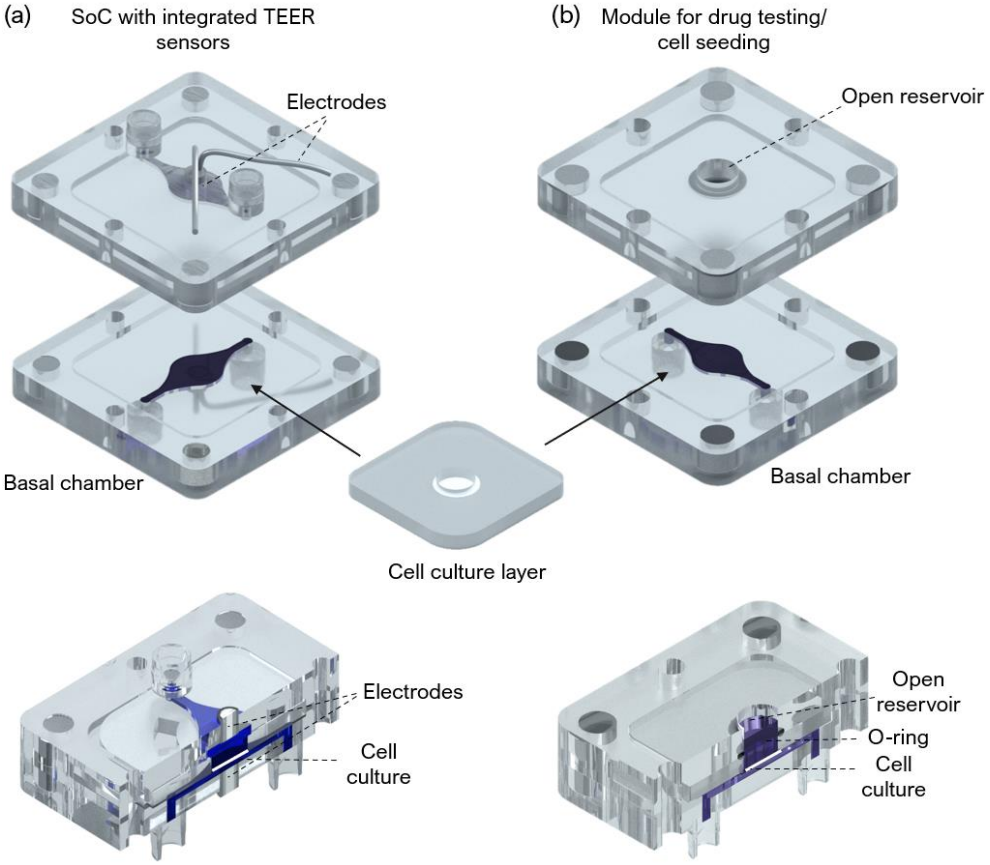

Figure 6. 2. Schematic design including an exploded view (top) and cut (bottom) of the (**a**) SoC device with integrated TEER sensors made of Ag/AgCl-sintered pellet electrode, insulating polyether ether ketone (PEEK) tubing and external silver tubing and (**b**) Module for drug testing/cell seeding with a central open reservoir, integrated O-ring and basal chamber for perfusion. The modular design and reversible sealing allow the modules to be easily exchanged without causing disruption and/or damage to the cell culture layer.

6.3.2 Computational Fluid Dynamic (CFD) simulations

To characterize the hydrodynamics of the developed SoC, 3D models of the fluidic compartments and scaffold domain were generated with CAD

(AutoCAD, Waltham, MA, USA) and imported to COMSOL Multiphysics™ (COMSOL Multiphysics GmbH, Gottingen, Germany) for finite element analysis (FEA).

The fluid was assumed as a homogeneous, incompressible Newtonian fluid. The density of the culture medium was assumed to be the same as water, 993.2 kg/m^3 and the dynamic viscosity $7.8x10^{-3}$kg/m/s at a temperature of 37°C. The boundary conditions were defined based on the inlet conditions for the flow rate (1.5 – 2 μl/min) and ambient pressure outlet conditions. COMSOL's Free and Porous Media Interface was used for modelling a combination of porous media and free flow domain. The Navier-Stokes equation (incompressible flows) was used to model the free flow in both the apical and basolateral chambers, and the Brinkman equations were applied to the porous domain (the scaffold layer) (**Appendix B.4**). At the interface between free and porous media flow, the implemented boundary conditions between these domains enforces continuity for the velocity and for the pressure.

Using COMSOL, different types of configurations were studied, namely, single tangential flow, parallel tangential flow and cross flow, and the shear stress distribution in the scaffold domain was obtained. Th scaffold porosity was set to 93% according to the manufacturer, to model the first days of cell culture. Scaffold permeability was obtained experimentally by applying Darcy's law (**Figure B. 7** and **Appendix B.5**). The permeability was set to 10^{-16} m^2 to represent the scaffold structure after cell growth and ECM deposition, according to the values on the literature for collagen-based hydrogels [29]. The parallel flow for the culture of epidermal cells under submerged conditions was studied by modelling a monolayer on top of the dermal compartment. For all solid walls, no slip boundary conditions were set. For all models, the "extra fine" mesh (under COMSOL calibration for general physics) was chosen, automatically assigning mesh sizes (**Figure B. 8 and Figure B. 9**).

6.3.3 Primary cells and cell maintenance

Primary human dermal fibroblasts isolated from neonatal foreskin (HDFn, CellnTec; Stauffcherstr, Switzerland) were maintained in Fibroblast Growth medium (FGM) composed of Iscove's Modified Dulbecco's Medium (IMDM, Gibco, Waltham, MA, USA) supplemented with 10% fetal bovine serum (FBS, Gibco, Waltham, MA, USA), at 37 °C in a 5% $C0_2$ humidifier, following supplier's instructions. HDFns were used for up to 10 passages and subcultured at a 90% confluency.

Primary human epidermal keratinocytes isolated from neonatal foreskin (HEKn, Gibco, Waltham, MA, USA) were maintained in keratinocyte growth medium (KGM) composed of EpiLife medium (Gibco, Waltham, MA, USA), supplemented with 0.06 mM calcium and keratinocyte growth factor (HKGS, Gibco, Waltham, MA, USA), at 37 °C in a 5% CO_2 humidifier incubator. The KGM medium was replaced every other day until the cells reached 50% confluency. At this point the medium was replaced every day. In these experiments, 6^{th} passage HEKn were used, subcultured at 70-80% confluency. All cultures were routinely monitored for contaminations.

6.3.4 Generation of dermal equivalents

The formation of the fully-human dermal equivalent was achieved by seeding HDFns within the Alvetex® scaffolds (REPROCELL Europe Ltd., Glasgow, UK) and by stimulating them to proliferate and secrete endogenous dermal ECM (**Appendix B.7**). These scaffolds have void sizes of 33 – 55 μm and 93% porosity, making them the ideal structure for the dermal cells to penetrate and lay down the fibroblast-derived matrix. The duration of the dermis culture was first studied and optimized off-chip, without perfusion [30]. Different perfusion configurations (parallel and cross flow) were tested using the developed platform to understand its impact on the dermis formation (**Figure 6. 3**).

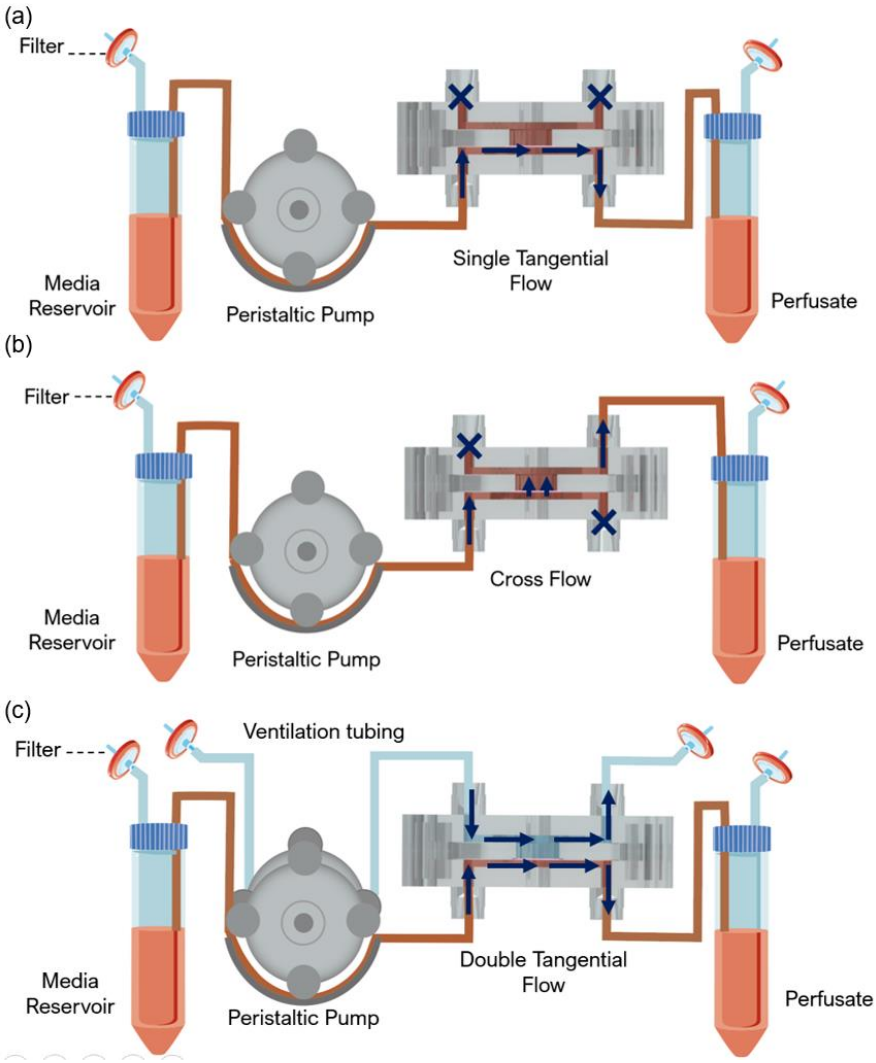

Figure 6. 3. Schematic representation of the different flow configurations used during dermal and epidermal culture. The top image shows the cross-flow configuration in which the flow enters the device through the basal chamber, passes through the scaffold and leaves through the apical chamber. Middle image shows single tangential flown in which the cell culture media is pumped through the basal chamber's inlet and leaves though the basal chamber's outlet without crossing the scaffold. Bottom image shows tangential parallel flow with air pumped through the apical chamber and media pumped through the basal chamber to establish an air-liquid interface.

Briefly, Alvetex® scaffolds were pre-treated with 70% ethanol to render its hydrophilicity followed by two washes with phosphate buffered saline (PBS)

(**Figure 6. 4.a**). Different concentrations of HDFns ($5x10^6$, $10x10^6$, $20x10^6$ cells/mL) were seeded directly on the Alvetex® scaffolds in 35 μL FGM medium and incubated at 37ºC, in a humidified atmosphere of 5% CO_2 for 1.5 hours (**Figure 6. 4.b**). Dermal equivalents were maintained on fabricated supports, which could fit in 6-well plates and kept under static conditions, as controls. After the cell adhesion period, 6 ml of FGM + 100 μg/mL ascorbic acid 2-phospahe (Sigma-Aldrich, St. Louis, MO, USA) was applied to the bottom of each well to flood the cell culture insert. The controls were maintained for 6 days, changing the medium after 3 days, to study the formation of the dermal equivalent without perfusion.

Dermal equivalents were generated under dynamic perfusion using the developed SoC device (**Figure 6. 4.c**). After the cells adhered to the scaffold structure, the cell culture layer was introduced into the device, between the apical and basal chambers. The single tangential flow configuration was achieved by connecting the inlet ports of the lower compartments to 3-stop Tygon® LMT-55 Tubing (Ismatec; Cole-Parmer GmbH, Wertheim, BW, Germany) mounted on a multichannel peristaltic pump (LABV1 with a MC10 pump head, Baoding Shenchen Precision Pump Co., LTD, Baoding, China) (**Figure 6. 3.a**). The tubing was connected to a media reservoir to supply the culture media to the SoC. A filter (Whatman GmbH, Dassel, Germany) placed at the reservoir allowed permanent gas exchange. The medium was pumped from the reservoir through the inlets of the basal chambers and left the SoC through the basal outlets. The inlets and outlets of the apical chamber were closed with mini-luer plugs (microfluidic ChipShop, Jena, DE, Germany).

The crossflow configuration was established by connecting the inlet port of the lower compartment to the tubing mounted on the peristaltic pump and the outlet of the top compartment was connected to the external reservoir (**Figure 6. 3.b**). The other ports were closed with the mini-luer lids. The medium was pumped from the reservoir through inlet of basal chambers, cross the scaffold and left the SoC through the apical outlet. With both configurations, the dermal equivalent in culture chamber of the device was perfused with FGM + 100 μg/mL ascorbic acid 2-phosphate at a flow rate of 1.5 μL/min.

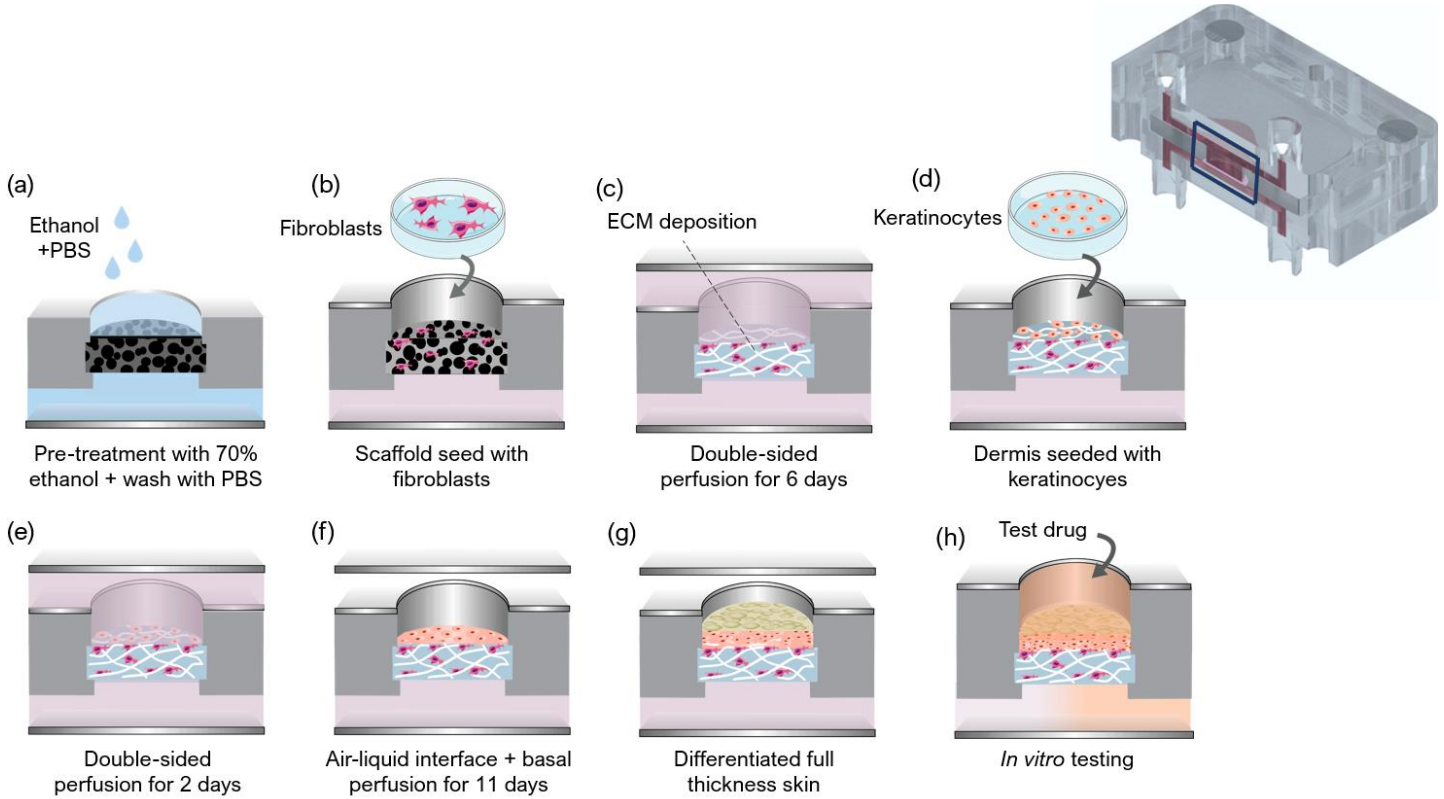

Figure 6. 4. Schematic representation of the developed methodology for generation of a skin-on-a-chip model based on a fibroblast-derived matrix. The process can be divided in three main steps: (a) – (c) the development of a mature dermis, (d) – (e) the culture of epidermal cells under submerged conditions with double perfusion and (f) the culture of the epidermis at the air-liquid interface until a fully differentiated skin is generated. (g)-(h) After 11 days, a stratified epidermis on top of a mature dermis is obtained and in vitro testing can be performed on chip.

6.3.5 Generation of FTSm on the SoC

The protocol to generate full-thickness and fully human skin model inside the OoC is depicted Figure 6.4. The process can be divided in three main steps: the development of a mature dermis, the culture of an epidermal cell monolayer on top of the dermis under submerged conditions, and the culture of the epidermis at the air-liquid interface (ALI) until a fully-differentiated skin is produced (**Appendix B.8**).

As a first step, dermal models were generated by seeding HDFns onto Alvetex® scaffolds using the seeding module and maintained for 6 days using the perfusion module as explained in section 2.4 (**Figure 6. 4.a – Figure 6. 4.c**). The FTSm was generated by seeding HEKn cells onto the dermal equivalents in KGM containing high calcium concentration (1.5 mM) (**Figure 6. 4.d**). HEKns were harvested by trypsinization and 30 µL of cell suspension $5.0x10^6$ cells/mL was pipetted directly on top of the mature dermis, followed by a 3-hour incubation period for cell adhesion, at 37 °C in a 5% CO2 incubator. After this period, double-sided parallel perfusion was established using the perfusion module (**Figure 6. 4.e**). For this, the inlet ports on the top and lower compartments were connected to the tubing mounted on the peristaltic pump and connected to a media reservoir with supplemented KGM medium. The medium was pumped from the reservoir through the inlets of the apical and basolateral chambers and left the SoC through the apical and basolateral outlets. With this configuration, the dermal equivalent in culture chamber of the device was double-sided perfused with KGM at a flow rate of 2 µL/min. The controls were maintained under submerged conditions in KGM containing high calcium concentration (1.5 mM), using the fabricated supports 6-well plates, without perfusion

After 48h, the models were raised to ALI and cultured in KGM containing 1.5 mM calcium, supplemented with 10 ng/mL KGF (Keratinocyte growth factor, Gibco, Waltham, MA, USA) and 100 µg/mL ascorbic acid 2-phosphate. The dynamic perfusion was maintained up to a further 11 days (**Figure 6. 4.f**). The formation of a differentiated epidermis was achieved by pumping the medium only through the basolateral chamber while pumping air through the apical

(**Figure 6. 3.c**). A flow rate of 1.5 µl/ml was established for medium and air flow. The overall setup used for dynamic perfusion of FTSm can be seen in **Figure B. 10**.

For the controls, the FTSm were raised to ALI by removal of the medium in the upper compartment and culture in 4 mL KGM containing 1.5 mM calcium, supplemented with 10 ng/m and 100 µg/mL ascorbic acid 2-phosphate. This volume resulted in the basal side of the skin tissue to be in contact with the media and the upper surface to remain exposed to the air. The incubation continued at 37°C in 5%CO_2 for 11 days, changing the media every two days, to allow the formation of a FTSm.

6.3.6 Histochemistry and Immunofluorescence analysis of the skin

The reconstructed tissues were fixed in 10% neutral buffered formalin (Sigma), immediately after being taken out of chip. The samples were embedded in paraffin to allow for transverse sectioning. Paraffin-embedded sections (5 µm-thick) were de-paraffined and re-hydrated for morphological evaluation by staining with haematoxylin and eosin (H&E) through standard methods.

Immunofluorescence analysis was performed to detect significant markers related to dermal maturation and epidermal differentiation. Skin sections were deparaffinized using HistoChoice® (Sigma-Aldrich) and incubated in a dry chamber at 65ºC during 30 minutes. Then, skin sections were hydrated during 5 minutes in a gradient of ethanol solutions (100%, 96% and 70%). The antigen retrieval was performed by heating in citrate buffer (pH=6). For anti-collagen IV antibody, the antigen retrieval was followed by proteinase K [20µg/mL in Tris-EDTA (TE) Buffer] incubation for 30 seconds at 37ºC with 10 minutes of cooling at room temperature. Immunofluorescence staining of sections was performed using the following primary antibodies: 1:500 anti-collagen IV (Abcam), 1:10 anti-cytokeratin 10 (Progen), 1:1000 anti-cytokeratin 14 (Abcam), 1:100 anti-cytokeratin 15 (Sigma-Aldrich), 1:250 anti-fibronectin (Abcam), 1:50 anti-filaggrin (Invitogen) and 1:100 anti-collagen I (Abcam) diluted in a solution with PBS-BSA 1% with overnight incubation in humidified chamber at 4˚C. Secondary antibodies, 1:1000

Alexa Fluor® 488 Goat Anti-Rabbit IgG (Invitrogen) or 1:1000 FITC Goat Anti-Mouse IgG (Sigma-Aldrich), diluted in a solution with PBS-BSA 1%, were then added with an incubation of 2 hours. The used antibodies are described in **Table B. 1**. Nuclei were stained with 1 μg/mL of 4,6-diamidino-2-Phenylindole (DAPI, Invitrogen) and slides were mounted with Vectashield (Vector Laboratories). Images were obtained using the Nikon Eclipse TE2000-S fluorescence microscope (Nikon instruments, USA) and analysed with the ImageJ software.

6.3.7 TEER measurements

TEER was measured using the SoC with integrated tetrapolar electrodes and an EVOM voltohmmeter (WPI Europe, Friedberg, Germany). The voltohmmeter supplies an AC square-wave current of ±10 μA at 12.5 Hz through the outer current carrying electrodes and measures the voltage drop across the inner voltage-sensing electrodes. This technique was used to measure the TEER of 3 batches of FTSm generated on-chip and 3 batches of FTSm generated off-chip (controls). TEER was recorded after 11 days of culture at ALI, following completion of the FTSm. For the controls, the cell culture layer was removed from their original supports and transferred to the a SoC module with integrated electrodes. The ALI was interrupted by pumping PBS in the basal and apical chambers to bridge an electrical connection between top and bottom sensors. TEER was recorded for 5 minutes to achieve stabilization, at room temperature. TEER was also measured for a blank scaffold to take into account the contribution of the geometry of the fluidic chambers and subtracted from each recording. The values in $\Omega \cdot cm^2$ were obtained by multiplying the obtained electrical resistance by the skin surface area.

6.3.8 Permeation assays

Permeation assays were conducted following TEER measurement for 3 batches of FTSm generate on-chip and 3 baches of FTSm generated off chip. The drug testing module was used to perform the permeation experiments *in situ* (**Figure 6. 4.h**). The culture media reservoir was replaced with a reservoir containing the receiver solution (PBS) to be supplied in the basal compartment. The perfusates

samples flowing out from the basal chamber were collected directly in a 96-well plate, according to predetermined time intervals (**Figure 6. 5**).

The donor compartment was filled with 100 μL of fluorescein isothiocyanate (FITC) - dextran with average molecular weight 4.4 kDa (FD-4, Sigma-Aldrich) at a 2.5 mg/mL concentration in PBS. The donor compartment was covered with PCR tape to minimize evaporation. The perfusate was collected into a different well every 30 minutes for 6 hours, after application of the donor solution (**Figure B. 11**). This was achieved by pumping the receiver solution at 8 μL/min flow rate. The concentrations of the skin-permeated FITC-dextran were determined by fluorescence spectroscopy (SLM 8100, SLM Instruments Inc., Rochester, NY, USA) at excitation and emission wavelengths of 495 and 519 nm, respectively. The concentrations were calculates using a calibration curve. Then, the concentrations were converted in cumulative amounts of FD-4 that permeated per unit skin surface area of skin and plotted against time. The slope of the linear portion of the area-normalized cumulative amount profiles were used to calculate the flux value and permeability coefficient, following Fick's first law (**Equation 5.3**).

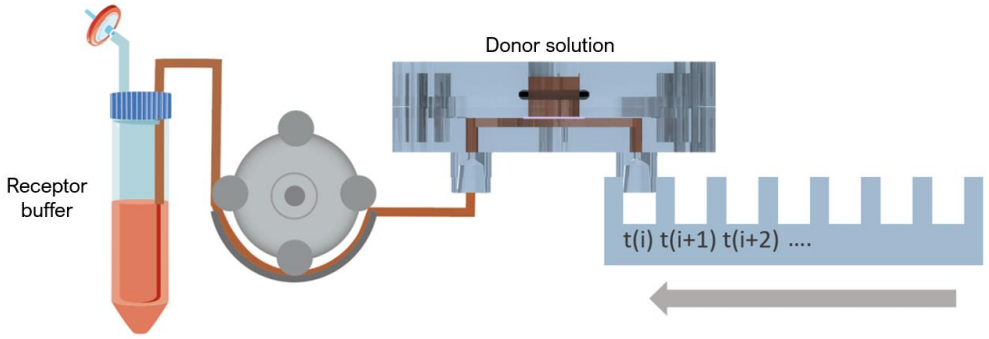

Figure 6. 5. Schematic illustration of setup for permeation testing using the skin-on-a-chip device with the cell seeding/drug testing module. The donor solution is pipetted onto the dedicated reservoir and the receptor solution is pumped through the basal chamber at a defined flow rate. The devices are places on top of a 96-well plate and the perfusate is collected on the wells at the end of each time interval t.

6.3.9 Statistical analysis

Quantitative data are presented as a mean ± standard deviation (SD). The statistical significance was calculated using a unpaired Student's t-test. Statistical differences are noted as *, ** or ***, corresponding to $p<0.05$, $p<0.01$ and $p<0.001$, respectively.

6.4 Results

6.4.1 Organ-on-a-chip platform enables leakage-free and reversible sealing

Preliminary analysis was performed using dyes to ensure leakage-free sealing during culture. The assembled culture platform is shown in **Figure 6. 6.a,** with blue dye used to identify the distinct basal and apical compartments. Two perfusable chambers with independent fluid lines are separated by a scaffold/membrane and form apical and basal chambers, analogous to the structure commonly found in the standard in vitro insert models (eg.Transwell®). This geometry ensured that the communication between channels only occurs at the central area where the cells are seeded. The reversible sealing allows the cell culture layer to be introduced and removed from the different modules and handled independently from the fluidic network.

The flexibility of the modular SoC device was tested by integrating cell culture supports with different thicknesses and materials at the centre of the device. **Figure 6. 6.b** shows the PDMS cell culture layer with a central polystyrene scaffold (Alvetex®). The scaffold was chosen to reconstructed a skin model with a dermal and epidermal compartment inside the SoC device due to its high porosity (90-93%) and thickness (200 μm). These features provide cells with an environment and physical space in which to growth in 3D, mimicking in vivo microenvironment. Alternatively, standard micro-porous polycarbonate membranes with lower thickness for the development of an epidermal model can be integrated.

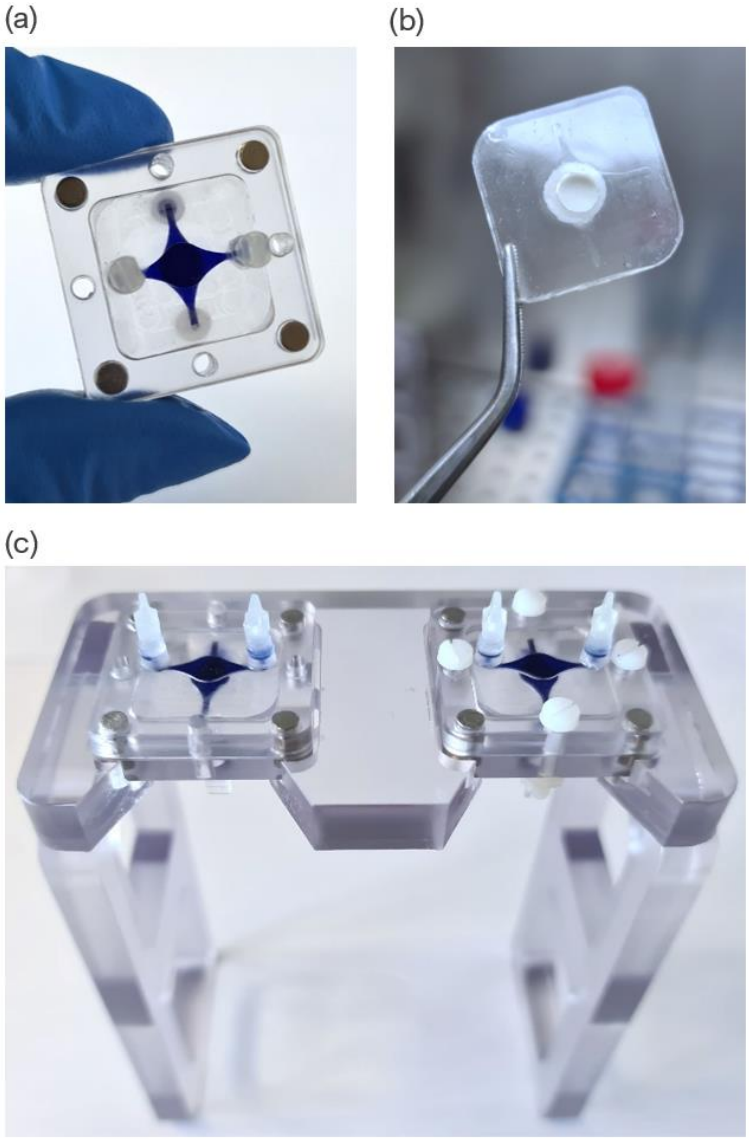

Figure 6. 6. Fabricated skin-on-a-chip (SoC) device with a modular and reversible sealing design. (a) Assembled device with blue dye used to distinct the apical and basal compartments. (b) Cell culture layer with a central porous scaffold sandwiched between a PDMS layer and a PCR tape. The reversible sealing approach allows the cell culture to be easily removed from the SoC platform. (c) Two assembled devices placed in a dedicated platform which includes magnets to ensure correct positioning of the chips during their manipulation. SoC on the left is sealed using only the magnetic latching and the SoC on the right is sealed using magnets and screws.

PCR tape was used for sealing the scaffold/membrane against the PDMS. However, the use of the PCR tape compromised the sealing at the interfaces between the perfusion layers and the cell culture layer. To solve this problem, the tape was covered with a thin layer of PDMS. The attraction forces between the magnets in each perfusion layer sealed the channels against the PDMS cell culture insert and established a liquid-tight seal capable of withstanding low pressures. The design includes holes for where screws can be added, ideal to achieve stable sealing during long-term cell culture. **Figure 6. 6.c** shows two SoC devices placed in a dedicated platform. The SoC on the left is sealed only using the magnets and the SoC on the right also includes screws. Each perfusion layer can be separately perfused with cell medium to maintain the cell culture or to introduce an experimental component.

6.4.2 SoC hydrodynamics

The hydrodynamics of the developed SoC platform with integrated porous scaffold was theoretically evaluated by performing FEA, using the software COMSOL. Simulations were performed to compare the velocity profiles and resultant mechanical forces from the different flow modalities employed for dermis formation (cross-flow and single tangential flow) and for the development of the FTSm (double tangential flow).

6.4.2.1 Dermis culture

Figure 6. 7 shows the results obtained by performing FEA using the designed SoC under single tangential flow (**Figure 6. 7.a**) and cross-flow (**Figure 6. 7.b**) conditions inside the developed SoC. Under single tangential flow, the velocity is mainly directed along the y-direction, whereas under cross flow the velocity is oriented along the z-direction (along the scaffold). The flow rate was set to a value of 1.5 μL/min for both flow conditions, whereas the outlet pressure was set to $P_{ref}=P_{atm}$. The simulations were performed for hydraulic permeabilities of 10^{-12} m^2 order magnitude to model an immature scaffold at day 1 of cell culture and 10^{-16} m^2 to model a mature dermis filled with extracellular matrix.

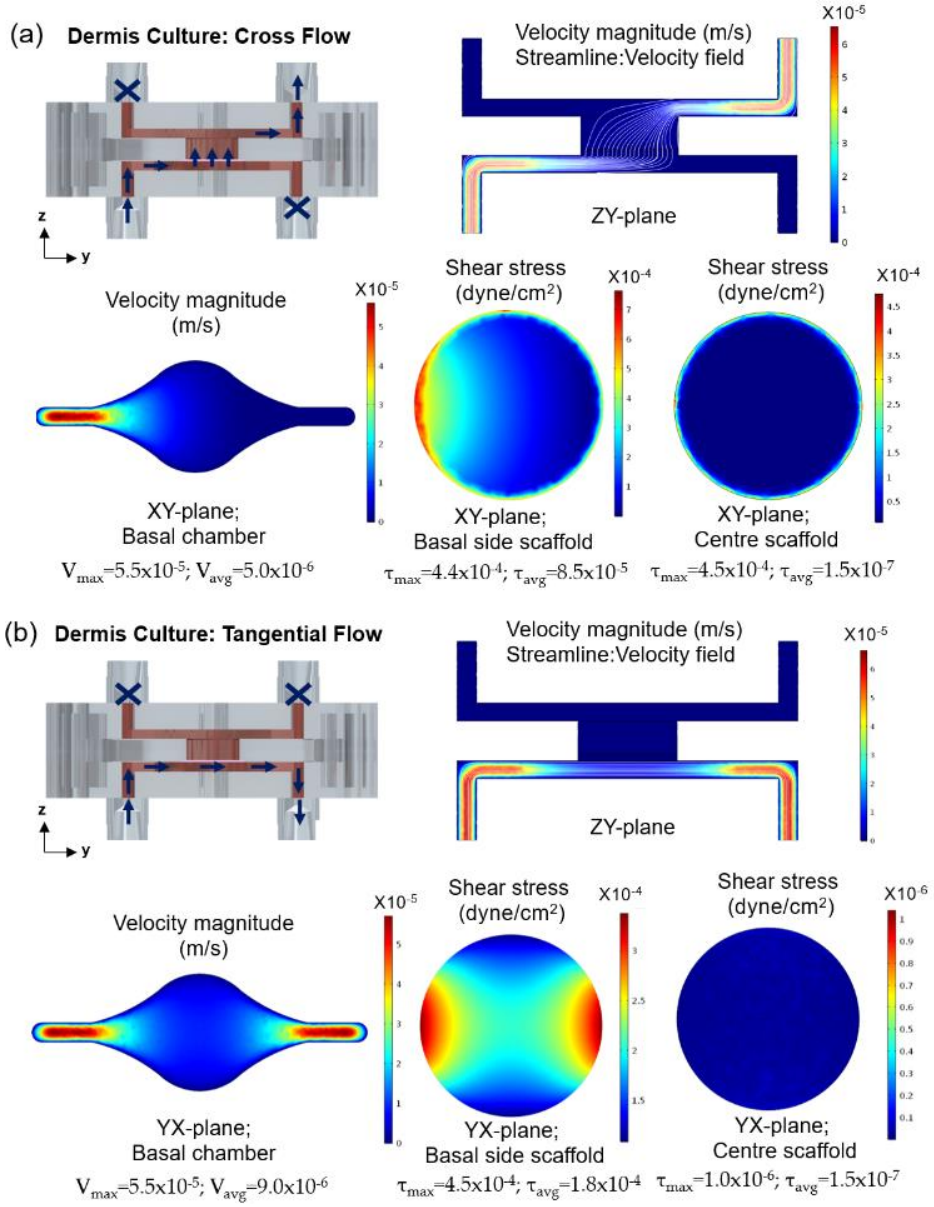

Figure 6. 7. Computational modelling depicts the fluidic mechanical conditions in the SoC and scaffold for dermis development, using two different perfusion methods (a) Forced convection intra-culture perfusion. The flow of medium is forced through the mass of cells and through the full culture thickness. (b) Tangential flow of medium. The flow of medium is not forced to pass through the mass of cells and through the full culture thickness. The resistance to fluid flow through the culture thickness is much higher than the resistance to fluid flow in a channel bellow the tissue. Streamlines and magnitude of velocity through the centre of the chamber on the y,z plane.

Using the cross-flow modality, a forced convection interstitial perfusion is established. The cell culture medium is forced to pass through the mass of cells and throughout the culture thickness. This eliminates paths of low resistance to fluid flow and all forced fluid passes through the culture at flow rates not deleterious to cells. For the cross-flow modality, the flow rate resulted in an average velocity (V_{avg}) of 5.0 x 10^{-6} m/s at the centre of the basal chamber and a velocity of 1.3 x 10^{-6} m/s at the scaffold region (**Figure B. 12.a)**. This flow modality results in a homogenous velocity profile across the scaffold along its thickness (z-direction) and diameter (y-direction). The resultant shear stress at the basal side of scaffold has an asymmetric distribution with a maximum value (τ_{max}) of 4.4 x 10^{-6} dyn/cm^2 in the region closer to the inlet and minimum values in the regions farthest away from the inlet. This value drops to an average (τ_{avg}) of 1.5 x 10^{-7} dyn/cm^2 in the scaffold with maximum values of 4.5 x 10^{-4} dyn/cm^2 at the outer zones. No significant differences on these parameters were observed for a mature dermis with increased permeability (**Figure B. 13.a).**

Using tangential flow, fluid passes along the tissue, but it is not forced to pass through it due to significantly lower resistance to flow in the channel compared to crossing the tissue barrier. For the single tangential flow, a V_{avg} = 9.0 x 10^{-6} m/s at the centre of the basal chamber was obtained. Using this modality, the fluid velocity values across the scaffold along the y-direction is very low with maximum values in zones closer to inlets/outlets of 1.6 x 10^{-9} m/s and approximately 1.0 x 10^{-10} m/s at the centre of the scaffold (**Figure B. 12.b)**. The velocity profile is also non-homogenous along the z-direction across the scaffold with a maximum value of 2.2 x 10^{-9} m/s closer to the basal fluidic network and reaching very low velocity magnitudes in the order of 10^{-10} m/s when reaching a distance of approximately 35 μm from the fluidic channel. The resultant shear stresses at the basal side of the scaffold have a symmetric distribution with higher values closer to the inlets/outlets of 4.5 x 10^{-5} dyn/cm^2. For a mature dermis, the velocities along the thickness and diameter of the scaffold as well as the shear stresses drop by several orders of magnitude and convection is reduced (**Figure B. 13.b**).

Comparing both perfusion modalities, for the same flow rate, the cross-flow results in higher velocity profiles across the scaffold and a more homogenous distribution not only along its diameter but also thickness. Using this configuration,

the streamlines pass through the scaffold. In contrast, tangential flow reduces the streamlines inside the scaffold. This phenomenon is dependent on the hydraulic permeability of the scaffold with a mature dermis decreasing convection. The resultant shear stresses are similar for both modalities, except for an outer region of the scaffold where higher values are reached for the cross-flow modality. Overall, these low values show that, during the dermis formation, the cells are protected from the shear stress inside the scaffold structure. In the porous medium, the global transport of momentum by shear stresses in the fluid is often negligible, because the pore walls impede the momentum transport to the fluid outside the individual pores. The low velocities in the tangential flow point to a dominance of diffusion for nutrient delivery.

6.4.2.2 Skin culture

Figure 6. 8 shows the results obtained by performing FEA using the designed SoC under double tangential flow for FTSm development. The flow rate was set to a value of 2 μL/min and the outlet pressure was set to $P_{ref}=P_{atm}$. This simulation was performed to study the hydrodynamics when developing FTSm under submerged conditions. The basal chamber delivers nutrients under the dermal construct and the apical chamber delivers nutrients to the HEKns layer on top the scaffold.

The basal chamber presents a V_{avg} =7.0 x 10^{-6} m/s and a maximum value of 1.0x10^{-6} m/s at the inlets/outlets. This velocity profile results in a symmetric shear stress distribution at the basal side of the scaffold with maximum value τ_{max}=3.5 x10^{-4} dyn/cm^2, closer to the inlets/outlets. The cell culture layer is asymmetrical positioned between the apical and basal chambers. At the apical chamber a "step chamber" with 2 mm in hight is present. This step chamber reduced the velocity magnitude at the cell culture area, thereby reducing both the average and maximum values of shear stresses that the cells experience at the apical side of the scaffold by approximately an order of magnitude compared to the basal side of the scaffold. The shear stress distribution at the apical side of the scaffold presents maximum values (3 x 10^{-5} dyn/cm^2) at the centre of the scaffold and lower values in the zones nearest the inlets and outlets (1 x 10^{-6} dyn/cm^2).

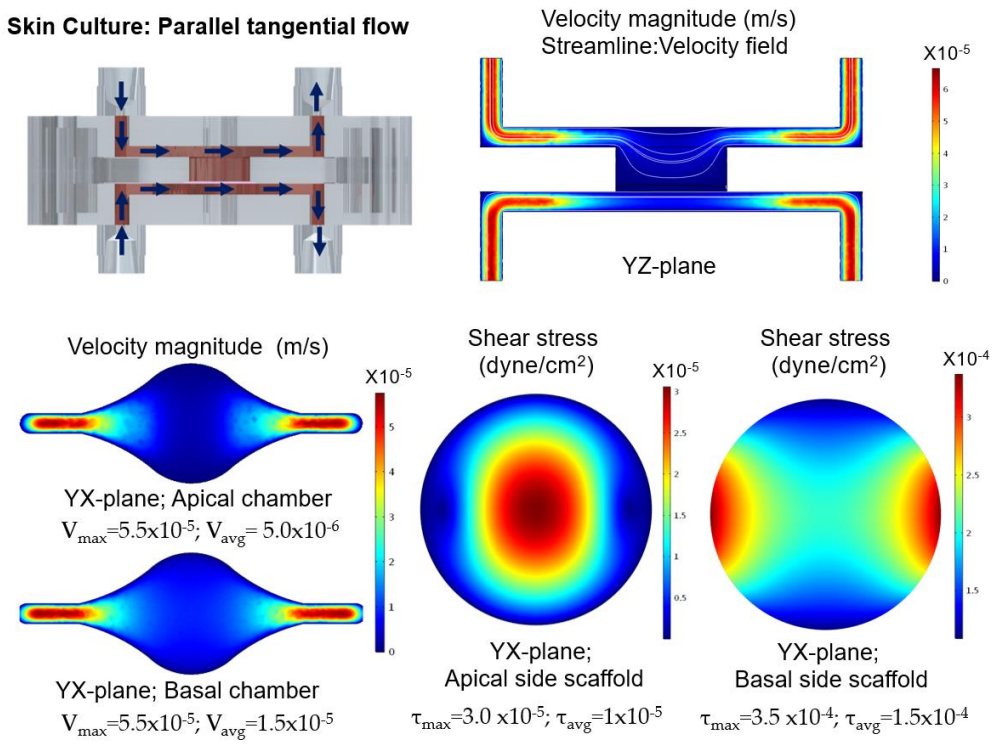

Figure 6. 8. Finite element analysis to study the hydrodynamic of the skin-on-a-chip platform during submerged conditions with apical and basal side perfusion (double tangential perfusion). Top images shows the streamlines and magnitude of velocity through the centre of the chamber on the y,z plane. Bottom images shows the velocity magnitude at the apical and basal chamber on the y,z plane (left) and the magnitude of the shear stress at the cell surface on the x,y plane at the apical and basal sides of the scaffold (middle and right, respectively).

6.4.3 Dermal maturation affects skin development

The developed SoC device was used to produce a fully human dermal compartment. Preliminary tests were performed to determine the optimized HDFn concentration range to produce a dermal construct capable of supporting the epidermis and avoid HEKn infiltration into the dermis. The influence of the dermis maturation on the epidermis formation was evaluated by seeding HEKns on top of dermal equivalents seeded with different HDFn concentrations (5×10^6, 10×10^6 and 20×10^6 cells/mL). These concentrations were tested on-chip using single

tangential flow for 6 days, followed by HKEns seeding and generation of a FTSm off-chip. **Figure 6. 9.** shows cross sections of FTSm generated using dermal constructs with 5× 10^6 (**Figure 6. 9.a**) and 20 × 10^6 cells/mL (**Figure 6. 9.b**).

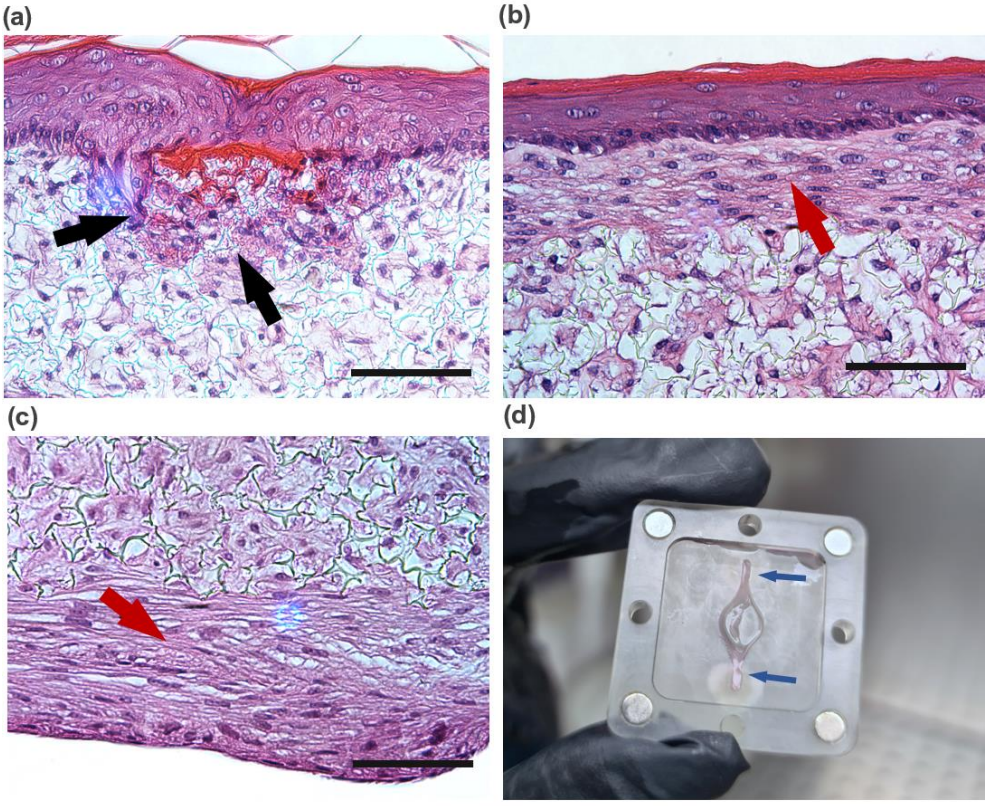

Figure 6. 9. Impact of the dermis maturation and ECM protein production on the support and development of a full thickness skin model. Representative H&E micrographs of full thickness skin equivalents (a) generated with less developed and mature dermal compartments by seeding 5x10^6 cells/mL, showing keratinocyte infiltration (black arrows), (b) generated with a mature dermal compartment by seeding 20x10^6 cells/mL, showing excessive extracellular matrix deposition (red arrows) and the apical side and (c) deposition at the basal side. Scale bares:100 um. (d) Photograph of the device basal chamber showing extracellular matrix deposited on the fluidic network and clogging the inlets/outlets (blue arrows).

As can be seen in FTSm seeded with a lower HDFn concentration, this leads to extensive HEKn infiltration into the dermal compartment. The epidermis grown on this dermal construct shows keratinocyte infiltration, resulting in areas of epidermal disorganization. The FTSm generated using a higher concentration shows

the presence of a differentiated and organized epidermis. No signs of keratinocyte infiltration can be seen in these constructs. However, a thick layer of fibroblasts and ECM can be seen on both sides of the scaffold, reaching a thickness of 105 ± 20μm at the apical side and 160 ± 45 μm at the basal side of the scaffold (**Figure 6. 9.c**). Half of the SoC devices generated with the highest dermal cell concentration led to an ECM deposition not only in the apical and basal sides of the scaffold structure but also in the basal chamber of the device. **Figure 6. 9.d** shows the SoC device with the excessive ECM deposition. The same phenomenon did not occur for lower HDFn concentrations. In particular, a concentration of 10×10^6 cells/mL cultured for 6 days minimized HEKn infiltration and, simultaneously, did not result in excessive ECM deposition. Therefore, this condition was used on the following experiments.

6.4.4 Flow stimulates production of endogenous ECM

For a seeding concentration of 10×10^6 cells/ml, different flow modalities were tested and its impact on cell proliferation and ECM deposition inside the scaffold structure were evaluated. Two flow conditions (tangential and cross flow) were tested and compared with a dermis developed under static conditions. As can be seen in **Figure 6. 10.a**, for both flow and static conditions, dermal HDFns show a relatively homogenous distribution within the scaffold's structure.

Using both tangential and cross flow, the HDFns proliferated inside the scaffold and also grew at the apical side of the structure. This can be seen in the representative H&E images by the presence of a layer of ECM deposited at the apical side of the scaffold, pointing to an increased synthesis of these proteins and fibres. During the culture of the dermal compartment, HDFns are stimulated to produce endogenous ECM which builds up and accumulate inside the scaffold. **Figure 6. 10.b** shows the ECM markers expressed in the dermal construct from 6 days.

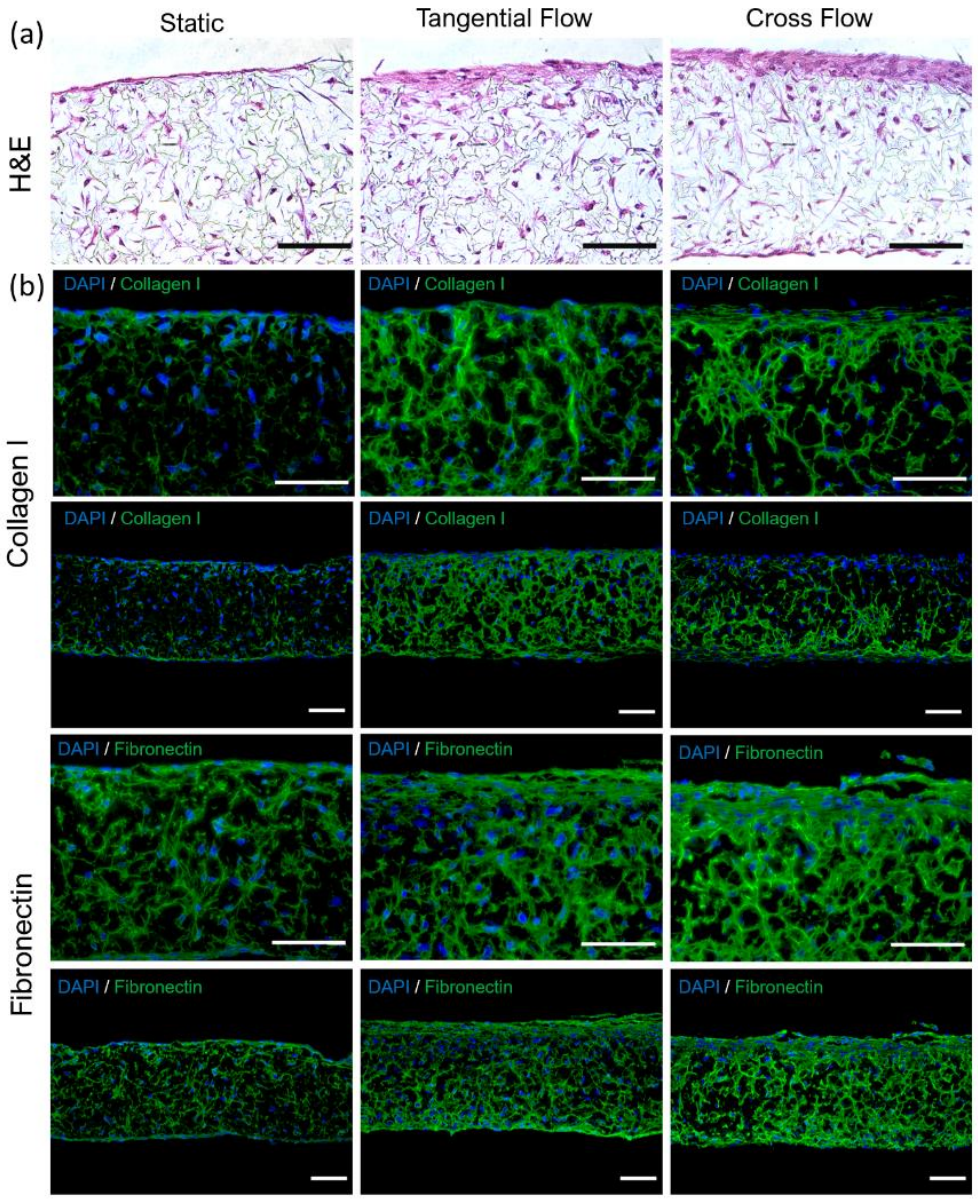

Figure 6. 10. Impact of the type of flow on the generation of a dermal equivalent based on a fibroblast derived matrix, after 6 days of culture. (a) Representative H&E images of two different batches of a dermal model cultured using single tangential flow, cross-flow and static conditions (control). (b) Representative immunofluorescence analysis showing ECM proteins (collagen type I and fibronectin) deposited on the dermal models. Nuclei are stained with DAPI (blue). Scale bares:100 μm.

Collagen I and fibronectin were detected within the dermal equivalents for all flow and static conditions. However, a clear increase in staining intensity can be observed for culture inside the chip, indicating an increased build-up and deposition of endogenous ECM proteins by HDFns within the scaffold, under perfusion. This was particularly seen for the deposition of collagen type I. The dermal compartment generated under static conditions shows a low intensity of this marker. Both flow conditions increased the intensity of the collagen type I markers. However, this effect was more pronounced and homogenous for the tangential flow. The cross-flow configurations present an inhomogeneous distribution of this protein. Both tangential and cross flow stimulated the production of fibronectin in a similar way.

6.4.5 OoC technology increases epidermal thickness and improves terminal differentiation

FTSms were maintained on-chip for 2 days under submerged conditions, followed by 11 days at the ALI, until complete development. The histological features of both models were evaluated and compared. **Figure 6. 11** shows representative histological sections performed for both the SoC and the static model. Both of them include a stratified and differentiated epidermis after 11 days at ALI. The organization was similar to the *in vivo* human skin, with columnar keratinocytes within the *stratum basale* undergoing sequential differentiation and forming the *stratum spinosum*, *stratum granulosum* and orthokeratinized corneal layers (*stratum corneum*). In both SoC and static models, terminally differentiated, keratinized corneocytes within the *stratum corneum* were stained pink by eosin and could be clearly seen at the outer part of epidermis. No differences were detected in the thickness of the corneal layers. Other histological features such as the presence of keratohyalin granules in the *stratum granulosum* could also be seen in both models. From the histological analysis, the major differences between the static and SoC models was the thickness of epidermal compartment, with the SoC presenting a significantly higher thickness than the static models. SoC models presented a mean thickness of 70 ± 30 μm and the static model a mean thickness of 41 ± 15 μm (value measured for N=3, at 3 coordinates). Furthermore, the presence of desmosomes can be clearly seen in the SoC, evidence of intercellular junctions which are indicative of cellular communication and mechanical integrity.

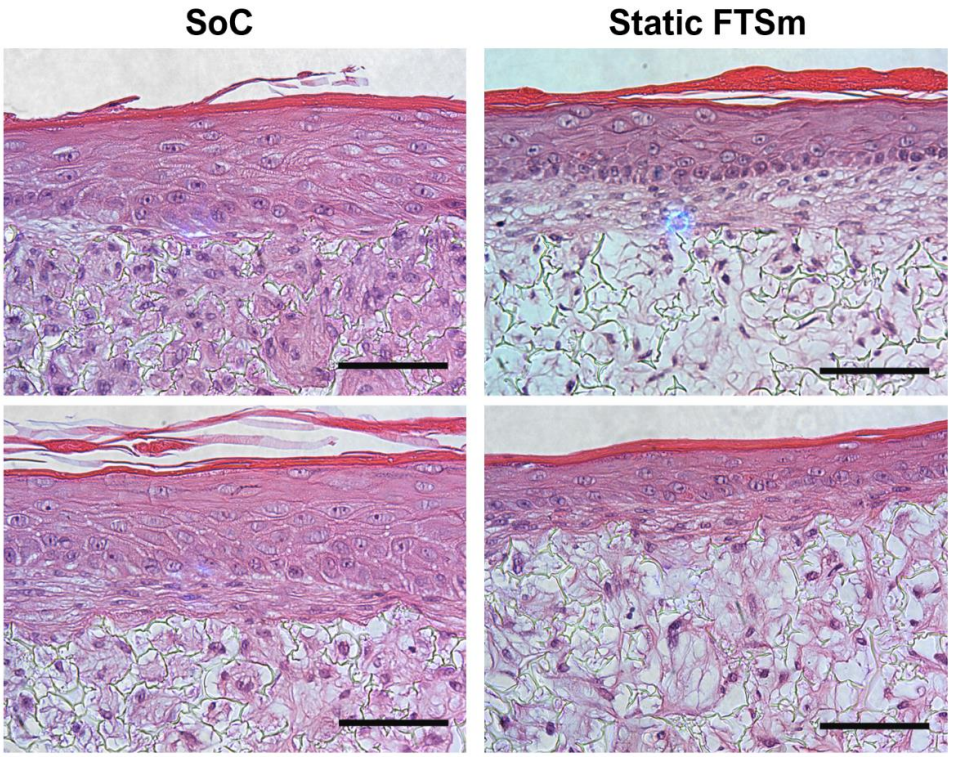

Figure 6. 11. Epidermal morphogenesis in full thickness skin-on-a-chip (SoC) models and full thickness skin models grown under static conditions (Static FTSm), grown for 11 days at the air-liquid interface (ALI). Representative H&E micrographs for 2 repetitions, showing thicker viable epidermis in the SoC model. Scale bars: 100 μm.

Figure 6. 12 shows the immunofluorescence characterization of a panel of ECM proteins expressed in the dermal compartment of the FTSm, for both SoC and static models. Collagen I and fibronectin were each detected within the dermal compartment for both models. These results replicated the observations of the dermis generated under perfusion conditions. A clear increase in staining intensity was observed for collagen I and fibronectin for the SoC models comparing to the static FTSm.

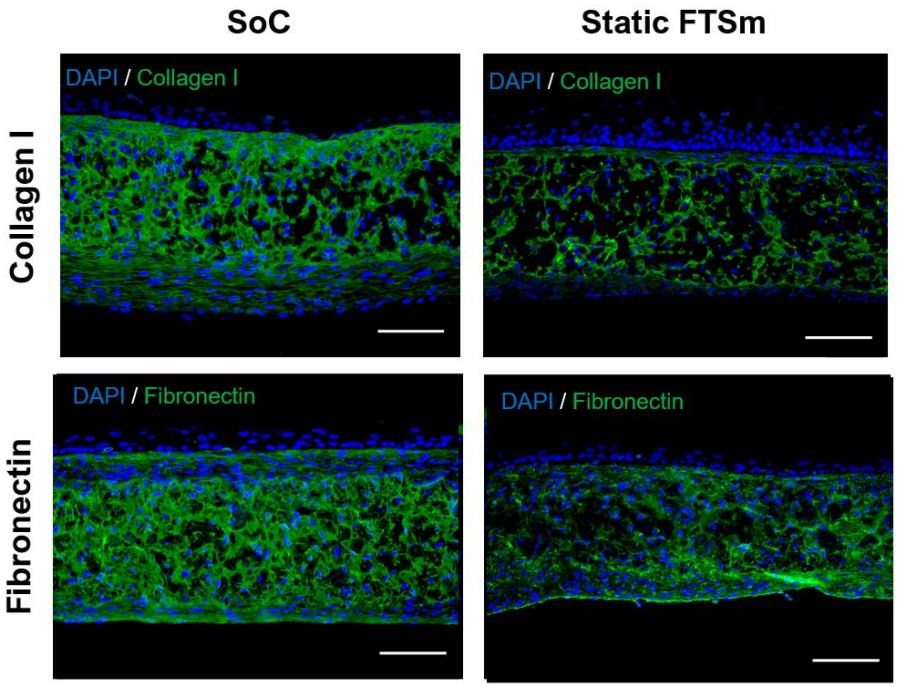

Figure 6. 12. Immunofluorescence analysis of full thickness skin-on-a-chip (SoC) model and full thickness skin model (FTSm) grown under static conditions. The models were generated by culturing the dermal compartment for 6 days, the allowing epidermal differentiation for 11 days at the air-liquid interface (ALI). Representative immunofluorescence images of extracellular matrix (ECM) proteins most often found in the epidermis (collagen I and fibronectin). Nuclei are stained with DAPI (blue). Scale bars: 100 um.

Finally, protein biomarkers representing various components of the epidermis compartment were assessed by immunofluorescence analysis (**Figure 6. 13**). HEKns at the basal layer express keratin 14 and, as they undergo a basal-to-suprabasal switch from keratin 14 to keratin 10, they move towards the surface and differentiate into the *stratum spinosum*. For both SoC and static models, the keratin 14 expression was localized mainly in the basal cell layer and keratin 10 was expressed in the living suprabasal cell layers. The increased expression of terminal differentiation markers filaggrin and involucrin in the upper layers demonstrated the more differentiated nature of the SoC model compared to the static FTSm.

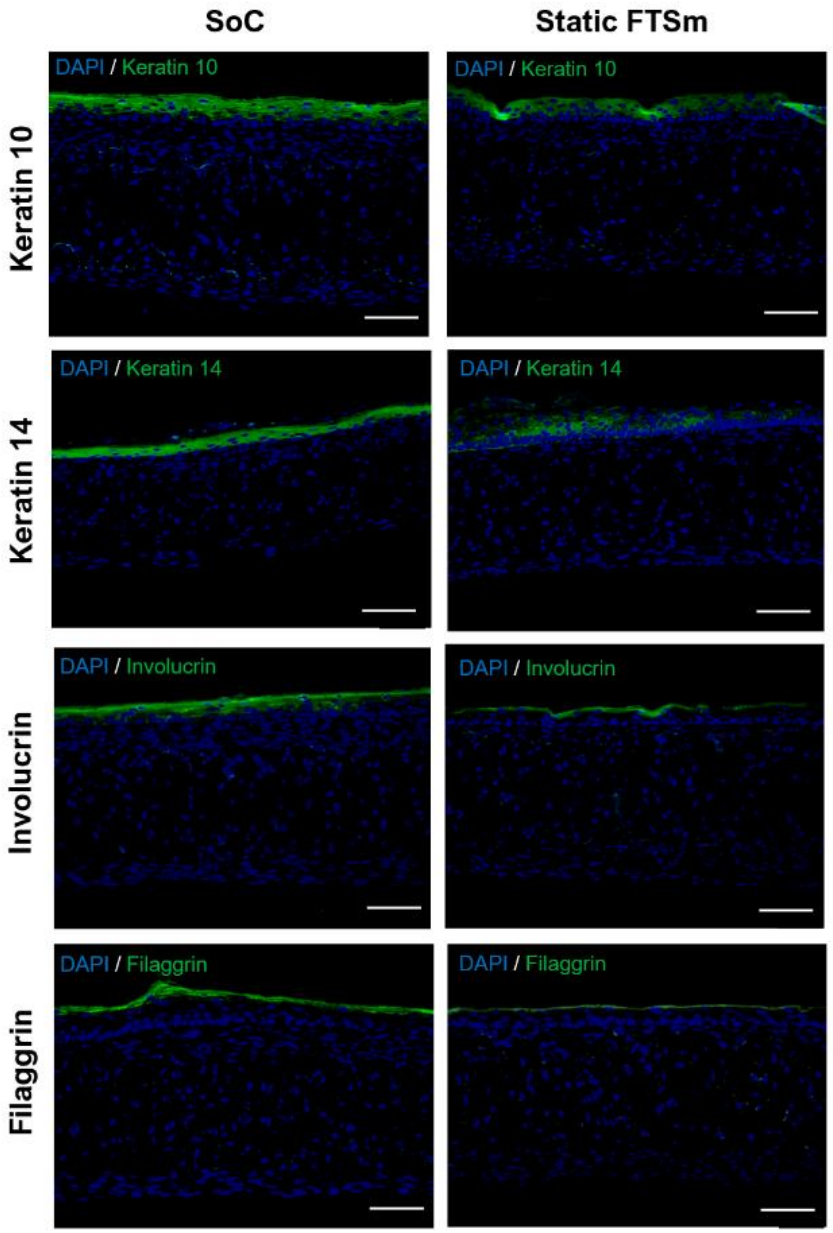

Figure 6. 13. Immunofluorescence analysis of full thickness skin-on-a-chip (SoC) model and full thickness skin model (FTSm) grown under static conditions. The models were generated by culturing the dermal compartment for 6 days, the allowing epidermal differentiation for 11 days at the air-liquid interface (ALI). Representative immunofluorescence images of proteins typically associated with epidermal differentiation (keratin 10, keratin 14, involucrin and filaggrin). Nuclei are stained with DAPI (blue). Scale bars: 100 μm.

6.4.6 SoC produces skin with increased barrier properties

The barrier function of the FTSms developed on chip (SoC) was compared with models grown off chip (static) by performing TEER measurements and permeation studies. TEER was measured using the SoC with integrated tetrapolar electrodes and an EVOM volt-ohmmeter. FTSms with TEER values ≤ 500 Ω·cm² were considered damaged/defective and excluded from the study.

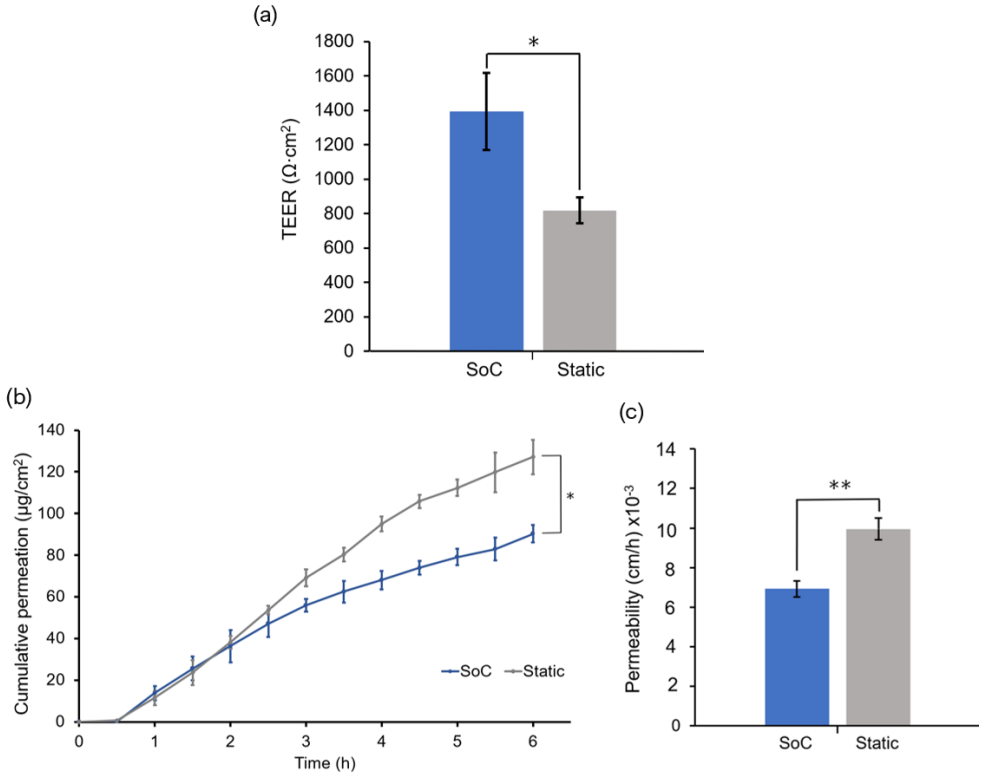

Figure 6. 14. Comparison of the skin barrier function between skin-on-a-chip (SoC) models and static models a) trans-epithelial electrical resistances (TEER) measurements measured using concentric Ag/AgCl electrodes and an EVOM system. The measurements were performed after 11 days of culture at the air liquid-interface by filling the apical and donor compartment with PBS (N=3 and n=2 SoCs and N=3 and different technical replicates: n=3,2,3). Models with TEER values ≤ 500 Ωcm² were excluded from the study. (b) cumulative permeation of FITC-dextran in SoC (N=3, n=1) and static control models (N=3, n=2). (c) permeability coefficient in SoC models and controls. Permeation testing was performed on tissue models generated for 11 days at air liquid-interface using the cell seeding/drug testing module. * and ** indicate statistically significant differences with $p < 0.05$ and $p < 0.01$, respectively. Error bars represent mean ± SD.

As shown in **Figure 6. 14.a,** the SoC model presents a significantly higher mean TEER than the static control. This value was 1393 ± 255 Ω·cm² for the SoC models (N=3) and 788 ± 78 Ω·cm² for the controls (N=3). **Figure 6. 14.b,** shows the cumulative amount of the FITC-dextran with molecular weight 4 KDa permeated through the FTSms developed on chip (SoC) and developed off chip (static), using the seeding/drug testing module. The lag time to steady-state was similar between the different models. The SoC models presented significantly lower mean FITC-dextran cumulative amounts at 6h (90±4 μg/cm²) as compared with the controls (127±8 μg/cm²). The steady-state flux was calculated from the slope of the linear portion of the cumulative amount and the permeability coefficient was calculated according to the Fick's first diffusion law (**Figure 6. 14.c**). The permeability coefficient was significant lower for SoCs as compared to the controls.

6.5 Discussion

6.5.1 Innovative chip design with integrated scaffold

In this study we present an innovative skin-on-a-chip device for development of a full thickness and fully human skin construct. The device includes a flexible architecture based on a modular and reusable approach. Conventional OoC are irreversible sealed, usually through plasma bonding, making it difficult the complete removal of the tissue for analysis [31]. The reversible-sealing feature allows easy removal of the skin tissue for histological and immunohistochemistry analysis without damaging the tissue as well as direct cell seeding. Furthermore, the device is fabricated using rapid prototyping and excludes the use of soft-lithography and plasma bonding, making it compatible with mass production [26]. Importantly, the innovative design made it possible to integrate a thick scaffold for *in-vivo* like 3D cell culture generation of the dermal compartment. This excluded the need to introduce animal-derived hydrogels which are known to be one of the major limitations of current skin models [32]. As far as we know, this is the first publication integrating an artificial scaffold on chip for generation of a fully differentiated full thickness skin. The integrated fluidic networks enable continuous flow of media for supply of nutrients and removal of metabolic wastes, recreating the role of *in vivo* vasculature.

The leakage-free sealing using magnets and/or screws results in the correct establishment of an air-liquid interface, necessary condition for epidermal differentiation. With the proposed design and setup, air is actively and continuously pumped to the apical side during skin cultivation.

6.5.2 *In-vivo* like dermal compartment generated under dynamic perfusion

One of the major challenges for the generation of a biomimetic skin model is the development of a dermal compartment with *in vivo*-like composition and mechanical environment while assuring its stability and reproducibility during culture and testing [32]. Typical FTSms generated inside an OoC device use animal-derived hydrogels to recreate the dermal compartment [23], [24], [33]–[37]. These constructs not only are not fully representative of the *in vivo* ECM, which comprises multiple types of collagens, fibrous proteins and proteoglycans but also suffer from fibroblast-mediated contraction and matrix degradation, limiting their lifespan, reproducibility and applicability [38]. In particular, the collagen detachment inside the SoC platform leads to various documented problems including the inability of maintaining a leakage-free fluid-tissue-air barrier and the inability of performing permeation assays *in situ* [39], [40]. For SoC applications, the materials used for the dermis construct should not only mimic the biophysical properties of the *in vivo* skin but also remain stable during cell culture. This has been achieved by performing chemical or physical modifications of the matrix through the addition of synthetic or natural polymers, for example, by combining fibrinogen with PEG [25]. However, the rheological behaviour of hydrogels makes them difficult to be manipulated and introduced in OoC devices in a reproducible manner [41].

Here, we propose an alternative approach by combining the use of an inert scaffold integrated on the chip with the concept of a fibroblast-derived matrix, where the dermal cells are stimulated to produce their own endogenous ECM components. Our group previously optimized this technique for the culture of a pigmented FTSm, under static conditions [30]. We showed that the developed model could maintain its architecture and function for up to 50 days at ALI. In this study, we evaluate the impact of the dynamic flow on the development a dermis construct and FTSm.

There is abundant evidence that mechanical forces are important for the architecture and physiology of multiple tissues such as the lung, bone and vascular tissues [42]. Furthermore, studies showed the effect of interstitial flown on fibroblasts, especially regarding its alignment [43][44]. The histological analysis of the generated dermal compartment showed that fibroblasts populate the scaffold and generate ECM proteins, giving rise to a mature *in vivo*-like dermal structure. Compared to the static culture, the development of a dermal compartment using dynamic flow resulted in increased deposition of ECM (fibronectin and collagen type I) onto the scaffold structure. The effect of the dynamic flow on ECM deposition could be clearly seen in the case of dermal compartments cultured for 6 days on-chip and for FTSm cultured for approximately 20 days on-chip. It can be hypothesized that this phenomenon is a result of increased interstitial flow. In a porous medium such as the dermal compartment, the pore walls impede the momentum transport of the fluid outside the individual pores. Consequently, shear stresses in the fluid are often negligible in this case. However, the dynamic flow can increase the convection necessary for the transport of nutrients through the interstitial space, mimicking important components of the microcirculation. This dynamic dermis-on-a-chip could be a relevant stand-alone model to study *in vivo*-like ECM deposition and remodelling. The development of the tissue using a porous polymeric scaffold can overcome important limitations of current SoC models due to its mechanical stability and robustness. Since this approach does not require exogenous animal-derived collagen hydrogels, the biologic variability is reduced. Moreover, since no hydrogels are introduced in the model, the manipulation of the device could be easily performed in a reproducible manner with syringe/peristaltic pumps.

The deposition of ECM (fibronectin and collagen type I) onto the scaffold structure was not significantly different between the different flow configurations. Finite element modelling was used as complementary tool to understand the hydrodynamic behaviour resulting from the different flow configurations. The theoretical analysis shows that the cross-flow configuration provides increased convection necessary for the transport of nutrients through the interstitial space, mimicking an important component of the microcirculation. However, in the experimental tests no significant differences were seen between the tangential and cross-flow configurations regarding cell proliferation and ECM synthesis. This

experiment could have been affected by the increased number of bubbles trapped in the fluidic networks when the cross-flow configuration was used. Future studies should be done towards the evaluation of flow rates that increase the effect of the mechanical forces acting on the cells in the interstitium.

6.5.3 Development of a FTSm under dynamic perfusion

The mature dermal matrix was then used to recreate a FTSm with added perfusion. Conventional skin models still have important limitations, including increased permeability and different architecture compared to native human skin [45]. One of the proposed explanations is the lack of *in vivo*-like mechanical forces, under static conditions. Using the developed platform, we generated mature pluristratified, orthokeratinized epidermal construct with increased thickness and barrier function. The models presented an organized cell morphology with the presence of basal keratinocytes undergoing sequential differentiation and stratification forming keratinocytes with a morphology characteristic of the *stratum spinosum* and *stratum granulosum*. Finally, the keratinocytes underwent terminal differentiation into anuclear, flattened corneocytes within the *stratum corneum* layers, similar to the *in vivo* skin. Contrary to other SoC studies, the *stratum corneum* was not significantly different from the controls [25]. Immunofluorescence analysis showed the presence of markers of basal, suprabasal and terminally differentiated cells expressed in the corresponding layers. Compared to the static model, the SoC showed increased expression of filaggrin, a skin barrier protein and differentiation marker, and a trend for increased involucrin expression. This is similar to the results obtained by other studies that used dynamic cultivation to generate a FTSm [36]. Filaggrin is a structural protein contributing to the integrity of the epidermal barrier, disturbed in atopic dermatitis [46]. Involucrin is an intermediate-stage differentiation marker that reinforces the skin barrier [47]. These results can explain the increased mean TEER values measured in the SoC devices.

It can be hypothesized that the differences between the SoC model and the controls are a result of the dynamic transport and interstitial flow inside the chip which can enhance the transport of nutrients and induce various morphogenetic effects [48]. Furthermore, the peristaltic flow may induce mechanical stretching, capable of generating a thicker epidermis [49]. It is documented that shear stresses

impact keratinocyte morphology with a magnitude of 0.06 dyn/cm^2 leading to morphological variation and cytoskeletal reorganization and a magnitude of 6 dyn/cm^2 resulting in cellular disruption [50]. Simulations were performed to calculate the shear stress and to study the hydrodynamics of the SoC during the 48h under submerged conditions with double tangential perfusion. The overall chamber design protects the cells from the effects of the shear stress and, combined with the use of small flow rates, resulted in a low shear stress with maximum magnitude of $3x10^5$ dyn/cm^2 at the centre of the apical chamber. These low values are not expected to have a significant impact on the cell morphology and behaviour. Thus, using the presented platform, the particular role of shear stress for skin optimization seems to be reduced. Higher shear rates could be easily achieved by tuning the flow rate. Interestingly, the SoC design results in shear stresses an order of magnitude higher at the basal chamber compared to the apical chamber. These are ideal conditions to cultivate cells at the basal side (e.g., endothelial cells) taking advantage of higher shear rates and to cultivate cells benefiting from lower shear (e.g., keratinocytes) at the apical side.

It is relevant to note that, in this study, the static FTsm present lower thickness and lower filaggrin expression than the models generated in our previous studies using primary HEKns at a 3rd passage [30]. This is possibly a consequence of the use of higher keratinocyte passage used (6th passage) and/or a result of a less optimized seeding protocol of the cells in a different insert geometry. Further studies should be performed to fully characterize the impact of the cell passage on the skin differentiation.

6.5.4 *In situ* TEER and permeation measurements

The developed SoC has been constructed with integrated sensors. Most OoC studies use fluorescent-labelled cells for visual inspection under a microscope. However, this becomes more difficult when producing 3D tissues such as the full thickness skin [51]. TEER is a promising parameter for non-destructive quantitative analysis of the skin barrier [52]. In this study, we used TEER to compare the barrier of the SoC models with the controls. The mean TEER of the skin tissues generated on chip was significantly higher than the skin tissues generated off-chip, without perfusion. This result correlates with the increased expression of filaggrin and involucrin in SoC models, both proteins that contribute to the integrity of the

epidermal barrier. The increase SoC barrier function can also be seen by its significantly lower FD4 permeability when compared to the controls. Previous permeation studies on chip reported no significant difference in regards to drug permeability as compared to the controls [36]. The authors cite contraction of the dermal compartment compromising the correct sealing of the skin model as a possible reason. This artifact was avoided in our platform through the use of a non-contractile integrated scaffold. The modular concept made it possible to easily place the cell culture insert into the dedicated drug testing module, avoiding the use of Franz diffusion cell experiments.

Taken together, this work demonstrates the potential of SoC platforms to increase the biomimicry of current FTSm. However, by comparing these results with published work from groups developing SoC models, it is possible to observe multiple inconsistencies regarding the effects of the OoC technology on the skin architecture and physiology. These differences can be explained by the group's widely different approaches regarding the materials used, cell types, OoC design and type of flow. Further progress needs to be done in the field of advanced skin models to understand what are the determinant variables to recreate models with increased skin differentiation and barrier function, closer to *in vivo* human skin.

6.6 Conclusion and outlook

We have developed a full thickness SoC model based on a fibroblast-derived matrix and with integrated sensors for real-time, non-destructive skin barrier evaluation. The platform has a modular and reversible sealing approach, resulting in a flexible architecture that allows the leakage-free integration of a porous scaffold. Further, it offers the advantages of performing downstream assays such as toxicity and permeation tests *in situ*. Interchangeable modules were developed to suit the specific requirements of an experiment. With the proposed platform, human fibroblasts are stimulated to produce their own extracellular matrix which deposits onto the scaffold structure, resulting in a fully human dermal compartment. Its non-contractile nature increased the stability and avoided the artifacts observed in conventional collagen-based structures. Perfusion during dermis generation

replicated the effects of interstitial flow and increased ECM deposition. Controlled perfusion and air flow resulted in a full thickness human skin model with *in vivo-like* characteristics, including a well-differentiated and organized epidermis with increased thickness and barrier function. In the future, additional cell types such as melanocytes, immune and endothelial cells could be integrated in the current SoC model to expand its applicability. Additionally, the use of iPSCs could be explored as tool towards personalized medicine, to model healthy and disease characteristics. Importantly, progress should be made to increase the automation of these devices to increase their utility for drug testing.

6.7 References

[1] D. Velasco, C. Quílez, M. Garcia, J. F. del Cañizo, and J. L. Jorcano, "3D human skin bioprinting: a view from the bio side," *J. 3D Print. Med.*, vol. 2, no. 3, pp. 141–162, 2018.

[2] W. Wang, K. J. Lu, C. H. Yu, Q. L. Huang, and Y. Z. Du, "Nano-drug delivery systems in wound treatment and skin regeneration," *J. Nanobiotechnology*, vol. 17, no. 1, pp. 1–15, 2019.

[3] A. Almeida, B. Sarmento, and F. Rodrigues, "Insights on in vitro models for safety and toxicity assessment of cosmetic ingredients," *Int. J. Pharm.*, vol. 519, no. 1, pp. 178–185, 2017.

[4] V. Zuang et al., EURL ECVAM Status Report on the Development, Validation and Regulatory Acceptance of Alternative Methods and Approaches (2015) EURL ECVAM Status Report 2015, no. September. 2015.

[5] G. A. Van Norman, "Limitations of Animal Studies for Predicting Toxicity in Clinical Trials: Is it Time to Rethink Our Current Approach?," *JACC Basic to Transl. Sci.*, vol. 4, no. 7, pp. 845–854, 2019.

[6] P. Avci *et al.*, "Animal models of skin disease for drug discovery," *Expert Opin. Drug Discov.*, vol. 8, no. 3, pp. 331–355, Mar. 2013.

[7] Junhee Seok *et al.*, "Genomic responses in mouse models poorly mimic human inflammatory diseases," *Proc. Natl. Acad. Sci. U. S. A.*, vol. 110, no. 9, pp. 3507–3512, 2013.

[8] S. H. Mathes, H. Ruffner, and U. Graf-Hausner, "The use of skin models in drug development," *Adv. Drug Deliv. Rev.*, vol. 69–70, pp. 81–102, 2014.

[9] N. J. Hewitt *et al.*, "Use of human in Vitro skin models for accurate and ethical risk

assessment: Metabolic considerations," *Toxicol. Sci.*, vol. 133, no. 2, pp. 209–217, 2013.

[10] A. Astashkina and D. W. Grainger, "Critical analysis of 3-D organoid in vitro cell culture models for high-throughput drug candidate toxicity assessments," *Adv. Drug Deliv. Rev.*, vol. 69–70, pp. 1–18, 2014.

[11] Y. Poumay and A. Coquette, "Modelling the human epidermis in vitro: Tools for basic and applied research," *Arch. Dermatol. Res.*, vol. 298, no. 8, pp. 361–369, 2007.

[12] Q. Wu *et al.*, "Organ-on-a-chip: Recent breakthroughs and future prospects," *Biomed. Eng. Online*, vol. 19, no. 1, pp. 1–19, 2020.

[13] G. A. Clarke *et al.*, "Advancement of sensor integrated organ-on-chip devices," *Sensors (Switzerland)*, vol. 21, no. 4, pp. 1–44, 2021.

[14] B. Ataç *et al.*, "Skin and hair on-a-chip: In vitro skin models versus ex vivo tissue maintenance with dynamic perfusion," *Lab Chip*, vol. 13, no. 18, pp. 3555–3561, 2013.

[15] H. E. Abaci, K. Gledhill, Z. Guo, A. M. Christiano, and M. L. Shuler, "Pumpless microfluidic platform for drug testing on human skin equivalents," *Lab Chip*, vol. 15, no. 3, pp. 882–888, 2015.

[16] J. J. Kim *et al.*, "A microscale, full-thickness, human skin on a chip assay simulating neutrophil responses to skin infection and antibiotic treatments," *Lab Chip*, vol. 19, no. 18, pp. 3094–3103, 2019.

[17] F. A. Alexander, S. Eggert, and J. Wiest, "Skin-on-a-chip: Transepithelial electrical resistance and extracellular acidification measurements through an automated air-liquid interface," *Genes (Basel).*, vol. 9, no. 2, 2018.

[18] I. Wagner *et al.*, "A dynamic multi-organ-chip for long-term cultivation and substance testing proven by 3D human liver and skin tissue co-culture," *Lab Chip*, vol. 13, no. 18, pp. 3538–3547, 2013.

[19] I. Maschmeyer *et al.*, "A four-organ-chip for interconnected long-term co-culture of human intestine, liver, skin and kidney equivalents," *Lab Chip*, vol. 15, no. 12, pp. 2688–2699, 2015.

[20] J. Kühnl *et al.*, "Characterization of application scenario-dependent pharmacokinetics and pharmacodynamic properties of permethrin and hyperforin in a dynamic skin and liver multi-organ-chip model," *Toxicology*, vol. 448, no. November 2020, 2021.

[21] M. Wufuer *et al.*, "Skin-on-a-chip model simulating inflammation, edema and drug-based treatment," *Sci. Rep.*, vol. 6, no. October, pp. 1–12, 2016.

[22] Q. Ramadan and F. C. W. Ting, "In vitro micro-physiological immune-competent model of the human skin," *Lab Chip*, vol. 16, no. 10, pp. 1899–1908, 2016.

[23] N. Mori, Y. Morimoto, and S. Takeuchi, "Skin integrated with perfusable vascular channels on a chip," *Biomaterials*, vol. 116, pp. 48–56, 2017.

[24] S. Lee, S. P. Jin, Y. K. Kim, G. Y. Sung, J. H. Chung, and J. H. Sung, "Construction of 3D multicellular microfluidic chip for an in vitro skin model," *Biomed. Microdevices*, vol. 19, no. 2, 2017.

[25] G. Sriram *et al.*, "Full-thickness human skin-on-chip with enhanced epidermal morphogenesis and barrier function," *Mater. Today*, vol. 21, no. 4, pp. 326–340, 2018.

[26] S. Schneider, D. Gruner, A. Richter, and P. Loskill, "Membrane integration into PDMS-free microfluidic platforms for organ-on-chip and analytical chemistry applications," *Lab Chip*, vol. 21, no. 10, pp. 1866–1885, 2021.

[27] M. Serra, I. Pereiro, A. Yamada, J. L. Viovy, S. Descroix, and D. Ferraro, "A simple and low-cost chip bonding solution for high pressure, high temperature and biological applications," *Lab Chip*, vol. 17, no. 4, pp. 629–634, 2017.

[28] P. Zoio, S. Lopes-ventura, and A. Oliva, "Barrier-on-a-chip with a modular architecture and integrated sensors for real-time measurement of biological barrier func- tion," pp. 1–20, 2021.

[29] V. Serpooshan *et al.*, "Reduced hydraulic permeability of three-dimensional collagen scaffolds attenuates gel contraction and promotes the growth and differentiation of mesenchymal stem cells," *Acta Biomater.*, vol. 6, no. 10, pp. 3978–3987, 2010.

[30] P. Zoio, S. Ventura, M. Leite, and A. Oliva, "Pigmented full-thickness human skin model based on a fibroblast-derived matrix for long-term studies," *Tissue Eng. Part C Methods*, pp. 1–12, 2021.

[31] Y. Temiz, R. D. Lovchik, G. V. Kaigala, and E. Delamarche, "Lab-on-a-chip devices: How to close and plug the lab?," *Microelectron. Eng.*, vol. 132, pp. 156–175, 2015.

[32] L. Valencia and J. L. Jorcano, "Skin-on-a-chip models : General overview and future perspectives Skin-on-a-chip models : General overview and future perspectives," vol. 030901, no. May, 2021.

[33] H. E. Abaci *et al.*, "Human Skin Constructs with Spatially Controlled Vasculature Using Primary and iPSC-Derived Endothelial Cells," *Adv. Healthc. Mater.*, vol. 5, no. 14, pp. 1800–1807, 2016.

[34] B. S. Kim, G. Gao, J. Y. Kim, and D. W. Cho, "3D Cell Printing of Perfusable Vascularized Human Skin Equivalent Composed of Epidermis, Dermis, and Hypodermis for Better Structural Recapitulation of Native Skin," *Adv. Healthc. Mater.*, vol. 8, no. 7, pp. 1–11, 2019.

[35] H. J. Song *et al.*, "Development of 3D skin-equivalent in a pump-less microfluidic chip," *J. Ind. Eng. Chem.*, vol. 60, pp. 355–359, 2018.

[36] K. Strüver, W. Friess, and S. Hedtrich, "Development of a Perfusion Platform for Dynamic Cultivation of in vitro Skin Models," *Skin Pharmacol. Physiol.*, vol. 30, no. 4, pp. 180–189, 2017.

[37] K. Schimek *et al.*, "Bioengineering of a full-thickness skin equivalent in a 96-well insert format for substance permeation studies and organ-on-a-chip applications," *Bioengineering*, vol. 5, no. 2, pp. 1–19, 2018.

[38] C. Frantz, K. M. Stewart, and V. M. Weaver, "The extracellular matrix at a glance," *J. Cell Sci.*, vol. 123, no. Pt 24, pp. 4195–4200, Dec. 2010.

[39] C. M. Gee, A. C. Watkinson, J. A. Nicolazzo, and B. C. Finnin, "The Effect of Formulation Excipients on the Penetration and Lateral Diffusion of Ibuprofen on and within the Stratum Corneum Following Topical Application to Humans," *J. Pharm. Sci.*, vol. 103, no. 3, pp. 909–919, 2014.

[40] Q. Zhang *et al.*, "Infrared Spectroscopic Imaging Tracks Lateral Distribution in Human Stratum Corneum," *Pharm. Res.*, vol. 31, no. 10, pp. 2762–2773, 2014.

[41] L. Valencia, V. C. Tejero, M. Clemente, I. Fernaud, and M. Holgado, "OPEN A new microfluidic method enabling the generation of multi - layered tissues - on - chips using skin cells as a proof of concept," pp. 1–14, 2021.

[42] R. Ogawa, "Chapter 9 - Mechanobiology and Mechanotherapy in Tissue Engineering," S. J. Lee, J. J. Yoo, and A. B. T.-I. S. T. R. Atala, Eds. Boston: Academic Press, 2016, pp. 165–181.

[43] C. P. Ng and M. A. Swartz, "Fibroblast alignment under interstitial fluid flow using a novel 3-D tissue culture model," *Am. J. Physiol. Circ. Physiol.*, vol. 284, no. 5, pp. H1771–H1777, May 2003.

[44] C. P. Ng and M. A. Swartz, "Mechanisms of Interstitial Flow-Induced Remodeling of Fibroblast–Collagen Cultures," *Ann. Biomed. Eng.*, vol. 34, no. 3, pp. 446–454, 2006.

[45] M. H. Mohammadi *et al.*, "Skin Diseases Modeling using Combined Tissue Engineering and Microfluidic Technologies," *Adv. Healthc. Mater.*, vol. 5, no. 19, pp. 2459–2480, 2016.

[46] B. Cabanillas and N. Novak, "Atopic dermatitis and filaggrin," *Curr. Opin. Immunol.*, vol. 42, pp. 1–8, 2016.

[47] E. Candi, R. Schmidt, and G. Melino, "The cornified envelope: a model of cell death in the skin," *Nat. Rev. Mol. Cell Biol.*, vol. 6, no. 4, pp. 328–340, 2005.

[48] M. A. Swartz and M. E. Fleury, "Interstitial Flow and Its Effects in Soft Tissues," *Annu. Rev. Biomed. Eng.*, vol. 9, no. 1, pp. 229–256, Jul. 2007.

[49] E. Tokuyama, Y. Nagai, K. Takahashi, Y. Kimata, and K. Naruse, "Mechanical Stretch on Human Skin Equivalents Increases the Epidermal Thickness and Develops the Basement Membrane," *PLoS One*, vol. 10, no. 11, p. e0141989, Nov. 2015.

[50] T. Agarwal, G. H. Narayana, and I. Banerjee, "Keratinocytes are mechanoresponsive to the microflow-induced shear stress," *Cytoskeleton*, vol. 76, no. 2, pp. 209–218, Feb. 2019.

[51] B. W. Graf and S. A. Boppart, “Imaging and Analysis of Three-Dimensional Cell Culture Models BT - Live Cell Imaging: Methods and Protocols,” D. B. Papkovsky, Ed. Totowa, NJ: Humana Press, 2010, pp. 211–227.

[52] B. Srinivasan, A. R. Kolli, M. B. Esch, H. E. Abaci, M. L. Shuler, and J. J. Hickman, “TEER measurement techniques for in vitro barrier model systems,” *J. Lab. Autom.*, vol. 20, no. 2, pp. 107–126, Apr. 2015.

Chapter 7

Barrier-on-a-chip with a modular architecture and integrated sensors for real-time measurement of biological barrier function

The contents of this chapter have been published in:

Zoio P, Ventura S, Oliva A. Barrier-on-a-Chip with a Modular Architecture and Integrated Sensors for Real-Time Measurement of Biological Barrier Function. *Micromachines*. 2021; 12(7):816. doi.org/10.3390/mi12070816

Author contributions:

Zoio P. performed the simulations (finite element analysis), designed and fabricated the platform and performed the TEER measurements on-chip. **Zoio P**. wrote the manuscript. Ventura S. contributed to the skin characterization. Oliva A. supervised the project, contributed to the integration of the electrodes inside the chip and revised the manuscript.

7.1 Abstract

Biological barriers are essential for the maintenance of organ homeostasis and their dysfunction is responsible for many prevalent diseases. Advanced *in vitro* models of biological barriers have been developed through the combination of 3D cell culture techniques and organ-on-chip (OoC) technology. However, real-time monitoring of tissue function inside the OoC devices has been challenging, with most approaches relying on off-chip analysis and imaging techniques. In this study, we designed and fabricated a low-cost barrier-on-chip (BoC) device with integrated electrodes for the development and real-time monitoring of biological barriers. The integrated electrodes were used to measure transepithelial electrical resistance (TEER) during tissue culture, thereby quantitatively evaluating tissue barrier function. A finite element analysis was performed to study the sensitivity of the integrated electrodes and to compare them with conventional systems. As proof-of-concept, a full-thickness human skin model (FTSm) was grown on the developed BoC, and TEER was measured on-chip during the culture. After 14 days of culture, the barrier tissue was challenged with a benchmark irritant and its impact was evaluated on-chip through TEER measurements. The developed BoC with an integrated sensing capability represents a promising tool for real-time assessment of barrier function in the context of drug testing and disease modelling.

7.2 Introduction

Biological barriers are crucial for the integrity and proper function of various organs, including the skin, brain, eye and blood vessels [1]. Disruption and dysfunction of barrier-forming tissues are an integral part of the pathophysiology of many disorders (skin barrier in psoriasis [2], blood–brain barrier in multiple sclerosis [3], blood retinal barrier in macular degeneration [4], endothelial barrier in neurodegenerative disorders and ischemic stroke [5,6]). An understanding of barrier function is essential when studying the causes and mechanisms of disease as well as when developing novel drugs and treatments.

The importance of biological barriers pressured the development of in vitro methods to recreate and characterize the tissue barrier function. Permeable cell culture supports (e.g., Transwell®) are often used to generate in vitro organ-tissue models [7-9]. However, these conventional culture systems do not provide a dynamic physicochemical microenvironment which plays an important role in maintaining the barrier function of tissues. Organ-on-chip (OoC) systems show great promise in overcoming these challenges by including key physical and biochemical parameters [10-12]. To maintain a suitable environment for tissue growth inside these systems it is necessary to monitor physiological parameters in real-time. Currently, monitoring tissue function inside the OoC mainly depends on endpoint assessment techniques. In particular, for 3D cell culture using scaffolds or membranes, this monitoring cannot be performed using conventional microscopy techniques due to difficulties with light penetration and scattering effects [13].

Transepithelial/transendothelial electrical resistance (TEER) has become a widely accepted method to evaluate the tissue barrier function in in vitro systems [14]. This method is a label-free alternative to the widely used conventional assays based on the transport of tracer compounds. TEER enables non-destructive, real-time quantification of the barrier function. Conventional TEER measurements are performed by introducing commercially available chopstick-type electrodes at both sides of a cellular barrier. The resistance of the path between the electrodes is determined by applying an alternating current (AC) signal at low frequency (typically 12.5 Hz). However, TEER readings using handheld chopstick electrodes

have low reproducibility due to variations in depth and/or the angle of immersion. Moreover, chopstick-type electrodes cannot deliver a uniform current density when large tissue culture inserts are used (>12 mm in diameter) [15]. Alternatively, EndOhm chambers contain fixed concentric electrodes, symmetrical positioned at both sides of the cellular barrier. This results in a more uniform current density when compared to chopstick electrodes and in a higher reproducibility [14]. However, cell culture inserts need to be manually transferred from the wells to the chambers which can increase the probability of tissue damage and contamination.

Just as in conventional systems, the TEER of a cellular barrier inside an OoC device can be measured by introducing electrodes on both sides of the cellular barrier. This has been achieved by inserting electrodes on the chip inlets/outlets [16-18], in a process similar to the introduction of the chopstick electrodes. Alternatively, the OoC with integrated TEER electrodes has been fabricated for development and monitoring of the blood–brain barrier [19,20], gastrointestinal tract [21,22] and airway epithelium [21]. The integration of the electrodes during the fabrication reduces the noise generated by electrode motion. However, most of the devices described in the literature require expensive processes and advanced microfabrication techniques for the development of the OoC and for the patterning of the TEER electrodes on the substrates of the channels, often requiring cleanroom access [23]. Currently, these costs of fabrication and the use of materials and strategies unsuitable for mass production are some of the major barriers delaying the transfer of the OoC to the industry [24]. Furthermore, the process of polydimethylsiloxane (PDMS) bonding makes it difficult to integrate scaffolds for 3D cell culture which are typically an order of magnitude thicker than membranes [25].

Here, we have developed a low-cost chip with a modular architecture and integrated custom-made tetrapolar electrodes for the development and monitoring of a biological barrier-on-chip (BoC). The fabrication of this platform does not require plasma bonding and it is cleanroom-free. The geometry of the custom-made electrodes integrated on the BoC is similar to the electrode arrangement on the EndOhm chamber, with a symmetric and concentric placement on both sides of the cellular barrier. Taking into account works from Odijik et al. [26] and Yeste et al.

[15], highlighting possible sources of error when integrating tetrapolar electrodes on OoC, we use finite element analysis (FEA) to determine the sensitivity distribution within the cell culture chamber. These simulations are performed for electrodes of different diameters and compared with FEA of chopstick electrodes for measuring the TEER in permeable inserts of a smaller (6.5 mm diameter) and larger culture area (12 mm diameter).

As proof-of-concept, we show the applicability of our device by developing a full-thickness human skin model (FTSm) inside the system. This is achieved by co-culturing primary human fibroblasts and primary human keratinocytes on an inert polymeric scaffold inserted between two perfusion channels. Various skin-on-a-chip (SoC) devices have been fabricated in an attempt of reproducing a skin model with a better barrier function by including fluidic forces [18-30]. However, SoC devices face multiple technical challenges, including the tendency of the hydrogel-based materials (e.g., collagen) to contract over time leading to tissue disruption and the difficulty in recreating the complex 3D architecture of the epidermis [31]. To our knowledge, until now, there is no description of a functional OoC combining 3D skin production with real-time TEER measurement. Here, we measured the TEER in real-time, following skin differentiation and resultant barrier formation. Histological analysis was performed on tissues representative of different stages of differentiation. TEER-on-chip measurements were performed to test the impact of a benchmark irritant on the tissue barrier function.

The presented platform is applicable to any biological barrier requiring an apical and basolateral chamber to mimic tissue–tissue, tissue–liquid and tissue–air interfaces. Moreover, the possibility of integrating other structures besides membranes (e.g., polymeric scaffolds) opens the door for reproducing tissues with an increased level of complexity.

7.3 Materials and Methods

7.3.1 Simulation Model

FEA was performed using the AC/DC module from the commercial software COMSOL Multiphysics v.5.3 (COMSOL Inc., Burlington, MA, USA) to map the sensitivity field (S) distribution for different tetrapolar electrode configurations placed within different chamber geometries. **Figure 7. 1** provides details of the different electrode and chamber configurations used for FEA: (1) BoC device with integrated custom-made electrodes with different dimensions (2 mm and 4 mm outer diameter) (**Figure 7. 1.a**); (2) conventional permeable insert model with chopstick electrodes and cell culture area with different dimensions (6.5 mm diameter and 12 mm diameter) (**Figure 7. 1.b**).

In more detail, the BoC model comprises two chambers and a small volume at the centre representing the 3D tissue. Concentric electrodes representing the current carrying (CC) and voltage sensing (VS) electrodes were placed in upper and lower surfaces on the top and bottom chambers. Two different electrode sizes were simulated: CC electrodes 0.8 mm + VS electrodes 2 mm diameter (BoC A) and CC electrodes 2 mm + VS electrodes 4 mm diameter (BoC B). The 3D geometry of the BoC and the complete mesh can be seen in **Figure 7. 2.a**. The tetrahedral mesh consisted of approximately 7×10^4 domain elements, 2×10^4 boundary elements, and 1×10^3 edge elements.

The insert model is a 3D representation of a conventional permeable support for cell culture and chopstick electrodes. The model was created for 12 mm (Insert A) and 6.5 mm (Insert B) diameter inserts. These diameters are widely used to generate biological barriers and recommended for normalizing TEER measurements performed with chopstick electrodes. The 3D geometry of this model and the complete mesh can be seen in **Figure 7. 2.b**. Complete mesh consists of approximately 2×10^5 domain elements, 2×10^4 boundary elements, and 1×10^3 edge elements.

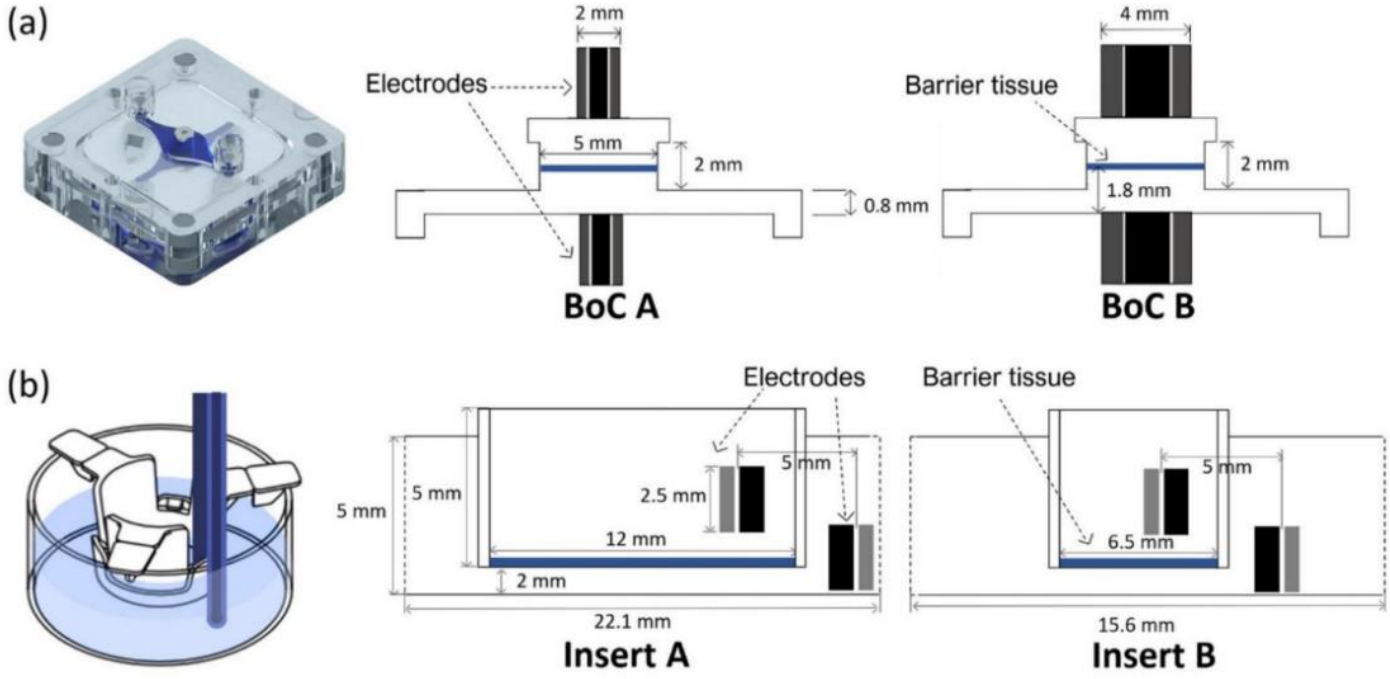

Figure 7. 1. Geometrical dimensions for the simulated models. (**a**) BoC (barrier-on-chip) model with integrated concentric electrodes of different sizes: current carrying (CC) electrodes 0.8 mm + voltage sensing (VS) electrodes 2 mm diameter (BoC A) and CC electrodes 2 mm + VS electrodes 4 mm diameter (BoC B). The image on the left are the 3D representations of the experimental setup. (**b**) Insert model with chopstick electrodes and insert of different diameters: 12 mm diameter (Insert A) and 6.5 mm diameter (Insert B). The image on the left is a schematic representation of the measurements using chopstick electrodes and an insert. The barrier tissue is represented in blue.

The electrical current (ec) interface of the AC/DC module was used to calculate the electric fields and current density distributions associated with the analysed electrode configurations. For all configurations, a constant DC current of 1A was injected through the CC electrodes and the pick-up, VS electrodes were set as floating potential and zero current. The other outer boundaries were defined as electrical insulations. For all models, the "extra fine" mesh (under COMSOL calibration for general physics) was chosen, automatically assigning mesh sizes. More details about the FEA parameters are provided as supplementary information (**Table C. 1**). To reduce the computational complexity of the simulations, time-independent DC simulations were performed. This is a valid approximation to the experimental apparatus since a low frequency (12.5 Hz) AC current was used.

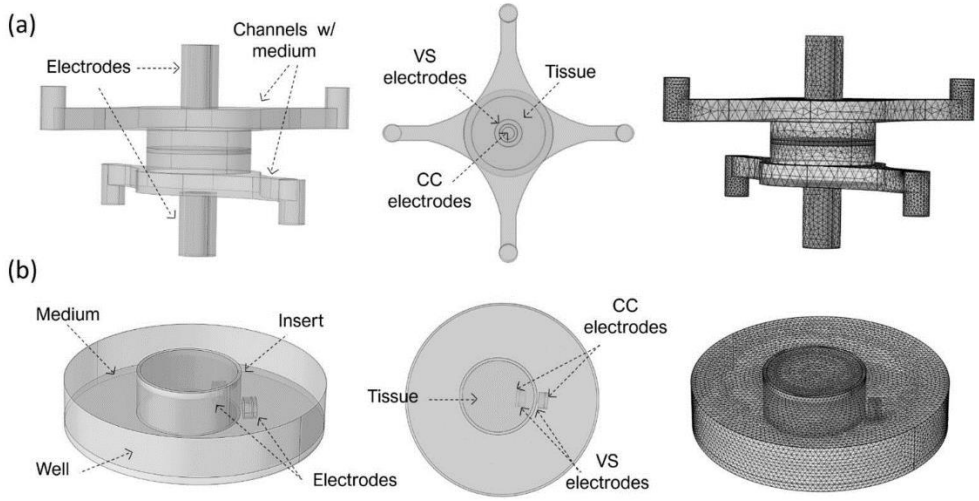

Figure 7. 2. Three-dimensional geometry and created mesh for finite element analysis (FEA) for (**a**) the BoC model with integrated electrodes (CC 0.8 mm + VS 2 mm diameter) and tetrahedral mesh consisting of approximately 7×10^4 domain elements, 2×10^4 boundary elements, and 1×10^3 edge elements and (**b**) the Insert model (insert of 12 mm diameter). Complete mesh consists of approximately 2×10^5 domain elements, 2×10^4 boundary elements, and 2×10^3 edge elements.

7.3.2 Sensitivity evaluation

The sensitivity of a small volume within the measured biomaterial is a measure of how much the resistivity of this volume contributes the total measured impedance, provided that the electrical properties are uniform throughout the material. For calculation of sensitivity, the reciprocity theorem was used (**Figure C. 1, Appendix C.2**) [32]. The sensitivity S of each zone can be calculated as reported by Grimnes and Martinsen [33]:

$$S = \frac{Jcc \cdot Jvs}{I^2} \qquad [7.1]$$

where $\boldsymbol{J_{CC}}$ is the current density field that results by using CC electrodes for current injection, $\boldsymbol{J_{VS}}$ is the current density field produced by reversing the setup and using the VS electrodes for current injection, and I is the magnitude of the applied current.

The sensitivity of a tetrapolar system was computed using FEA, by:

1. Applying a constant current I between the tCC electrodes and computing the current density field $\boldsymbol{J_{CC}}$ in each small volume in the material as a result of this current.

2. The CC and VS electrodes are exchanged, i.e., the same current I is injected between the voltage VS electrodes and again the resulting current density $\boldsymbol{J_{VS}}$ is computed in each small volume element.

3. The vector dot product between $\boldsymbol{J_{CC}}$ and $\boldsymbol{J_{VS}}$ in each volume element, divided by the current squared, is the sensitivity of the volume element.

Sensitivity can be positive, negative or zero depending on the angle between $\boldsymbol{J_{CC}}$ and $\boldsymbol{J_{VS}}$**.** Positive sensitivity means that an increase in electrical resistivity of a volume results in a corresponding increase in the measured electrical resistance. Conversely, negative sensitivity results in a decrease in the measured electrical resistance for the same increase in resistivity. In areas of zero sensitivity, a change in electrical resistivity does not notably affect the impedance. Since the sensitivity is normalised to the current, this distribution is independent of the current used.

Simulations were conducted with parametric sweeps of the TEER (from 10^1 to 10^4 $\Omega.cm^2$) spanning the range of the values reported in the literature for barrier tissues as well as simulating the growth and development of these tissues [24]. The sensitivity distribution along the cell barrier surface was simulated and compared between the different models.

7.3.3 Fabrication and assembly of barrier-on-a-chip (BoC) device

The fabricated device includes two polycarbonate compartments (apical and basal) and a central layer for tissue culture. The central layer is composed of polydimethylsiloxane (PDMS) and a thin layer of polymerase chain reaction (PCR) tape to seal a membrane or scaffold at the centre. The basal compartment includes a fluidic channel and inlet/outlet channels for perfusion with culture media or flow-through of a receiver solution in an *in vitro* test. The apical compartment presents the same fluidic structure and can be used for perfusion of culture medium (liquid-liquid interface) or ventilation (air-liquid interface). An exploded view of the BoC can be seen in **Figure 7. 3**. The design includes integrated magnets to correctly seal the cell culture layer between the apical and basal compartments.

The fluidic compartments and the molds used to produce the cell culture layer were designed in computer aided design (CAD) using Autocad 2017 (Waltham, MA, USA) and fabricated using computer numerically controlled (CNC) machining and laser machining (Xometry Europe GmbH, Ottobrunn, DE). The apical and basal chamber were constructed in polycarbonate with the following dimensions: 31.5 mm in length, 31.5 mm in width, 4 mm in heigh and a central cavity with 21 mm in length, 21 mm in width and 1 mm in height. The cavities were included on the fluidic chambers to accept the PDMS layer for skin culture. Each of the fabricated layers contained 4 neodymium magnets with 4 mm diameter and 3 mm height with a force of 3N each. The magnets were placed with polar opposites facing each other on the basal and apical layer. Both apical and basal compartments included a central circular opening housing the electrodes for TEER measurements. For the access ports, mini female luers (Microfluidic ChipShop, Jena, DE) were glued to the inlets and outlets into the upper and lower

polycarbonate housings with the channel features oriented to the interior of the device.

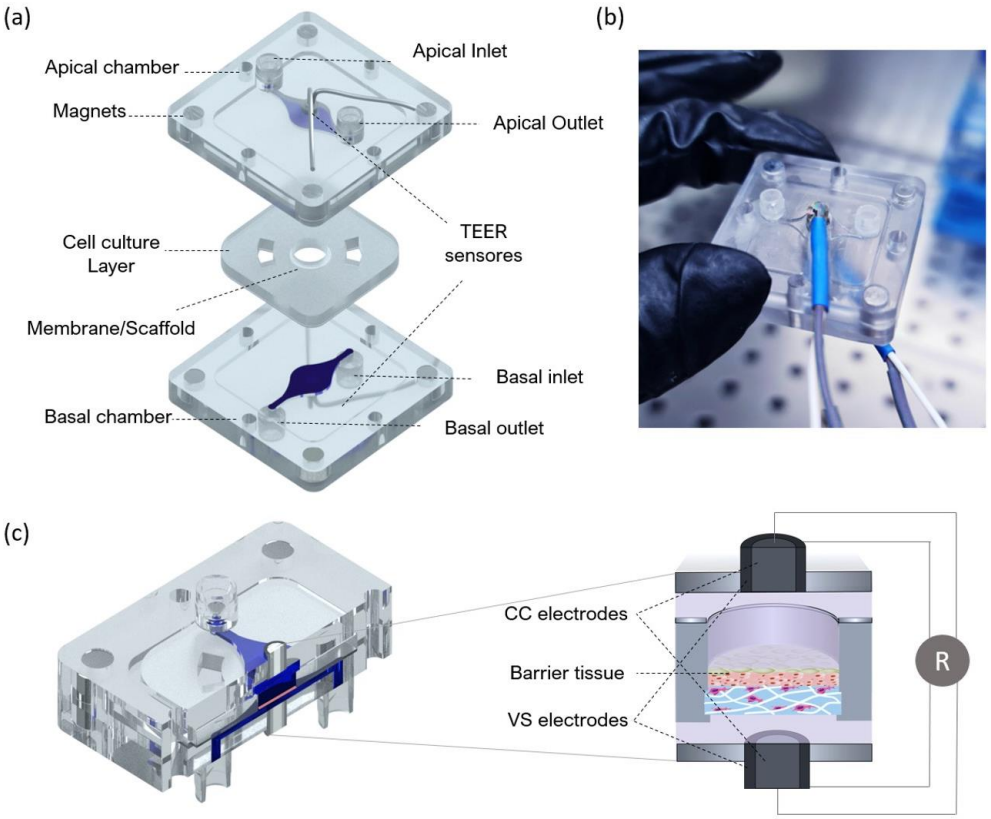

Figure 7. 3. Design of the BoC with integrated electrodes for TEER measurements. (a) Schematic exploded view of the BoC platform. The device consists of central insert for cell culture and two external compartments (apical and basal) for top and bottom perfusion with air and/or medium and integrated electrodes. The central insert layer is composed of polydimethylsiloxane (PDMS) and a thin layer of PCR tape sealing a membrane/scaffold. The top and bottom compartments are made of polycarbonate and include magnets at the corners to correctly seal the insert layer and establish interfaces (air-liquid and liquid-liquid) (b) Picture of the assembled device with integrated TEER sensors made of Ag/AgCl sintered pellet electrode, insulating polyether ether ketone (PEEK) tubing and external silver tubing. (c) Schematic representation of the BoC side view showing the fluid pathway, barrier tissue at the centre and concentric electrodes (CC and VS electrodes) positioned at the top and bottom chambers. The zoom-in panel showing the cross-section is not drawn to scale.

To obtain central layers for cell culture that could fit in the polycarbonate cavities, molds were fabricated using CNC machining and laser cutting. The base

of the mold was fabricated in poly(methyl methacrylate) (PMMA) and had 21 mm in length and 21 mm in width and included a central cylinder with 5 mm diameter and 2 mm height. The lateral and top pieces of the mold were fabricated with laser cutting using PMMA with 2 mm in thickness. The mold cavity was filled with degassed PDMS prepolymer mixed with curing agent (Sylgard 184, Dow Corning, Corning, NY) at a 10:1 (w/w) ratio. The assembled molds were clamped and placed in an oven for 12 hours at 65°C. The resulting PDMS layer was removed from the mold with the help of a razor blade. The polystyrene scaffolds (Alvetex®, REPROCELL Europe Ltd, Glasgow, UK) were cut with a 6 mm diameter puncher and sandwiched between the PDMS insert layer and PCR tape. To better seal the PDMS insert against the polycarbonate housing and avoid leakage, the PCR tape was covered with a thin PDMS layer. This geometry ensured that the communication between channels only occurred though the area at the centre where the cells were seeded. The modular approach of the design makes it possible to handle the cell culture layer independently from the fluidic network.

The electrodes integrated at the apical and basal layers were both made of a 0.8 mm diameter Ag/AgCl sintered pellet electrode (Neurospec AG, Stans, Switzerland), an electrical insulating polyether ether ketone (PEEK) tubing and silver tubing with 2 mm OD. They were concentrically assembled and installed on both perfusion chambers (**Figure 7. 3.b**). Liquid PDMS pre-polymer mixed with curing agent was applied to fill gaps and cured at 50°C for 24h to ensure leakage-free installation. The BoC devices were sterilized using UVC radiation before each experiment.

7.3.4 Primary cells and cell maintenance

Primary human foreskin-derived dermal fibroblasts (HDFn, CellnTec, Switzerland) were maintained in Fibroblast Growth medium (FGM) composed of Iscove's Modified Dulbecco's Medium (IMDM Gibco®, Waltham, MA USA) supplemented with 10% fetal bovine serum (FBS, Gibco®, Waltham, MA USA), at 37ºC in a 5% $C0_2$ humidifier, following supplier's instructions. HDFs were used for up to 10 passages and subcultured at a 90% confluency.

Primary human epidermal keratinocytes isolated from neonatal foreskin (HEKn, Gibco®, Waltham, MA USA) were maintained in keratinocyte growth medium (KGM) composed of EpiLife medium (Gibco®, Waltham, MA USA), supplemented with 0.06 mM calcium and keratinocyte growth factor (HKGS, Gibco®, Waltham, MA USA), at 37ºC in a 5% CO_2 humidifier incubator. The KGM medium was changed every other day until the cells reached 50% confluency. At this point the medium was changed every day. A low passage (4-5) and actively proliferating HEKns were used for successful 3D culture. All cultures were routinely monitored for contaminations.

7.3.5 Generation of full thickness equivalents on the BoC

The process of developing fully human FTSm can be divided in three main steps: the development of a mature dermis, the culture of HEKns on top of the dermis under submerged conditions, and the culture of the epidermis at the air-liquid interface (ALI) until a fully differentiated skin is produced. The protocol for generating a FTSm using a polystyrene scaffold and a fibroblast-derived matrix was adapted from [34]. Briefly, dermal models were generated by seeding HDFns (3.0×10^5 cells) onto Alvetex® scaffolds (REPROCELL Europe Ltd, Glasgow, UK) and incubating at 37ºC in a 5% CO_2 humidified incubator in FGM medium supplemented with 100 ug/mL L-Ascorbic acid 2-phosphate (Sigma-Aldrich). Dermal equivalents were maintained for 12 days on a 6-well plate under static conditions.

FTSm were generated by seeding HEKns onto the dermal equivalents and maintaining the tissue construct the BoC under submerged conditions for 2 days and ALI for up to 14 days. For this, HEKns were harvested by trypsinization and 30 µL of cell suspension ($5.0 \times 10^6 cells/mL$) was seeded on top of the dermal equivalent in KGM containing high calcium concentration (1.5 mM). The tissue construct was incubated for 3 hours for cell adhesion at 37ºC in a 5% CO_2 incubator. After the incubation period, the PDMS layer was inserted on the BoC, between the apical and basal chambers, and parallel perfusion was established. The inlet ports on the top and lower compartments were connected to the tubing mounted on the peristaltic pump and connected to a media reservoir with supplemented KGM medium. The medium was pumped from the reservoir through the inlets of the apical and basal

chambers and left the BoC through the apical and basal outlets. With this configuration, the FTSm in culture chamber of the device was double-sided perfused at a flow rate of 1.5 μL/min.

After 48h, the models were raised to ALI and cultured in KGM containing 1.5 mM calcium, supplemented with 10 ng/mL KGF and 50 μg/mL of L-Ascorbic acid 2-phosphate and maintained up to a further 14 days. For this, the medium was pumped only through the basal chamber at a flow rate of 1.5 μL/min and air was pumped through the apical chamber to allow the formation of a differentiated epidermis.

7.3.6 TEER measurements

TEER was measured with the EVOM volt-ohmmeter (WPI Europe, UK), using the tetrapolar method. The volt-ohmmeter supplies an AC square-wave current of ± 10 μA at 12.5 Hz through the outer CC electrodes and measures the voltage drop across the inner VS electrodes as shown schematically in Figure 7.3.c. This technique was used to measure TEER using conventional chopstick electrodes and concentric electrodes integrated in the BoC device. For both cases, each electrode pair contains a silver/silver-chloride pellet for measuring voltage and a silver electrode for passing current. TEER values were recorded during culture time from the last day under submerged conditions (day 0) until day 14 at ALI. For this, the medium was pumped through both the basal and apical chambers to bridge an electrical connection between top and bottom sensors. After a 10-minute TEER reading for each sample, the ALI was resumed. At the removal of the medium from the apical chamber, the TEER becomes immeasurable again due to the removal of the electrical bridge. These measurements were performed for 3 skin batches at each time point. TEER was also measured for a blank scaffold and subtracted from each recording.

The applicability of the TEER sensors for toxicological applications was accessed by delivering cell medium with 0.2% sodium dodecyl sulphate (SDS) to the basal side of the skin. TEER measurements were recorded at day 14 of ALI by pumping phosphate buffered saline (PBS) into the apical chamber and medium with SDS to the basal chamber to bridge an electrical connection between sensors.

Perfusion with SDS medium continued for 3 hours with TEER being measured every 15 minutes.

To better validate the custom-made tetrapolar electrodes, a comparison on the resistance readings was made between the BoC electrode system and the traditional chopstick electrodes. Chopstick electrodes are the conventional method to perform TEER readings on permeable cell culture inserts and present approximate uniform current distributions for small diameters and high TEER values. Since it is not possible to directly introduce the chopstick electrodes on the BoC device, a custom calibration chamber was designed and fabricated (**Figure C. 2**). The chamber was fabricated using precision milling and was designed to accommodate the PDMS insert layer while allowing for the same placement of the chopstick electrodes as in the conventional permeable inserts for cell culture.

7.3.7 Barrier function analysis with passive dye

The barrier function of the skin models was further assessed by the penetration of the passive dye lucifer yellow (Sigma-Aldrich) in combination with treatment with the detergent SDS. Solution of SDS 0.2% w/v in PBS was perfused at the apical chamber for 0, 1 and 3 hours. After perfusion with SDS, the models were washed three times with PBS. 1 mg/mL lucifer yellow was topically applied to the models for 30 minutes, followed by three washes with PBS. The tissues were fixed with neutral buffered 10% formalin solution (Sigma-Aldrich) and embedded in paraffin. Tissue sections were rehydrated and nuclei were stained with 1 μg/mL of 4,6-diamidino-2-Phenylindole (DAPI, Invitrogen) and slides were mounted with Vectashield (Vector Laboratories). Images were obtained using the Nikon Eclipse TE2000-S fluorescence microscope (Nikon instruments, USA) and analysed with the ImageJ software.

7.3.8 Histochemistry analysis

The modular architecture and reversible sealing have made it possible to easily open the platform and remove the tissue for analysis. The reconstructed tissues were fixed immediately after being taken out of chip in 10% neutral buffered formalin (Sigma). The samples were embedded in paraffin to allow for transverse sectioning. Paraffin-embedded sections (5 μm-thick) were de-paraffined and re-hydrated for morphological evaluation by staining with haematoxylin and eosin (H&E) through standard methods, as described in [35].

7.4 Results

7.4.1 Sensitivity distribution

In this study, the software COMSOL Multiphysics was used to model the complex BoC and Insert geometries and perform FEA. The sensitivity field along the tissue barrier area was evaluated using equation 7.1. This was used to determine the contribution of each zone of the tissue to the measured resistance for the different electrode configurations and chamber geometries.

Figure 7. 4 and **Figure 7. 5** show the planar sensitivity at the tissue culture plane and the normalized sensitivity (S_{normal}) profile along the line AA' when TEER is measured using a BoC device with integrated concentric electrodes (**Figure 7. 4**) covering ~ 15% of total culture area (BoC A) or covering ~ 65% of total culture area (BoC B) and when TEER is measured using chopstick electrodes and Insert with conventional sizes (**Figure 7. 5**): 12 mm diameter (Insert A) and 6.5 mm diameter insert (Insert B).

For all the setups, the sensitivity values are positive in the entire cell culture volume. Zones of negative sensitive can be seen close to the electrodes (**Figure C. 3**). The sensitivity is non-uniformly distributed with the highest values in the regions close to the electrodes and lowest values (normalized to 0%) in the regions further away from the electrodes. As expected, for both BoC and Insert models, regions closer to the electrodes contribute more to the measured resistance. Moving away from the electrodes, the sensitivity rapidly decreases. In the BoC device this can be

seen by the central areas of increased sensitivity bellow the electrodes, for both configurations (**Figure 7. 4**). In the insert models, sensitivity peaks can be seen in the periphery bellow the electrodes, representation a higher contribution of these regions to the resistance measurement (**Figure 7. 5**). For these configurations, sensitivity valleys can also be observed in the areas in the middle of pair electrodes, especially for the model Insert B.

A range of the most common TEER values measured on barrier tissues (10^1 to 10^4 $\Omega.cm^2$) were used to study the dependency of this parameter on the sensitivity field. For all the models, there was a dependency of the TEER on the sensitivity, with higher TEER values resulting in a decrease in the peak sensitivity. Thus, resulting in a more uniform sensitivity field.

Concerning the BoC models (**Figure 7. 4**), it could be theorized that larger electrodes, covering more tissue area, could result in a more uniform sensitivity. However, this was only verified for very low TEER values (10^1 $\Omega.cm^2$). For most TEER values ($\geq 10^2$ $\Omega.cm^2$), the smaller electrode assembly (BoC A) results in a more uniform sensitivity than the larger electrode assembly (BoC B). In particular, for BoC A, TEER values of 10^2 $\Omega.cm^2$ result in a maximum sensitivity deviation of 17% at the centre of the tissue when comparing with the periphery. TEER values $\geq 10^3$ Ω cm^2 result in a maximum sensitivity deviation of 10% at the centre when comparing with the periphery.

For most TEER values, BoC B results in larger differences between the zones of the culture area. For BoC B and TEER of 10^1 Ω cm^2, the central area has a sensitivity 70% higher compared with the periphery. For TEER values $\geq 10^2$ Ω cm^2 the central area has a sensitivity 42% higher compared with the periphery. For the model BoC A, no sensitivity differences were seen for TEER values greater than 10^3 Ω cm^2 and for the model BoC B, no sensitivity differences were seen for TEER values greater than 10^2 Ω cm^2.

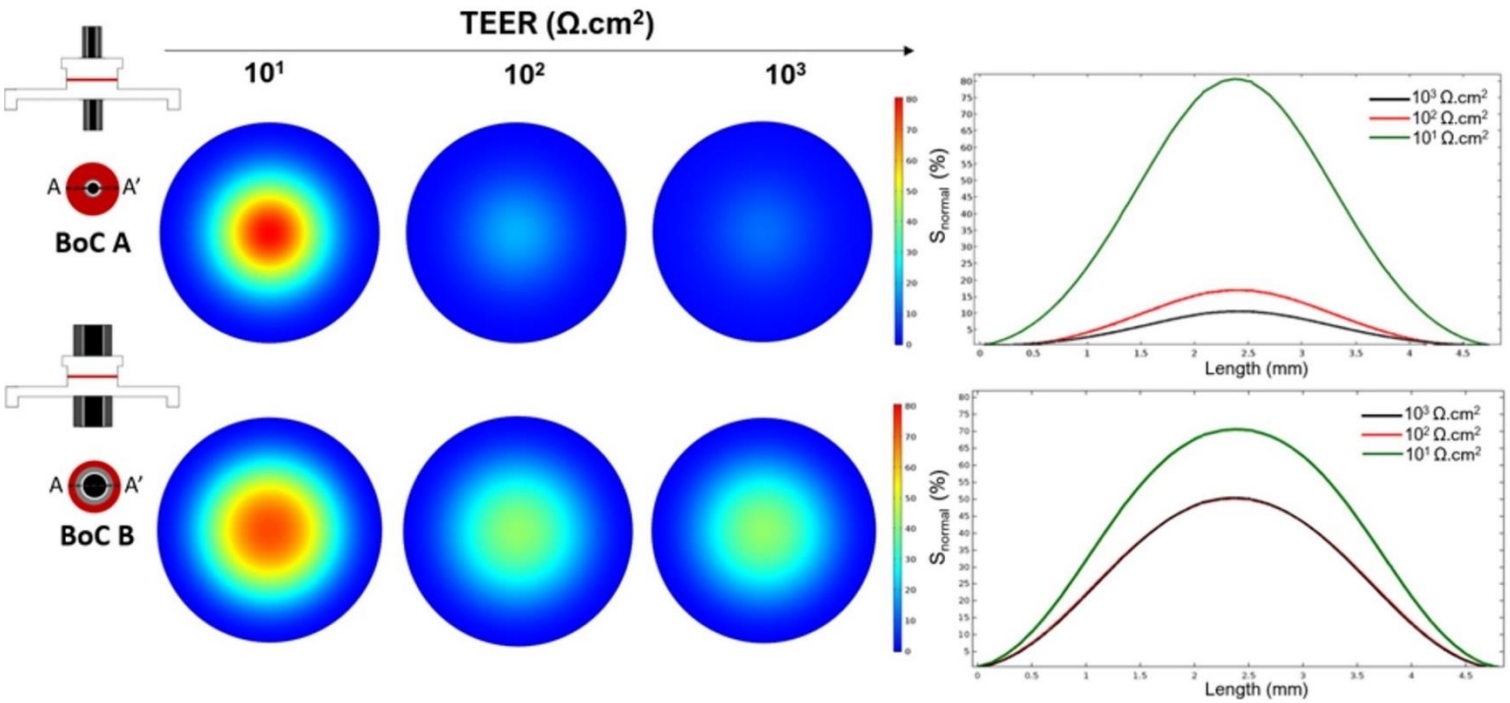

Figure 7. 4. Normalized sensitivity distribution (Snorm) including the planar sensitivity distribution along the cell barrier surface (rainbow color map) in the x-y plane and sensitivity distribution along the cell barrier though the axis (lines AA') shown in the scheme of the model at the left, when TEER is measured for the BoC device with concentric electrodes occupying 15% total area (BoC A) and occupying 65% total area (BoC B) and when TEER is measured. A Snorm value of 0% represents the zone of lower sensitivity

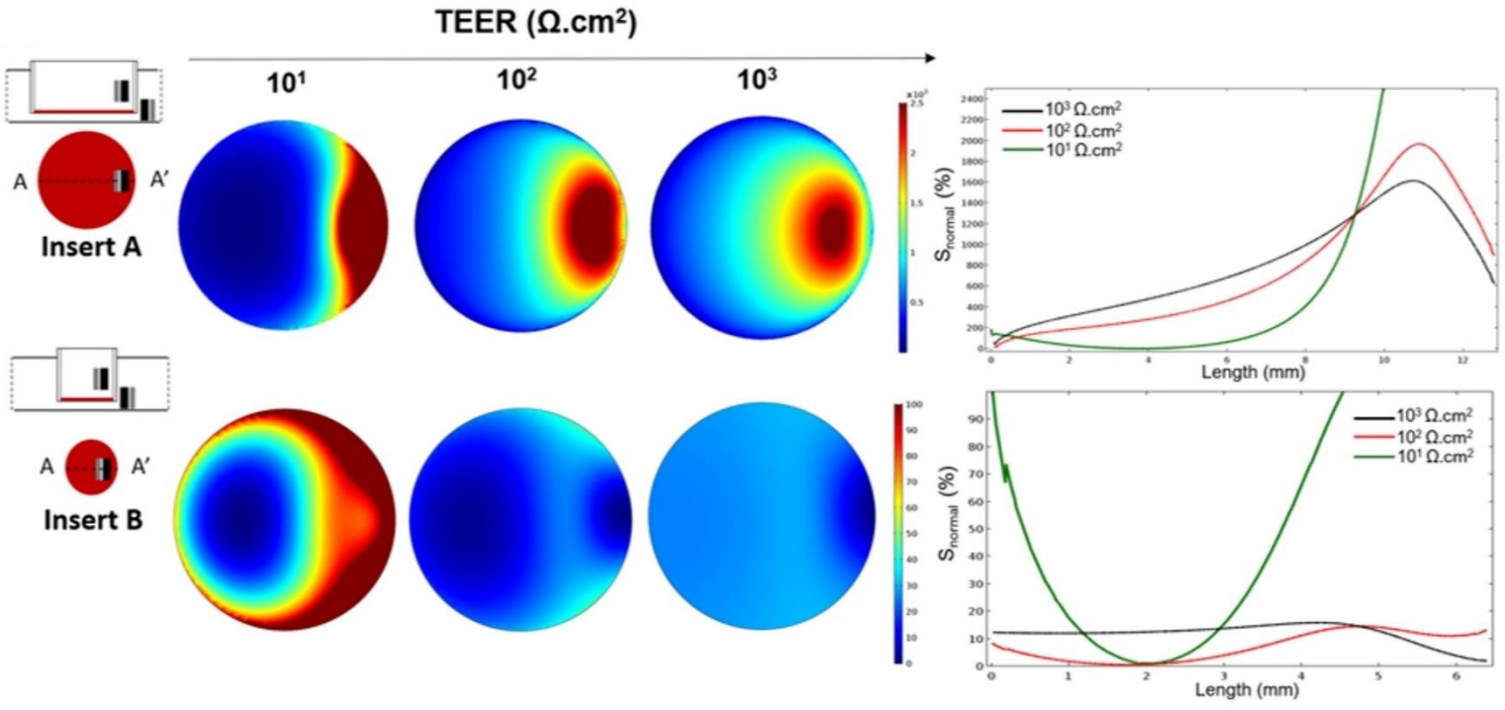

Figure 7. 5. Normalized sensitivity distribution (S_{norm}) including the planar sensitivity distribution along the cell barrier surface (rainbow color map) in the x-y plane and sensitivity distribution along the cell barrier though the axis (lines AA') shown in the scheme of the model at the left, when TEER is measured using chopstick electrodes in a insert culture insert with 12 mm diameter (Insert A) and 6.5 mm diameter (Insert B). Results are presented for different TEERS (10^1 -10^3 Ω.cm^2). A S_{norm} value of 0% represents the zone of lower sensitivity. Note that axis have different scales.

Another feature that has an impact on the sensitivity is the geometry and dimensions of the chambers. The sensitivity field in the Insert model is less uniform as its diameter increases, because larger inserts have zones further away from the chopstick electrodes that contribute little to the measurement (**Figure 7. 5**). For example, for the model Insert A and TEER values between 10^1 and 10^3 Ω cm^2, the sensitivity field below the electrodes contribute 10^3 % more to the measured resistance compared to the regions further away from the electrodes. Thus, resistance measurements performed with this configuration are only representative of small zone of the total culture area, revealing an error when multiplying the measured values by the total area. The most uniform sensitivity distribution was found for the Insert B model when measuring a tissue in the range of 10^3 Ω cm^2, with maximum sensitivity deviations of 15%. For the calibration chamber, the sensitivity distribution is less homogenous due to the narrowness of the chamber obstructing the electrical current to flow through the cell barrier in areas away from the electrodes (**Figure C. 4**).

7.4.2 Barrier-on-chip with integrated sensors: design and operation

The fabricated BoC consists of two polycarbonate layers that firmly press the central PDMS layer containing a 200 μm thick porous scaffold through magnetic latching or by using screws. Screws were used for long-term studies (tissue formation) and magnetic latching for shorter experiments (irritant exposure). The fabrication of the device was completely cleanroom-free and excluded the use of plasma activation. The BoC correctly sealed the tissue between the basal and apical sides with no signs of fluid leakage. Two isolated chambers were obtained, compatible with the establishment of ALI or liquid-liquid interface. Also, since the basal and apical chambers were electrically isolated from one another, TEER measurements could be successfully performed. For this, electrodes were inserted on both chambers and fixed with PDMS, securing the position of the electrodes, therefore eliminating measurement errors due to variation in electrode placement, which can occur when inserting wires manually to the in/outlets.

Geometrical dimensions of the fabricated BoC slightly differed from those in model BoC A (**Figure 7. 1.a**) and resulted in an asymmetric placement of the cell

culture insert between the electrodes. The sensitivity distribution for this electrode configuration were calculated as in the previous simulation study (**Figure C. 5**). The asymmetric placement of the cell culture resulted in a sensitivity approximately 20% higher at the centre when comparing with the periphery.

The electrode system incorporated in the BoC was compared to the conventional chopstick electrodes. For this, a calibration chamber was designed and fabricated using precision milling. This calibration chamber could accommodate the insert layer from the BoC and was compatible with the use of chopstick electrodes to perform TEER measurements. Each measurement was performed during 10 minutes and the variation during this period was recorded. The TEER data obtained with the two devices showed a correlation slope of approximately 0.86 (**Figure C. 6**). The values from the chopstick system were lower than the values obtained from the electrodes incorporated in BoC. However, the two systems presented a linear correlation. Compared with the BoC electrodes, measurements done by the chopstick electrodes, resulted in significant variability, mainly due to gesture errors using these electrodes. The electrode position could not be defined precisely and this caused the fluctuations. TEER values obtained using chopstick electrodes presented high variability during the 10-minute period reaching 37% variability in the TEER reading. This was also probably due to an incorrect immersion of the chopsticks using the calibration chamber. TEER measurements obtained using the electrodes integrated in BoC device were very stable and presented a maximum deviation of 5% the TEER value for each measurement.

7.4.3 Reconstructed skin-on-a-chip recapitulating in vivo skin

A fully human dermis was developed off chip by seeding HDFns on a porous and inert scaffold. For 12 days, these cells were stimulated to produce extracellular-derived matrix (ECM) components which built up and accumulated inside the scaffold. The resultant structure can be seen in **Figure 7. 6** (top left), with a homogeneous distribution of HDFns and fibroblast-derived matrix deposited all over the scaffold.

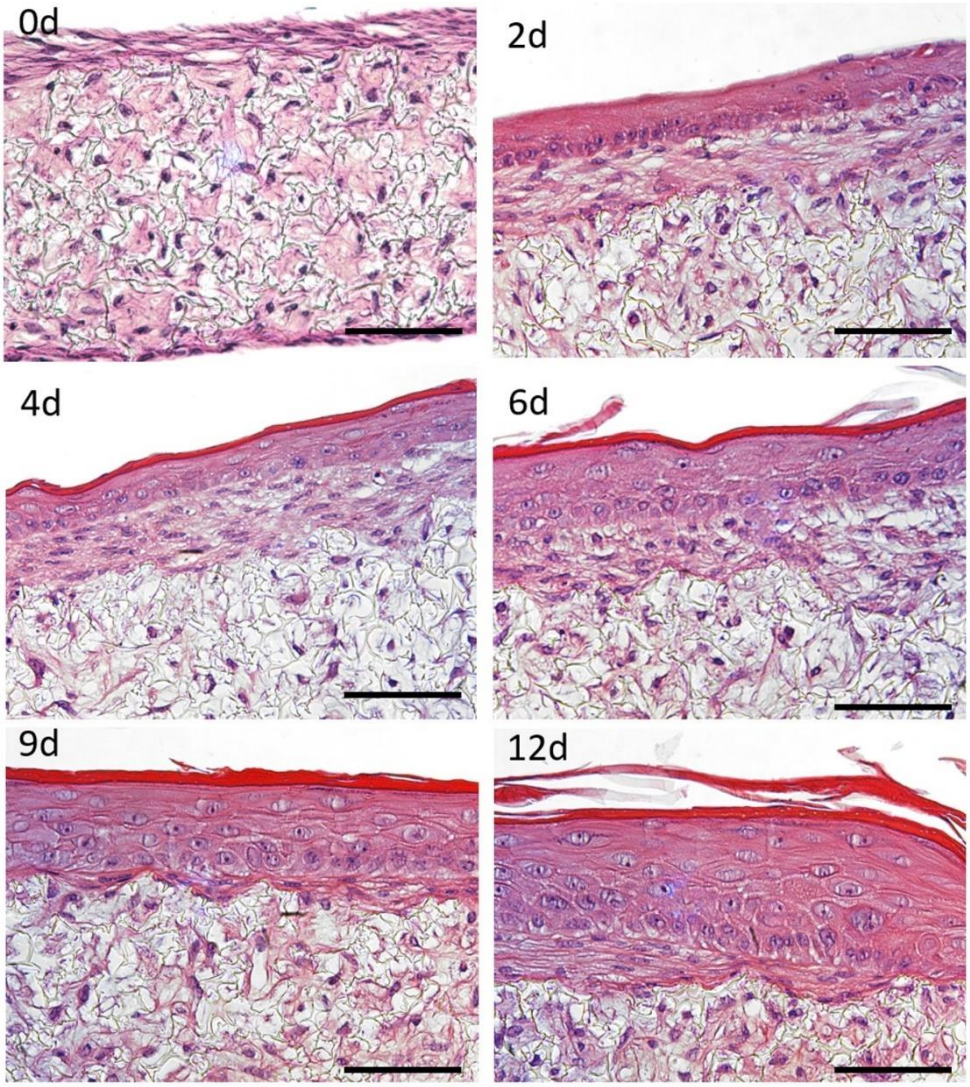

Figure 7. 6. Representative images of haematoxylin and eosin (H&E) stained histological cross sections of a full thickness skin model (FTSm) cultured for different times (0, 2, 4, 6, 9 and 12 days) at the air-liquid interface (ALI). Primary human epidermal keratinocytes isolated from neonatal foreskin (HEKns) were seeded on top of a dermis cultured for 12 days and maintained at ALI for up to 12 days to promote epidermal differentiation. Scale bars: 100 μm.

After maturation, the generated dermis was inserted into the BoC and a FTSm was developed during 12 days. For this, HEKns were seeded on top of the dermis and, after 2 days under submerged conditions, medium was perfused via

basal chamber. The scaffold structure allowed passive diffusion of fresh nutrients to the basal layer of cells and waste products from the cells. Nutrient-depleted medium was pumped out of the chamber via the outlet. The apical surface of FTSm was exposed to ambient air to stimulate differentiation into a stratified layer at the ALI.

FTSm structure was monitored over time and histological cross sections were analysed employing H&E staining to demonstrate the capability of FTSm to reflect the human skin anatomy (**Figure 7. 6**). In the early culture phase, HEKns formed a continuous layer on top of the dermis (**Figure 7. 6** top right). After 4 to 6 days of culture at the ALI, cells in the basal layer began to develop a cubic morphology and HEKns appeared to flatten in higher cell layers. Furthermore, a single cell layer with granula and the *stratum corneum* was detectable (**Figure 7. *6*** middle). In the late culture phase, from 9 to 12 days, the epidermal differentiation was complete and the thickness of the viable cell layers and the thickness of the *stratum corneum* increased (**Figure 7. 6** bottom). After 12 days of culture, FTSm displayed a native human skin-like morphology, including a well-organized, orthokeratinized epidermis over a fibroblast-populated dermis. H&E staining reveals all layers of the epidermis: *stratum basale*, *stratum spinosum*, *stratum granulosum* and *stratum corneum*. Other histological features include desmosome junctions between keratinocytes and it is possible to distinguish keratohyalin granules in the granular layer.

7.4.4 Real time measurement of skin barrier formation

The integrity of the tissue barrier was evaluated by measuring TEER on-chip during 14 days of culture (**Figure 7. 7**). To measure the TEER of these cultures, ALI was interrupted and PBS was pumped into the apical chamber. This completed the electrical circuit between the electrodes integrated in the apical chamber and the electrodes integrated in the basal chamber. The TEER of the tissue was recorded continuously for 10 min to capture fluctuations in the measurement. PBS was then removed from the apical chamber and air was pumped to maintain the ALI.

Under submerged conditions, the TEER values varied between 66 and 106 $\Omega.cm^2$ for the different tissue batches. During epidermal differentiation at ALI, electric resistance increased significantly reaching 503 ± 150 $\Omega.cm^2$ after 4 days of

culture at ALI and 663 ± 133 Ω.cm² after 8 days of culture. At day 12, a mean value of 1050 ± 180 Ω.cm² was obtained, indicating the formation of a permeability barrier and multi-layered epithelia. For all the independent batches of FTSm, the TEER values remained approximately stable after 12 days at ALI. The shift of the electrical properties of the FTSm during the epidermal differentiation could be attributed to architectural changes of the tissue with the progressive formation of tight-junctions and *stratum corneum*. The integrated home-made electrode showed stable TEER monitoring, without significant variation during the 10-minute measurements.

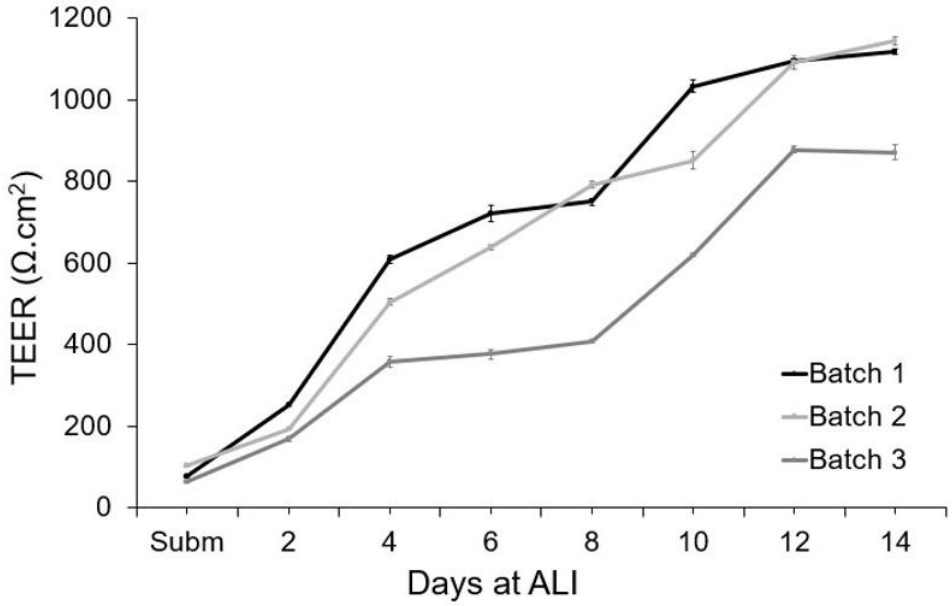

Figure 7. 7. TEER measurements performed with the concentric electrodes integrated in the BoC device and an EVOM system. Measurements were performed from day 0 (submerged conditions) to day 14 at ALI for 3 different batches of FTSm grown on-chip (N=3 and n=1). Data represents the average TEER values registered during a 10-minute measurement for each point. Data dispersion during this period is used to calculate the standard deviation. Error bars represent mean ± standard deviation.

7.4.5 Real time TEER measurement as a parameter to assess drug irritation

Figure 7. 8.a depicts the impact of chemical disruption of FTSm by exposing the upper layer to 0.2% SDS. TEER values were monitored continuously for 3 hours

and registered every 15 minutes. The batches of FTSm had mean TEER values of 1086 ± 239 Ω.cm² before exposure. Upon exposure of the tissue to the test substance SDS at t=0, the TEER values remained relatively stable for 15 minutes. After 0.25 h, the TEER value abruptly drops linearly, reaching a final value of 53 ± 66 Ω.cm² at t=3h. The designed system allows for continuous TEER observation during permeation studies whereas static experiments only permit singular measurements before and after the experiment.

In parallel to the TEER measurements, morphological analysis of the SDS-treated and control FTSm was undertaken. The tissue damage induced by the cytotoxic benchmark and the resultant disruption of the skin barrier was visualized by topical application of 0.2 % SDS for 0 (control), 1 and 3 hours followed by the observation of the passive diffusion of the hydrophilic fluorescent dye, lucifer yellow (**Figure 7. 8.b** left). When the dye was applied to an untreated skin model it was retained in the *stratum corneum* and no diffusion was observed in the epidermis or into the dermal layer, showing the integrity of the skin barrier for this molecule. For skin models treated with SDS, a total penetration of the dye could be seen (**Figure 7. 8.b** right). A complete lack of epidermal integrity was observed for skin models treated with 0.2% SDS for 3 hours and it was possible to observe tissue damage.

7.5 Discussion

7.5.1 Overview of the BoC design

A BoC device consists in two perpendicular chambers separated by a membrane, establishing two separate compartments (basal and apical). Here, we improve on the conventional BoC setup by designing a flexible platform with a modular architecture and incorporated sensors. Contrary to conventional systems, with the developed BoC it is possible to integrate scaffolds which are typically an order of magnitude thicker than membranes. The developed BoC does not require plasma bonding and it is cleanroom-free.

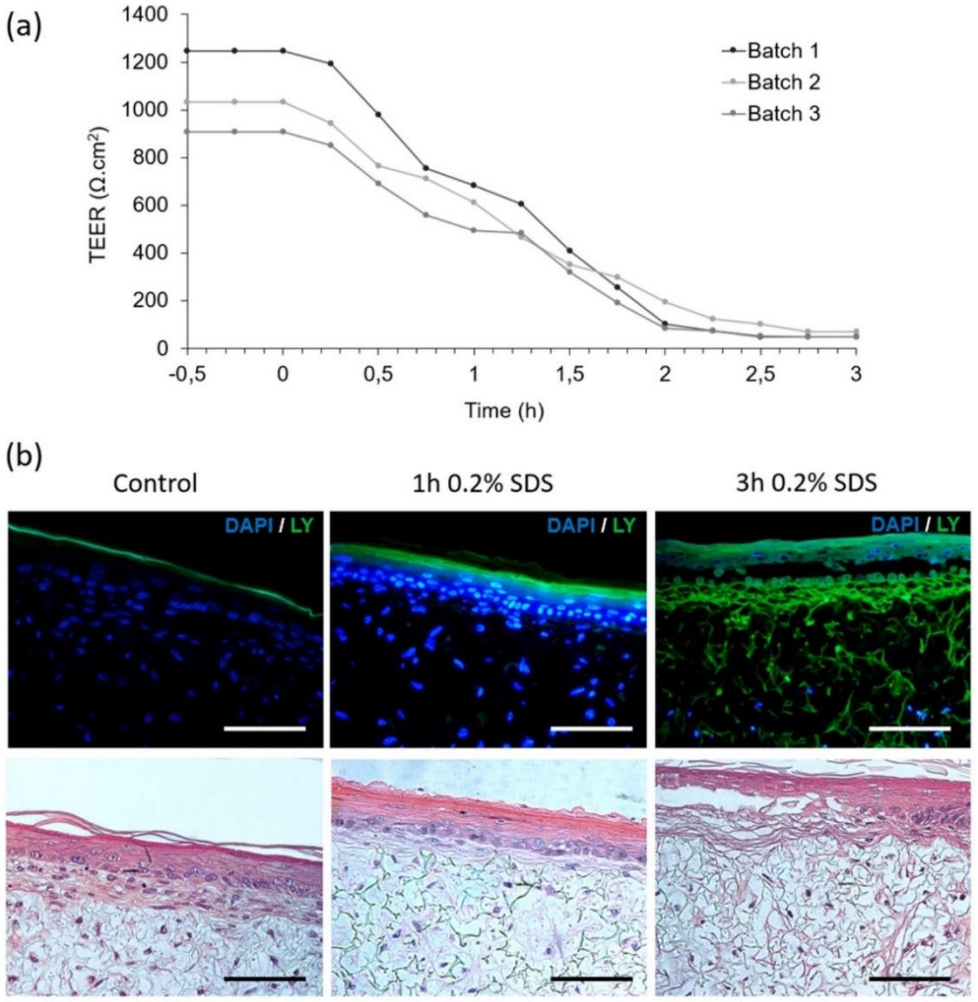

Figure 7. 8. Assessment of barrier damage from the exposure to a benchmark irritant (0.2% SDS) (a) TEER measurements performed with concentric electrodes integrated in the BoC device and an EVOM system. Measurements were performed over time before and after exposure to 0.2%SDS in PBS (at time=0) for 3 batches of FTSm grown for 14 days on chip. (b) Assessment of barrier resistance in FTSm: representative fluorescence (top) and H&E images (bottom) cultured for 14 days at ALI and exposed to 02% SDS for 0 (control), 1 and 3 hours, followed by the application of the green fluorescent dye lucifer yellow (LY, green) for 30 min to assess barrier integrity. Cell nuclei were stained by DAPI (blue). Scale bars: 100 μm.

The monitoring of tissue function inside the OoC devices has been challenging, frequently requiring removal of tissue from its original housing. Conventional analysis occurs exclusively at the endpoint, limiting the possibility of monitoring changes over time. In this work, we integrate low-cost commercial electrodes in the BoC device for real-time TEER measurement during tissue formation. To reduce the measurement errors by variations in electrode placement, we integrated immobilized TEER electrodes directly within the chip model and in close proximity to the tissue. This not only reduces the contribution of electrical resistance from the cell culture medium but also the signal noise generated by the electrode motion.

7.5.2 Theoretical analysis of the sensitivity distribution

Odijik *et al* pointed out the problems resulting from integrating electrodes in the conventional BoC configuration which result in a frequent overestimation of TEER values [26]. The group highlighted the importance of studying the geometry and placement of the electrodes to prevent measurement errors. In our work, the sensitivity field along the tissue barrier area was evaluated using FEA for different tetrapolar electrode configurations and chamber geometries. The relevance of using FEA to study the sensitivity of tetrapolar electrode systems was experimentally confirmed by several studies using phantoms [36-38]. Overall, the simulations show that the sensitivity is dependent on the electrode geometry, cell culture area, TEER value and chamber geometry. In particular, the use of chopstick electrodes results in non-uniform current distribution along the cell culture surface and non-uniform sensitivity distribution. This results in an error when normalizing by multiplying by the culture area and a consequent overestimation of the TEER. Experiments using the calibration chamber showed that TEER readings with handheld chopstick electrodes are highly dependent on the electrode positioning and the variances in depth and angle of immersion result in low precision. These factors result in measurement errors, especially for larger culture inserts and can explain why, for the same cell and tissue types, a wide range of TEER values have been reported in the literature. These findings are in accordance with previous studies [15,26].

When using custom designed and embedded TEER electrodes, it is particularly important to ensure a uniform sensitivity across the tissue. To study the impact of the size electrodes integrated in the BoC, we compared a larger electrode assembly (covering ~ 65% of total culture area) to a smaller electrode assembly (covering ~ 15% of total culture area). No advantages in sensitivity distribution were seen using the larger electrodes in the BoC with the chosen geometry for TEERs ≥ 10^2 Ω.cm^2. Taking this into account, the smaller electrode configuration was chosen for BoC fabrication. For TEER values ≥ 10^3 Ω.cm^2, a homogenous sensitivity distribution is achieved with a maximum deviation of 10% for a symmetric tissue placement between the electrodes and 20% for asymmetric tissue placement (experimental conditions).

7.5.3 Experimental analyses of the BoC with integrated electrodes

Various studies where electrodes are integrated on BoC devices highlight the importance of designing configurations compatible with the optical visualization of the cell culture. This is usually achieved by using complex manufacturing process [39, 40]. Although optical visualization can be useful for monitoring 2D cell cultures, its relevance for in vivo-like 3D tissues grown on membranes or scaffolds is very limited. In this study we integrate TEER electrodes that cover part of the cell culture area. Although this affects chamber visualization it is still possible to detect trapped bubbles, contaminations and other relevant findings. Furthermore, the modular chip architecture using magnets/screws, makes it possible to open the device and remove the cell culture insert for further testing and imaging techniques.

The designed BoC system was successfully fabricated and the custom-built electrodes based on the FEA were integrated on the system without disrupting the culture conditions. To test the potential of the fabricated BoC system to develop complex biological barrier tissues, a state-of-the-art FTSm was grown and monitored on-chip. ALI was successfully established on the BoC device, a key feature for epidermal differentiation. This feature is also ideal for establishing other complex models such as lung-on-a-chip since respiratory tract epithelial cells interact with both liquid and air *in vivo* [41].

To date, much progress has been made to develop biomimetic FTSm using OoC devices. However, none combines a functional OoC for 3D skin production with real-time TEER measurement. Ramadan and Ting performed TEER measurements on-chip to study interactions between HEKns and monocytes, however, their system was only used for 2D cell culture with perfusion [42]. Alexander *et al* modified an automated intelligent mobile lab for in vitro diagnostics (IMOLA-IVD) with integrated TEER sensors from Cellasys to suit a reconstructed epidermis model [43]. However, the skin model was not developed on-chip. Our device could provide a reliable, low-cost platform for the formation of complex biological barriers such as FTSms and for the real-time, non-destructive monitoring of its function.

7.5.4 Real-time TEER measurement for evaluation of topical irritants

TEER analysis was used to evaluate the stage of skin differentiation and the impact of a topical irritant. Polarized keratinocytes begin a complex differentiation process from day 0 under submerged conditions until day 12 at ALI, when a totally differentiated structure is already present. The increasing TEER levels with time during FTSm formation reflect the overall ion barrier of the stratum corneum and tight junction formation which regulate the movement of ions across the paracellular pathway. The FTSm reached values of 1050 ± 180 $\Omega.cm^2$ which are comparable to the values obtained in previous studies for similar models [44-46].

In addition to monitoring epidermal differentiation, TEER measurements have the potential to be employed as a real-time non-destructive analysis tool in the context of drug testing. In fact, TEER analysis is now used as a testing parameter of the Organization for Economic Co-operation and Development (OECD) test guidelines (TG) 430 in order to classify ingredients for their capacity to modify the skin barrier (skin corrosivity in rat skin) [47]. To test the applicability of the developed device as a complement for skin toxicity testing, we performed TEER measurements while exposing the skin to a benchmark irritant (SDS) for 3 hours. The disruption of barrier function was monitored in real-time and resulted in a decrease in TEER values. The impact of the irritant on the skin barrier was also shown by the penetration of the aqueous-soluble lucifer yellow dye. These

experiments show the potential of the developed BoC with integrated sensors for on-chip assessment of tissue barrier integrity in the context of drug testing. In contrast to conventional testing procedures, TEER measurements allows real-time monitoring, comparison of individual tissues before and after treatment and can be combined with other standard endpoint assays.

7.6 Conclusions

In this work, we presented a low-cost BoC with a modular architecture and integrated electrodes for real-time, non-destructive TEER measurements. The integrated tetrapolar electrode configuration resulted in a more homogenous sensitivity distribution along the culture area when compared with conventional chopstick systems. Furthermore, its positioning reduced the contribution of the electrical resistance from the cell culture medium and the signal noise generated by the electrode motion. A state-of-the-art FTSm was developed inside the BoC by providing a dynamic microenvironment and by correctly establishing an ALI. TEER measurements were performed in real-time to monitor the tissue development and its increase reflected tight junction formation and *stratum corneum* accumulation. Further, our results suggests that the BoC platform incorporating embedded TEER sensors present the opportunity of conducting drug testing directly on the platform, with key diagnostic parameters being monitored in real-time. In particular, TEER measurements can be useful to monitor the effect of irritants on biological barriers. Given the flexibility of the platform, additional cell types could be added to the FTSm and other epithelial tissues could be reconstructed and monitored. This advanced BoC system modelling complex biological barrier tissues (physiological and pathological states) present the potential to revolutionize pharmaceutical, toxicological and cosmetic applications.

7.7 References

[1] Yeste J, Illa X, Alvarez M, Villa R. Engineering and monitoring cellular barrier models. *J Biol Eng*. 2018;12:18. doi:10.1186/s13036-018-0108-5

[2] Montero-Vilchez T, Segura-Fernández-Nogueras MV, Pérez-Rodríguez I, et al. Skin Barrier Function in Psoriasis and Atopic Dermatitis: Transepidermal Water Loss and Temperature as Useful Tools to Assess Disease Severity. *J Clin Med*. 2021;10(2):359. doi:10.3390/jcm10020359

[3] Ortiz GG, Pacheco-Moisés FP, Macías-Islas MÁ, et al. Role of the blood-brain barrier in multiple sclerosis. *Arch Med Res*. 2014;45(8):687-697. doi:10.1016/j.arcmed.2014.11.013

[4] Cunha-Vaz J, Bernardes R, Lobo C. Blood-retinal barrier. *Eur J Ophthalmol*. 2011;21 Suppl 6:S3-S9. doi:10.5301/EJO.2010.604

[5] Maiuolo J, Gliozzi M, Musolino V, et al. The "Frail" Brain Blood Barrier in Neurodegenerative Diseases: Role of Early Disruption of Endothelial Cell-to-Cell Connections. *Int J Mol Sci*. 2018;19(9):2693. doi:10.3390/ijms19092693

[6] Bernardo-Castro S, Sousa JA, Brás A, et al. Pathophysiology of Blood-Brain Barrier Permeability Throughout the Different Stages of Ischemic Stroke and Its Implication on Hemorrhagic Transformation and Recovery. *Front Neurol*. 2020;11:594672. doi:10.3389/fneur.2020.594672

[7] Chung HH, Mireles M, Kwarta BJ, Gaborski TR. Use of porous membranes in tissue barrier and co-culture models. *Lab Chip*. 2018;18(12):1671-1689. doi:10.1039/c7lc01248a

[8] Yonker LM, Mou H, Chu KK, et al. Development of a Primary Human Co-Culture Model of Inflamed Airway Mucosa. *Sci Rep*. 2017;7(1):8182. doi:10.1038/s41598-017-08567-w

[9] Bluhmki T, Bitzer S, Gindele JA, et al. Development of a miniaturized 96-Transwell air-liquid interface human small airway epithelial model. *Sci Rep*. 2020;10(1):13022. doi:10.1038/s41598-020-69948-2

[10] Vernetti LA, Senutovitch N, Boltz R, et al. A human liver microphysiology platform for investigating physiology, drug safety, and disease models. *Exp Biol Med (Maywood)*. 2016;241(1):101-114. doi:10.1177/1535370215592121

[11] Yin F, Zhu Y, Zhang M, Yu H, Chen W, Qin J. A 3D human placenta-on-a-chip model to probe nanoparticle exposure at the placental barrier. *Toxicol In Vitro*. 2019;54:105-113. doi:10.1016/j.tiv.2018.08.014

[12] Stucki AO, Stucki JD, Hall SRR, Felder M, Mermoud Y, Schmid RA, Geiser T, Guenat OT. A lung-on-a-chip array with an integrated bio-inspired respiration mechanism. Lab Chip. 2015;15:1302–10. doi:10.1039/c4lc01252f.

[13] Graf BW, Boppart SA. Imaging and analysis of three-dimensional cell culture models. *Methods Mol Biol*. 2010;591:211-227. doi:10.1007/978-1-60761-404-3_13

[14] Srinivasan B, Kolli AR, Esch MB, Abaci HE, Shuler ML, Hickman JJ. TEER measurement techniques for in vitro barrier model systems. *J Lab Autom*. 2015;20(2):107-126. doi:10.1177/2211068214561025

[15] Yeste J, Illa X, Gutiérrez C, et al. Geometric correction factor for transepithelial electrical resistance measurements in transwell and microfluidic cell cultures. J. Phys. D Appl. Phys. 2016, 49, 375401. doi:10.1088/0022-3727/49/37/375401.

[16] Kim HJ, Huh D, Hamilton G, Ingber DE. Human gut-on-a-chip inhabited by microbial flora that experiences intestinal peristalsis-like motions and flow. *Lab Chip*. 2012;12(12):2165-2174. doi:10.1039/c2lc40074j

[17] Shin W, Wu A, Massidda MW, et al. A Robust Longitudinal Co-culture of Obligate Anaerobic Gut Microbiome With Human Intestinal Epithelium in an Anoxic-Oxic Interface-on-a-Chip. *Front Bioeng Biotechnol*. 2019;7:13. doi:10.3389/fbioe.2019.00013

[18] Sriram G, Alberti M, Dancik Y et al. Full-thickness human skin-on-chip with enhanced epidermal morphogenesis and barrier function. *Materials Today*. 2018;21(4):326-340. doi:10.1016/j.mattod.2017.11.002.

[19] Booth R, Kim H. Characterization of a microfluidic in vitro model of the blood-brain barrier (μBBB). *Lab Chip*. 2012;12(10):1784-1792. doi:10.1039/c2lc40094d

[20] Jeong S, Kim S, Buonocore J, et al. A Three-Dimensional Arrayed Microfluidic Blood-Brain Barrier Model With Integrated Electrical Sensor Array. *IEEE Trans Biomed Eng*. 2018;65(2):431-439. doi:10.1109/TBME.2017.2773463

[21] Henry OYF, Villenave R, Cronce MJ, Leineweber WD, Benz MA, Ingber DE. Organs-on-chips with integrated electrodes for trans-epithelial electrical resistance (TEER) measurements of human epithelial barrier function. *Lab Chip*. 2017;17(13):2264-2271. doi:10.1039/c7lc00155j

[22] Drieschner C, Könemann S, Renaud P, Schirmer K. Fish-gut-on-chip: development of a microfluidic bioreactor to study the role of the fish intestine in vitro. *Lab Chip*. 2019;19(19):3268-3276. doi:10.1039/c9lc00415g

[23] Arık YB, van der Helm MW, Odijk M, et al. Barriers-on-chips: Measurement of barrier function of tissues in organs-on-chips. *Biomicrofluidics*. 2018;12(4):042218. doi:10.1063/1.5023041

[24] Ramadan Q, Zourob M. Organ-on-a-chip engineering: Toward bridging the gap between lab and industry. *Biomicrofluidics*. 2020;14(4):041501. Published 2020 Jul 14. doi:10.1063/5.0011583

[25] Schneider S, Gruner D, Richter A, Loskill P. Membrane integration into PDMS-free microfluidic platforms for organ-on-chip and analytical chemistry applications. *Lab Chip*. 2021;21(10):1866-1885. doi:10.1039/d1lc00188d

[26] Odijk M, van der Meer AD, Levner D, et al. Measuring direct current trans-epithelial electrical resistance in organ-on-a-chip microsystems. *Lab Chip*. 2015;15(3):745-752. doi:10.1039/c4lc01219d

[27] Kwak BS, Jin SP, Kim SJ, Kim EJ, Chung JH, Sung JH. Microfluidic skin chip with vasculature for recapitulating the immune response of the skin tissue. *Biotechnol Bioeng*. 2020;117(6):1853-1863. doi:10.1002/bit.27320

[28] Kim JJ, Ellett F, Thomas CN, et al. A microscale, full-thickness, human skin on a chip assay simulating neutrophil responses to skin infection and antibiotic treatments. *Lab Chip*. 2019;19(18):3094-3103. doi:10.1039/c9lc00399a

[29] Mori N, Morimoto Y, Takeuchi S. Perfusable and stretchable 3D culture system for skin-equivalent. *Biofabrication*. 2018;11(1):011001. doi:10.1088/1758-5090/aaed12

[30] Wufuer M, Lee G, Hur W, et al. Skin-on-a-chip model simulating inflammation, edema and drug-based treatment. *Sci Rep*. 2016;6:37471. doi:10.1038/srep37471.

[31] Mori N, Morimoto Y, Takeuchi S. Skin integrated with perfusable vascular channels on a chip. *Biomaterials*. 2017;116:48-56. doi:10.1016/j.biomaterials.2016.11.031

[32] van der Helm MW, Henry OYF, Bein A, et al. Non-invasive sensing of transepithelial barrier function and tissue differentiation in organs-on-chips using impedance spectroscopy. *Lab Chip*. 2019;19(3):452-463. doi:10.1039/c8lc00129d.

[33] Grimnes S, Martinsen Ø. Sources of error in tetrapolar impedance measurements on biomaterials and other ionic conductors. *J Phys D: Appl Phys*. 2006;40:9-14. doi:10.1088/0022-3727/40/1/S02.

[34] Zoio P, Ventura S, Leite M, Oliva A. Pigmented full-thickness human skin model based on a fibroblast-derived matrix for long-term studies [published online ahead of print, 2021 Jun 19]. *Tissue Eng Part C Methods*. 2021;10.1089/ten.TEC.2021.0069. doi:10.1089/ten.TEC.2021.0069

[35] Capallere C, Plaza C, Meyrignac C, et al. Property characterization of reconstructed human epidermis equivalents, and performance as a skin irritation model. *Toxicol In Vitro*. 2018;53:45-56. doi:10.1016/j.tiv.2018.07.005

[36] Canali C, Mazzoni C, Larsen LB, et al. An impedance method for spatial sensing of 3D cell constructs--towards applications in tissue engineering. *Analyst*. 2015;140(17):6079-6088. doi:10.1039/c5an00987a.

[37] Rabbani KS. Focused Impedance Method: Basics and Applications. In: Simini F., Bertemes-Filho P, eds. *Bioimpedance in Biomedical Applications and Research.* Springer, Cham. 2018: 137-186. doi:10.1007/978-3-319-74388-2_9.

[38] Roy SK, Karal MAS, Kadir MA, Rabbani KS. A new six-electrode electrical impedance technique for probing deep organs in the human body. *Eur Biophys J*. 2019;48(8):711-719. doi:10.1007/s00249-019-01396-x

[39] Henry OYF, Villenave R, Cronce MJ, Leineweber WD, Benz MA, Ingber DE. Organs-on-chips with integrated electrodes for trans-epithelial electrical resistance (TEER) measurements of human epithelial barrier function. *Lab Chip*. 2017;17(13):2264-2271. doi:10.1039/c7lc00155j.

[40] Booth R, Noh S, Kim H. A multiple-channel, multiple-assay platform for characterization of full-range shear stress effects on vascular endothelial cells. *Lab Chip*. 2014;14(11):1880-1890. doi:10.1039/c3lc51304a.

[41] Saygili E, Yildiz-Ozturk E, Green MJ, Ghaemmaghami AM, Yesil-Celiktas O. Human lung-on-chips: Advanced systems for respiratory virus models and assessment of immune response. *Biomicrofluidics*. 2021;15(2):021501. doi:10.1063/5.0038924.

[42] Ramadan Q, Ting FC. In vitro micro-physiological immune-competent model of the human skin. *Lab Chip*. 2016;16(10):1899-1908. doi:10.1039/c6lc00229c.

[43] Alexander FA, Eggert S, Wiest J. Skin-on-a-Chip: Transepithelial Electrical Resistance and Extracellular Acidification Measurements through an Automated Air-Liquid Interface. *Genes (Basel)*. 2018;9(2):114. doi:10.3390/genes9020114.

[44] Kandárová H, Liebsch M, Schmidt E, et al. Assessment of the skin irritation potential of chemicals by using the SkinEthic reconstructed human epidermal model and the common skin irritation protocol evaluated in the ECVAM skin irritation validation study. Altern Lab Anim. 2006;34(4):393-406.

[45] Jung KM, Lee SH, Jang WH, et al. KeraSkin-VM: a novel reconstructed human epidermis model for skin irritation tests. Toxicol In Vitro. 2014;28(5):742-750.

[46] Akagi T, Nagura M, Hiura A, Kojima H, Akashi M. Construction of Three-Dimensional Dermo-Epidermal Skin Equivalents Using Cell Coating Technology and Their Utilization as Alternative Skin for Permeation Studies and Skin Irritation Tests. Tissue Eng Part A. 2017;23(11-12):481-490.

[47] OECD. Test No. 430: In Vitro Skin Corrosion: Transcutaneous Electrical Resistance Test *(TER), OECD Publishing, Paris*. 2004. doi: 10.1787/9789264071124-en.

Chapter 8

Conclusion and future work

8.1 Conclusions

8.1.1 Overview

Drug development is a slow and costly process affected by the high attrition rates in clinical trials. Although animal models have contributed to the development of numerous drugs and therapies and to expand our understanding of physiology and disease states, species-to-species variations hampers translation of *in vivo* results to human clinical trials. There is an increasing need for more predictive models of human organs to study healthy and disease conditions as well as for preclinical research, to promote identification of new drug targets and to reduce cost of drug development. This need prompted the development and expansion of the organ-on-a-chip (OoC) field. Taking advantage of the available fabrication techniques and biomaterials, this field provides new opportunities for engineering a controlled culture environment that resembles the *in vivo* microenvironment of an organ by tuning mechanical, biochemical and geometrical aspects. Since OoC platforms allow the use of human cells it is possible to overcome the species-to-species variations. Furthermore, the possibility of integrating electrodes for continuous monitoring tissue viability and function allows better control and automation.

One important application of OoC systems is modelling biological barriers (epithelia and endothelia). These barriers are crucial to main organ homeostasis and proper function of multiple organs, including skin, eye, brain and gut. Their disruption plays an integral role in the pathophysiology of many prevalent diseases. An understanding of barrier function is essential for studying mechanisms of diseases and for the development of new drugs and treatments. The work here described was aimed at developing an OoC system focused on the development of an *in vitro* skin barrier. However, as described in Chapter 7, the flexibility of the developed platform theoretically allows the development of different biological barriers. The development of an OoC platform for the generation of a full thickness skin model (FTSm) is a particularly interesting challenge due to 3D complexity of the skin tissue, with a multi-layered epidermal architecture on top of the dermal compartment filled with a combination of

multiple proteins and fibres, with a specific mechanical and biochemical microenvironment. Other interesting features of the skin culture is the need to establish a leakage-free air-liquid interface for correct tissue differentiation and for long culture times (at least 3 weeks) to produce full thickness skin.

In the introductory **Chapter 2**, the current available skin models, including the commercial products were discussed. It was possible to conclude that, although over the last few decades, techniques for culturing 3D skin cells have resulted in significant advancements in the field of skin tissue engineering, current available human skin models still lack complexity, present weaker barrier properties compared to *in vivo* human skin and lack vascularization which results in restricted nutrient supply and cell-cell interactions

In the introductory **Chapter 3**, a detailed review of the developed skin-on-a-chip (SoC) platforms was given. It was possible to conclude that the existent studies demonstrate the potential of SoC platforms for a multitude of applications ranging from disease modelling to drug testing. However, by comparing the results obtained from the different groups it is possible to observe inconsistencies regarding the effects of the OoC technology on the skin architecture and physiology. Some groups even report negative effects from the development of skin models inside the chip, with dynamic perfusion. This is the case of the work from Lee *et al* in which dynamic perfusion resulted in a negative effect on the *stratum corneum* homogeneity, resulting in a "leakier" barrier [1].

Chapter 4 to **Chapter 7** described the experimental methods and results generated during the thesis work with the goal of developing new advanced skin models for drug testing and disease modelling. **Chapter 4** and **Chapter 5** focused on the development of mechanical stable skin model, generated off chip, and the performance of preliminary tests to access its potential for drug testing. **Chapter 6** focused on the development of an organ-on-a-chip platform for the growth of a physiologically relevant skin model with dynamic perfusion. Finally, in **Chapter 7**, the focus was on the integration of sensors on the developed device for maintenance and real-time evaluation of biological barriers.

Particular conclusions and main achievements from the experimental work are listed in the following points:

In **Chapter 4** an innovative protocol to generate FTSm was described. By using an inert porous scaffold and by stimulating the dermal fibroblasts to produce extracellular matrix (also called fibroblast-derived matrix) it was possible to obtain a model without added exogenous animal-derived hydrogels. An epidermis with a well-organized and multi-layered structure was successfully produced on top of the dermal compartment. The potential of this model for achieving higher complexity was further demonstrated by successfully reproducing skin pigmentation. The use of the scaffold to recreate the dermal compartment resulted in a non-contracting and stable structure, allowing the possibility of integrating the model in OoC devices. Importantly, we showed that the innovative protocol could produce a skin model that could be maintained for at least 50 days. The expected impact of this protocol is the potential of reducing the dependence on animal models, especially for long-term studies of skin diseases and safety and efficacy assessment of novel drugs. Its longevity and robustness allow the experimental testing phase to be lengthened. The presence of active melanocytes at the dermal-epidermal junction makes this model the ideal platform to study skin pigmentation disorders.

In **Chapter 5,** the potential applications for the skin models developed using the protocol described in **Chapter 4** were investigated. Particular attention was given to the potential of these models to be used for studies of skin irritation, according to OECD performance standards and for transdermal permeation studies, using different standard drugs. It was shown that the model has a penetration profile for a benchmark irritant similar to accepted models, consistent with formation of an intact and robust skin barrier which conforms to OECD regulatory guidelines. The irritation and transdermal permeation tests showed the potential of the models to offer an alternative solution to the current commercial models. Moreover, it was shown that transepithelial electrical resistance (TEER) measurements can complement cell viability assays, resulting in a more comprehensive analysis of skin irritation and opening the possibility of identifying sub-irritative effects. The potential impact of this study is the availability of an open-source alternative to current commercial models for drug testing, to speed up the translation of new candidate therapeutics to the clinic and/or the

market. Furthermore, the open-source protocol could circumvent the limitations of the commercial models related to their lack of transparency.

In **Chapter 6**, the protocol developed on Chapter 4 was adapted for generation of skin inside a OoC. A platform with a modular architecture and a reversible sealing approach was designed and fabricated. This resulted in a flexible architecture and allowed the leakage-free integration of a porous scaffold. Further, it offered the advantages of performing downstream assays such as toxicity and permeation tests *in situ*. Interchangeable modules were developed to suit the specific requirements of an experiment. In this proposed platform, human fibroblasts are stimulated to produce their own extracellular matrix (ECM) which is deposited onto the scaffold structure, resulting in a fully human dermal compartment. Its non-contractile nature increased the stability and avoided the artifacts observed in conventional collagen-based structures. Perfusion during dermis generation replicated the effects of interstitial flow and increased ECM deposition. A state-of-the-art FTSm was developed inside the OoC by providing a dynamic microenvironment and by correctly establishing an air-liquid interface (ALI). Controlled perfusion and air flow resulted in a FTSm with *in vivo-like* characteristics, including a well-differentiated and organized epidermis with increased thickness and barrier function. In **Chapter 3**, the limitations of current SoC devices were shown, most of them using a 2D cell configuration or integrating contractile hydrogels. The proposed SoC is expected to offer a mechanically stable and physiologically relevant alternative to the existent models. Furthermore, the simplicity of the design and fabrication process makes the SoC device easily reproducible for a large array of research laboratories.

Lastly, in **Chapter 7**, the possible applications of the developed OoC were further described for multiple biological barriers [Barrier-on-chip (BoC)]. Electrodes were successfully integrated in the platform described in **Chapter 6** which allowed real-time evaluation of the biological barrier. Using finite element analysis (FEA), it was possible to show the limitations of common electrode configurations reported in literature for performing TEER measurements. It has been evidenced that TEER can be erroneously determined if the entire cell culture area does not contribute equally to the measurement as assumed in the common

formulas to calculate TEER. A tetrapolar configuration based on a symmetric concentric placement of electrodes at the apical and basal sides of the cell culture was proposed as an accurate measurement system. The system resulted in a more homogenous sensitivity distribution along the culture area when compared with conventional chopstick systems. TEER measurements were performed in real-time to monitor the skin development and its increase reflected tight junction formation and *stratum corneum* accumulation. Further, our results suggest that the BoC incorporating embedded TEER sensors presents the opportunity of conducting drug testing directly on the platform, with key diagnostic parameters being monitored in real-time. In particular, TEER measurements can be useful to monitor the effect of irritants on biological barriers. Given the flexibility of the platform, additional cell types could be added to the FTSm and other epithelial tissues could be reconstructed and monitored. This advanced BoC system modelling complex biological barrier tissues (physiological and pathological states) presents the potential to revolutionize pharmaceutical, toxicological and cosmetic applications.

Overall, three main goals were achieved during the thesis. One was the development of a new culture protocol for skin development with a microenvironment more representative of human skin, without the use of exogenous animal-derived components. The model by itself has the potential to offer an alternative to commercial approaches for topical drug testing, including assays requiring long-term skin cultivation. The second main achievement was the development of an OoC platform for formation of biological barriers, including a FTSm. The platform was used to produce an advanced skin model with increased differentiation and barrier properties. Finally, this work successfully showed that TEER is a promising tool for real-time evaluation of the tissue barrier function.

8.2 Future work

8.2.1 Optimizing chip performance and reproducibility

The impact of different operation conditions should be further investigated and fine-tuned towards the development of reproducible and standardized SoC models. During this work, only flow rates of 1.5– 2 μL/min were studied for both dermal and full thickness skin formation. In the literature, a vast range of flow rates from 1 μL/min to 125 μL/min have been used. It would be important to study the impact of higher flow rates and increased interstitial flow, using the same platform, for both dermal and full-thickness skin formation.

In **Chapter 6**, it was reported that tissues generated on the developed chip presented high variability, with a significant percentage presenting area of defective epidermal differentiation. This resulted in TEER values with increased variability compared to the controls. It was hypothesized that these defects could result from the presence of trapped air bubbles in the basal chamber and/or due to scaffold deformation, observed in a percentage of the experiments. Further chip optimizations should be performed by including bubble traps and pillars at the basal chamber to support the scaffold and prevent its deformations or collapse at the central part. Addition of phaseguide technology could help achieve control over filling of the fluidic structure and avoiding trapping air bubbles during the process [2]. This technique is based on the introduction of a line of material or change in geometry, resulting in an abrupt change in capillary pressure and inducing a controlled, step-wise advancement of the liquid (**Figure 8. 1.a**). **Figure 8. 1.b** shows the design of the OoC described in **Chapter 6** and **Chapter 7** with added phaseguides.

Furthermore, future steps should be employed to create automated monitoring systems, similar to the setup proposed by Alexander.Jr *et al* [3]. During skin formation, ALI is established by pumping air to the apical interface and medium at the basal interface. In **Chapter 7**, an OoC with integrated electrodes is described for real-time TEER measurement. To perform these measurements, the

medium was manually pumped through both the basal and apical chambers to bridge an electrical connection between top and bottom sensors. After removal of the medium from the apical chamber, the TEER becomes immeasurable again due to the removal of the electrical bridge. Overall, the process relied on manual procedures to pump and remove the liquid for the measurements. In the future, an automated fluidic system should be implemented to automatically monitor the TEER of the skin models over the culture period. The automated TEER monitoring and acquisition system should be capable of performing programmed test schema with frequent media change.

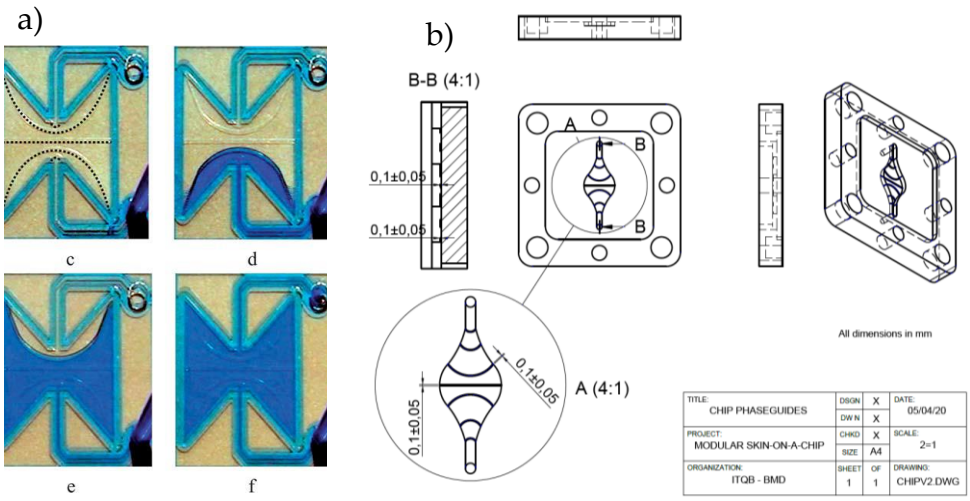

Figure 8. 1. Phaseguide technology a) Filling of a chamber with a complex geometry, with added phaseguides (viualized by dashed lines in 1) results in the structure being completely filled with liquid [2]. b) technical drawings of the organ-on-a-chip described in Chapter 6 and Chapter 7 with added phaseguides.

8.2.2 Improving physiological relevance

In the SoC platform described in **Chapter 6** and **Chapter 7**, keratinocytes are used to reproduce the epidermis and fibroblasts are used to reproduce the dermal compartment. Although fibroblasts are the most abundant cells of the dermis, this compartment also hosts nerve and vascular networks, macrophages, mast cells, lymphocytes, adipocytes, Schwann cells, and stem cells [4]. It also includes blood

vessels, nerves, glands and hair follicles. Depending on the particular application, other components could be introduced in the model.

Endothelial cells could be easily introduced in the current model. After dermis generation and keratinocyte seeding, the cell culture layer can be easily flipped and endothelial cells seeded at the basal side, using the drug testing/ cell seeding module. As described in **Chapter 3,** Wufuer *et al* proposed a model consisting of 3 layers in which epidermal, dermal and endothelial components were culture [5]. The endothelial component was important to recreate inflammation and edema and to evaluate the efficacy of therapeutic drugs. The paracellular permeability of endothelial cells is controlled by protein complexes which act as a fluid permeability barrier. The increased permeability of endothelial cells can be a result of various pathological conditions or a result of skin irritation and produces erythema and edema [6]. By adding endothelial cells to the platform proposed in **Chapter 6** and **Chapter 7**, the study could expand the findings from Wufuer *et al* by providing a co-culture of 3 skin compartments with a 3D architecture and *in-vivo* like microenvironment. The TEER sensors would give real-time information regarding the endothelial permeability barrier.

The physiological relevance of the skin models could also be increased by adding immune components. The toxicity of a topically applied chemical can elicit adverse dermal allergenic/immunogenic responses [7]. Typically, skin sensitization mechanisms are tested using skin models. Thus, there is the need to establish alternative skin sensitization models incorporating human cells. The SoC platform proposed in this thesis offers a suitable experimental setup to generate an advanced immunocompetent model. The basal fluidic network system allows immune cells to circulate and simulate physiologically relevant cell-cell interactions in skin models [8]. Incorporation of multiple cells, including immune components, could be realized with the use of induced pluripotent stem cells (iPSCs) [9]. This model may also provide a more personalized or patient-specific approach to study diseases.

8.2.3 Melanoma-on-a-chip

Cutaneous melanoma is a potentially lethal cancer with increasing incidence worldwide [10]. Despite advances in the treatment of cutaneous melanoma, there is

still a high percentage of patients who do not respond or develop resistance to these treatments. The development of *in vitro* melanoma models mimicking the complexity of *in vivo* microenvironment could surpass the limitations of 2D cell culture and improve the translation from preclinical studies to human clinical trials. Currently, the main challenges in cancer research are the development of *in vivo*-like tumour microenvironment *in vitro* and the development of efficient methods for screening anticancer drugs [11]. Typically, cancer responses to biochemical and biomechanical stimuli are evaluated using static conditions, without including a model of blood flow. However, it has been shown that flow in a vascular network is crucial for evaluation of tumour activity and drug screening [12]. The OoC described in this thesis could be the ideal tool to model cancer and metastasis formation. In particular, melanoma cell lines could be added to the full thickness SoC with a fibroblast-derived matrix on the dermal compartment to generate a physiologically relevant melanoma-on-a-chip. The incorporation of fluidic flow, including interstitial flow and *in vivo*-like ECM is expected to offer physiological conditions where important cell-cell and cell-matrix interactions are recreated. The melanoma-on-a-chip could be used to screen new therapeutic agents.

8.2.4 Exploring other biological barriers

Finally, the described platform could be used in the future to recreate other biological barriers including the blood-brain barrier, blood-retinal barrier, endothelial barrier and lung tissue. The flexibility of the device allows introduction of scaffolds and membranes of different thicknesses and materials, tailored to the specific organ and applications. An understanding of barrier function is essential when studying the causes and mechanisms of disease as well as when developing novel drugs and treatments. For all the mentioned barriers, the integrated TEER sensors can give important information regarding barrier state. The platform could be also used to model the disruption and dysfunction of these barrier-forming tissues, which are an integral part of the pathophysiology of many disorders including multiple sclerosis, macular degeneration, neurodegenerative disorders and ischemic stroke.

8.2.5 References

[1] S. Lee, S. P. Jin, Y. K. Kim, G. Y. Sung, J. H. Chung, and J. H. Sung, "Construction of 3D multicellular microfluidic chip for an in vitro skin model," *Biomed. Microdevices*, vol. 19, no. 2, 2017.

[2] P. Vulto, S. Podszun, P. Meyer, C. Hermann, A. Manz, and G. A. Urban, "Phaseguides: A paradigm shift in microfluidic priming and emptying," *Lab Chip*, vol. 11, no. 9, pp. 1596–1602, 2011.

[3] F. A. Alexander, S. Eggert, and J. Wiest, "Skin-on-a-chip: Transepithelial electrical resistance and extracellular acidification measurements through an automated air-liquid interface," *Genes (Basel).*, vol. 9, no. 2, 2018.

[4] L. Valencia and J. L. Jorcano, "Skin-on-a-chip models : General overview and future perspectives Skin-on-a-chip models : General overview and future perspectives," vol. 030901, no. May, 2021.

[5] M. Wufuer *et al.*, "Skin-on-a-chip model simulating inflammation, edema and drug-based treatment," *Sci. Rep.*, vol. 6, no. October, pp. 1–12, 2016.

[6] T. Welss, D. A. Basketter, and K. R. Schröder, "In vitro skin irritation: facts and future. State of the art review of mechanisms and models," *Toxicol. Vitr.*, vol. 18, no. 3, pp. 231–243, 2004.

[7] D. Y. S. Chau, C. Johnson, S. Macneil, J. W. Haycock, and A. M. Ghaemmaghami, "The development of a 3D immunocompetent model of human skin," *Biofabrication*, vol. 5, no. 3, 2013.

[8] A. Pupovac, B. Senturk, C. Griffoni, K. Maniura-Weber, M. Rottmar, and S. L. McArthur, "Toward Immunocompetent 3D Skin Models," *Adv. Healthc. Mater.*, vol. 7, no. 12, pp. 1–11, 2018.

[9] L. J. van den Broek, L. I. J. C. Bergers, C. M. A. Reijnders, and S. Gibbs, "Progress and Future Prospectives in Skin-on-Chip Development with Emphasis on the use of Different Cell Types and Technical Challenges," *Stem Cell Rev. Reports*, vol. 13, no. 3, pp. 418–429, 2017.

[10] E. Erdei and S. M. Torres, "A new understanding in the epidemiology of melanoma," *Expert Rev. Anticancer Ther.*, vol. 10, no. 11, pp. 1811–1823, Nov. 2010.

[11] X. Liu *et al.*, "Tumor-on-a-chip: from bioinspired design to biomedical application," *Microsystems Nanoeng.*, vol. 7, no. 1, p. 50, 2021.

[12] Y. Nashimoto *et al.*, "Vascularized cancer on a chip: The effect of perfusion on growth and drug delivery of tumor spheroid," *Biomaterials*, vol. 229, p. 119547, 2020.

Appendix

Supplementary information, figures and tables

A Supplementary information Chapter 5

A.1 Franz cell adaptors

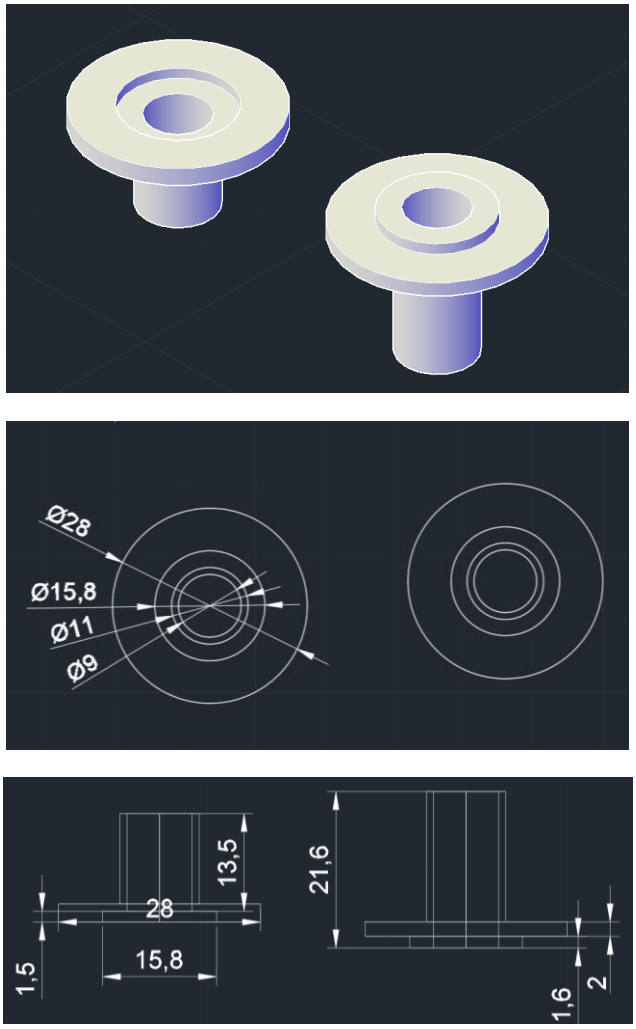

Figure A. 1. AutoCaD designs of the tailor-made full thickness skin model (FTSm) adapter to correctly seal and place the tissue in the centre of a Franz Cell. The Adapter consists of 2 parts and is designed to fit exactly in a 16 mm Franz Cell. The lower part has as a small cavity to take up the FTSm. The upper part tightly fixes the margin of the skin model while leaving open an exposure area of 9 mm in diameter. The design facilitates dermal absorption assays under standardized conditions. Dimensions are in mm. Different views: isometric, top and front.

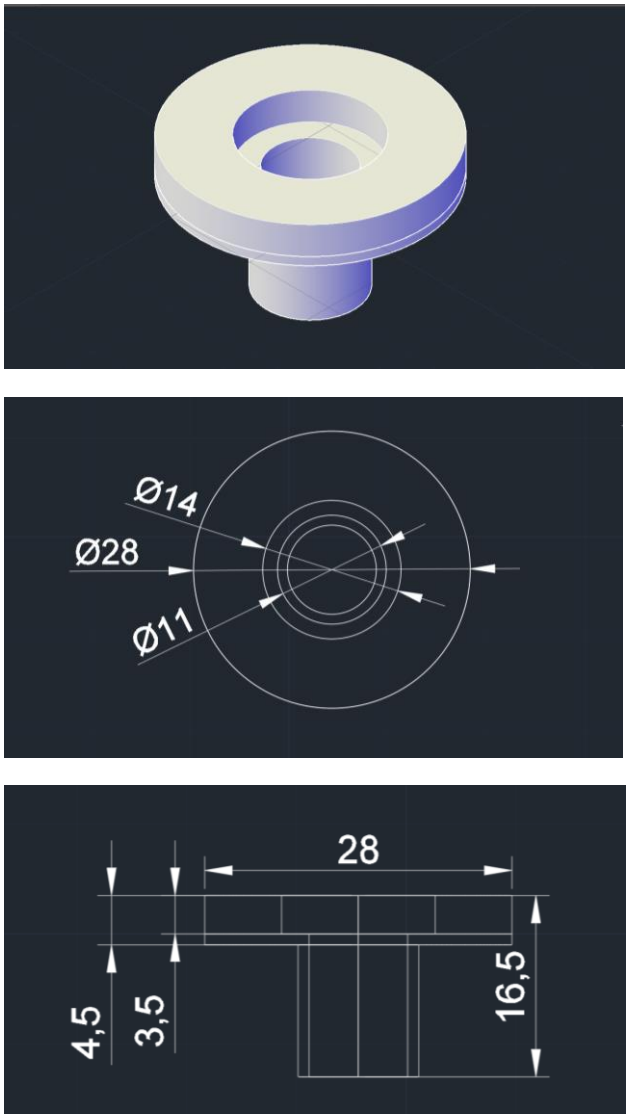

Figure A. 2. AutoCaD designs of the tailor-made adaptor for reconstructed skin models (RHEm) grown in Millicell® Standing cell culture inserts to correctly seal and place the tissue in the centre of a Franz Cell. The Adapter consists of 1 part and is designed to fit exactly in a 16 mm Franz Cell. The lower part has as a central cavity to take up the insert well. An O-ring is fitted of the cell culture insert. The Franz cell upper part tightly fixes the margin of the skin model while leaving open an exposure area of 9 mm in diameter. The design facilitates dermal absorption assays under standardized conditions. Dimensions are in mm. Different views: isometric, top and front.

A.2 Experimental setup for permeation assays

Figure A. 3. Experimental setup of the permeation testing using Franz cells. Top: Photograph of fabricated tailor-made full thickness skin model (FTSm) adapters using 3D printing. The FTSm is lower part has as a small cavity to take up the FTSm. The upper part tightly fixes the margin of the skin model while leaving open an exposure area of 9 mm in diameter. The design facilitates dermal absorption assays under standardized conditions. Dimensions are in mm. Different views: isometric, top and front.

A.3 Skin model defects

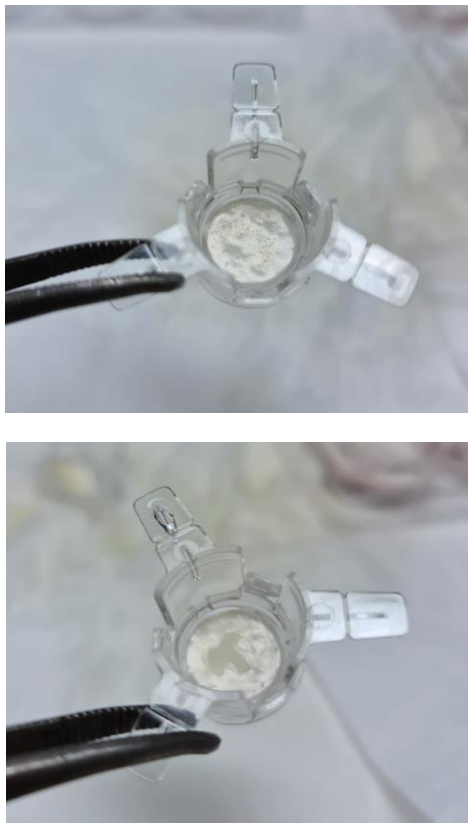

Figure A. 4. Alvetex inserts showing at the centre small defects (top) and an extreme defect (bottom). In this area no epidermis is present, resulting in a low TEER values compared to a non-defective model.

B Supplementary information Chapter 6

B.1 Technical drawings

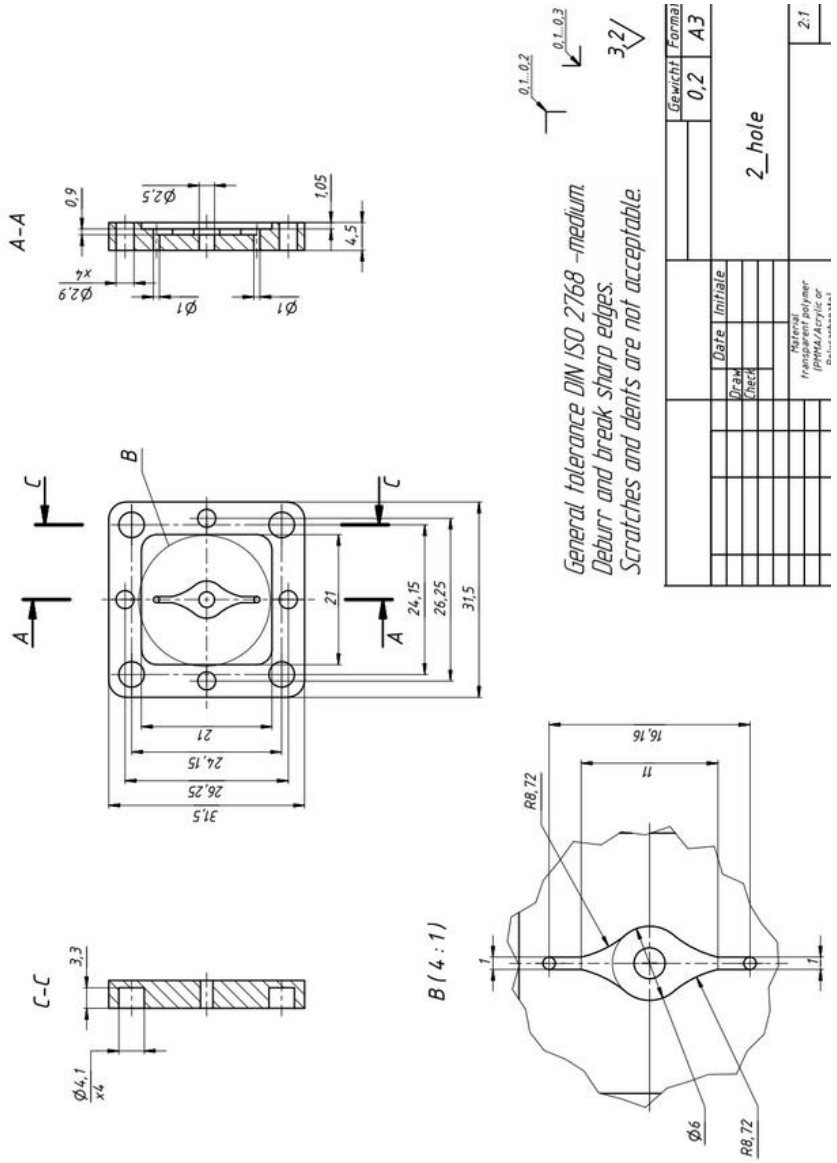

Figure B. 1. Technical drawing of the skin-on-a-chip perfusion module

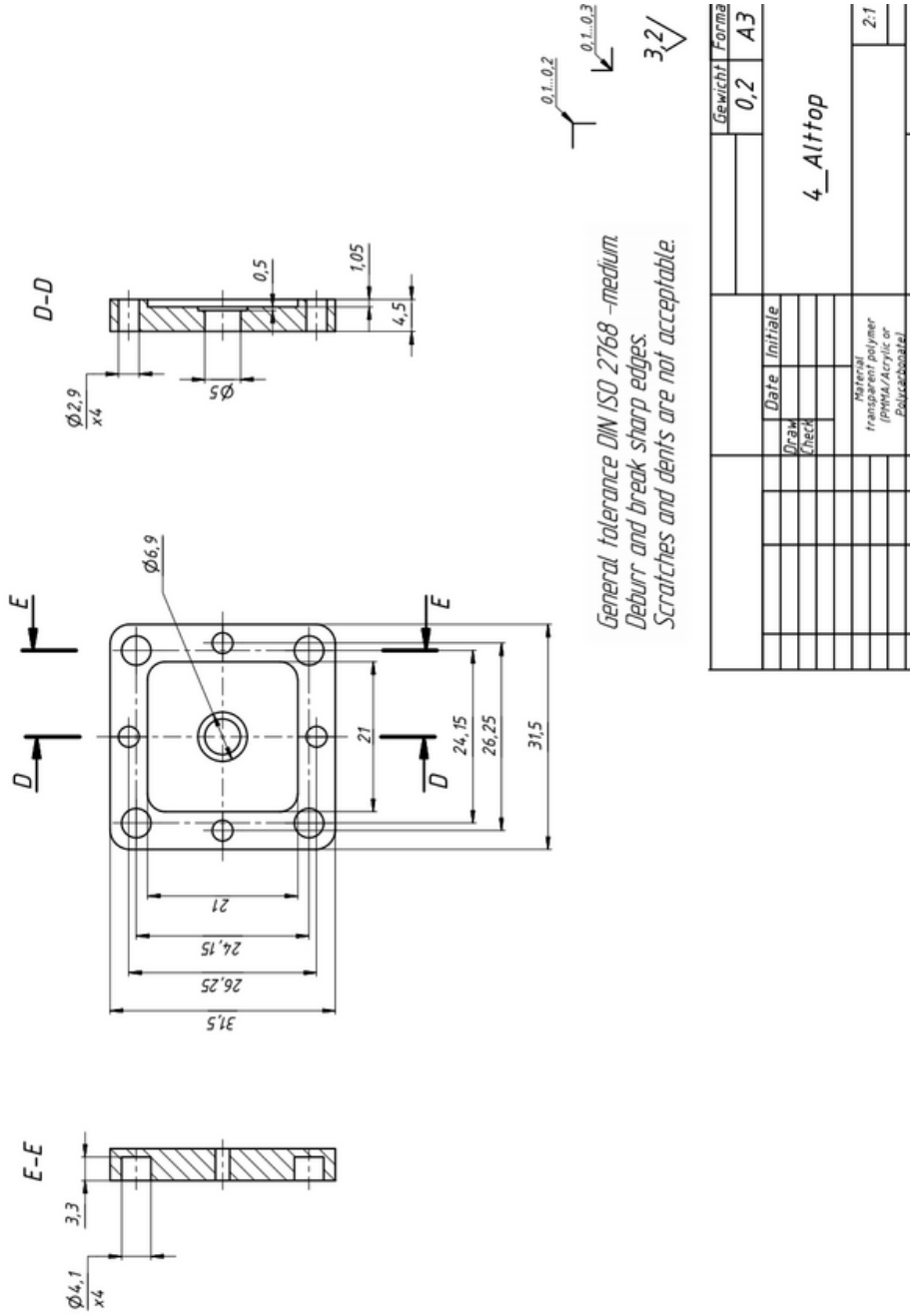

Figure B. 2. Technical drawing of the skin-on-a-chip cell seeding module

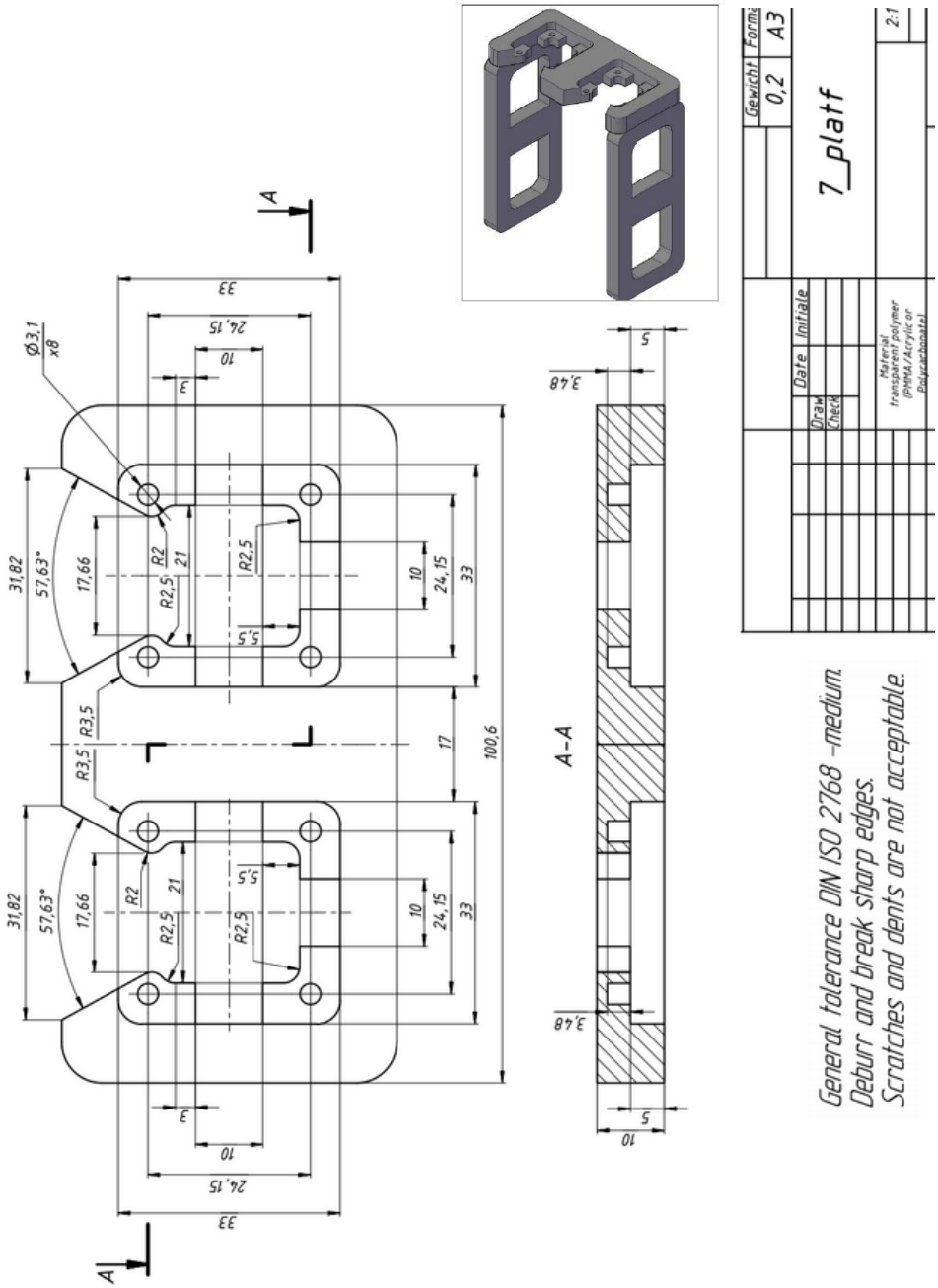

Figure B. 3. Technical drawing of the skin-on-a-chip support

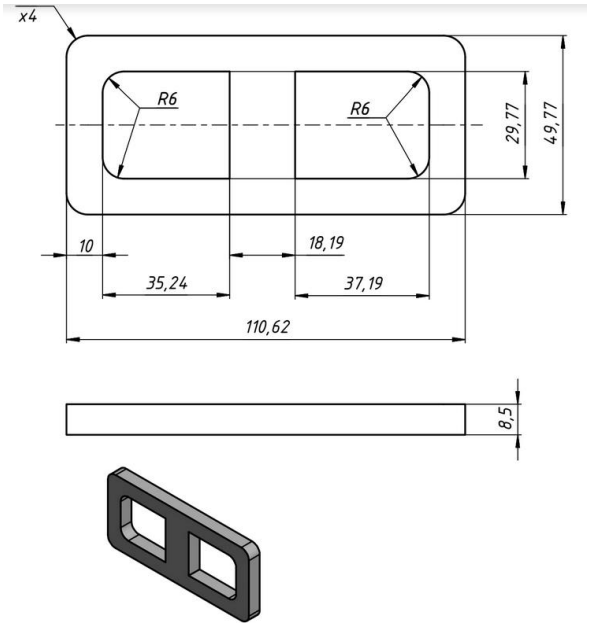

Figure B. 4**.** Technical drawing of the skin-on-a-chip support (leg)

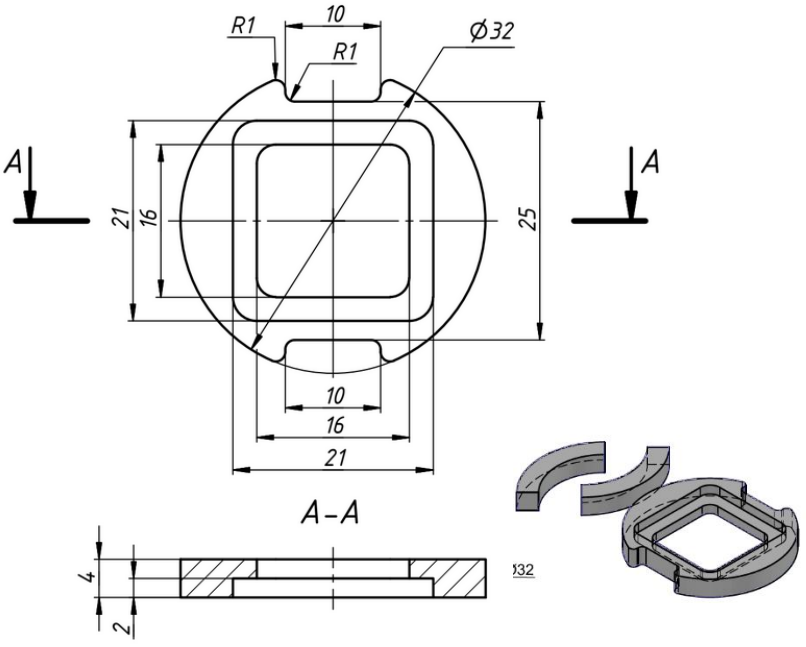

Figure B. 5. Technical drawing of the support for the controls

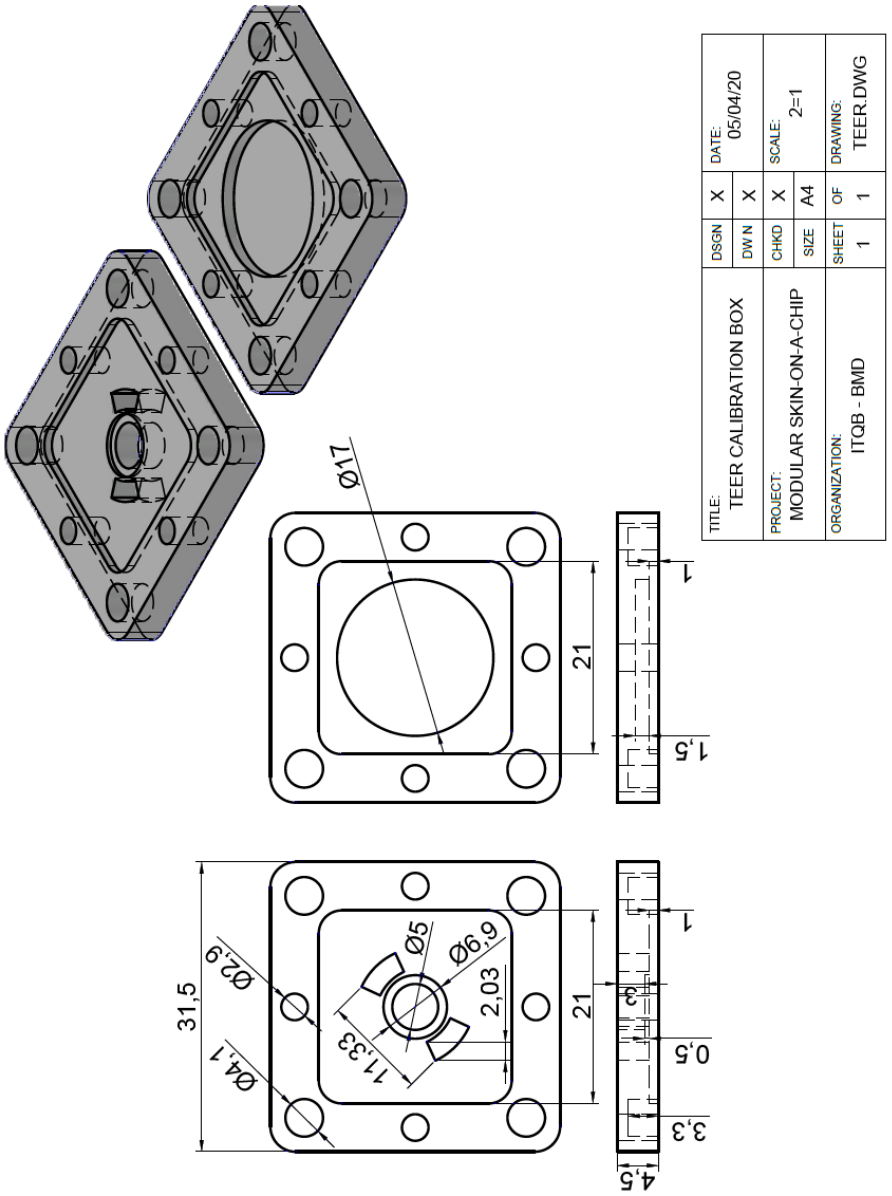

Figure B. 6. Technical drawing of the calibration chamber

B.2 Protocol for the fabrication of the SoC device (design with Easel and precision milling)

Note: This protocol was used to fabricate the preliminary SoC devices, using Fab Labs. A Fablab is a small-scale space equipped with an array of computer-controlled (CNC) tools and it is closely aligned with the do-it yourself (DIY) movement and open-source software. During the thesis first years it was possible to optimize the fabrication protocols and achieved considerable reproducibility. However, errors of ± 0.5 mm were observed even with the optimized protocols. In the final year, a high precision manufacturing service (Xometry) was used to fabricate the SoC device.

Materials: Software AutoCad, Adobe Ilustrator, Easel (CAD/CAM software from Inventables), PMMA/polycarbonate (5 mm thickness), bits (0.8 mm and 2 mm diameter), 3D carving machine (Inventables Carvey), wrenches (13 and 17 mm)

1. SoC designs made with software AutoCad need to be converted from .dxf (CAD file) to .svg (Vectorial Graphic) which can be done using Adobe Illustrator. Import files (.svf) to software Easel.

Caution: Care must be taken in regards to the design scale (scale by 100%; Scale:1; Unit(s):1; in millimeters) when importing to a different software.

2. Define the type of cut and its depth for each design element using Easel. To correct irregularities in the PMMA thickness, first cut a thickness of 0.5 mm using the mode "Fill". Then, create the internal chamber (Cut depth 1 mm, Mode "Fill"), magnet spaces (Cut depth 3.1 mm, Mode "Fill") and bolt spaces (Cut depth 5 mm, Mode "Fill");

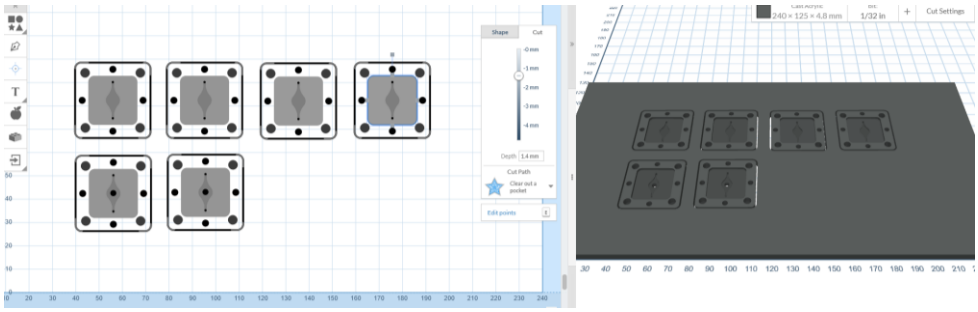

Software Easel (Inventables)

3. Design the perfusion path (Cut depth 1 + 1 mm, Mode "Fill") and, finally, the outside path (Cut depth 5 mm, Mode "Outline").

Caution: When cutting the outside path of the design there is a risk of the design breaking free and becoming damaged by the bit. Tabs should be added to act as small bridges between the cutout design and the stock material around it. Examples of tabs: 4 tabs, length 5 mm, height 0.2 mm;

4. Define cut settings (feed rate, plunge rate, depth per pass and fill method). The feed rate is the distance the bit moves through the project in one minute in inches per minute (IPM)). Depth per pass is how deeply the bit goes into the material every time it starts a new toolpath (in mm). Cut settings internal chamber using a 2.0 mm bit: 500 mm/min feed rate, 200 mm/min plunge rate and 0.3 mm depth per pass. Cut settings of the perfusion path using a 0.8 mm bit: 230 mm/min feed rate, 130 mm/min plunge rate and 0.2 mm depth per pass. Cut setting of the outside path using the 2 mm bit: 450 mm/min feed rate, 130 mm/min plunge rate and 0.3 mm depth per pass. For the fill method, the offset mode was used.

Caution: As a general rule, it is not recommend using a depth per pass that is greater than half the cutting diameter of the bit.

5. Obstructions and debris need to be removed from the working table of the Carvey machine. Position the PMMA sheet against the stops at the lower left-hand corner of the board, then use the "Smart clamp" (this clamp has a sensor which allows the CNC to automatically locate a zero point for the Z axis) with the appropriately sized bolts to loosely secure the material.

Caution: Note that the Smart Clamp has an L-shaped groove on its underside which must be mated with the similarly shaped protrusion on the base plate. When the material is thicker than the protrusion, take care to ensure that the clamp is properly aligned with the base plate.

CNC machine (Carvey, Inventables)

6. Choose appropriately sized clamps, bolts, and step-blocks to make sure that the material is strongly and evenly secured to the bed. To maximize clamping strength, always choose the shortest pieces of clamping hardware that will still allow for proper tool clearance. Insert the chosen bit in the nut and tighten it with the wrenches. If you want to replace it with a milling bit of the same shank diameter, simply slide the new bit into the collet and re-tighten the collet nut to secure.

B.3 Protocol for the assembly of the SoC device

Materials: Poly(dimethylsiloxane) (PDMS), fabricated PMMA/polycarbonate perfusion layers and insert layer molds, polypropylene (PP) mini female luer interfaces, neodymium magnets, UHU Max Repair extreme glue, Loctite surface activator, cyanoacrylate adhesive, PCR tape, Alvetex scaffold, polycarbonate membranes.

1. After fabricating the PMMA perfusion layers using precision milling, neodymium magnets (4x3 mm) are glued to the surfaces such that the apical and basal perfusion layers have opposite magnetic poles facing one another.

2. Mini female luer interfaces are glued to the surface at the inlets/outlets using a 6 mm diameter metal tube for alignment. First, the surface activator is applied to both surfaces (PMMA/polycarbonate and PP). After waiting 60 seconds for the activator to completely dry, the metal tube is placed in the mini female luer hole and the cyanoacrylate is applied only to the PP surface (use the glue

sparingly, approximately one drop). The parts are pressed together immediately and hold in place for 30 seconds or until bond sets. Remove the metal tube while pressing the luer interface down. Test the basal and apical perfusion layers using a syringe with a luer to mini-luer interface to make sure the inlets/outlets are not clogged with glue.

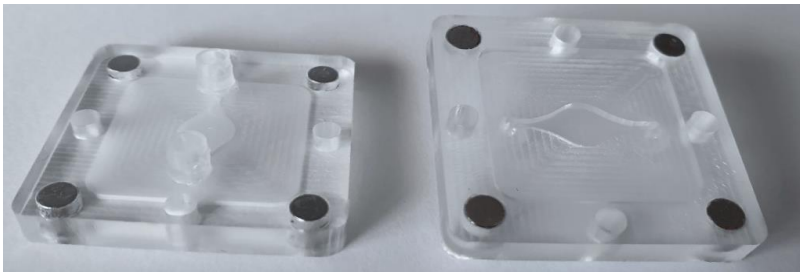

Apical and basal PMMA layers with inserted magnets and mini female luer interfaces

3. For PDMS layer fabrication the next steps are followed:

   i. PDMS poured into a disposable cup in a 10:1 weight ratio of monomer to curing agent;

   ii. Components vigorously mixed with a spatula until the mixture appears white due to the bubbles formed during mixing;

   iii. Prepolymer mixture is then introduced in a vacuum chamber and degassed until all the bubbles disappear (between 40-50 min);

   iv. Assemble the fabricated molds for the scaffold layer;

Molds for PDMS inserts

v. After degassing, the prepolymer is inserted onto the molds with a 1 ml syringe avoiding formation of additional bubbles. Close the acrylic mold;

vi. Introduce the mold in an oven at 60ºC for at least 2 hours to cure the PDMS (it is possible to leave it overnight)

vii. After curing the PDMS, the molds are extracted from the oven and allowed to cool down to room temperature for 5-10 min.

viii. Open the mold and carefully remove the PDMS layer with the help of a small spatula and scalpel. A scalpel is used to trace the periphery of the layers and remove excess PDMS.

4. Using a 6 mm diameter puncher, cut various circular membranes (Alvetex, polycarbonate or other membrane materials).

5. Using a 5 mm diameter puncher, punch holes in the PCR tape and cut it into a square that fits in a petri dish. Place the PCR tape at the bottom of a petri dish, making sure it is completely straight and pressed against the bottom.

Material needed to assemble the insert layer (PDMS + scaffold + PCR tape with thin layer of PDMS)

6. Using a 1ml syringe place 1.5 mL PDMS at the center of the petri dish. The goal is to obtain a thin layer of PDMS. Use a brush to spread the PDMS evenly over the surface. Place it the oven at 60ºC for 1h30.

7. With scissors cut the PCR tape covered with a PDMS thin film into squares of approximately 3x3 cm. Remove excess PDMS from the 5mm diameter hole using a puncher. Carefully assemble the scaffold layer (PDMS + 6 mm Alvetex/Polycarbonate + PCR tape with thin film).

Insert layer with PDMS layer + membrane/scaffold + PCR tape. Left: Insert layer with Alvetex. Right: insert layer with polycarbonate membranes

B.4 Mathematical modelling of the skin

The different layer of the skin can be considered porous materials. These materials consist of a solid structure (porous matrix) with voids (pores). The total size of the material is much bigger than the mean pore diameter and a detailed description, down to the resolution of every pore, is not feasible in most cases. A macroscopic approach must be used to model these structures by homogenization of the porous and fluid media into a single medium.

Two variables are important to characterize the porous material: the porosity (ε_p) and the permeability (k) in m². The porosity describes the ratio of void/pore volume to total volume and the permeability specifies the ability of a fluid to pass through it. Alternative hydraulic conductivity, K in m/s can be used.

$$\frac{k}{\mu} = \frac{K}{\rho g}$$

Where Darcy's model gives the transport model applicable for flow in the dermis. This model is widely used for calculating flow through interstices in a porous medium. It can be used to model low-velocity flows or media where the permeability and porosity are very small. In a porous medium, the global transport of momentum by shear stresses in the fluid is often negligible, because the pore walls impede the momentum transport to the fluid outside the individual pores. Darcy's law in combination with the continuity equation and equation of state for the pore fluid provide a complete mathematical model suitable for a wide variety of applications involving media flows, for which the pressure gradient is the major driving force.

Darcy's law describes fluid movement through interstices in a porous medium. Because the fluid loses considerable energy to frictional resistance within pores, flow velocities in porous media are very low. It states that the velocity field is determined by the pressure gradient, the fluid viscosity and the structure of the porous medium

$$\boldsymbol{u} = -\frac{k}{\mu}\nabla p \text{ or } \boldsymbol{u} = -\frac{K}{\rho g}\nabla p$$

where $\mathbf{u}$ is the Darcy's velocity in m/s, k is the permeability of the porous medium in m^2, u is the fluid's dynamic viscosity in Pa.s, and p is the pressure in Pa

Combining the Darcy's law with the continuity equation

$$\frac{\partial}{\partial t}(\rho\varepsilon_p) + \nabla \cdot (\rho \boldsymbol{u}) = \boldsymbol{Q_m}$$

Where p is the density of the fluid in kg/m^3, ε_p is the porosity and ε_p and $\boldsymbol{Q_m}$ is a mass source term. Porosity is defined as the fraction of the control volume that is occupied by pores. Thus, the porosity can vary from zero for pure solid regions to unit for domains of free flow.

For simulation of an open channel and an adjacent porous structure such as the case of the SoC device with the perfusion channels and integrated scaffold/dermal compartment, typically Darcy's law is incorporated adjacent to Navier-Stokes. However, this approach does not account for viscous effects arising from the free media flow, which may still be important in the region close to the free-porous structure. Depending on the pore size and its distribution and fluid properties, it can be an oversimplification to employ Darcy's law.

The Brinkman equations account for momentum transport by macroscopic viscous effects as well as pressure gradients stemming from microscopic shear effects inside each pore channel and can be considered an extension of Darcy's Law. The Brinkman equations describe fluids in porous media for which the momentum transport withing the fluid due to shear stresses is of importance. This mathematical model extends Darcy's Law to include a term that accounts for viscous transport in the momentum balance.

For an incompressible flow, the density stays constant in any fluid particle, which can be expressed as:

$$\frac{\partial}{\partial t}(\rho\varepsilon) + u \cdot \nabla\rho = 0$$

Equation S3.2 and equation S3.4 taken together can be simplified into the following form of the continuity equation

$$\rho\nabla \cdot \boldsymbol{u} = \boldsymbol{Q_m}$$

Q_m accounts for mass deposit and mass creation in domains, and the mass exchange is assumed to occur at zero velocity.

Flow in the free channel is described by the stationary, incompressible Navier-Stokes equations:

$$\rho(\boldsymbol{u} \cdot \nabla)\boldsymbol{u} = -\nabla \cdot [-p\boldsymbol{I} + \mu(\nabla \boldsymbol{u} + (\nabla \boldsymbol{u})^T)]$$

$$\nabla \cdot \boldsymbol{u} = 0$$

Where $\boldsymbol{u}$ refers to the velocity in the open channel in m/s. In the porous domain:

$$\frac{\mu}{k}\boldsymbol{u} = \nabla \cdot [-\rho\boldsymbol{I} + \frac{\mu}{\varepsilon_P}(\nabla \boldsymbol{u} + (\nabla \boldsymbol{u})^T)]$$

B.5 Experimental measurement of scaffold permeability

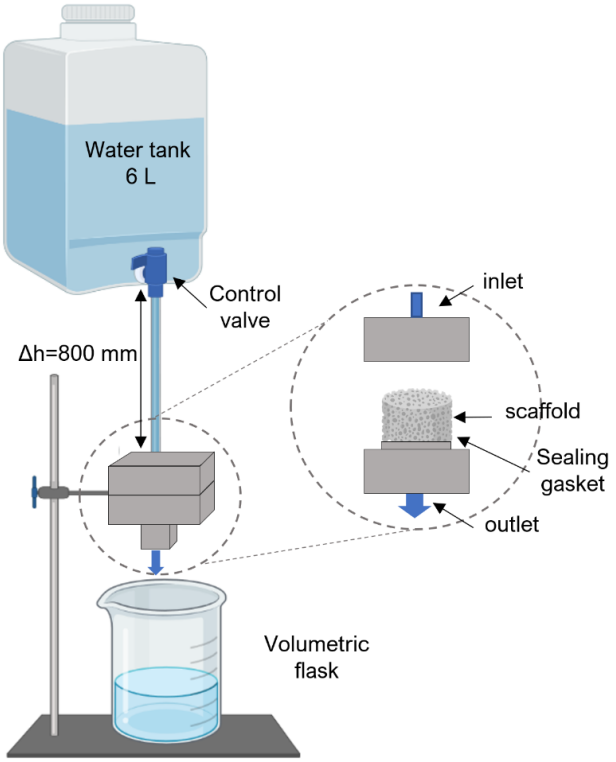

Figure B. 7. Setup used for experimentally measuring the permeability of the scaffold. The fluid holding tank contained a measured volume of 6 L. This large tank provided constant hydrostatic pressure, p, and was set at a height, Dh, of 800 mm above the sample. The hydrostatic pressure was calculated as follows: $P = \rho_w \Delta h g = 7833\ Pa = 0.07829\ atm$, where ρ_w is the density of water (1000 kg/m^3 at 25°C), g is the gravitational force (9.8 m/s) and h is the total height of the system in meters (0.8). In order to conduct each permeability test, the specimen was placed into the clamping device and the time required for 400 mL of fluid to pass into the graduated container was measured.

Darcy's law was used to calculate the experimentally determined intrinsic permeability values:

$$k = \frac{Q\mu\Delta x}{AP}$$

where Q is the volumetric fluid flow rate, μ is the dynamic viscosity of the fluid, Δx is the thickness of the porous medium and P is the applied pressure difference. The calculated values for permeability for the scaffold were k=2.676 darcy (2.641×10^{-12} m^2). The calculated $k=10^{-12}$ m^2 and porosity=90% corresponds to the scaffold at time t=0 on the cell seeding day. On the following days, the cells are stimulated to produce extracellular matrix which deposits onto the structure of the scaffold. This results in a gradual decrease in permeability values and pore size. The final values were obtained from the literature, for collagen gels. Since this is the main extracellular matrix being deposited on the scaffold, it is a good approximation. Values between $k=10^{-13}$ - 10^{-18} are reported in the literature for collagen gels.

B.6 Finite element analysis: Geometry and mesh

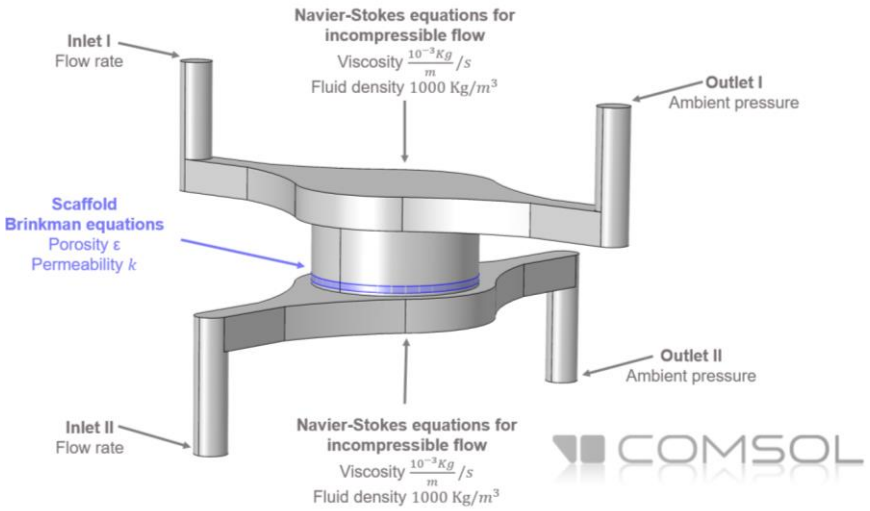

Figure B. 8. Depiction of the modelling geometry and domains for the SoC device with free flow domain where Navier-Stokes equations where applied and porous structure where Brinkman equations where applied.

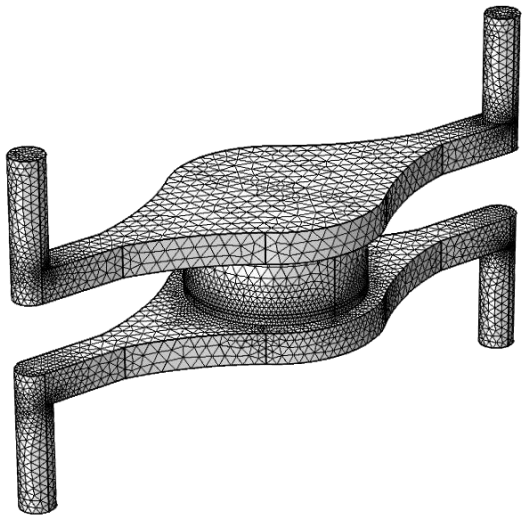

Figure B. 9. Mesh created using COMSOL: Maximum element size 0.411 mm, minimum element size 0.0775 mm, maximum element growth rate 1.12, curvature factor 0.5 and resolution of narrow 0.8.

B.7 Protocol for the development of a dermis-on-a-chip

1st part: Scaffold pretreatment, trypsinization, seeding

This protocol to produce dermis-on-a-chip is performed after fibroblast expansion;

Material: Sterilized PMDS inserts, 2x 6-well plates, 70% ethanol, supplemented IMDM medium, PBS, Trypsin/accutase, 50 mL falcons, eppendorf, trypan blue, pipettes.

1) Before starting the experiment, PDMS insert layers are sterilized using UVs 10 minutes each side. PMMA supports (or aluminum grids) are also sterilized, first by submerging in 70% ethanol for 10s and then using UVs for 10 minutes (each side);

2) Scaffold pretreatment:

   i. Prepare two 6-well plates for the scaffold pretreatment. One 6-well plate with 3x wells with 70% ethanol, 3x with PBS and the other plate with one well filled with fibroblast medium for each insert layer;

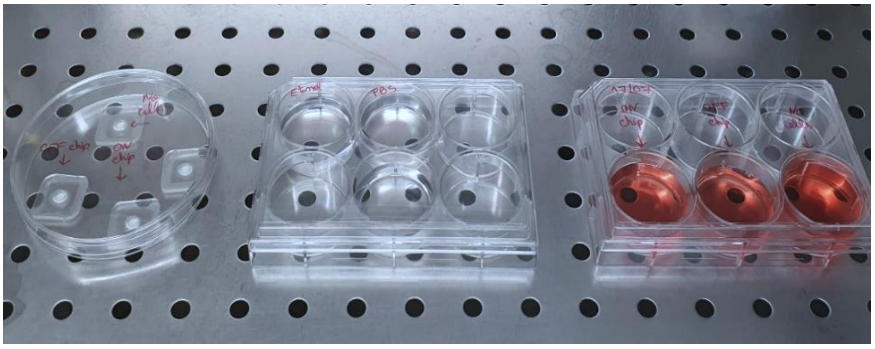

Scaffold pre-treatment. Left: Sterilized insert layer with alvetex, Centre: 6-well plate with 70% ethanol and PBS; Right: 6-well plate with supplemented fibroblast medium

   ii. Pretreat the scaffold layer by immersion in 70% ethanol. Add enough ethanol to completely cover the scaffold;

iii. Carefully remove the ethanol solution and immediately wash the scaffold layer in PBS (1 minute). Make sure the level of the PBS raises over the Alvetex membrane;

iv. Repeat the process using supplemented cell medium. To avoid drying, leave this layer in the final medium wash until required. Incubate at 37 °C with 5 % CO_2 until seeding step;

3) Harvest the fibroblasts by trypsinization (using 0.05% trypsin-EDTA):

i. Aspirate medium from the flask;
ii. Wash with 4 mL PBS. Aspirate PBS from the flask;
iii. Add 4 ml of trypsin solution for a T-175 flask (gently rock the flask to ensure entire surface is covered);
iv. Incubate fibroblasts at room temperature until approximately 90% cells are rounded up (generally 5 min). Observe the progress of trypsinization under the microscope. Hit the flask laterally to detach cells from the surface of the flask;
v. Add 8 ml (double volume) of fibroblast growth medium (FGM) to block trypsin;

4) Transfer the fibroblasts into 50 mL falcons and centrifuge at 2840 rpm at 4ºC for 5 minutes;

5) Aspirate the supernatant and carefully resuspend the fibroblasts in 30 μL medium for each Alvetex. Transfer suspension to an Eppendorf and count the cells;

6) Place the inserts in the dedicated supports. Seed 3.0×10^5 human dermal fibroblasts per Alvetex insert in 30 ul media. (10×10^6 cells/mL). With this concentration the liquid should have a high viscosity and be mostly retained in the scaffold. When seeding remove the wash medium and carefully dispense the cell suspension directly onto the center of the scaffold without touching the membrane;

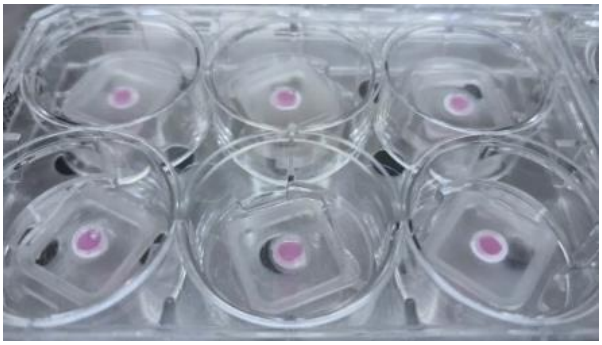

Cell suspension seeded into the scaffolds

7) Incubate at 37°C, in a humidified atmosphere of 5% CO_2 in air for 1.5 hours, for cell adhesion;

2nd part: Chip sterilization, setup preparation using peristaltic pumps

Material: sterilized chips units (2 chips: 4 PMMA parts), sterilized mini luers (male and lid), sterilized tygon tubes, bolts and nuts, reservoir with filter, 4x 10 ml syringes, 2x 1 ml syringes, plastic tweezers, sterilized absorbent paper.

1) Sterilization: Before starting the experiment, mini luer connectors are sterilized by soaking in 70% ethanol for 1 minute and subsequently by applying UV irradiation for 10 minutes. PMMA parts of the chip and tubes are sterilized by applying UV irradiation for 10 minutes (each side). Tubes with connectors are rinsed with 70 % ethanol to ensure sterility;

2) Setup preparation:

   i. Using a syringe, rinse the tygon tubes with PBS to remove the ethanol;

   ii. Using tweezers, connect the tygon tubes to the the reservoir, being careful not to damage them; Place a filter on one of the reservoir's outlets;

3) Fill the reservoir with the FGM + 100 μg/ml ascorbic acid (protect from light with aluminium);

4) Use the peristaltic pumps to completely fill the tubes with medium and remove the PBS;

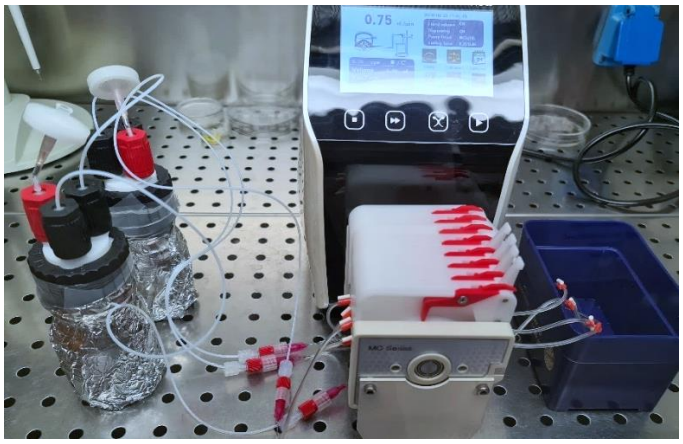

Reservoirs filled with medium and peristaltic pump

5) After the incubation period (approximately 1.5h), with a sterilized absorbent paper, clean any excess medium from the scaffold layer, being careful not to damage it. Using appropriate plastic tweezers, transfer this piece to the sterilized SoC parts;

6) If needed, add bolts and nuts to ensure better sealing. In that case, first close the inlets/outlets by placing mini luer lids. Then, proceed with placing the sterilized bolts in the dedicated holes. Place the chips in the dedicated platform;

7) Connect the sterilized tubes (with the mini male luer connectors) to the mini female luer connectors in the chip;

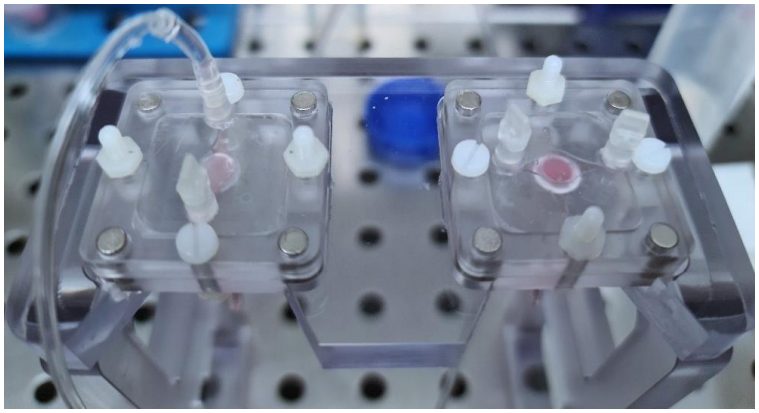

Assembled dermis-on-chip on the platform with different flow configuration

B.8 Protocol for the development of a skin-on-a-chip

This protocol is performed after incubation of the dermal equivalent for at least 6 days and after expansion of keratinocytes;

1st part: Typsinization and cell seeding

1) Supports are sterilized, first by submerging in 70% ethanol for 5 minutes and then using UVs for 10 minutes (each side);

2) Harvest the keratinocytes by trypsinization (using 0.05% trypsin-EDTA):

   i. Remove the medium from culture flasks by aspiration. Wash with 4 ml PBS;
   ii. Add 4 ml of trypsin for a T-175. Rock the flask back and forth to ensure even coating. Place the T-flask into the incubator for 2-3 minutes. Monitor the trypsinization progress at room temperature under an inverted microscope;
   iii. Add 8 ml of warm blocking solution medium [keratinocyte growth medium (KGM)+ 2% FBS] to block trypsin. Gently rock the flask to homogenize);

3) Harvest and transfer cell suspension into a 50 ml falcon. Rinse the flask with an additional 5 ml blocking solution and transfer the solution into the same falcon;

4) Centrifuge cells at 1500 rpm and 4ºC for 7 minutes to pellet the cells;

5) Aseptically aspirate the supernatant, being careful not to dislodge the cell pellet. Resuspend the cells in 30 µL of medium (for each insert) by gently pipetting the cells to break up the clumps. Count the cells with a hemocytometer or cell counter;

6) Pipette 30 µL of cell suspension with $5x10^6$cells/mL in each insert;

7) Incubate at 37 °C in a humidified atmosphere, 5% CO_2 for 3 hours for cell adhesion;

2nd part: Chip sterilization, setup preparation

1) Setup preparation:

i. Rinse the tubes with ethanol followed by a PBS rinse;

ii. Using tweezers, connect the tygon tubes to the tubes in the reservoir, being careful not to damage them; Place a filter on one of the reservoir's outlets;

iii. Fill the reservoir with KGM containing high calcium concentration (1.5 mM);

2) Using the peristaltic pumps fill the tubes with medium and remove the PBS;

3) After the incubation period (approximately 3 h), with a sterilized absorbent paper, clean any excess medium from the scaffold layer, being careful not to damage it. Using appropriate plastic tweezers, transfer this piece to the sterilized SoC parts.

4) If needed, add bolts and nuts to ensure better sealing. In that case, first close the inlets/outlets by placing mini luer lids. Then, proceed with placing the sterilized bolts in the dedicated holes. Place the chips in the dedicated platform.

5) Connect the sterilized tubes (with the mini male luer connectors) to the mini female luer connectors in the chip:

i. First, with the apical inlets/outlets closed with luer lids, connect tubes to the basal perfusion side and pump cell medium until the basal chamber is filled;

ii. After filling the tube circuit with cell medium, remove the luer lids from the apical chambers and connect the tubing. Pump cell medium until the apical chamber is filled;

Caution: Before leaving the biosafety hood make sure the screw caps in the reservoir are tightly closed.

6) Establish double-perfusion at a flow rate of 2 μL/min for 2 days;

3rd part: Skin culture on-chip under air-liquid interface (ALI)

After culture for 2 days under submerged conditions, return the setup to the biosafety hood;

1) Change the medium in the reservoir for KGM containing 1.5 mM calcium, supplemented with 10 ng/mL KGF and 100 μg/mL ascorbic acid 2-phosphate (protect from light with aluminium).

2) Using a syringe exert negative pressure to remove the medium from the apical chamber; Close the apical chamber with mini luer lids;

3) Using the peristaltic pumps, fill the basal chamber with medium;

7) Remove the luer lids from the apical chamber and connect air tubes to the apical inlets and outlets

8) Place the setup at an incubator. Establish basal perfusion at a flow rate of 1.5 μL/min for 11 days;

B.9 Experimental setup skin-on-a-chip

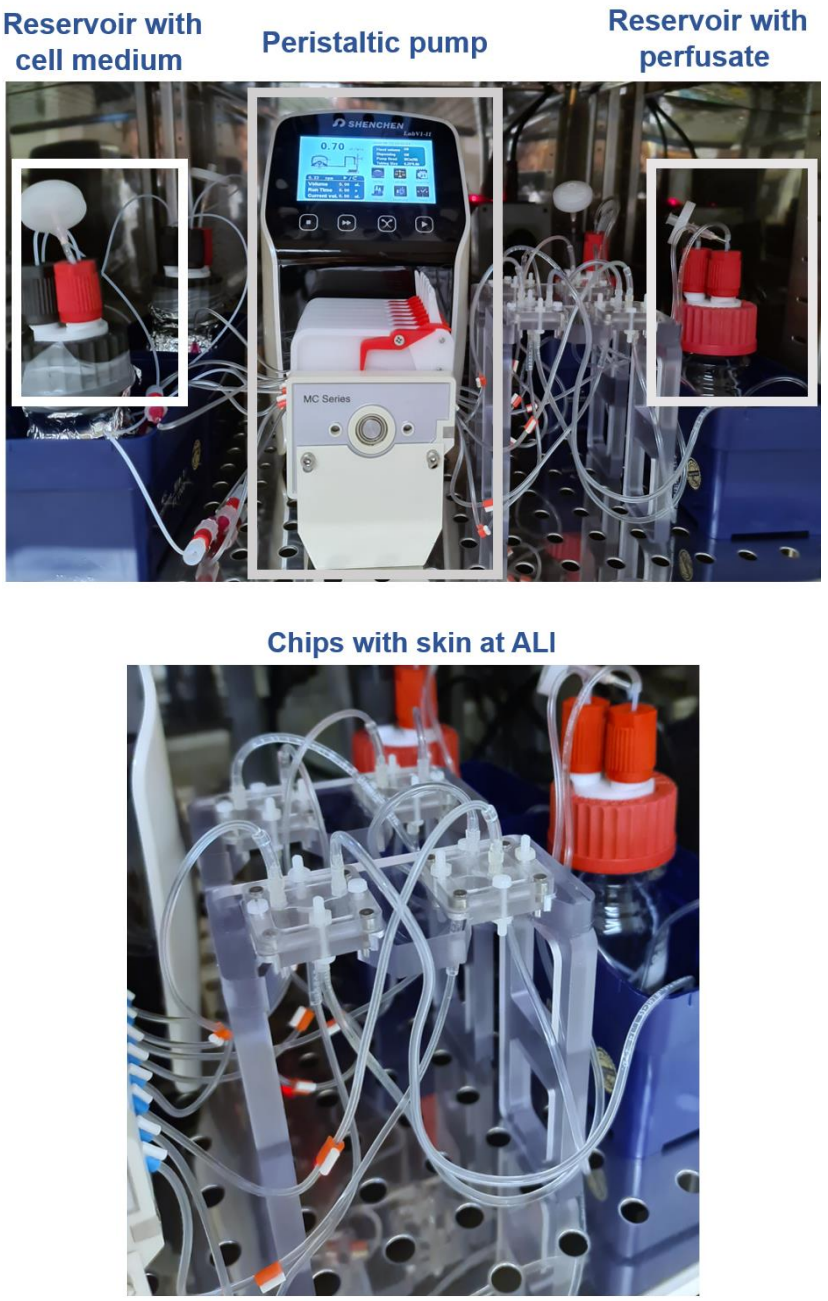

Figure B. 10. Setup for dynamic perfusion of full thickness skin

B.10 Antibodies for immunohistochemistry analysis

Primary antibody	Reference	Primary antibody dilution	Antigen Retrieval	Blocking	Secondary antibody dilution
K10 (Mouse)	Progen, 11414	1:10	Citrate buffer; 20 min (4 x 2min)	PBS-BSA 0,1%; 15min	mouse FITC (1:500)
K14 (Mouse)	Abcam, ab7800	2ug/mL	Citrate buffer; 20 min (4 x 2min)	PBS-BSA 0,1%; 30min	mouse FITC (1:500)
K15 (Rabbit)	Sigma, SAB4501658	1:100	Citrate buffer; 20 min (4 x 2min)	PBS-BSA 0,1%; 15min	Rabbit 488 (1:500)
Involucrin (Mouse)	Sigma, SAB4200794	1:200	Citrate buffer; 20 min (4 x 2min)	PBS-BSA 0,1%; 15min	mouse FITC (1:500)
Collagen I (Rabbit)	Abcam, ab34710	1:100	Citrate buffer; 20 min (4 x 2min)	PBS-BSA 0,1%; 30min	Rabbit 488 (1:500)
Collagen IV (Rabbit)	Abcam, ab6586	1:500	Citrate buffer; 20 min (4 x 2min)	PBS-BSA 0,1%; 15min	Rabbit 488 (1:500)
Fibronectin (Rabbit)	Abcam, ab2413	1:250	Tris-EDTA/0,05% Tween 20; 20 min (4 x 2min)	PBS-BSA 0,1%; 15min	Rabbit 488 (1:500)
Filaggrin (Mouse)	Thermofisher, MA5-13440	1:50	Citrate buffer;20 min (4 x 2min)	PBS-BSA 0,1%; 15min	mouse FITC (1:500)

Secondary antibodies

INVITROGEN, A-11008	Alexa Fluor® 488 Goat Anti-Rabbit IgG (H+L) Antibody (Molecular Probes®)
Sigma, F0257	FITC Goat Anti-Mouse IgG

Table B. 1. Antibodies used for skin characterization

B.11 Experimental setup *in situ* permeation assays

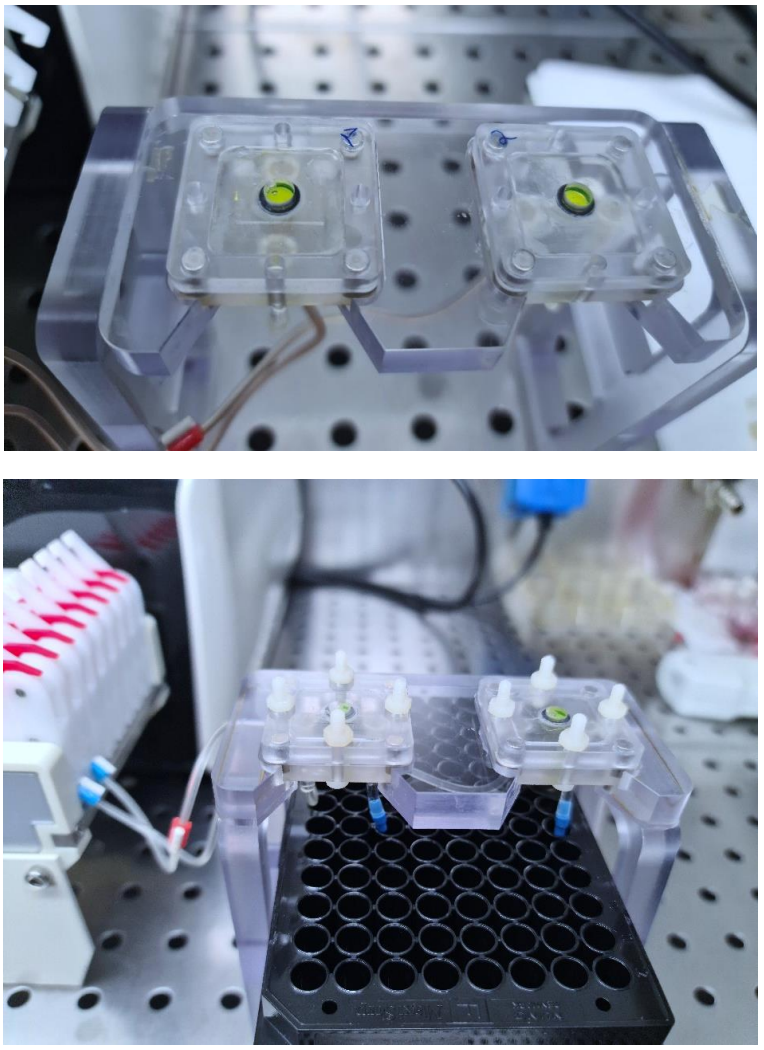

Figure B. 11. Setup for permeation assays on-chip

B.12 Results finite element analysis

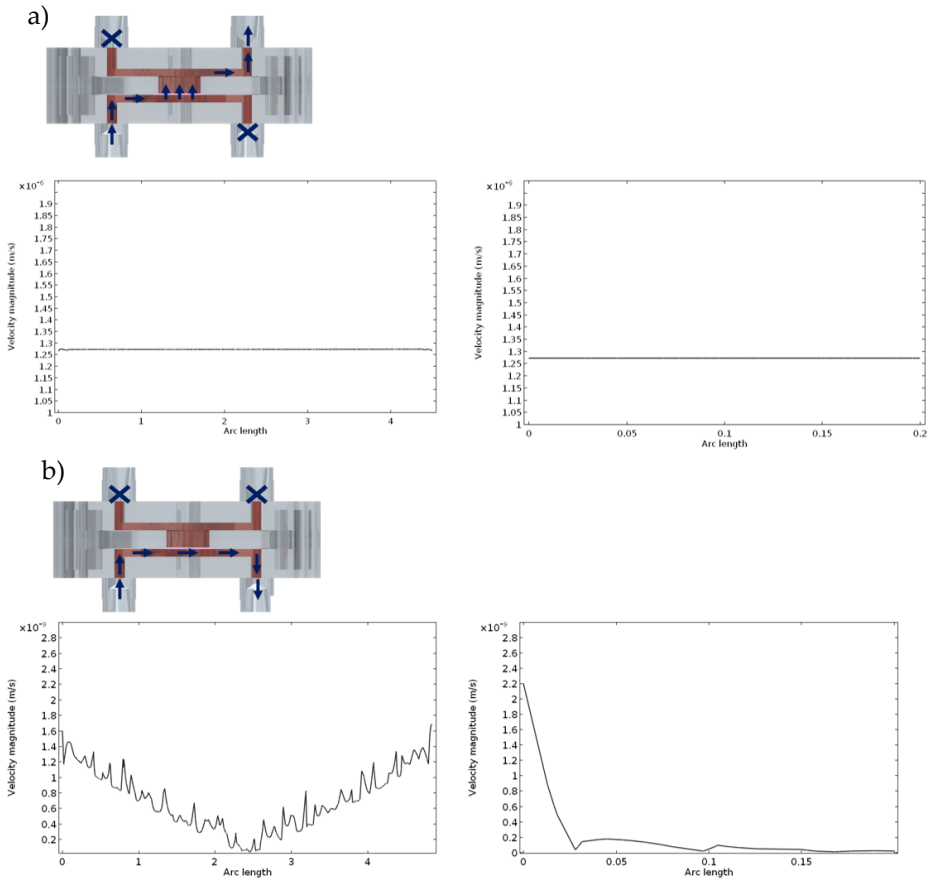

Figure B. 12. Velocity magnitude (m/s) at the scaffold region along the y-direction (left) and z-direction (right) for (a) the cross-flow configuration and (b) tangential flow configuration. Simulations performed for a scaffold permeability 10^{-12} m^2.

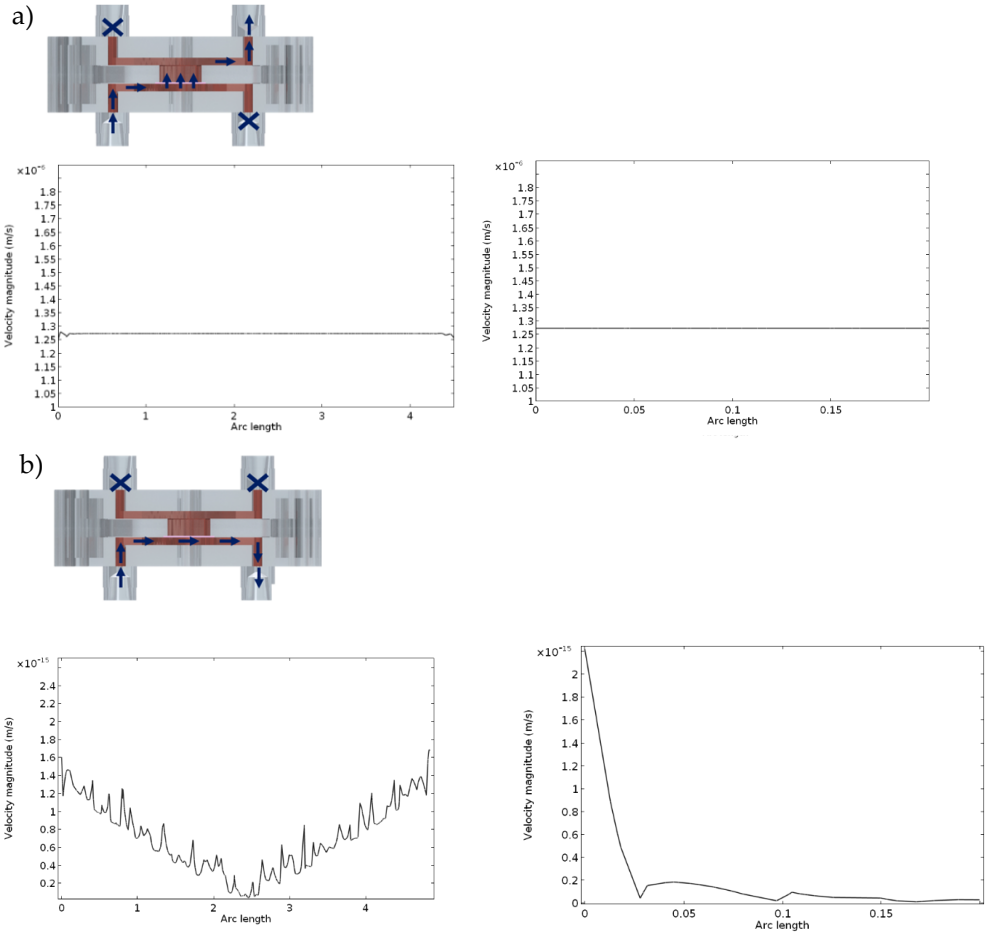

Figure B. 13. Velocity magnitude (m/s) at the scaffold region along the y-direction (left) and z-direction (right) for (a) the cross-flow configuration and (b) tangential flow configuration. Simulations performed for a scaffold permeability 10^{-16} m^2.

C Supplementary information Chapter 7

C.1 Parameters for finite element analysis

Name/Description	Symbol	Expression/Value
Medium electrical conductivity	σ_m	1.5 [S/m]
Medium relative permittivity	ε_m	78
Tissue height	h	100 [μm]
Normalized transepithelial electrical resistance	TEER.A	10^1 - 10^4 [Ω.cm^2]
Current	I	1 [A]
Tissue conductivity	σ_t	$\frac{h}{TEER.A}$ [S/m]

Table C. 1. Summary of the parameters used in the simulation study

C.2 Theory sensitivity distribution

In tetrapolar resistance measurements, electrical fields and current densities develop in 3D space, resulting in different contributions of separate volume elements to the final measured resistance. At every point in the measured volume, the current flow is described by the current density $\boldsymbol{J}$ (A/m^2). The local current density gives rise to a local electrical field. Geselowitz *et al* showed that this generated field is picked up the strongest by the readout electrodes, when this is field is exactly in line with the field that would exist when the same current was sent through the readout electrodes instead of through the excitation electrodes [1]. The interchangeability of the excitation and readout electrode pairs is Geselowitz's reciprocity theorem. On the basis of this theorem, authors calculated a sensitivity coefficient for every small volume element, quantifying the extent to which it contributes to the total measured impedance. As this sensitivity coefficient is based on the extent to which the generated and measured fields line up, it contains the dot product of two vectors.

Grimnes and Martinsen calculated the sensitivity coefficient based on the dot product of the current densities Metherall *et al* had used the dot product of the developed electric fields in earlier work. In this chapter we follow the formulations of Grimnes et al. for the sensitivity coefficient S (equation 7.1) [3, 4]. The higher the value for the sensitivity coefficient, the more a change in the resistivity of this volume element will affect the total resistance. As the resulting scalar field may possess positive and negative values depending on the orientation of the two lead fields, the measured impedance may either increase, decrease or be entirely unaffected in consequence of a conductivity change in a particular region. A negative sensitivity means that an increase in the resistivity of this volume element will, maybe surprisingly but not counterintuitively, result in a lower total measured resistance. **Figure C. 1** illustrates schematically the formation of the measurement sensitivity of a tetrapolar impedance measurement in a homogeneous cylinder. Electrode distances affect whether superficial or deep regions are more efficiently sampled and the regions of negative sensitivity lay near the electrodes, where the two lead fields have antiparallel components

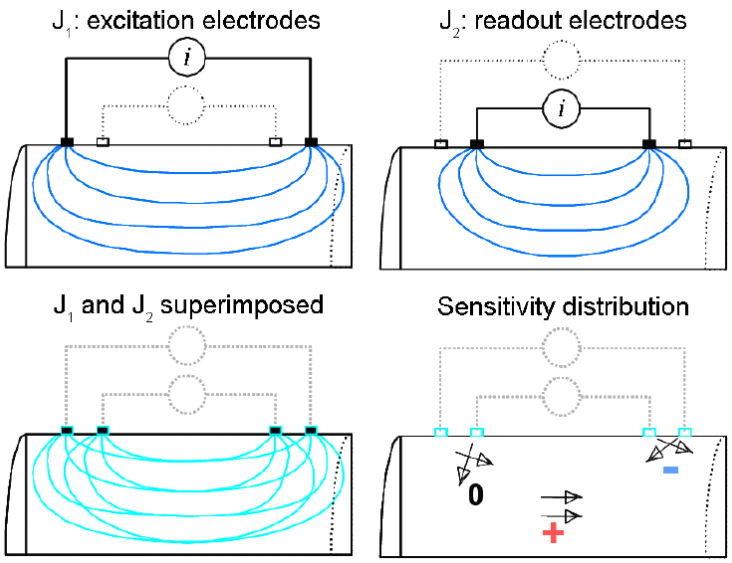

Figure C. 1. Schematic illustration of the sensitivity distribution of four-terminal impedance sensing in a uniformly conductive cylinder. The electrical field arising when current is applied between the excitation electrodes is superimposed on the electric field arising when the same current is applied between the readout electrodes (following the reciprocity theorem). Where the fields align, the resulting sensitivity is high; where the fields are perpendicular the resulting sensitivity is 0; and where the fields oppose each other the resulting sensitivity is negative. Adapted from Kauppinen *et al*. [4]

References:

[1] Geselowitz, D.B. (1971). An application of electrocardiographic lead theory to impedance plethysmography. *IEEE Transactions on Biomedical Engineering*, (1): 38-41.

[2] Grimnes, S. & Martinsen, Ø.G. (2007). Sources of error in tetrapolar impedance measurements on biomaterials and other ionic conductors. *Journal of Physics D: Applied Physics*, **40**(1): 9-14.

[3] Metherall, P., Barber, D., Smallwood, R. & Brown, B. (1996). Three-dimensional electrical impedance tomography. *Nature*, **380**(6574): 509.

[4] Kauppinen, P., Hyttinen, J. & Malmivuo, J. (2006). Sensitivity distribution visualizations of impedance tomography measurement strategies. *International Journal of Bioelectromagnetism*, **8**(1): 1-9.

C.3 Design calibration chamber

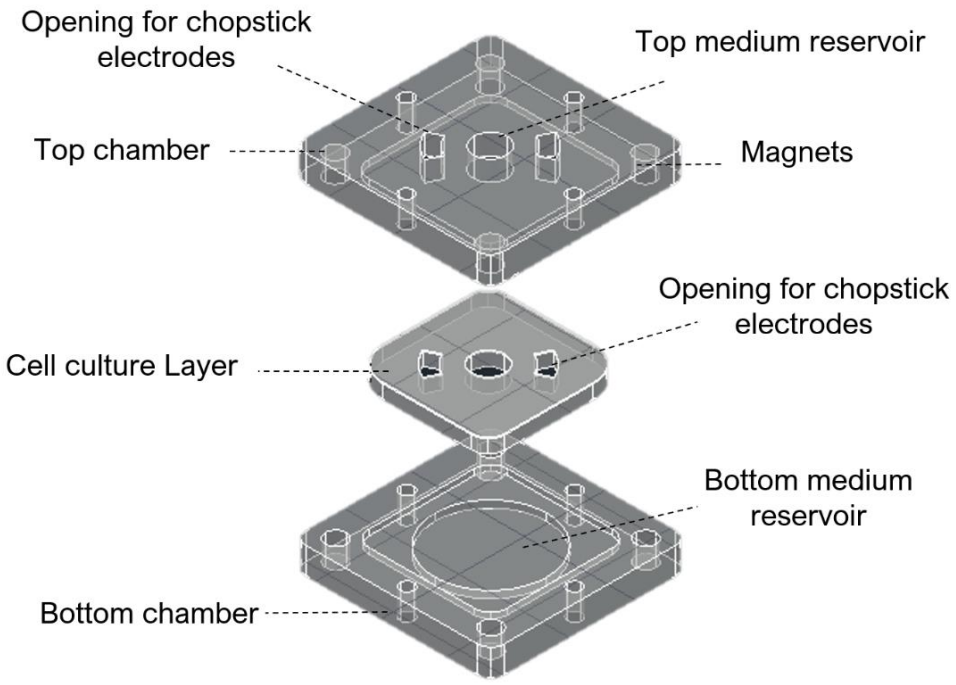

Figure C. 2. Schematic exploded view of the calibration chamber with openings to inset chopstick electrodes for TEER measurements. The calibration chamber consists of a top and bottom chamber including a top and bottom medium reservoir and opening for chopstick electrodes. The chamber was designed to accommodate the PDMS insert layer while allowing for the same placement of the chopstick electrodes as in a Transwell®.

C.4 Results finite element analysis

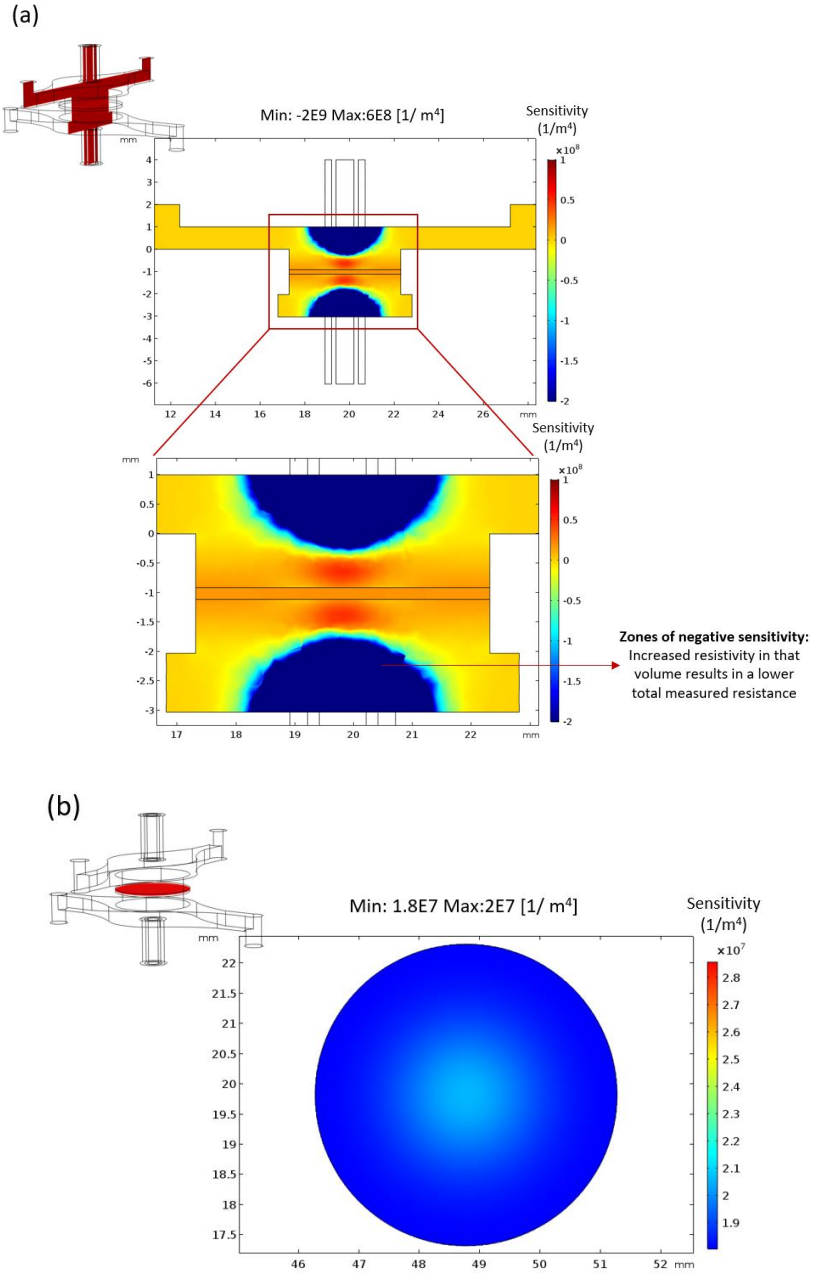

Figure C. 3. Sensitivity distribution (rainbow color map) using the BoC A and TEER 10^3 Ω.cm^2 along (a) a longitudinal cut in the y-z plane and (b) along the cell barrier in the x-y plane.

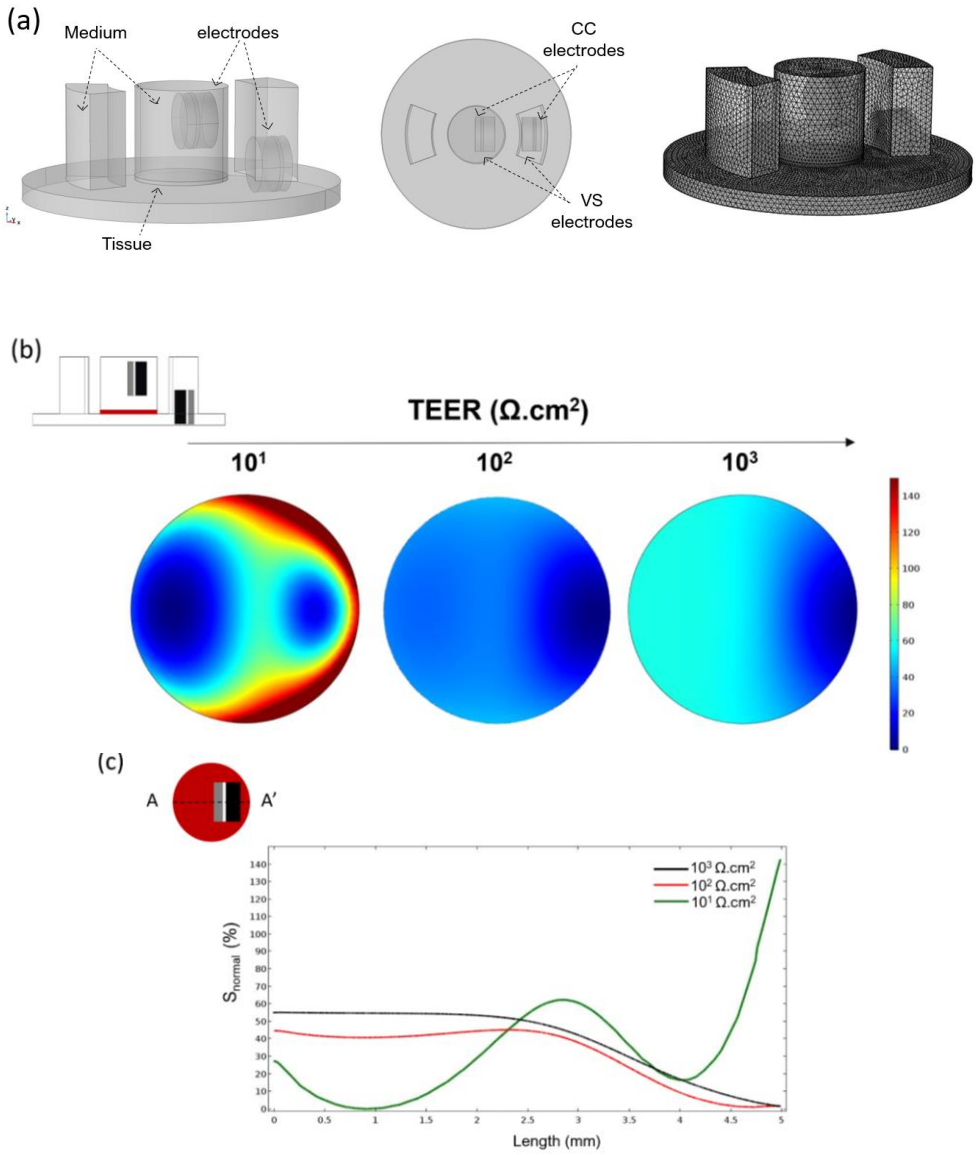

Figure C. 4. TEER measurement calibration device. (a) 3D geometry and created mesh for finite element analysis (FEA) (b) Normalized sensitivity distribution (S_{norm}) including the planar sensitivity distribution along the cell barrier surface (rainbow color map) in the x-y plane and sensitivity distribution along the cell barrier though the axis (lines AA′) shown in the scheme of the model at the left. Results are presented for different TEERS (10^1-10^3 Ω.cm^2). A S_{norm} value of 0% represents the zone of lower sensitivity. Note that axis have different scales.

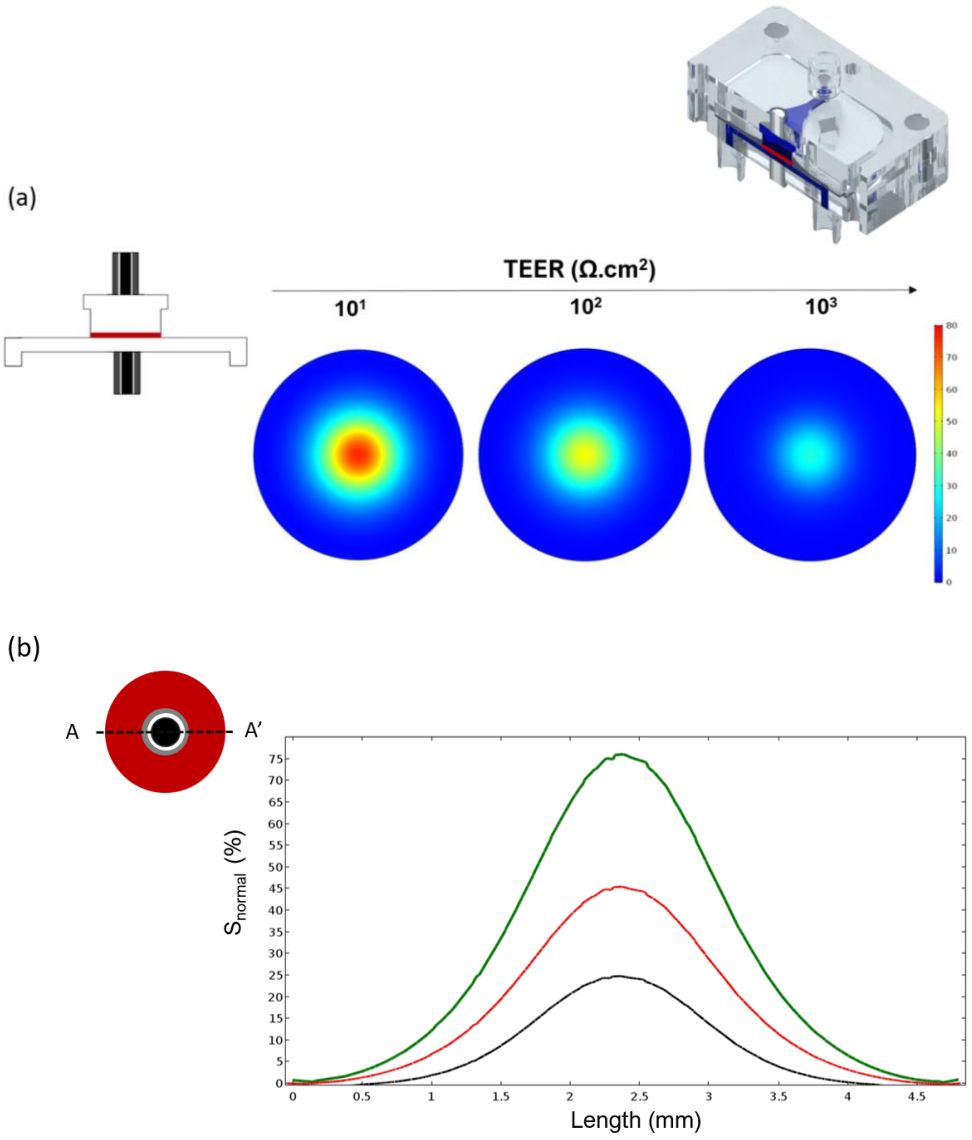

Figure C. 5. BoC A with asymmetric placement of cell culture insert. Normalized sensitivity distribution (S_{norm}) including the planar sensitivity distribution along the cell barrier surface (rainbow color map) in the x-y plane and sensitivity distribution along the cell barrier though the axis (lines AA') shown in the scheme of the model at the left, when TEER is measured. Results are presented for different TEERS (10^1 -10^3 Ω.cm^2). A S_{norm} value of 0% represents the zone of lower sensitivity. Note that axis have different scales.

C.5 Results calibration

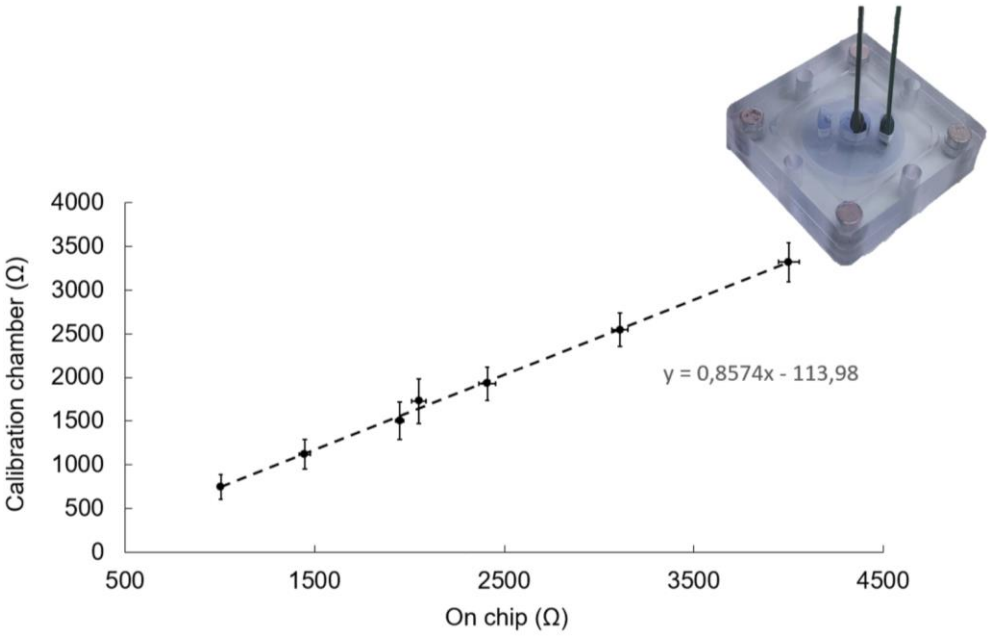

Figure C. 6. TEER measurement calibration device. Resistance readings from the calibration device and the BoC with integrated electrodes showing a linear correlation. Picture of the assemble device with chopstick electrodes (Top-right).

Patrícia Zoio, PhD Candidate

Contacts

patricia.zoio@itqb.unl.pt
pattie.zoio@gmail.com

+351 91 506 30 66

Lisbon, Portugal

PROFILE: Patrícia Zoio is a PhD candidate at the Institute of Chemical and Biological Technology from the NOVA University of Lisbon. Patricia's research interests lie on the interplay between biology and technology with special focus on organ-on-a-chip technology, tissue engineering and computational modelling and simulations. During her PhD, she worked on the design and fabrication of an innovative organ-on-a-chip platform with integrated sensors for the development of a full-thickness human skin model. Patrícia is the first author in multiple articles published in peer-review journals focused on organ-on-a-chip technology and tissue engineering.

RESEARCH EXPERIENCE

10/2016 – 02/2022 (expected)
Institute of Chemical and Biological Technology (ITQB-NOVA), Oeiras, Portugal
PH.D. Candidate in Advanced Integrated Microsystems

- *Advanced skin model*

Developed a new protocol for the generation of a scaffold-based full-thickness skin model without using exogenous animal-derived materials. Contrary to conventional skin models, the developed tissue preserves its architecture and homeostasis for more than 6 weeks. The model demonstrated structural characteristics and barrier properties parallel to the native skin. Skin permeation and irritation tests were performed, according OCDE guidelines, using reference drugs. Skills: cell culture, tissue engineering, toxicology in vitro;

- *Modular and reversibly sealed organ-on-a-chip device*

Designed and fabricated an innovative organ-on-a-chip platform with a module-based architecture and a removable cell culture insert. A polymeric scaffold was integrated in the device to reproduce tissues with a high level of complexity. A skin model with increased thickness and enhanced barrier function was successful produced on the developed chip. Skills: Computer aided design (CAD), computer modelling and simulations (fluid dynamics), rapid prototyping, microfluidics;

- *Sensors for real-time evaluation of biological barriers*

Integrated sensors on a organ-on-a-chip device for real-time, non-destructive evaluation of the tissue barrier function. Performed finite element modelling to study the sensitivity distribution of a tetrapolar electrode concentric arrangement for transepithelial electrical resistance measurements. Skills: computer modelling and simulations (electromagnetics), electronics;

09/2017 – 03/2018
INESC Microsystems and Nanotechnologies, Lisbon, Portugal
Internship

-Microfluidic device for tissue culture

Designed and fabricated a micro-physiological system using micro/nanofabrication techniques. Skills: CAD design, plasma bonding, precision liquid pumping, photoresist molding, soft lithography (PDMS).

02/2014 – 05/2015
Institute of Biophysics and Biomedical Engineering (IBEB), Lisbon, Portugal
M.S. Candidate in Biomedical Engineering

- *Modelling an electromagnetic actuation system for the manipulation of microdevices in blood vessels*

Performed finite element analysis to identify coil configurations that would allow the control of magnetic devices at different size scales in blood vessels. The simulations showed that it is possible to control the magnetic force and toque acting on a microdevice through the fields produced by Maxwell and Helmholtz coils, respectively. Skills: computer modelling and simulations (electromagnetics. Hydrodynamics, particle tracing);

- Design of a proof-of-concept electromagnetic actuation system
Designed and built a prototype of a magnetic actuation system to control devices with sizes ≥ 100 μm. The system was fabricated from the ground up, using a do-it-yourself approach. Skills: electromagnetics, mechanics;

07/2012 – 10/2012
International Iberian Nanotechnology Laboratory (INL), Braga, Portugal
Internship

- Tailored magnetic nanoparticles for optimizing magnetic fluid hyperthermia
Synthesized and characterized iron oxide magnetic nanoparticles for magnetic fluid hyperthermia. The magnetic loss processes in magnetic nanoparticles were studied. Specific loss power values were obtained for different iron oxide magnetic nanoparticles, synthesized by different chemical routes. Skills: Nanoparticle characterization techniques (TEM, STEM, x-ray powder diffraction), magnetic measurement techniques (vibrating sample magnetometer, SQUID).

PUBLICATIONS:

Peer-reviewed publications
- **Zoio P**, Lopes-Ventura S, Marto J, Oliva A. Open-source human skin model with *in vivo*-like barrier for drug irritation and permeation testing. *ALTEX – Alternatives to animal experimentation. 2022;*

- **Zoio P, Oliva A.** Skin-on-a-chip technology: Microengineering physiologically relevant in vitro skin models. *Pharmaceutics.* 2022;

- **Zoio P**, Lopes-Ventura S, Oliva A. Biomimetic Full-Thickness Skin-on-a-Chip Based on a Fibroblast-Derived Matrix. *Micro*. 2022; 2(1):191-211. https://doi.org/10.3390/micro2010013;

- Hall Michael J.; Lopes-Ventura S; Neto M; Charneca J; **Zoio P**; Seabra M; Oliva A; Barral D, Reconstructed human pigmented skin/epidermis models achieve epidermal pigmentation through melanocore transfer. Submitted to *Pigment cell & Melanoma;*

- **Zoio P**, Lopes-Ventura S, Oliva A. Barrier-on-a-Chip with a Modular Architecture and Integrated Sensors for Real-Time Measurement of Biological Barrier Function. *Micromachines*. 2021; 12(7):816. doi.org/10.3390/mi12070816;

- **Zoio P,** Ventura S, Leite M, Oliva A. Pigmented Full-Thickness Human Skin Model Based on a Fibroblast-Derived Matrix for Long-Term Studies. *Tissue Eng Part C Methods*. 2021;27(7):433-443. doi:10.1089/ten.TEC.2021.006;

- Esmail A, Pereira JR, **Zoio P**, Silvestre S, Menda UD, Sevrin C, Grandfils C, Fortunato E, Reis MAM, Henriques C, Oliva A, Freitas F. Oxygen Plasma Treated-Electrospun Polyhydroxyalkanoate Scaffolds for Hydrophilicity Improvement and Cell Adhesion. *Polymers*. 2021; 13(7):1056. https://doi.org/10.3390/polym13071056;

In preparation
- Ventura S, Leite M, **Zoio P**, Cabeçadas J, Rosa J, Pereira T, Pojo M, Oliva A. Reconstructed three-dimensional melanoma skin model for screening therapies. Submitted to *Biomaterials Science*.

SCIENTIFIC CONFERENCE PRESENTATIONS

Oral communications
- Invited speaker at the joint ASCCT – ESTIV webinar "Maturing three-dimensional toxicology models of the barrier organs: Examples from lung and skin" with a presentation entitled "Full-thickness skin-on-a-chip model for in vitro drug testing and disease modelling" (2022).

- Invited speaker at the11th edition World Conference on Alternatives and Animal Use in the Life Sciences (WC11) with a presentation entitled "Skin-on-a-chip with integrated sensors and a modular architecture for drug screening and disease modelling" (Maastricht, The Netherlands) (2021).

Oral communications (cont.)

- Invited speaker at the 7th edition of the workshop on Biomedical Engineering with a presentation entitled "Magnetic actuation of microdevices for biomedical applications" (Lisbon, Portugal) (2015).

- Invited speaker at the summer school "Dual-imaging of Nano/Microsized Theranostics" at the Charité University with a presentation entitled "Nanorobot navigation using an MRI system" (Berlin, Germany) (2013).

Poster communications

- Rafael A, Pereira J, Esmail A, **Zoio P** *et al***.** Production of 3D biocomposite scaffolds based on polyhydroxyalkanoates (PHAs) and Fucopol. Presented at the Microbiotec21 (Lisbon, Portugal) (2021);

- **Zoio P**, Oliva A. Fully Human Skin-on-a-chip with integrated sensors and a modular architecture for drug screening and disease modelling. Presented at the 11th edition World Conference on Alternatives and Animal Use in the Life Sciences (Maastricht, The Netherlands) (2021);

- Ventura S, Leite M, **Zoio P**, Pojo M, Oliva A. *In vitro* 3D human melanoma skin model for therapeutic studies. Presented at the cutaneous melanoma meeting (Lisbon, Portugal) (2021);

- Rafael A, Pereira J, Esmail A, **Zoio P** *et al***.** Polyhydroxyalkanoates (PHAs) And Fucopol Scaffolds For Tissue Engineering Applications. Presented at the Global Summit on Biomaterials and Applications (Valencia, Spain) (2021);

- Lopes-Ventura S, **Zoio P**, Oliva A. Reconstructed Fully-Humanized Skin model for therapeutic biomedical applications. Presented at the Champalimaud Foundation, Lisbon, Portugal (2020);

- **Zoio P**, Lopes-Ventura S, Oliva A. Fully Humanized Skin-on-a-chip for medical applications: Combining microtechnology with 3D tissue engineering to develop human skin. Presented at the European Commission JRC, Ispra, Italy (2019).

GRANTS AND AWARDS

- Early career Scientist Award attributed by the Physicians Committee for Responsible Medicine (2021);

- Best Poster Award attributed by European Society of Toxicology *in vitro* (ESTIV) at the 11th World Congress on Alternatives to Animal Use in Life Sciences WC11 (2021);

- Early-Career Scientist Award attributed by the People for ethical treatment of animals (PETA) (2019);

- Best Poster award attributed by the European Commission (JRC) at the Conference on "Non-animal approaches in Science" (2019);

- Best Abstract at the 7th edition of the Workshop on Biomedical Engineering (2016).

EDUCATION

01/2020 – 07/2020
Nova School of Business and Economics (NOVA SBE), Carcavelos, Portugal
StartUp Research Post-Graduation program
International and interdisciplinary Post-Graduation course brought together by scientists and entrepreneurs. During the program, the hypothesis of creating a start-up in field of organ-on-a-chip technology was evaluated. A final pitch was given to entrepreneurs in the pharmaceutical industry.

EDUCATION (cont.)

05/2019 (1 week)
European Commission Joint Research Centre, Ispra, Italy
JRC Summer School on "Non-Animal Approaches in Science: Challenges and Future directions"
During the European Commission JRC Summer School, it was possible to share knowledge and experience on the latest non-animal approaches used in research and testing including in vitro methods and computational modelling.

01/2017 – 07/2017
Institute of Chemical and Biological Technology (ITQB-NOVA), Oeiras, Portugal
Ph.D., Program Molecular Biosciences curricular units
Core training: Biotechnology, Systems Biology, Protein and Biogenesis DNA and RNA biology;
Specic training profile: Technologies for Biopharmaceutical Development, Nanoprocesses for Life Sciences, Bioprocess data analysis, Tools for Discovery and Preclinical research.

09/2013 – 05/2015
Faculty of Sciences of the University of Lisbon
M.S.C., Biomedical Engineering and Biophysics
Main subjects: Nanotechnology; Medical Robotics; Tissue Engineering; Stem cells; Neuroscience; Bioelectriciy; Signal Processing; Medical Equipment; Human Anatomy; Human Physiology; Biostatistics.

SCIENCE COMMUNICATION

Interviews given to the press: Portuguese Vegetarian Association, Smack.pt from Impresa (the major portuguese media conglomerate), Weggan magazine. Invited speaker at the International congress CouraVeg 2019. Scientific research shared by PETA (.uk and .org).

ITQB-UNL | Av. da República, 2780-157 Oeiras, Portugal
Tel (+351) 214 469 100 | Fax (+351) 214 411 277

www.itqb.unl.pt